FITNESS-FOR-SERVICE ASSESSMENT FOR THERMAL HOT SPOTS AND CORROSION IN PRESSURE VESSELS

PATTARAMON TANTICHATTANONT

FITNESS-FOR-SERVICE ASSESSMENT FOR THERMAL HOT SPOTS AND CORROSION IN PRESSURE VESSELS

by

Pattaramon Tantichattanont ©

A Thesis submitted to the School of Graduate Studies
In partial fulfillment of the requirement for the degree of
Doctor of Philosophy in Engineering

Faculty of Engineering and Applied Science

Memorial University of Newfoundland

December 1, 2006

St. John's Newfoundland and Labrador, Canada

ABSTRACT

Corrosion and thermal hot spots are typical of damage occurring in pressure vessels, piping or storage tanks used in industrial processes. Structural integrity of such components needs to be evaluated periodically to determine the acceptability for continued service. The ability to demonstrate structural integrity of an in-service component containing damage is termed as Fitness-for-Service (FFS) assessment.

In the present thesis, the Remaining Strength Factor (RSF) is chosen to quantify FFS assessments. Three alternative methods for Level 2 FFS assessments (according to API 579) of pressure components are proposed. Damage due to corrosion and thermal hot spots is considered. The methods are based on variational principles in plasticity, the limit load multiplier m_α-method, reference volume and the concept of decay lengths in shells. The m_α-method has been shown to provide acceptable approximations to limit load of various mechanical components and is thus employed as one of the bases of the recommended calculations for RSF in the current study.

The effects of local damage on a shell structure are normally restricted to a limited volume in the vicinity of the damage termed as reference volume. The use of reference volume instead of the entire volume of the structure gives a better approximation of limit load multipliers. In the present study, reference volume is characterized by using decay lengths of shells. Decay lengths for spherical and cylindrical shells are derived based on

elastic shell theories. The derived decay lengths are also used to specify the limit of what can be called “local” damage. They allow one to examine the interaction between decay effects in two perpendicular directions. The local damage limit is defined as the maximum size of damage beyond which pure equilibrium stress occurs at some place inside the damaged area. If the damage in a component is larger than this limit, it can be deemed as “global.” For global damage, the “failure” load is as if the damage extends to the entire component and the classical lower bound RSF_L is used.

The stretching and bulging effects due to the damage are studied. For highly localized damage, the effects of stretching action dominate the behavior of the damage and surrounding areas. The damaged spot tends to open up instead of forming a bulge. The limit defining the threshold to dominance of stretching action is proposed by using an approximate equilibrium calculation and yield-line analysis.

The usefulness and effectiveness of the three recommended methods are demonstrated through illustrative examples. The recommended approaches are validated by detailed inelastic finite element analysis. Recommendations and relevant observations for general shapes have been made. Detailed procedures and useful aids for FFS assessments are provided.

ACKNOWLEDGEMENTS

I owe my gratitude to all the people who have made this thesis possible. First and foremost I wish to express my deep gratitude to my supervisors, Dr. R. Seshadri and Dr. S. M. R. Adluri, for their tireless support, guidance and technical discussions during the entire course of my doctoral program. Thanks are also directed to Dr. S. Iyer, Dr. W. Reinhardt and Dr. K. Munaswamy for their helpful comments. The financial support provided by NSERC and the Faculty of Engineering and Applied Science, Memorial University of Newfoundland are gratefully acknowledged.

I would like to extend my acknowledgements to my friends in the Asset Integrity Management Research Group for their interesting discussions and kind assistance. I also would like to thank all my friends for their constant support and friendship. Last but not least, I owe my deepest thanks to my family: my father, my mother and both of my brothers; for their inspiration, encouragement and understanding through all these years.

TABLE OF CONTENTS

LIST OF TABLES

LIST OF FIGURES

LIST OF APPENDICES

LIST OF ACRONYMS AND ABBREVIATIONS

ANSI	American National Standards Institute
API	American Petroleum Institute
ASME	American Society of Mechanical Engineers
CA	Corrosion Allowance
FCA	Future Corrosion Allowance
FEA	Finite Element Analysis
FFS	Fitness-for-service
LTA	Locally Thinned Area
RSF	Remaining Strength Factor
RTA	Round Thin Area

LIST OF SYMBOLS

Symbols

a, b	Half length and width of an equivalent rectangular damaged area
a_L, b_L	Extent of local damage for cylinder
A	Area of the crack or defect
B, n	Creep parameters for second stage power law creep
c	Bulging displacement for ellipsoidal bulge
D	Nominal outside diameter; Flexural rigidity of shell
D_i	Inside diameter
D_{maz}	Maximum diameter of the component due to bulging
D_o	Original diameter of the component
$\dot{D}$	Increment of plastic dissipation per unit volume
d	Depth of corrosion
e	Distance between thickness centerlines of corroded and uncorroded areas
E	Modulus of elasticity
E_{eff}	Effective elastic modulus based on the concept of reference volume
E_0	Original Young's modulus of material
E_j	Joint efficiency
E_s	Modified Young's modulus
f	Safety factor
$f(s_{ij})$	Yield function
F	Functional
G	Shear modulus
h	shell thickness
h_c	corroded thickness
J_2	Second invariant of the stress deviator tensor
K	Shear rigidity of shell
k	Yield stress in pure shear; Shell parameter; Element number
l	Characteristic length used in shell theory
L	Length of cylinder
$L(\cdots)$	Operator for shell having the form of a surface of revolution

L_{msd} Distance between flaw and major structural discontinuity

L_v Thickness averaging zone

m Exact limit load multiplier or safety factor; The number of harmonics

m^0 Statically admissible upper bound multiplier

m' Lower bound multiplier from Mura's formulation

m_α Improve lower bound multiplier

m^* Kinematically admissible multiplier

m_L Classical lower bound multiplier

m_d^0 Upper bound multiplier for damaged component

m_u^0 Upper bound multiplier for undamaged pipe

M Folias factor; Bending moments per unit length

M_p Plastic moment

N Normal forces per unit length; Total number of elements in FEA; Hardening exponent

p_1, p_2 Roots of Donnell's equation

p Internal pressure

P_d Design pressure

P_x, P_y, P_z Components of body forces in x, y and z directions, respectively

q Modulus adjustment index, intensity of a continuous distributed load

Q_e Effective generalized stress

r Aspect ratio of damaged spot

r_1, r_2 Radii of curvature of a shell in meridian plane and in the normal plane perpendicular to meridian, respectively

$r_d l$ Decay length of a spherical shell loaded by a concentrated normal force

R_i Inner radius

R_o Outer radius

RSF_α Improved lower bound RSF based on m_α -multiplier

RSF_a Allowable RSF

RSF_i Inelastic RSF

RSF_L Lower bound RSF

RSF_r Recommended RSF

RSF_U Upper bound RSF

R_b Radius of the bulge

R_C Inner radius of the corroded part of the component

R_t Remaining thickness ratio

s	Corrosion axial length
s_{ij}	Deviatoric stress
s_{ij}^0	Statically admissible deviatoric stress field under applied load $m^0 T_i$
$\bar{s}_{ij}^0$	Statically admissible deviatoric stress field under applied load T_i
S_T	Surface of the body where surface traction is prescribed
S_v	Surface of the body where velocity is prescribed
t	Nominal wall thickness
t_C	Corroded thickness
$t_{\min}$	Minimum required wall thickness
t_{mm}	Minimum measured remaining wall thickness.
T	Temperature
T_i	Applied surface traction
U_d	Distortion energy
$\dot{u}$	Velocity field
$\bar{u}, \bar{v}, \bar{w}$	Non-dimensional displacement components
v_i	Velocity vector
v_i^*	Kinematically admissible velocity
V	Volume of the component; Angle of rotation of a tangent to a meridian
V_D	Volume of the damaged spot
V_R	Reference volume
V_T	Total volume
V_I	Undamaged adjacent volume
w_1, w_2	Longer and shorter side of an approximate rectangular flat plate
W_{ext}	External work
W_{int}	Internal energy dissipation
x, y, z	Rectangular coordinates
x_c, x_l	Decay length in the circumferential and axial directions of cylinder

Greek Symbols

α	Thermal coefficient; Ramberg-Osgood constant; Slope factor for linear interaction curve
α_1, α_2	Real parts of roots p_1, p_2
α_{eff}	Effective thermal coefficient based on the concept of reference volume
β	Shell parameter for cylinder
β_1, β_2	Imaginary parts of roots p_1, p_2

δ_b	Radial displacement of the bulge
δ_{ij}	Kronecker delta
ΔT	Temperature change due to formulation of hot spot
ε	Strain
ε_b	Maximum membrane strain at the crown of bulging
$\dot{\varepsilon}$	Strain rate
$d\varepsilon_{ij}^{P}$	Plastic strain increment
$\dot{\varepsilon}_{ij}^{*}$	Kinematically admissible strain rate
γ	Engineering shear strain; Integration constant for sphere; parameter for surface area of ellipsoid
η	non-dimensional variable for linear interaction curves
Φ	Stress function
φ	Angle defined a parallel plane
φ_a	Hot spot or corrosion included angle
φ_b	Included angle of the bulge
φ_d	Decay angle based on an applied normal concentrated load
φ^0	Point function introduced in the yield criterion
κ	Change in curvature; non-dimensional variable for elliptic interaction curves
λ	Metal loss parameter; parameter representing the thinness of shell
$d\lambda$	Positive scalar of proportionality in the flow rule
μ	Plastic flow parameter
ν	Poisson's ratio
Σ	Yielding surface
θ	Angle defined a meridian plane
σ_e	Equivalent stress
$\sigma_{ij}, \sigma'_{ij}$	Stress tensor
σ_{fail}	Nominal hoop stress at failure
σ_{flow}	Flow stress
σ_y	Yield stress
$\sigma_1, \sigma_2, \sigma_3$	Principal stresses
ξ	non-dimensional variable for damage in cylindrical shell
ψ_d	Decay angle based on edge moment effects
ψ_L	Transition angle from small to intermediate of hot spot
ζ	Iteration variable
∇^2	Laplacian operator

Subscripts

c	Circumferential direction
D	Parameters in the damaged part of the component
e	Von Mises equivalent
I	Parameters in the adjacent part
i, j	Tensorial indices
k	Element number
L	Lower bound; Quantities at the extent for local damage
r	Radial direction
T	Quantities at transition point
u	Upper bound
U	Parameters in the undamaged part of the component
α	Parameters based on m_α method

Superscripts

0	Statically admissible quantities
*	Kinematically admissible quantities;
	Quantities at the threshold to dominance of membrane and bending effect
c	Complementary solution

CHAPTER 1

INTRODUCTION

1.1. BACKGROUND

Structural integrity assessment of mechanical components and structures is of considerable importance in a number of industrial sectors. The ability to demonstrate structural integrity of an in-service component undergoing damage is termed as integrity assessment or Fitness-for-Service assessment and is extensively dealt with by recommended practices and procedures such as API 579 (American Petroleum Institute, 2000) and R6 (Nuclear Electric, 1995).

Fitness-for-Service (FFS) evaluations are conducted periodically to determine whether the component with existing flaws or damage is suitable for continued service until the end of some desired period of operation such as the next shutdown, a specific future date or the end of its useful life. The assessments include determination of current serviceability to ensure safe operation in the present condition, and remaining service life

of the equipment or structure. Sometimes it can be used to assess the component suitability for planned modifications or upgrades.

For pressurized equipment in operating plants, API 579 prescribes three levels of structural integrity evaluations. Levels 1 to 3 are progressively more sophisticated. Each assessment level provides a balance between the degree of conservatism, the amount of required input, the skill of the practitioner, the complexity of analysis effort and the accuracy of the procedure. Level 1 assessments are the most conservative screening criteria that generally include the use of charts and tables, which can be implemented by plant technicians with minimal inspection requirements. Level 2 assessments involve detailed calculations intended for use by plant engineers with the help of a recommended procedure on a routine basis without too much complication. Level 3 assessments require a rational analysis by specialists where advanced computational techniques such as full scale nonlinear finite element modeling are engaged.

The procedures in API 579 are developed to overcome the shortcomings of the former inspection codes for pressure vessels and piping which are mainly based on empirical data and past experience (Sims, Hantz and Kuehn, 1992). Extensive validations based on both numerical analysis and physical testing are applied to various damage modes such as metal loss and crack-like flaws. In that regard, further enhancements to Level 2 procedures for damaged areas such as hot spots and corrosion effects are of interest.

Localized corrosion damages and thermal hot spots are typical of damage that occurs in ageing pressure vessels, piping or storage tanks, e.g., corrosion-damaged pipelines in Trans Alaska Pipeline System (TAPS) and Prudhoe Bay network (Fineberg, 2006; Loy, 2006). Corrosion spots are considered to be locally thinned areas (LTA) for the purpose of evaluation. External corrosion can occur in pressure components exposed to hostile surrounding environments such as buried or submerged metallic piping systems. The primary protection for external corrosion is a coating or lining of the outside surface. A corrosion protection system will be a secondary protection. Internal corrosion is caused by corrosive products inside the pressurized component for instance natural gas and petroleum products transported in pipelines or corrosive products inside pressure vessels. Although B31.X code equation does not explicitly account for corrosion tolerance in t_{nom}, corrosion allowance is sometimes specified at the design stage to accommodate in-service corrosion that is likely to occur. Corrosion damage can be detected by the use of ultrasonic devices on the exterior of storage tanks or pressure vessels, or by the use of in-line inspection vehicles called 'Smart Pigs'[1] in pipelines.

Thermal hot spots are caused by damage due to local loss of refractory lining on the inside wall of pressure components or due to mal-distribution of flow containing catalyst and reactive fluids. They are detected through thermography or temperature sensitive paints on the outside of the vessel. Although thermal hot spots are caused by loss of refractory lining on the inside wall of the pressure components, it also results in

[1] *Smart Pig* : An electronic internal inspection device placed inside the pipeline to provide data about the condition of the pipeline, such as measuring dents or locating corrosion (Westwood and Hopkin, 2004)

higher temperature on the outside wall of the component. This temperature change can be noticed by the color of the temperature sensitive paints on the outside.

An FFS assessment is required to determine the acceptability of a component containing hot spots or corroded areas for continued service. The parameter generally used in such assessments is the Remaining Strength Factor (RSF). The RSF is defined as the ratio of the limit load (pressure) of the damaged component to that of the undamaged component. Limit load indicates the reaching of certain predefined failure criteria and not necessarily physical collapse. If the calculated RSF is greater than or equal to the allowable RSF, the damaged component is termed as fit-for-service and no repair/rework are warranted. If the calculated RSF is less than the allowable value (or if the vessel is shown to have sustained damage beyond some unacceptable repair threshold), the component can be repaired, rerated or some form of remediation can be applied to combat the severity of the operating environment.

1.2. PRESENT STUDY

The existing procedures for RSF calculation pertaining to corrosion damage, such as API 579, are mostly limited to cylindrical components and the recommendations are based on empirical relationships. However, there are no recommendations for pressure components containing thermal hot spots. Seshadri (2004) addressed this to calculate an RSF for cylinders with thermal hot spots. The current work extended this.

One of the objectives of the current research is to study the factors affecting structural integrity of pressure vessels with typical damage so as to provide practical, simple and theoretical-grounded Level 2 techniques to determine the remaining strength factors of such components. The evaluation procedures in the present study are developed based on the concept of reference volume, application of the variational principles in plasticity and the estimation of limit load multipliers.

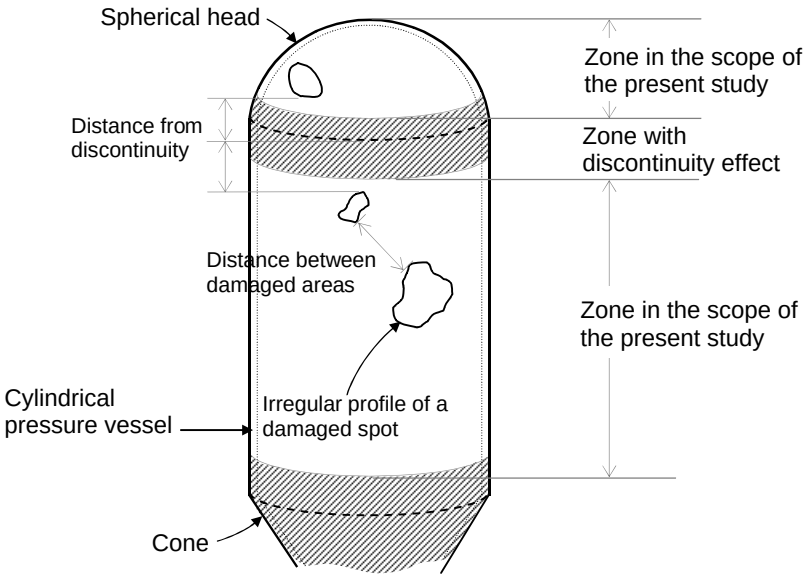

Figure 1.1 Damaged spots in cylindrical pressure vessel with spherical head

The behaviour of pressure vessels at limit state including the effect of membrane and bending actions is studied for different sizes of the damaged zone. The size of damage to be defined as “local” and “global” is specified by using shell theory and the interaction of damage in circumferential and axial directions of a cylinder is investigated. The minimum distance between a damaged spot and structural discontinuities and between multiple damages such that no interaction occurs are also studied. Although the

current study is focused on spherical and cylindrical pressure vessels, the recommended methods are shown to be applicable to pressure components of other shapes due to the shape-independence feature of the RSF used. An example of a pressure vessel with typical damages is shown in Figure 1.1.

1.3. OBJECTIVES OF THE RESEARCH

The objectives of the current research are to:

1. Develop Level 2 structural integrity assessment procedures to evaluate the remaining strength factors for pressure vessels (cylinders and spheres) containing corrosion damage or thermal hot spots using limit load multipliers. The recommendations will be validated using in-elastic finite element analysis.

2. Investigate the decay lengths for a variety of pressure component configurations based on elastic shell theory. The decay lengths will be used

    - to specify the size of damage that can be classified as “local” for different shell geometries and examine its implications.

    - to identify the reference volume participating in plastic action and use it to identify whether interaction occurs between multiple damage zones.

    - to investigate the effect of having different decay lengths along longitudinal and circumferential directions of cylinders.

3. Study the stretching and bulging effects due to damage and their interaction.

4. Estimate bulging displacement using the simplified theory.

5. Provide detailed procedures, examples and other aids (MATLAB and Spreadsheet files) useful for Level 2 assessment of damage due to corrosion and thermal hot spots in spherical and cylindrical pressure vessels.

1.4. SCOPE OF THE STUDY

The current study will focus on estimating remaining strength factors for pressure vessels with the shape of a sphere or a cylinder. The study of the fitness-for-service assessment methodology assumes elastic-plastic ductile material which is able to absorb significant deformation beyond the elastic limit without the danger of fracture. Strain hardening is assumed to be small. If the strain hardening is significant, a flow stress is used instead of the actual yield stress. This will accommodate different materials with differing tangent moduli.

Internal pressure is assumed to be the only significant load. The study will focus on pressure vessels with thermal hot spots and part-wall internal or external volumetric corrosion damage. Corrosion damage will be considered for vessels with the remaining thickness ratio (defined as the ratio of the corroded wall thickness to the nominal thickness) not less than 0.5. The discontinuity of corrosion damage is assumed to be tapered down smoothly and corrosion damage is considered as blunt or non-crack like flaws.

All pressure retaining items with pressure greater than 15 psig are designed to appropriate codes and standards and also need to be registered according to legal requirement. The components studied in the current work are assumed to be originally designed and constructed in accordance with a recognized code or standard. It is assumed that the operating condition of the vessel is not in the creep range of the material, i.e., temperatures for carbon steel do not exceed 750°F (400°C). Therefore, the assessments proposed in the current study are not valid for coal fired plants operating at a higher temperature environment. Thermal hot spots and corrosion damage are assumed to be remote from other major structural discontinuities, such as nozzles, or geometry changes such as cone-to-cylinder junctions (hatched region of Figure 1.1), or knuckles in hemispherical heads. It is also assumed that the corrosion and thermal hot spots do not significantly overlap with each other.

1.5. STRUCTURE OF THE THESIS

This thesis is organized in nine chapters. The first chapter introduces the background to the problem, objectives and scope of the study. The second chapter presents a review of literature. The theoretical aspects of plasticity, the classical lower and upper bound theorems and limit load multipliers are discussed. A brief outline of the existing Level 2 fitness-for-service evaluation methods for pressure vessels containing corrosion damage or thermal hot spots is provided. Shell theory which is fundamental to the study of decay length is reviewed.

Chapter 3 provides the principles for an improved lower bound limit load estimation called the m_α-method which is the basis of the current research. The concepts used in the m_α-method including theorem of nesting surfaces, leap-frogging of iterations to the limit state and Mura's extended variational formulation are discussed.

Chapter 4 studies the factors influencing the behavior of pressure vessels containing typical damage. Similarities and differences in the behavior of pressure components with corrosion damage and thermal hot spots are discussed. The general methodology of the proposed Level 2 Fitness-for-Service assessment based on the concept of reference volume is also presented.

In Chapter 5, finite element modeling details for the present study including geometry and constraints, material models and samples of typical mesh are given. Advantages and disadvantages of different element types used in this research are also discussed.

Chapter 6 discusses in detail decay length estimation for spherical and cylindrical shells using elastic theory. Comparison of decay lengths for different shell shapes and application of decay lengths to the current research is discussed.

Chapters 7 and 8 discuss recommendations for remaining strength factors. Illustrative numerical examples are provided. The extent of local damage and interaction of damage is investigated. The threshold to dominance of membrane and bending effects for sphere and cylinder are also suggested using an approximate method. The recommended procedure is validated by Level 3 inelastic finite element analysis.

Chapter 9 includes summary of the current work, conclusions and recommendations for future work.

CHAPTER 2

LITERATURE REVIEW

This chapter reviews briefly the theoretical background in plasticity and limit analysis including limit load multipliers and estimations of remaining strength factor for pressure vessels. Theory of cylindrical shells and the more general theory of shells of surface of revolution are presented. These theories will be applied in the investigation of decay length. Literature regarding Fitness-for-Service assessments for pressure components containing corrosion and thermal hot spots from previous investigations and existing standards and procedures is reviewed and discussed.

2.1. PLASTICITY

Theory of plasticity is the basis for limit analysis in which the components or structures are assumed to reach a certain limiting plastic state of the material before failure. Plasticity is defined as the behavior of solid bodies where permanent deformation occurs under the action of external loads, whereas elasticity is the behavior of solid

bodies in which they return to the original shape when the external forces are removed (Mendelson, 1968).

2.1.1. Criteria for Yielding

The basic theory of yielding is well known (Beer and Johnston, 2002). The following is included for review purposes. When the stress is uniaxial, a yield point at which the material begins to deform plastically can be readily determined. However, when the material is subject to multiaxial stresses, *yield criteria* are used in deciding which combination of multiaxial stresses will cause yielding. The most common yield criteria for metal structures will be briefly discussed below.

(a) Tresca Criterion (Maximum Shear Stress Theory)

This theory assumes that yielding will occur when the maximum shear stress in multiaxial state of stress reaches the value of the maximum shear stress occurring under simple tension test. The maximum shear stress is equal to half the difference between the maximum and minimum principal stresses. For simple tension, only one principal stress exists and $\sigma_2 = \sigma_3 = 0$. If the principal stresses are σ_1, σ_2 and σ_3 ($\sigma_1 > \sigma_2 > \sigma_3$), the Tresca criterion then asserts that yielding will occur when

$$\left|\sigma_1 - \sigma_3\right| = \sigma_y \tag{2.1}$$

A plot for Tresca yield criterion for a 2D-stress state is shown in Figure 2.1a. The Tresca criterion is in fair agreement with experiments and is used to a considerable extent

by designers (Kachanov, 1971) since it is easy to apply and is slightly conservative compared to the von Mises criterion.

(b) Von Mises Criterion (Distortion Energy Theory)

Strain energy is energy stored in the material due to elastic deformation. This deformation can be viewed as a combination of volume change and angular distortion without volume change. The latter stores the shear strain energy or distortion energy, which has been shown to be a primary cause of failure. Detailed experiments showed that hydrostatic pressure has negligible effect on the yielding thereby indicating that the material in the plastic range can be considered as incompressible. This observation is used by von Mises criterion (and the maximum shear stress theory) to derive the yield function.

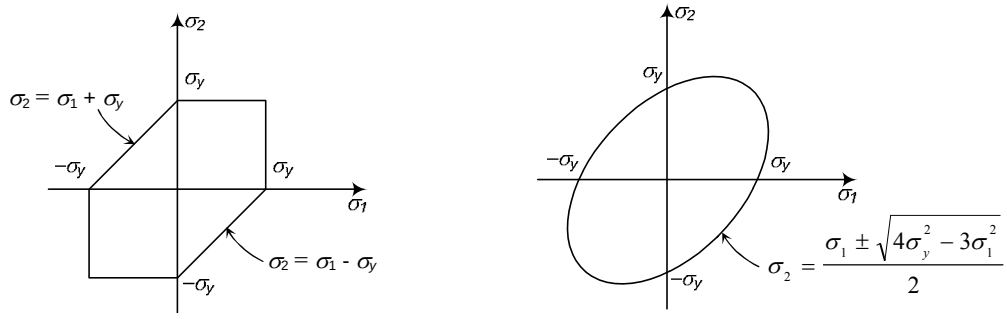

(a) (b)

Figure 2.1 Yield criteria in σ_1 - σ_2 plane (a) Tresca criterion (b) von-Mises criterion**.**

The distortion energy theory assumes that yielding begins when the distortion energy equals the distortion energy at yield in simple tension. The distortion energy can

be calculated as $U_d = \frac{1}{2G} J_2$, where, G is the shear modulus and J_2 is the second invariant of the deviatoric stress tensor which can be written in terms of principal stresses as $J_2 = \frac{1}{6}[(\sigma_1 - \sigma_2)^2 + (\sigma_1 - \sigma_3)^2 + (\sigma_3 - \sigma_2)^2]$. At the yield point in simple tension, $J_2 = \frac{1}{3}\sigma_y^2$. The yield condition therefore becomes

$$\frac{1}{2}[(\sigma_1 - \sigma_2)^2 + (\sigma_1 - \sigma_3)^2 + (\sigma_3 - \sigma_2)^2] = \sigma_y^2 \tag{2.2}$$

Equation (2.2) plots as an ellipse in the σ_1 - σ_2 plane (Figure 2.1b).

The von Mises yield criterion is widely used because it is smoothly differentiable and is without abrupt changes as is the case with Tresca criterion.

2.1.2. Yield Surface

In general, a yield criterion will depend on a complete three-dimensional state of stress at the point under consideration. For a material loaded to the initial yield, the relationship for a yield criterion can be expressed as,

$$f(\sigma_{ij}) = K \tag{2.3}$$

where, σ_{ij} is a stress tensor in three dimensional space, K is a known function (which can be selected as zero if desired). Equation (2.3) is called *yield function* and represents a hypersurface called *yield surface*. Any point on this surface represents a point at which yielding can begin.

In the *Haigh-Westergaard stress space* for principal stress $(\sigma_1, \sigma_2, \sigma_3)$ coordinate system, a line having equal angles with the coordinate axes (i.e., $\sigma_1 = \sigma_2 = \sigma_3 = \sigma_m$) corresponds to a hydrostatic stress state where the deviatoric stresses are equal to zero. The yield surface is plotted as a cylinder or prism along this line for von Mises or Tresca criterion, respectively. The intersection of this yield surface with any plane perpendicular to the centerline will produce a curve called the *yield locus* (Figure 2.2).

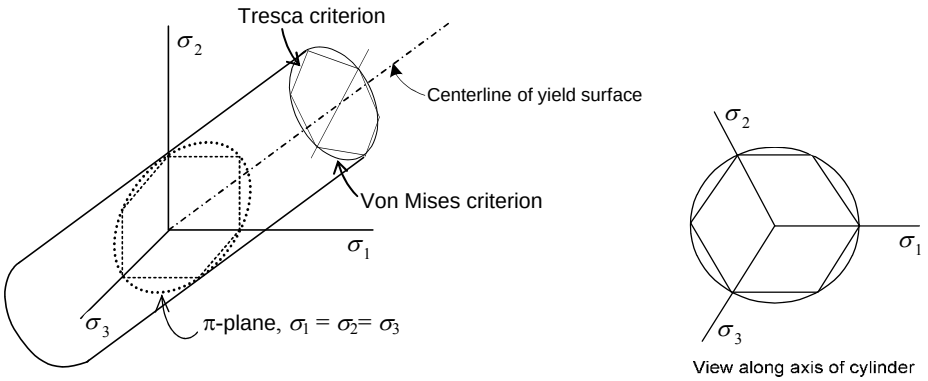

(a) (b)

Figure 2.2 (a) Yield surfaces and (b) Yield locus for Tresca and von Mises criteria

2.1.3. Theory of Plastic Flow

In the elastic range, the strains are linearly related to the stresses by Hooke's law and can be computed directly from the current state of stress regardless of how it was reached. The relationship will be nonlinear in the plastic range and can not be uniquely determined by the current stresses but depends on the whole history of loading. In order to determine the strains, it becomes necessary to compute the increments of plastic strain

throughout the loading history and then obtain the total strains by integration or summation. Yield criteria are used to prescribe the onset of plastic deformation. Further plastic strain increment is related to the state of stress through the flow rule.

The general form of the flow rule for ideal plasticity[1] can be written as

$$d\varepsilon_{ij}^{P} = d\lambda \frac{\partial f(\sigma_{ij})}{\partial \sigma_{ij}} \tag{2.4}$$

where, $d\varepsilon_{ij}^{P}$ is the plastic strain increment at any instant of loading and f is a yield function. The flow parameter $d\lambda$ is equal to zero when the material behaves elastically or $f(\sigma_{ij}) < K$ and has a positive value when plastic flow takes place or $f(\sigma_{ij}) = K$. The direction cosine of the normal to the yield surface is proportional to $\partial f / \partial \sigma_{ij}$. Therefore, Eq. (2.4) implies that the plastic flow vector is directed along the normal to the yield surface.

The *associated flow rule* corresponding to the von-Mises criterion can be expressed in the form

$$d\varepsilon_{ij}^{P} = d\lambda s_{ij} \tag{2.5}$$

where, s_{ij} is the deviatoric stress. Since plastic stress and strain are related by the infinitesimal strain *increments* and deviatoric stresses, it is convenient to divide the strains and strain rates by the increment of time and write the equilibrium equations. These equations remain homogeneous in time which acts only as a scaling parameter.

[1] plastic deformation without hardening

2.1.4. Drucker's Postulate

Consider an element that has an initial stress σ'_{ij} lying inside or on the current position of yielding surface Σ (point A in Figure 2.3). Let some external loading add stresses until a state of stress σ_{ij} on the yield surface is reached (point B). Only elastic changes have taken place so far. Next, an infinitesimal stress increment $d\sigma_{ij}$ (which produces small plastic strain increments $d\varepsilon_{ij}^{P}$ as well as elastic increments) is applied. The state of stress is now changed from point B to point C. Let this external loading be applied and then removed. The state of stress is returned to σ'_{ij} along an elastic path $\mathrm{C} \rightarrow \mathrm{A}$. The changes are assumed to take place sufficiently slowly for the process to be regarded as isothermal. The total work done over the cycle is

$$\delta W = \left(\sigma_{ij} - \sigma'_{ij}\right) d\varepsilon_{ij}^{P} + d\sigma_{ij} d\varepsilon_{ij}^{P} \tag{2.6}$$

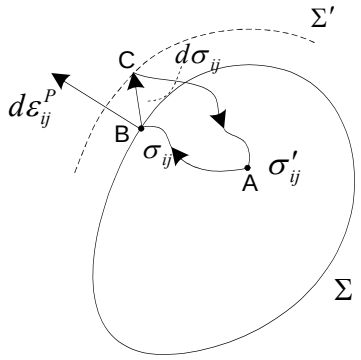

Figure 2.3 Loading surfaces (Hill, 1950).

Drucker's postulate states that the prolongation of plastic deformation of a hardening medium requires additional work done or $\delta W > 0$. The work done will be

equal to zero only for purely elastic changes. The second term in Eq. (2.6) corresponds to strain-hardening and has positive value. This term is equal to zero in the case of perfectly plastic material.

Since the magnitude of $\sigma_{ij} - \sigma'_{ij}$ can always be made larger than that of $d\sigma_{ij}$, it follows that

$$\left(\sigma_{ij} - \sigma'_{ij}\right) d\varepsilon_{ij}^{P} > 0 \tag{2.7}$$

From inequality (2.7), the scalar product of the vector of additional stresses $\sigma_{ij} - \sigma'_{ij}$ (vector AB) and the vector $d\varepsilon_{ij}^{P}$ is positive. This means that these vectors always generate an acute angle. Consequently, we deduce the convexity of the yielding surface with respect to the origin of the vector space. This will be used in explaining Mura's extended variational principle in plasticity which is the basis of the m_α-method.

2.2. LIMIT ANALYSIS

Complete plastic analyses of practical engineering structures are generally difficult and time-consuming. If the failure prevention of a structure is the main interest of the analysis, it is justified to concentrate on the collapse state of the structure or the "limit state." In classical limit analysis, material nonlinearity is included by assuming the material behavior to be perfectly plastic while geometric nonlinearity is ignored. The bounding theorems are used to provide lower and upper estimates of the exact limit load.

2.2.1. Classical Upper and Lower Bound Theorems

The *upper bound theorem* states that if an estimate of the limit load of a structure is made by equating the internal rate of dissipation of energy to the rate of external work for any strain and displacement field which corresponds to a postulated mechanism of deformation, the limit load estimate will be either too high or correct (Calladine, 2000).

Applying the principle of virtual work, the upper-bound theorem may be expressed as

$$\int_{S_T} T_i \dot{u}_i dS \leq \int_{V_T} \dot{D} dV \tag{2.8}$$

where, T_i are the tractions acting on the surface S_T, $\dot{u}_i$ are the postulated displacement rates, $\dot{D}$ are the corresponding increment rates of plastic dissipation per unit volume, and V_T is the total volume.

The *lower bound theorem* states that if any stress distribution throughout the component or structure can be found, which is everywhere in equilibrium internally, balances the external loads and at the same time does not violate the yield condition, then the corresponding applied loads will be less than, or at most equal to, the exact limit load and will be carried safely by the structure.

The upper bound limit analysis can be viewed as the "geometry" approach in which the mode of deformation and energy balance are considered and a limit load is arrived at without considering the equilibriums equations. In contrast, the lower bound limit analysis is the "equilibrium" approach in which the equilibrium equations and yield

condition are satisfied and an estimate of collapse load is obtained without considering the mode of deformation (Calladine, 2000).

2.2.2. Admissible multipliers

Consider an arbitrary structure with volume V and surface S disjointed in two parts S_T and S_v, i.e., $S = S_T \cup S_v$. The body is subjected to a surface force traction T_i prescribed on S_T and geometric constraints over the remainder of the total surface S_v. Let m be a multiplier and consider the structure under the loads mT_i as m is slowly increased from zero. When the value of m is sufficiently small, the structure behaves elastically. As m increases, a part in the body reaches the plastic state. The plastic region spreads further as the multiplier increases. The safety factor s is defined as the smallest value of m for which the structure can undergo an increase in deformation without increase in load. The set of loads corresponding to the impending plastic flow is called the limit load of the structure. Thus, the safety factor is the ratio of the limit load to the actual load (T_i).

(a) Kinematically Admissible Multipliers, m^*

A velocity field, v_i is called *kinematically admissible* if it satisfies velocity (or displacement) constraints and if the total external rate of work done by the actual loads on this velocity field is positive. Therefore, the conditions for a kinematically admissible velocity field are as following;

$$\delta_{ij} v_{i,j} = 0 \qquad \text{in } V$$

$$v_i = 0 \quad \text{on } S_v \qquad (2.9)$$

$$\int_{S_T} T_i v_i dS > 0$$

where, δ_{ij} is Kronecker delta. Note that the first of Eqs. (2.9) is due to incompressibility condition.

Let the generalized strain-rate vector associated with a given kinematically admissible velocity field be designated by $\dot{\varepsilon}^*$, where the asterisk is used to indicate that this is not necessarily the actual strain-rate vector but one that is kinematically admissible. If the von Mises yield criterion is applied, plastic strains occur when the deviatoric stresses are on the yield surface or $\frac{1}{2} s_{ij} s_{ij} = k^2$, where, k is the yield limit in pure shear. The kinematically admissible multiplier m^* is then defined by the ratio of the internal and external energy dissipation as

$$m^* = k \int_V \left(2\dot{\varepsilon}_{ij}^* \dot{\varepsilon}_{ij}^*\right)^{1/2} dV \Big/ \int_{s_T} T_i v_i^* dS, \qquad (2.10)$$

where, $\dot{\varepsilon}_{ij}^* = (v_{i,j}^* + v_{j,i}^*)/2$ in V, and constraint conditions from Eqs. (2.10) are applied.

(b) Statically Admissible Multiplier, m^0

A *statically admissible* stress field, σ_{ij}^0 is defined as one which is in internal equilibrium with the external load $m^0 T_i$, and nowhere exceeds the yield limit. The multiplier m^0 corresponding to such a stress field is called a *statically admissible multiplier*. Therefore,

$$\begin{aligned} \sigma^0_{ij,j} &= 0 && \text{in } V, \\ \sigma^0_{ij} n_j &= m^0 T_i && \text{on } S_T, \\ f(s^0_{ij}) &= \tfrac{1}{2} s^0_{ij} s^0_{ij} - k^2 \le 0 && \text{in } V, \end{aligned} \tag{2.11}$$

where, s^0_{ij} is the statically admissible deviatoric stress ($s^0_{ij} = \sigma^0_{ij} - \delta_{ij}\sigma^0$), $\sigma^0 = \sigma^0_{kk}/3$. Note that the first and second of Eqs. (2.11) are equilibrium equations and the third of Eqs. (2.11) is the yield function.

These two classical multipliers are the basis of other improved lower bound multipliers applied in the current research as will be further explained in Chapter 3.

2.3. THEORY OF SHELLS

In the present research, pressure vessels of practical shapes, such as cylinder and sphere will be studied. The volume that participates in localized plastic collapse due to corrosion damage or thermal hot spot will be investigated. For this, shell theory needs to be used. Basic shell theory is well known (Timoshenko, 1970; Ugural, 1999) and it is included for review purposes. Solutions for a circular cylindrical shell under arbitrary load will be reviewed first while a more general theory of shell of surface of revolution is subsequently discussed.

2.3.1. Circular Cylindrical Shell

Kraus (1967), among several others, derived the governing equations for circular cylindrical shells with bending resistance under arbitrary loads. The governing equations are derived from the equations of static equilibrium; the relationships between strains, changes of curvature and the displacements; and the relationships between the stress resultants and the strains.

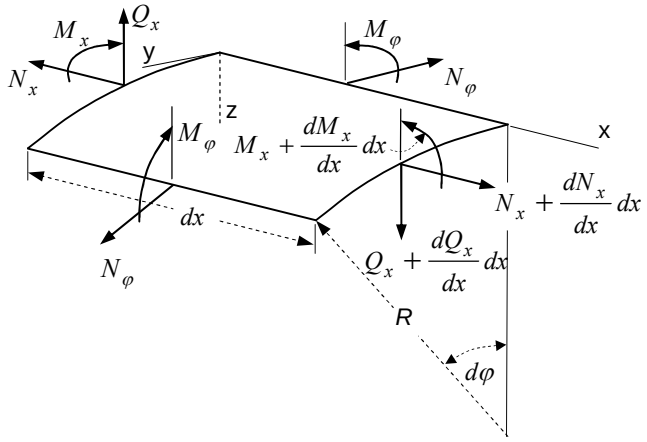

Figure 2.4 Forces and moments acting on a cylindrical shell element.

If the shells are thin, the transverse shearing force makes a negligible contribution to the equilibrium of forces in the circumferential direction. The equations of equilibrium of the cylindrical shell (Figure 2.4) are,

$$\frac{\partial N_x}{\partial x} + \frac{\partial N_{x\varphi}}{\partial \varphi} + q_x = 0, \qquad \frac{\partial N_{\varphi x}}{\partial x} + \frac{\partial N_\varphi}{\partial \varphi} + q_\varphi = 0$$

$$\frac{\partial^2 M_x}{\partial x^2} + 2\frac{\partial^2 M_{x\varphi}}{\partial x \partial \varphi} + \frac{\partial^2 M_\varphi}{\partial \varphi^2} - \frac{N_\varphi}{R} - q_z = 0 \tag{2.12}$$

where, N are the normal forces per unit length of sections, q is the intensity of a continuous distributed load, M are the moments per unit length of sections and R is the radius of the cylinder.

If the shell is assumed to have small curvature (shallow shell), the stretching displacement u_s has negligible effect on the changes of curvature and twist. Shallow shells are shells in which the slope of its middle surface (described by $z = z(\mathbf{x}, y)$) is very small and satisfies the requirements $(\partial z/\partial x)^2 \ll 1$ and $(\partial z/\partial y)^2 \ll 1$. For circular cylindrical shells, these conditions are satisfied automatically since $\partial z/\partial x = 0$ and $\partial z/\partial y = r - r\cos(d\varphi) \approx 0$. The relationship between the strains (ε), changes in curvature (κ), relative angle of twist (τ) and the displacements (u_x, u_s and w) as shown in Figure 2.5 can be expressed as

$$\varepsilon_x = \frac{\partial u_x}{\partial x}, \quad \varepsilon_s = \frac{\partial u_s}{\partial s} + \frac{w}{R}, \quad \gamma_{xs} = \frac{\partial u_s}{\partial x} + \frac{\partial u_x}{\partial s},$$

$$\kappa_x = -\frac{\partial^2 w}{\partial x^2}, \quad \kappa_s = -\frac{\partial^2 w}{\partial s^2}, \quad \tau = -2\frac{\partial^2 w}{\partial x \partial s}. \tag{2.13}$$

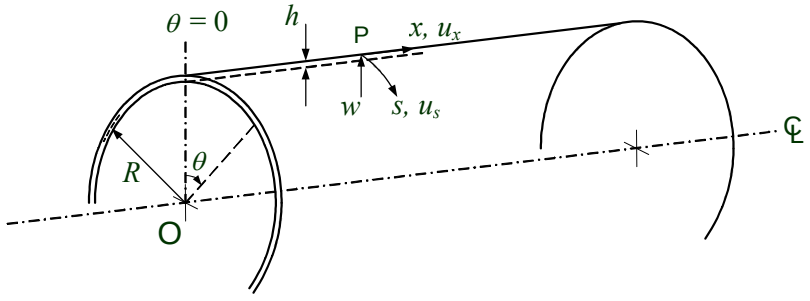

Figure 2.5 Thin Cylindrical Shell.

The behavior of a thin cylindrical shell of small curvature is similar to that of a thin plate except for the presence of N_s/R in the third equilibrium equation and *w/R* in the definition of the circumferential normal strain. Finally, the stress resultants and stress couples are related to the strains and changes of curvature as

$$N_x = K[\varepsilon_x + \nu\varepsilon_s], \quad N_s = K[\varepsilon_s + \nu\varepsilon_x], \quad N_{xs} = N_{sx} = Gh\gamma_{xs}$$

$$M_x = D[\kappa_x + \nu\kappa_s], \quad M_s = D[\kappa_s + \nu\kappa_x], \quad M_{xs} = M_{sx} = Gh^3\tau/12 \tag{2.14}$$

where, $K = Eh/(1-\nu^2)$ and the flexural rigidity of shell, $D = Eh^3/12(1-\nu^2)$.

The governing equations of the cylindrical shell that relate the displacements and surface loadings can be accomplished by substitution of Eqs. (2.13) and (2.14) into Eq. (2.12). The governing equations have the form

$$\frac{\partial^2 u_x}{\partial x^2} + \frac{1-\nu}{2}\frac{\partial^2 u_x}{\partial s^2} + \frac{1+\nu}{2}\frac{\partial^2 u_s}{\partial x \partial s} + \frac{\nu}{R}\frac{\partial w}{\partial x} = P_x$$

$$\frac{1-\nu}{2}\frac{\partial^2 u_s}{\partial x^2} + \frac{1-\nu}{2}\frac{\partial^2 u_s}{\partial s^2} + \frac{1+\nu}{2}\frac{\partial^2 u_x}{\partial x \partial s} + \frac{\partial}{\partial s}\left(\frac{w}{R}\right) = P_s \tag{2.15}$$

$$\frac{h^2}{12}\nabla^4 w + \frac{1}{R}\left(\frac{w}{R} + \frac{\partial u_s}{\partial s} + \nu\frac{\partial u_x}{\partial x}\right) = P_z$$

where, $P_x = -\frac{(1-\nu^2)}{Eh}q_x$, $P_s = -\frac{(1-\nu^2)}{Eh}q_s$, $P_z = -\frac{(1-\nu^2)}{Eh}q$, and $\nabla^2 = \frac{\partial^2}{\partial x^2} + \frac{\partial^2}{\partial s^2}$.

The solutions of Eqs. (2.15) can be decomposed into particular and complementary components corresponding to the contributions from the distributed

surface loadings and edge loadings, respectively. Therefore, only the complementary component is of interest in the determination of decay length as mentioned in Chapter 1.

Donnell (1933) manipulated Eqs. (2.15) to achieve a decoupled eighth-order differential equation for the radial displacement *w*. In the absence of surface loadings, Donnell's equations in a non-dimensional coordinate system are

$$\overline{\nabla}^8 \overline{w} + 4k^4 \left(\frac{\partial^4 \overline{w}}{\partial \theta^4} \right) = 0 \tag{2.16a}$$

$$\overline{\nabla}^4 \overline{v} = (2+\nu)\left(\frac{\partial^3 \overline{w}}{\partial \theta^2 \partial \varphi} \right) + \left(\frac{\partial^3 \overline{w}}{\partial \varphi^3} \right) \tag{2.16b}$$

$$\overline{\nabla}^4 \overline{u} = \nu \left(\frac{\partial^3 \overline{w}}{\partial \theta^3} \right) - \left(\frac{\partial^3 \overline{w}}{\partial \theta \, \partial \varphi^2} \right) \tag{2.16c}$$

where, $\overline{\nabla}^2 = \frac{\partial^2}{\partial \theta^2} + \frac{\partial^2}{\partial \varphi^2}$ and the non-dimensional variables are defined as $\theta = \frac{x}{R}$, $\varphi = \frac{s}{R}$, $\overline{v} = \frac{u_s^c}{R}$, $\overline{u} = \frac{u_x^c}{R}$, $\overline{w} = \frac{w^c}{R}$ and $4k^4 = 12\left(1-\nu^2\right)\left(R/h\right)^2$. The superscript *c* indicates complementary solution. For any known mechanical or thermal loading Eq. (2.16a) can be solved for *w* and then u_x and u_s can be obtained as the solutions of (2.16b) and (2.16c).

In the case of cylindrical shell subjected to axisymmetric longitudinal bending, the displacements are independent of the circumferential coordinate *s* and the last of Eq. (2.15) can be reduced to

$$\frac{d^4 w}{dx^4} + 4\beta^4 w = \frac{P_z}{D} \qquad \text{where, } \beta^4 = \frac{3(1-\nu^2)}{R^2 h^2}. \tag{2.17}$$

Equations (2.16) will be used in Chapter 6 to calculate the decay length for circular cylindrical shell in the circumferential direction and Eq. (2.17) will be used to determine decay length in the longitudinal direction.

2.3.2. Shells Having the Form of a Surface of Revolution

A brief review of the governing equations for a more general case of shells of surface of revolution is presented in this section. Complete details in the derivation are provided by Timoshenko (1970) as well as others, such as Kraus (1967), Ugural (1999) and Lukasiewicz (1979).

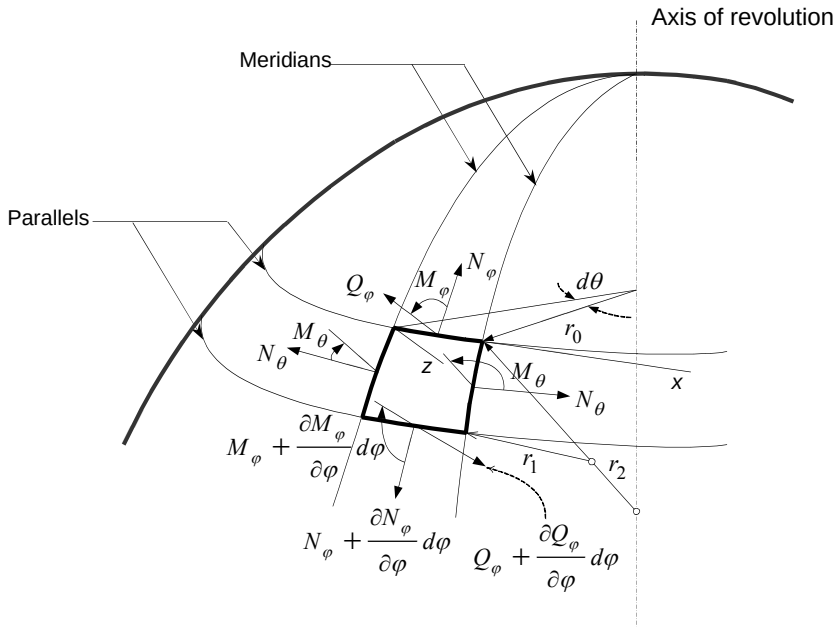

Figure 2.6 Shells having the form of a surface of revolution (Timoshenko, 1970).

Shells having the form of surfaces of revolution find extensive application in various kinds of containers, tanks, and domes. A surface of revolution is obtained by

rotation of a plane curve about an axis lying in the plane of the curve. This curve is called the "meridian" and its plane is a meridian plane. The conditions of equilibrium of an element of the shell bounded by two adjacent meridian planes and two sections perpendicular to the meridians are considered (Figure 2.6).

Due to the symmetry, only normal stresses will act on the two sides of the element that are in the meridian planes. The stresses can be reduced to the resultant force $N_\theta r_1 d\varphi$ and resultant moment $M_\theta r_1 d\varphi$, which are independent of the angle θ. The external load acting upon the element can be resolved into two components $P_y r_1 r_2 \sin\varphi \; d\varphi \; d\theta$ and $P_z r_1 r_2 \sin\varphi \; d\varphi \; d\theta$ tangent to the meridians and normal to the shell, respectively. If the change of curvature is neglected, three equations of equilibrium can be expressed as

$$\frac{d}{d\varphi}(N_\varphi r_0) - N_\theta r_1 \cos\varphi - r_0 Q_\varphi + r_0 r_1 q_y = 0$$

$$N_\varphi r_0 - N_\theta r_1 \sin\varphi - \frac{d(Q_\varphi r_0)}{d\varphi} + q_z r_1 r_0 = 0 \qquad (2.18)$$

$$\frac{d}{d\varphi}(M_\varphi r_0) - M_\theta r_1 \cos\varphi - Q_\varphi r_1 r_0 = 0$$

Equations (2.18) contain five unknown quantities, three resultant forces (N_φ, N_θ, and Q_φ) and two resultant moments (M_θ and M_φ). The number of unknowns can be reduced to three by expressing the membrane forces and the moments in terms of the displacement components *v* and *w* using Hooke's law as,

$$N_\varphi = \frac{Eh}{1-\nu^2}\left[\frac{1}{r_1}\left(\frac{dv}{d\varphi}-w\right)+\frac{\nu}{r_2}\left(v\cot\varphi-w\right)\right]$$

$$N_\theta = \frac{Eh}{1-\nu^2}\left[\frac{1}{r_2}\left(v\cot\varphi-w\right)+\frac{\nu}{r_1}\left(\frac{dv}{d\varphi}-w\right)\right] \qquad (2.19)$$

$$M_\varphi = -D\left[\frac{1}{r_1}\frac{d}{d\varphi}\left(\frac{v}{r_1}+\frac{dw}{r_1 d\varphi}\right)+\frac{\nu}{r_2}\left(\frac{v}{r_1}+\frac{dw}{r_1 d\varphi}\right)\cot\varphi\right]$$

$$M_\theta = -D\left[\frac{1}{r_2}\left(\frac{v}{r_1}+\frac{dw}{r_1 d\varphi}\right)\cot\varphi+\frac{\nu}{r_1}\frac{d}{d\varphi}\left(\frac{v}{r_1}+\frac{dw}{r_1 d\varphi}\right)\right]$$

Three equations with three unknown quantities v, w, and Q_φ can be obtained by substitution of expressions (2.19) into Eqs. (2.18). By using the third of Eqs. (2.18) the shearing force Q_φ can be eliminated and the three equations reduced to two equations of the second order with the unknowns v and w. Timoshenko (1970) introduced the use of two new variables, the angle of rotation of a tangent to a meridian V and the quantity U, to further simplify the equations,

$$V = \frac{1}{r_1}\left(v+\frac{dw}{d\varphi}\right) \quad \text{and} \quad U = r_2 Q_\varphi \qquad (2.20)$$

Consider the equilibrium of the portion of the shell above the parallel circle defined by the angle φ. Assuming there is no load applied to the shell, this equation gives

$$2\pi\ r_0 N_\varphi \sin\varphi + 2\pi\ r_0 Q_\varphi \cos\varphi\ = 0 \qquad (2.21)$$

Therefore,

$$N_\varphi = -Q_\varphi \cot\varphi = -\frac{1}{r_2} U \cot\varphi \tag{2.22}$$

Substituting N_φ from Eq. (2.22) into the second of Eqs. (2.18), for $r_0 = r_2 \sin\varphi$ and $Z = 0$, we obtain

$$N_\theta = -\frac{1}{r_1 \sin\varphi}\left[N_\varphi r_0 + \frac{d}{d\varphi}(Q_\varphi r_0) \right] = -\frac{1}{r_1}\frac{dU}{d\varphi} \tag{2.23}$$

From the first two equations of Eqs. (2.18), expressions for N_φ and N_θ in (2.19), and Eqs. (2.22) and (2.23), the equation relating U and V is

$$\frac{r_2}{r_1}\frac{d^2U}{d\varphi^2} + \frac{1}{r_1}\left[\frac{d}{d\varphi}\left(\frac{r_2}{r_1}\right) + \frac{r_2}{r_1}\cot\varphi - \frac{r_2}{r_1 h}\frac{dh}{d\varphi}\right]\frac{dU}{d\varphi} - \frac{1}{r_1}\left[\frac{r_1}{r_2}\cot^2\varphi - \nu - \frac{\nu}{h}\frac{dh}{d\varphi}\cot\varphi\right]U = EhV \tag{2.24}$$

By substituting expressions of M_φ and M_θ in (2.19) into the third of Eqs. (2.18), the second equation for U and V is obtained as

$$\frac{r_2}{r_1}\frac{d^2V}{d\varphi^2} + \frac{1}{r_1}\left[\frac{d}{d\varphi}\left(\frac{r_2}{r_1}\right) + \frac{r_2}{r_1}\cot\varphi + 3\frac{r_2}{r_1 h}\frac{dh}{d\varphi}\right]\frac{dV}{d\varphi} - \frac{1}{r_1}\left[\frac{r_1}{r_2}\cot^2\varphi - \nu - \frac{3\nu}{h}\frac{dh}{d\varphi}\cot\varphi\right]V = -\frac{U}{D} \tag{2.25}$$

If the thickness of the shell is constant, the terms containing a factor $dh/d\varphi$ vanish. Introducing the notation

$$L(\cdots) = \frac{r_2}{r_1}\frac{d^2(\cdots)}{d\varphi^2} + \frac{1}{r_2}\left[\frac{d}{d\varphi}\left(\frac{r_2}{r_1}\right) + \frac{r_2}{r_1}\cot\varphi\right]\frac{d(\cdots)}{d\varphi} - \frac{r_1\cot^2\varphi}{r_2 r_1}(\cdots) \tag{2.26}$$

Eqs. (2.24) and (2.25) simplified to two simultaneous differential equations of the second order as

$$L(U) + \frac{\nu}{r_1} U = EhV$$
$$L(V) - \frac{\nu}{r_1} V = -\frac{U}{D} \tag{2.27}$$

The application of these differential equations to determine a decay length in spherical shells will be further explained in Chapter 6.

2.4. FITNESS-FOR-SERVICE

Fitness-for-service assessments are quantitative engineering evaluations that are performed to demonstrate the structural integrity of an in-service component containing a flaw or damage. Three levels of assessment are presented by API 579 in Section 2.4.1 as given below:

Level 1 – The assessment procedures included in this level are intended to provide conservative screening criteria that can be utilized with a minimum amount of inspection or component information. Level 1 assessments may be performed by either plant inspection or engineering personnel.

Level 2 – The assessment procedures included in this level are intended to provide a more detailed evaluation that produces results that are more precise than those from a Level 1 assessment. In a Level 2 Assessment, inspection information similar to that

required for a Level 1 assessment are needed; however, more detailed calculations are used in the evaluation. Level 2 assessments would typically be conducted by plant engineers, or engineering specialists experienced and knowledgeable in performing FFS assessments.

Level 3 – The assessment procedures included in this level are intended to provide the most detailed evaluation which produces results that are more precise than those from a Level 2 assessment. In a Level 3 Assessment the most detailed inspection and component information is typically required, and the recommended analysis is based on numerical techniques such as the finite element method. A Level 3 analysis is primarily intended for use by engineering specialists experienced and knowledgeable in performing FFS assessments.

As mentioned previously, the current study aims at deriving Level 2 methods for FFS assessment of pressure vessels with corrosion or hotspot damage.

This following presents a summary of the primary investigations that have been reported in the literature on failure due to corrosion damage and thermal hot spots. Numerous models have been proposed for evaluation of corroded components. Several standards have incorporated the assessment methodology for continuing service of components containing corrosion spots. A vast majority of these studies are limited to analysis and assessment of pipes and sometimes cylindrical vessels.

2.4.1. FFS Assessment for Thermal Hot Spots

Although thermal hot spot is known to be one of the common types of damage that occurs in ageing pressure vessels, the studies of hot spot FFS evaluation procedures are meager compared to other damages such as crack-like flaws. The few studies that have focused on hot spots are mostly restricted to assessment of cylindrical shells.

Du Preez (1995) investigated the characteristics of hot spots that would cause cyclic plasticity or ratcheting in particular vessels of conical and cylindrical shape. It was concluded that ratcheting can be present in the cases of large hot spot size and high temperature difference between hot spot and average temperature. It was suggested that a condition which is within the shakedown regime should be selected as a basis for continuous operation and hot spots which fall in the cyclic plasticity and ratcheting regimes are only acceptable with a restriction on the total accumulated strain during the lifetime of the vessel.

Radakovic, Zhao and Lucas (2004) performed heat transfer and stress analysis to identify conditions that can lead to hot spots on the shell and potential failure of the shell plate in blast furnace bustle pipe. It was concluded that thinning of the shell due to corrosion combined with high shell temperature has contributed to cracking and bulging of the shell plate.

Seshadri (2004) proposed a Level 2 FFS assessment for hot spots based on elastic analysis. The localized effect of discontinuities on the cylindrical shell is discussed and the concept of reference volume is introduced as the “kinematically active” portion that

participates in plastic action. The reference volume is defined by using a characteristic length called "decay length" of a cylinder. The decay length is the distance from the applied force to the point where the effect of the force is almost completely dissipated and becomes negligible. In order to determine a decay length in the circumferential direction of a cylinder, the effects of line load applied along the generator of cylindrical shells is used. A decay length in longitudinal direction can be determined by using the solution for differential equations of cylindrical shell subjected to an axisymmetric loading.

The remaining strength factor is suggested based on the m_α -multiplier. In order to verify the evaluation assessment, inelastic finite element analyses are carried out on the basis that there is post-yield strain hardening in the material with the plastic modulus of 3447 MPa (500 ksi) -compared to E = 207 GPa (30×10^3 ksi), and the maximum strain is limited to 1%. It is concluded that the recommended RSF calculated using m_α -multiplier provides close lower bound approximation compared with a nonlinear finite element model. This and associated work is used and extended in the present research. The relevant theory using m_α-method, etc., is summarized in the next chapter.

It may be noted that the plastic tangent modulus used in the above study is somewhat high and is perhaps not the most preferred. In that sense, the numerical data presented in (Seshadri, 2004) can be improved upon. However, the proposed ideas are still very useful for the simple and yet practical Level 2 assessment of RSF. The present research includes the use of decay lengths and other intuitive concepts meshed with variational principles. Thus, the application of reference volume and the estimation of

decay lengths for cylindrical shells will be explored further in the present research. The RSF evaluation procedures discussed by Seshadri (2004) will be the basis of the recommended RSF for the current work.

At the current stage, there is no design standard for hot spot evaluation in pressure vessels. Procedures and rules for hot spot evaluation are currently being developed to be added to section 14 of API 579 by considering fatigue and creep damages (Osage, 1997). It should also be noted in addition that the entire API 579 document is being re-developed in conjunction with the American Society of Mechanical Engineers (ASME) to provide a common document as a Standard issued by both societies (Furtado and May, 2004).

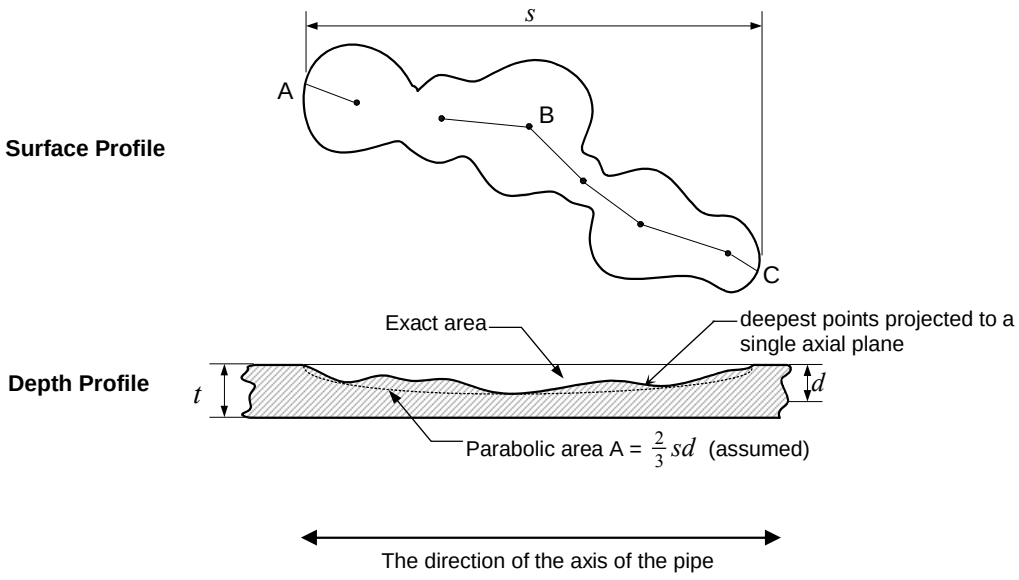

Figure 2.7 Metal loss and analysis parameters used in the effective area method

2.4.2. FFS Assessment for Corrosion Damage in Cylindrical Shells

The study of pressure vessels containing blunt metal-loss defects or corrosion damage, usually considered as a locally thinned area (LTA), has been far more elaborate compared to that for thermal hot spot problems. However, most studies are on the evaluation of piping and cylindrical vessels. The most widely used criteria in North America for the assessment of corroded pipes called "effective area methods" include ASME B31G (ASME/ANSI, 1984), Modified B31G and PRC RSTRENG (Kiefner and Vieth, 1989). The standard for conducting FFS assessments for pressurized components in oil and gas sector is API 579 (API, 2000) in which the procedures are based on ASME B31G and the RSTRENG criteria.

Note that for crack-like defects and defects caused by stress corrosion cracking (SCC), the failure mechanism is based on material toughness and the evaluation procedures are different. SCC is cracking due to a process involving conjoint corrosion and straining of a metal due to residual or applied stress (Arup and Parkins, 1979). This requires specific combinations of metal and environment such as chloride cracking of stainless steel or hydrogen embrittlement of high strength steels (Cottis, 2000). This type of corrosion is currently dealt with by Level 3 assessment according to API 579 and is not of direct interest in the current research.

The effective area method was first developed from a semi-empirical fracture mechanics relationship by Maxey, et al. (1972). The method assumes that the strength loss due to corrosion is proportional to the amount of metal loss measured axially along

the pipe (*s*). To accommodate for the irregular corrosion profiles, the profile of the flaw is measured and the deepest points (path A-B-C) are projected to a single axial plane for analysis as shown in Figure 2.7.

The remaining strength factor is based on a Dugdale plastic-zone-size model and a "Folias" factor. Folias factor is a bulging stress magnification factor used in through-wall crack in pressurized cylinder (Folias, 1969). An empirical flaw-depth-to-pipe-thickness relationship is used to modify the Folias factor to account for part-through wall effects based on "effective" cross sectional area. This method assumes that the flaw fails when the stress in the flaw reaches the flow stress, σ_{flow}. The nominal pipe wall hoop stress at failure in the flaw is given by

$$\sigma_{fail} = \sigma_{flow}\left[\frac{1 - A/A_o}{1 - A/A_o\,(M^{-1})}\right] \tag{2.28}$$

where, A is the corroded area in the cross section, A_o is the original cross sectional area, M is Folias factor. The term in the bracket is proposed as the effects from effective area for a surface flaw.

(a) ASME B31G criterion

The expression for nominal hoop stress at failure σ_{fail} of a flaw used by ASME B31G is

$$\sigma_{fail} = 1.1\sigma_y RSF\,; \qquad RSF = \left[\frac{1 - (2/3)(d/t)}{1 - (2/3)(d/t)(M^{-1})}\right] \tag{2.29}$$

where, σ_y is the yield stress, d is the maximum depth of corrosion and t is the pipe thickness. The Folia factor, used in this assessment is a function of the corrosion axial length s, the pipe diameter D, and t as $M = \sqrt{1 + 0.8\left(\frac{s^2}{Dt}\right)}$.

It can be observed by comparison of Eq. (2.28) and (2.29) that this method assumes that flow stress $\sigma_{flow} = 1.1\sigma_y$. The flow stress used in this method is conservative when compared with yield stress for cylinders calculated using von-Mises criterion with elastic-perfectly plastic model which is equal to $2/\sqrt{3}\,\sigma_y$ or $1.15\,\sigma_y$. The corrosion flaw is assumed to have a parabolic shape and hence parameter $A = 2/3sd$ and $A_0 = st$. The two-term form of the Folias bulging factor is used to simplify the calculation. However, this two-term factor is only applicable to flaws with $s/\sqrt{Rt} < 6.3$ and $d/t \geq 0.175$. Beyond this length, the flaw depth is limited to 10 percent of the wall thickness. This limitation results in a discontinuity in the flaw assessment criterion that contributes frequently to excessively conservative evaluations of LTAs in pipelines.

(b) Modified ASME B31G criterion

The Modified B31G criterion attempts to reduce B31G simplifying assumptions and associated conservatism. The Modified B31G criterion is given by

$$\sigma_{fail} = \left(\sigma_y + 10{,}000\ \text{psi}\right) \cdot RSF\ ; \qquad RSF = \left[\frac{1 - 0.85(d/t)}{1 - 0.85(d/t)\left(M^{-1}\right)}\right] \tag{2.30}$$

where, $M = \sqrt{1 + 0.6275\left(\frac{s^2}{Dt}\right) - 0.003375\left(\frac{s^2}{Dt}\right)^2}$ for $\frac{s^2}{Dt} \le 50$ and $M = 0.032\frac{s^2}{Dt}$ for $\frac{s^2}{Dt} > 50$.

The flow stress used in Modified B31G is less conservative than B31G. For high strength pipeline material such as API 5L X80, the flow stress calculated by using Eq. (2.30) is $1.125\sigma_y$. For lower strength material such as API 5L grade A, with a yield stress of 30000 psi, the flow stress becomes $1.333\sigma_y$. This assumes that the material attains significant amount of strain hardening after yield. An empirical fit factor of 0.85 is also used in this criterion instead of the "2/3" area factor resulting from the assumed parabolic shape. In addition, the more accurate 3-term expression for the Folias bulging factor is utilized and hence the discontinuity that exists in B31G is eliminated.

(c) RSTRENG

The more accurate computation of the effective area is developed by applying more detailed corrosion profiles with the help of PC-based software known as RSTRENG.

RSTRENG uses the less conservative definition of flow stress and the 3-term Folias bulging factor described in the Modified B31G. The equivalent axial profile can be made by plotting points along the deepest path of the contour map, often referred to as the critical thickness profiles (CTP) or "river bottom" of the flaw (Figure 2.8). RSTRENG computes the failure pressure based upon all possible flaw geometries along the river

bottom and reports the lowest as its result. Although RSTRENG provides more accurate results, difficulties can often arise because of a large amount of information must be collected.

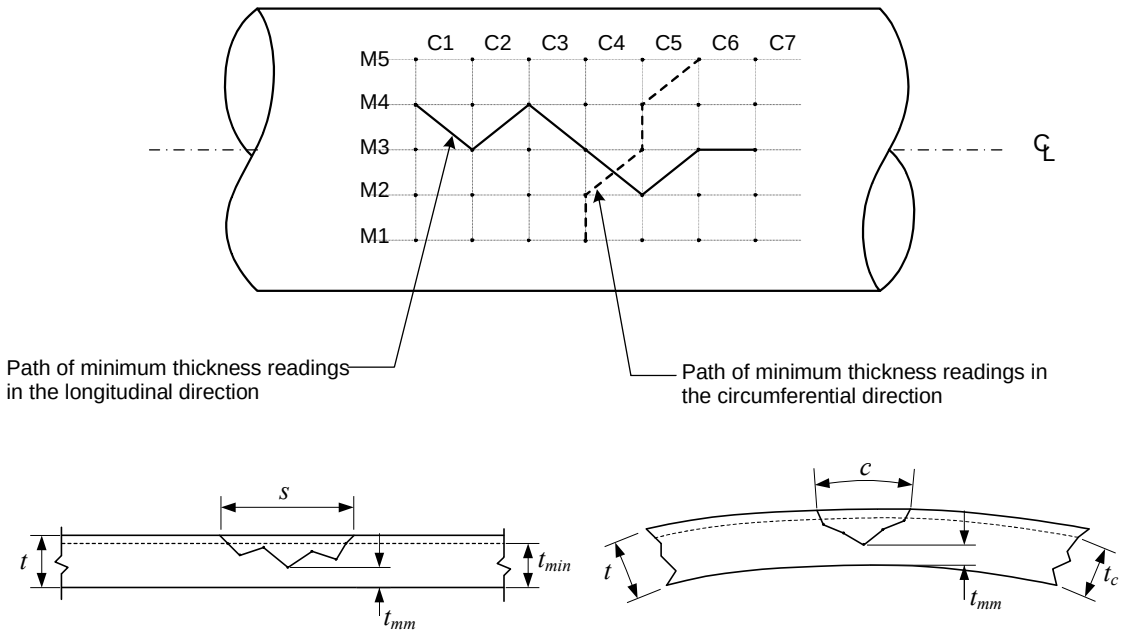

(a) Longitudinal CTP (b) Circumferential CTP

Figure 2.8 Procedure to establish the critical thickness profiles (CTP).

Note that the effective area method is a strength dependent method in which material toughness is not considered. Toughness is the ability of the material to withstand fracture. This implies the assumption of ductile material which is able to undergo large deformation before failure and the failure is non-crack-like. The assumption of ductile mechanism is also used in the current research.

The advantages of the effective area methods for corrosion flaw assessment lie in their simplicity and their experimental validation. The effective area methods have been validated by experiments and field failures on pipeline steels. Numerous additional experiments have been conducted and modifications to the criteria are suggested to reduce the conservatism. Extensions of the method to include some specific areas such as spirally oriented corrosion, corrosion longer than one pipe diameter, interaction of axial and circumferential separation of axially oriented corrosion defects, etc., have been investigated through experiments by Coulson and Worthingham (1990), Mok, et al. (1990, 1991), Hopkins and Jones (1992), and Jones et al. (1992).

Although corrosion in cylindrical shells has been examined by many researchers, the proposed criteria are mostly empirical based and do not consider the effects of damages in circumferential direction.

(d) Level 1 Method of Assessment from API 579

The assessment procedures for API 579 are based on the ASME B31G and the RSTRENG criteria. The API 579 assessment provides a consistent result for regions of metal loss with significant thickness variability (Osage, 2001). Two acceptance criteria are included, a simple Level 1 criterion based on length and depth dimensions (Sec. 5.4.2) and a more complex Level 2 criterion relying on the detailed cross-sectional profile. Different assessment criteria are used for stress in the circumferential and longitudinal directions to properly account for pressure and supplemental loads.

The assessment procedures for circumferential stress in pressure vessels with LTA subject to internal pressure are as shown below. Based on the thickness profile, the remaining thickness ratio, R_t, and the metal loss damage parameter, λ, are computed as

$$R_t = \frac{t_{mm} - FCA}{t_{\min}} \quad \text{and} \quad \lambda = \frac{1.285s}{\sqrt{Dt_{\min}}} \tag{2.31}$$

where, t_{mm} is minimum measured remaining wall thickness, FCA is future corrosion allowance, and $t_{\min}$ is minimum required wall thickness determined in accordance with the original construction code.

The stress at failure of LTA is computed as

$$\sigma_{fail} = \frac{\sigma_y \cdot RSF}{0.9}; \qquad RSF = \frac{R_t}{1-(1-R_t)M^{-1}} \tag{2.32}$$

where, $M = \sqrt{1+0.48\lambda^2}$.

The geometrical limitations on the region of local metal loss are $L_{msd} \geq 1.8\sqrt{Dt_{\min}}$, $R_t \geq 0.20$ and $t_{mm} - FCA \geq 2.5\,\text{mm}$, where, L_{msd} is the shortest distance between the edge of corrosion area and the discontinuity.

The first limitation, as in this thesis, requires that the LTA be located away from a structural discontinuity and any local effects associated with the discontinuity will decay to negligible value such that the stress field at the LTA will be predominantly membrane. The second of these limitations is due to the absence of validation results for deep corrosion profiles. It can be seen that evaluation is valid for corrosion loss up to 80% of

design thickness. The third limitation is to confine the minimum remaining thickness to prevent both leakage and mechanical damage to a component.

It can be noticed from Eq. (2.32) that the criteria for API 579 are based on Folias factor as in ASME B31G. The flow stress is also assumed to be equal to $\sigma_y/0.9$ (= $1.111\ \sigma_y$) similar to that of ASME B31G. However, the empirical relationship accounts for surface flaw effects based on the remaining thickness ratio. This implies rectangular shape of corrosion. Therefore, API 579 is expected to provide more conservative results than ASME B31G.

(e) Level 2 Method of Assessment from API 579

If there are significant variations in the thickness profile, the Level 2 assessment can be used to provide a better estimate of the RSF (API 579, Sec. 5.4.3). The inherent strength of the actual thickness profile is evaluated using an incremental approach to ensure that the weakest ligament is identified and properly evaluated. The limitations are checked using Eqs. (2.31) and an additional condition that $\lambda \le 5.0$. The procedure is similar to the RSTRENG method by using the same river-bottom methodology except that a different value of the Folias factor is used in the procedure, i.e,

$$M^i = \left[\frac{1.02 + 0.4411(\lambda^i)^2 + 0.006124(\lambda^i)^4}{1.0 + 0.02642(\lambda^i)^2 + 1.533(10^{-6})(\lambda^i)^4} \right]^{0.5} \qquad (2.33)$$

The criteria in API 579 appear to be suitable and applicable for evaluation of the remaining strength of LTA in cylindrical pressure vessels and piping under internal pressure loading.

One of the most significant limitations of the API 579 assessment procedure is the requirement that the LTA be located a minimum distance of $L_{msd} = 1.8\sqrt{Dt}$ from the nearest discontinuity. This length is essentially equal to $2.5\sqrt{Rt_{\min}}$ which is the decay length in axial direction for cylinders. This is the decay length used in the present work as explained in Section 6.2. Harvey (1991) obtained an analogous length of a cylindrical vessel to be considered as an infinitely long beam by using theory of beam on elastic foundation. It is also implies that API 579 uses the same decay length in the circumferential direction of the cylinder.

Seshadri (2004) proved that the decay length in circumferential is much larger than that of axial direction. Hence, this criterion of API 579 is not good from the interaction point of view for damage located near other damages or discontinuities in circumferential direction. Decay length in the circumferential direction will be further investigated in the current research in order to use it to find the RSF.

Different curvatures of the axial and the circumferential directions of a cylindrical shell affect the decay lengths in those directions differently. Hence, it is anticipated that the decay lengths associated with other shapes of pressure vessels (such as sphere, cone and torus) are different from that of a similar cylindrical shell. Thus, the minimum distance to a major structural discontinuity from an LTA without inducing interaction

effects is increased from that of API 579. One of the objectives of the present research is to utilize the theory of shells to estimate the minimum distance of the damages such as corrosion and thermal hot spots from the closest discontinuity.

(f) The m_α-method

Indermohan and Seshadri (2004) proposed a Level 2 FFS methodology for evaluating corrosion in cylindrical shells. It is similar to the previously discussed FFS assessment procedures for hot spots by Seshadri (2004). Thin cylindrical shells with radius to thickness ratio equal to 52.8 subject to internal corrosion of various sizes are studied. The remaining thickness ratios are taken as 0.9, 0.8, and 0.6. The results are compared with inelastic finite element analysis results. The material is modeled by using plastic modulus of 3447 MPa (500 ksi) and the criterion of 1% membrane strain limit is used. It is concluded by them that the RSF obtained are conservative and comparable with nonlinear FEA results.

Ramkumar and Seshadri (2005) extended the application of the assessment to a thicker cylindrical shell with radius to thickness ratio 32.6 for both internal and external corrosion. The RSF and limit pressure computed from the proposed method are compared with the results from finite element analysis using the same model and yield criteria as (Indermohan and Seshadri, 2004). The results are also compared with the results according to ASME B31G. The comparison showed the variation of the RSF and limit pressure of the LTA followed a similar pattern when variational method and inelastic FEA were used and the results from the variational method are conservative. Moreover,

the remaining strength factor evaluated by using the ASME B31G criterion is shown to underestimate the effect of corrosion damage in some cases.

The method proposed by Indermohan and Seshadri and extended later on by Ramkumar and Seshadri is shown to provide a simple and useful Level 2 FFS assessment to evaluate the effects of damage due to corrosion which reduce the conservatism compared with the ASME B31G criterion. Moreover, the reference volume approach overcomes the limitation of other evaluation methods by considering the circumferential extent of corrosion. However, it should also be mentioned that the plastic modulus of 500 ksi used in their work may be somewhat high and need to be used only for appropriate cases.

The corrosion areas studied in both works are limited to the aspect ratio of 1 to 1, 1 to 2 and 2 to 1. Further application of the method to cylindrical vessels with corrosion regions of various aspect ratio is of interest for the current research. The method will also be applied in conjunction with decay lengths calculated from shell theory to spherical pressure components.

(g) Comparison of Existing Procedures

Osage, et al. (2001) compared the existing assessment criteria for blunt LTA (non-crack like) in cylindrical shells by considering the maximum acceptable flaw dimensions in vessels which maintain their maximum allowable working pressure. The models are compared in terms of acceptable flaw depth ratio (d/t) and $L/\sqrt{Rt}$ and also in terms of remaining wall thickness (t_{mm}) and flaw length/vessel diameter (s/D). They suggested that

most of the criteria overlap significantly except for the Modified B31G criterion which provides the least conservative results for permissible flaw sizes. The "modified Level 1" criterion is recommended based on the adaptation of API Level 1 and Level 2 criteria and the curve fit factor $A/A_o = 0.85d/t$ similar to the Modified B31G criterion. Although this method offers a continuous criterion with low variability of safety factor, the results are shown to be more conservative than those obtained from ASME B31G criterion for LTA with $s/\sqrt{Rt} < 6.3$.

2.4.3. FFS Assessment for Corrosion Damage in Non-cylindrical Shells

Little technical development and experimental validation has been performed for corrosion damage in non-cylindrical pressure vessels and corrosion damage near structural discontinuities. The LTA assessment procedures for spherical shells and formed heads in API 579 are based on the procedures used for cylinders. However, in the Level 2 assessment procedures, the Folias factor developed for spherical shells is used in place of Eq. (2. 33).

$$M^i = \frac{1.0005 + 0.49001(\lambda^i)^2 + 0.32409(\lambda^i)^2}{1.0 + 0.50144(\lambda^i) - 0.011067(\lambda^i)^2} \tag{2.34}$$

Sims (1992) studied local Round Thin Areas (RTA) in cylinders and spheres with similar dimensions. The results indicate that for a given shell diameter and thickness, and RTA diameter and depth, the RSF for a cylinder is greater than that for a sphere. If the Folias factor for the sphere is used in the API 579 Level 2 assessment, this same trend

occurs. This can also be supported by the concept of reference volume as will be shown in the Chapter 7.

In API 579, the assessment procedures for LTA in conical shells located away from major structural discontinuities are also based on the procedures used for cylinders. The distance is specified to be the same as in the evaluation of cylindrical shell. However, the minimum required thickness is based on the construction code for conical shells and the inside diameter is specified to be the diameter at the center of the LTA. As discussed earlier, this distance can be improved upon by using theory of shells to obtain a decay length in a conical shell.

2.5. CLOSURE

The current chapter reviewed the theories in plasticity and limit analysis generally employed in evaluation of pressure vessels with local damages. An overview of the existing Fitness-for-Service assessments for thermal hot spot and corrosion damage is presented. It is observed that there is a lack of procedures for evaluating RSF for thermal hot spots in pressure vessels. Most of the FFS assessments for corrosion damage are designed for cylindrical shells and only consider the longitudinal extent of damage. An improved Level 2 procedure can be developed to overcome these limitations and offers a better understanding of the behavior of corrosion damage and thermal hot spots in pressurized components.

CHAPTER 3

THE m_α-MULTIPLIER METHOD

Limit load of a structure can be conservatively approximated by using statically admissible or lower bound limit load multipliers. The improved lower bound m_α -multiplier developed by Seshadri and Mangalaramanan (1997) is shown to provide close lower bound estimates to a variety of practical mechanical components including pressurized components of various shapes. Hence the m_α- multiplier will be the main multiplier applied to assess the strength of damaged pressure vessels in the current research. The theoretical background and application of the m_α- multiplier method will be discussed in this chapter.

3.1. BACKGROUND

Mura and coworkers (1963, 1965) introduced the concept of integral mean of yield criterion that allows the pseudo-elastic distributions of stresses to lie outside the

yield surface. Seshadri and Mangalaramanan (1997) applied this concept in conjunction with successive elastic finite element analyses, the concept of leap-frogging to the limit state and the theorem of nesting surfaces to develop an improved lower bound m_α-multiplier. The concept of reference volume is used to narrow the upper and lower bound spread for localized plastic collapse. The m_α-multiplier is proved to be robust (Fowler, 1998; Ralph, 2000) and applicable to determine lower bound estimation of limit load for a range of mechanical components (Pan and Seshadri, 2002; Reinhardt and Seshadri, 2003).

Indermohan and Seshadri (2004) recommended the m_α-multiplier method to evaluate the remaining strength factor (RSF) for cylinders with thermal hot spots. Ramkumar (2005) showed that the method provided lower bound RSF approximation for cylindrical shells with locally thinned area (LTA). The m_α-multiplier method will be applied to estimate RSF of spherical and cylindrical containing local corrosion damage or thermal hot spots in the current research.

3.2. GENERAL CONCEPTS

The theories used in the derivation of the m_α-multiplier method include the theorem of nesting surfaces, Mura's extended variational principle in plasticity and the concept of reference volume. These are briefly discussed below.

3.2.1. Theorem of Nesting Surfaces

In the steady state creep analysis, the constitutive equation is given by $\frac{d\varepsilon}{dt} = B\sigma^n$ where, B and n are creep parameters. Using elastic analogy, Hoff (1954) replaced the creep problem by a problem in nonlinear elasticity with the stress-strain law $\varepsilon = B\sigma^n$. The value of exponent $n = 1$ is analogous to linear elasticity, while $n \to \infty$ resembles perfect plasticity.

The effective generalized stress for the entire volume Q_e, is then given by,

$$Q_e = \left[\frac{1}{V} \int_V \sigma_e^{n+1} dV \right]^{1/(n+1)} \tag{3.1}$$

where, σ_e is equivalent stress.

Calladine and Drucker (1962) extended the work of Hoff and suggested the theorem of nesting surfaces. The theorem essentially shows that the functional $Q_e(\sigma_e)$ is strictly monotonically increasing with the exponent n. It is bounded from below by the result for $n = 1$ and from above by the limiting functional as $n \to \infty$. Boyle (1982) deduced that if hypersurfaces $Q_e(\sigma_e) = constant$ in stress space are considered, they must nest inside each other for increasing n. For a linear elastic material $n = 1$, the reference stress is expressed as

$$Q_e = \left[\frac{1}{V} \int_V \sigma_e^2 dV \right]^{1/2} \tag{3.2}$$

The above equation can be written using a finite element discretization scheme as

$$Q_e = \left[\frac{1}{V} \sum_{k=1}^{N} \sigma_{ek}^2 \Delta V_k \right]^{1/2} \tag{3.3}$$

where, k is element number and N is the total number of elements.

3.2.2. Mura's Extended Variational Formulation and Application

Mura and Lee (1963) showed by means of variational principles that the safety factor, the kinematically admissible multiplier and the statically admissible multiplier for a body made of perfectly plastic material and subjected to a given surface traction are actually extremum values of the same functional under different constraint conditions.

In a lower bound limit analysis, a statically admissible stress field cannot lie outside the yield surface, and in an upper bound analysis, the stress associated with a kinematically admissible strain rate field in calculating the plastic dissipation should lie on the yield surface. Mura, et al., (1965) eliminated such a requirement by further introducing the concept of integral mean of yield criterion,

$$\int_{V_T} \mu^0 [f(s_{ij}^0) + (\varphi^0)^2] dV = 0 \tag{3.4}$$

where, the superscript *"0"* refers to statically admissible stress distributions that are in equilibrium and μ^0 is the flow parameter from the associated flow rule. The deviatoric stress s_{ij}^0 corresponds to the impending limit state, where, $s_{ij}^0 = m_d^0 \bar{s}_{ij}^0$ and m_d^0 is the limit load multiplier and the deviatoric stress $\bar{s}_{ij}^0$ equilibrates the applied set of loads. The

parameter φ^0 is a point function that takes on a value of zero if s_{ij}^0 is at yield and remains positive below yield.

Mura's extended variational principle leads to a new lower bound multiplier m' smaller than the unknown actual collapse load multiplier m and can be expressed as

$$m' = \frac{m^0}{1 + \max[f(s_{ij}^0) + (\varphi^0)^2]/2k^2} \leq m \tag{3.5}$$

Equation (3.5) includes the classical definition of lower bound multiplier where $\max[f(s_{ii}^0) + (\varphi^0)^2] = 0$, with Eq. (3.5) reducing to $m^0 \leq m$.

Since s_{ij}^0 corresponds to the deviator of the stress state for impending plastic flow, $s_{ij}^0 = m^0 \bar{s}_{ij}^0$, where, $\bar{s}_{ij}^0$ represents the deviator of the stress state for applied traction T_i. The von Mises yield criterion is given by $f(s_{ij}) = \sigma_e = \frac{3}{2} s_{ij} s_{ij} - \sigma_y^2$ and the associated flow rule can be expressed as $\dot{\varepsilon}_{ij} = \mu(\partial f / \partial s_{ij})$ where, $\mu \geq 0$. Mura and co-workers have shown that m^0, μ^0 and φ^0 can be determined by rendering the functional F stationary in

$$F = m^0 - \int_{V_T} \mu^0 [f(s_{ij}^0) + (\varphi^0)^2] dV \tag{3.6}$$

leading to the set of equations

$$\frac{\partial F}{\partial m^0} = 0, \quad \frac{\partial F}{\partial \mu^0} = 0, \quad \frac{\partial F}{\partial \varphi^0} = 0 \tag{3.7}$$

For the von Mises yield criterion, the functional becomes

$$F = m^0 - \int_{V_T} \mu^0 \left[\frac{3}{2} (m^0)^2 \bar{s}_{ij}^0 \bar{s}_{ij}^0 - \sigma_y^2 + (\varphi^0)^2 \right] dV \tag{3.8}$$

Assuming a constant flow parameter μ^0 and setting $\delta F = 0$, the foregoing functional can be written in a finite element scheme, for $\varphi^0 = 0$, as

$$m^0 = \frac{\sigma_y \sqrt{V_T}}{\sqrt{\sum_{k=1}^{N} (\sigma_{ek})^2 \Delta V_k}} \tag{3.9}$$

where, N is the total number of elements, σ_{ek} and ΔV_k are the equivalent stress and volume of element *k*, and V_T is the total volume of the component.

Combining Eqs. (3.2) and (3.9) yields

$$m^0 = \frac{\sigma_y}{Q_e} \tag{3.10}$$

Therefore, m^0 is related to the reference stress Q_e and Mura's formulation is related to the theorem of nesting surfaces.

Equation (3.5) for m' can be rewritten in terms of the maximum equivalent stress σ_M^0 in a component as

$$m' = \frac{2m^0 \sigma_y^2}{\sigma_y^2 + (m^0)^2 (\sigma_M^0)^2} \tag{3.11}$$

Statically admissible stress fields and kinematically admissible strain fields can be obtained from linear elastic analyses by using a modulus adjustment scheme. The first

linear analysis is a conventional elastic analysis and the elastic modulus of all elements can be modified in the second analysis using the equation

$$E_s = \left(\frac{\sigma_{arb}}{\sigma_e} \right)^q E_0 \tag{3.12}$$

where, q is a modulus adjustment parameter nominally taken as one. The iteration can be repeated any number of times until convergence is obtained. An iteration variable ζ is now introduced in a manner that infinitesimal changes of the elastic modulus in successive elastic analysis would induce a corresponding change $\Delta\zeta$. As ζ increases with the iterations, m^0 and m' should ideally converge uniformly to the exact value of the safety factor m.

3.2.3. Reference Volume

When plastic collapse occurs over a localized region of a component, the calculation based on the total volume V_T would give an overestimated value of m^0 and underestimated value of m'. Moreover, the use of V_T can also give value that does not converge to the exact multiplier m. The reference volume concept is then introduced to identify the "kinematically active" portion of the structure that participates in the plastic actions. Equation (3.9) can be written in terms of the reference volume, V_R, as

$$m^0(V_R) = \frac{\sigma_y \sqrt{V_R}}{\sqrt{\sum_{k=1}^{\alpha} (\sigma_{ek})^2 \Delta V_k}} \tag{3.13}$$

where, $V_R = \sum_{k=1}^{\alpha} (\Delta V_k)$, and $\alpha < N$.

The elements are arranged in the descending order of energy dissipation

$$(\sigma_{e1}^0)^2 \Delta V_1 > (\sigma_{e2}^0)^2 \Delta V_2 > \cdots > (\sigma_{eN}^0)^2 \Delta V_N \tag{3.14}$$

As k is increased from 1 to N, the value of m^0 increases for any given linear elastic iteration. The variation of m_1^0 and m_2^0 with volume corresponding to the first and second linear elastic FEA is shown in Figure 3.1. The theorem of nesting surfaces is valid if $m_1^0 > m_2^0$ which is when $V \geq V_R$. The phrase "m_α-method" refers to the use of α elements in the finite element discretization scheme that pertains to the identification of an appropriate reference volume.

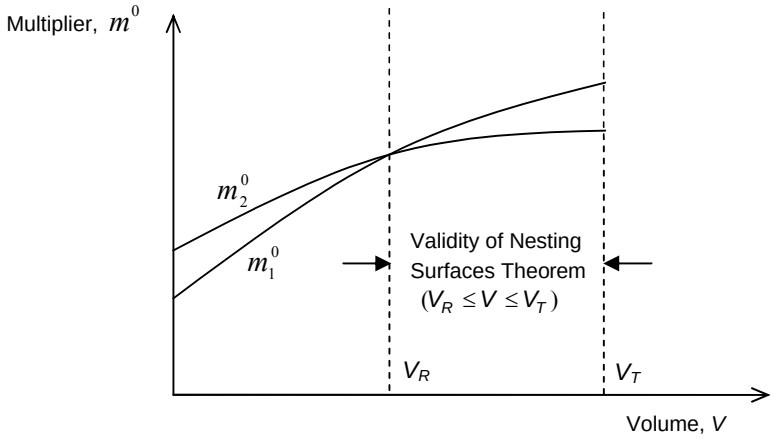

Figure 3.1 Identification of the reference volume, V_R.

3.3. THE m_α-MULTIPLIER

By using the new lower bound multiplier m' from Mura's variational principle, the m_α -multiplier can be determined by the concept of leap-frogging[1] to the limit state of two successive finite element analyses.

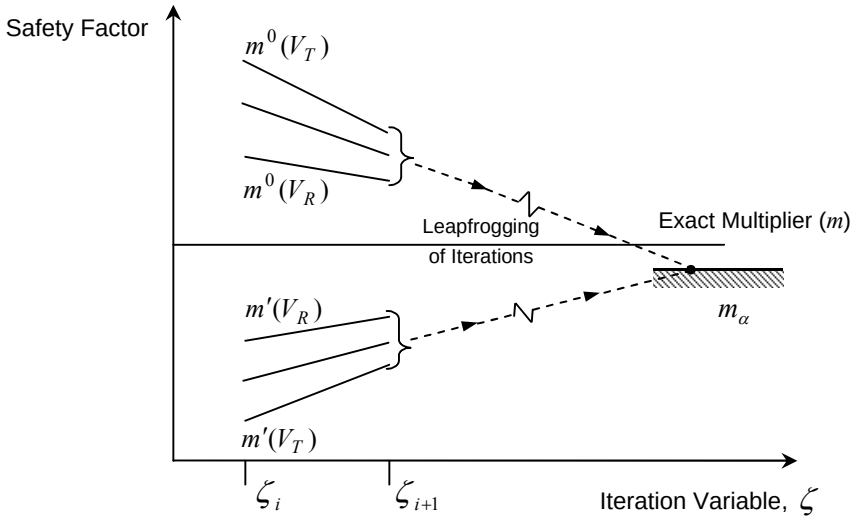

Figure 3.2 Leap-frogging to the limit state (Seshadri and Mangalaramanan, 1997).

Equation (3.9) can be expressed in terms of iteration variable ζ as

$$m'(\zeta) = \frac{2m^0(\zeta)\sigma_y^2}{\sigma_y^2 + [m^0(\zeta)]^2[\sigma_M^0(\zeta)]^2} \tag{3.15}$$

In terms of finite differences, we have

[1], 'leap-frogging' refers to the use of two iterations to obtain an estimate of the 'exact' multiplier by using the concept of reference volume

$$\Delta m' = \left.\frac{\partial m'}{\partial m^0}\right|_{\zeta_i} \cdot (\Delta m^0) + \left.\frac{\partial m'}{\partial \sigma_M^0}\right|_{\zeta_i} \cdot (\Delta \sigma_M^0) \tag{3.16}$$

where, $\zeta = \zeta_i$ corresponds to the *i*-th iteration. For a limit state $\zeta = \zeta_\infty$, we define

$$\Delta m' = m_\alpha - m_i', \quad \Delta m^0 = m_\alpha - m_i^0 \quad \text{and} \quad \Delta \sigma_M^0 = \frac{\sigma_y}{m_\alpha} - \sigma_{Mi}^0 \tag{3.17}$$

where, m_α is the value to which m' and m^0 are conjectured to converge by the idea of leap-frogging of iterations as shown in Figure3.2.

Substitution of Eqs. (3.16) and (3.17) into Eq. (3.15) yields the quadratic equation

$$Am_\alpha^2 + Bm_\alpha + C = 0 \tag{3.18}$$

where, $A = (m_i^0 \bar{\sigma}_{Mi}^0)^4 + 4(m_i^0 \bar{\sigma}_{Mi}^0)^2 - 1$, $B = -8m_i^0 (m_i^0 \bar{\sigma}_{Mi}^0)^2$, $C = 4(m_i^0)^3 \bar{\sigma}_{Mi}^0$ and $\bar{\sigma}_{Mi}^0 = \dfrac{\sigma_{Mi}^0}{\sigma_y}$. The values for m_i^0 and σ_{Mi}^0 are calculated from the results of any linear elastic FEA iteration. Although the m_α method was intended for two iterations, more iterations would provide a better estimation.

Equation (3.18) is a polynomial of second degree and the m_α-multiplier can be solved for the larger of the two possible solutions as

$$m_\alpha = 2m^0 \frac{2\left(\frac{m^0}{m_L}\right)^2 + \sqrt{\frac{m^0}{m_L}\left(\frac{m^0}{m_L} - 1\right)^2 \left(1 + \sqrt{2} - \frac{m^0}{m_L}\right)\left(\frac{m^0}{m_L} - 1 + \sqrt{2}\right)}}{\left(\left(\frac{m^0}{m_L}\right)^2 + 2 - \sqrt{5}\right)\left(\left(\frac{m^0}{m_L}\right)^2 + 2 + \sqrt{5}\right)} \tag{3.19}$$

where, $m_L \left(= \sigma_y / \sigma_M^0\right)$ is the classical lower bound multiplier . It should be noted that the solution for m_α vanishes (becomes imaginary) if $m^0 / m_L > 1 + \sqrt{2}$.

Reinhardt and Seshadri (2003) showed that m_α estimates are lower bounds in the great majority of cases. Although, the m_α-multiplier could be 5% on the upper bound side in the cases where the upper-bound multiplier is not so close to the exact multiplier, this may be considered as acceptable within engineering accuracy. Pan and Seshadri (2002) applied the m_α-multiplier to various types of practical mechanical components. Despite its complicated theoretical background and derivation, the formulation and application of m_α has been proved to be practicable and straightforward for determining lower bound approximations. Hence, the m_α -multiplier is used as the basis of RSF_α in the proposed assessment.

3.4. CLOSURE

The m_α-method has been shown to provide reasonable lower bound approximations to limit loads of various mechanical components. The background and theoretical aspects of the method are discussed in detail in the current chapter. The application of the m_α–multiplier to evaluate pressure components with local damages such as corrosion damage and thermal hot spots will be presented in Chapter 4.

CHAPTER 4

GENERAL METHODOLOGY FOR PROPOSED LEVEL 2 FITNESS-FOR-SERVICE ASSESSMENTS

Structural integrity of an in-service component containing damages such as corrosion and thermal hot spots have to be evaluated regularly so as to certify the acceptance and safety of continued service of the component. Level 1 Fitness-for-Service (FFS) assessments such as those recommended by API 579 can be used as basic screening criteria by plant technicians. Level 2 FFS assessments are recommended procedures which are less conservative but involve more detailed calculations intended for use by plant engineers.

This chapter discusses general methodology of the proposed Level 2 FFS assessments for pressure vessels containing thermal hot spots or corrosion damages. The factors influencing the failure of damaged pressure components are presented. The similarities and differences between edge effects due to corrosion damage and those due

to thermal hot spots are investigated. The parameters taken into consideration, the assumptions and failure criteria for the proposed FFS assessments are discussed. Procedures for Level 2 evaluation of corrosion damage or thermal hot spots in spherical and cylindrical shells including the concept of reference volume, distinction of local and global damage and calculation of equivalent stresses are then explained in detail.

4.1. FACTORS INFLUENCING CORROSION AND THERMAL HOT SPOT FAILURE

The complexity of obtaining an accurate FFS evaluation for a pressure component containing a flaw lies in the involvement of a number of parameters affecting the behavior of the flaw and the failure of the component. Experimental studies showed that the failure of corroded component can occur either by ductile failure (non crack-like flaws) or toughness dependent failure (crack-like flaws) as pointed out in Chapter 2. The current study focuses on the behavior of non-crack-like (or blunt) corrosion.

As discussed earlier, in order to determine strength of such corroded components, corrosion damage is considered as locally thinned area (LTA). Osage, et al. (2001), among others, investigated the applicable criteria for acceptance of LTA in pipe and cylindrical vessels. The global schematic of the factors contributing to failure of LTA is illustrated in Figure 4.1. Failure occurs when the effect of driving forces which induce the stresses and strains exceeds the material resistance.

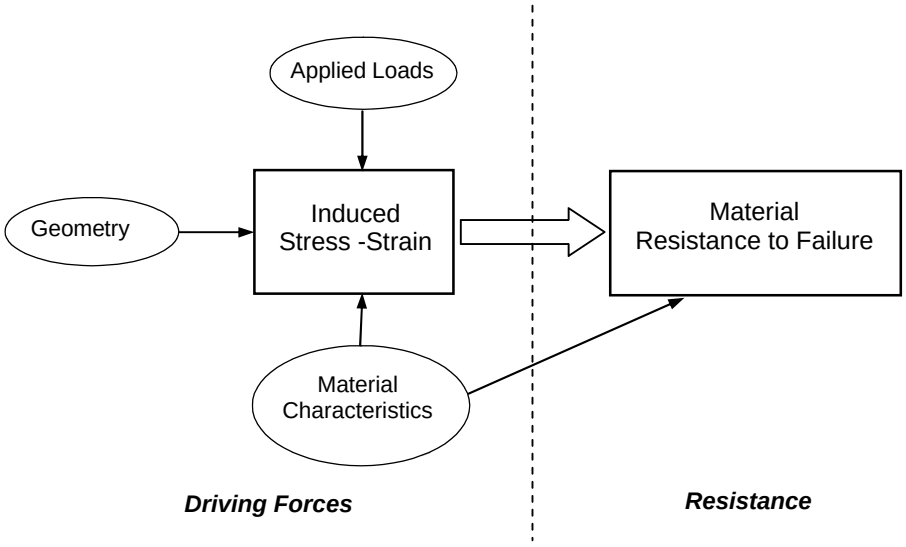

Figure 4.1 Schematic diagram of primary factors controlling the behavior of locally thinned areas (Osage et al., 2001).

Table 4.1 Parameters likely to influence the behaviour of pipeline defects

Applied Global Loadings	Geometry	Material Characteristics
Internal pressure Uniform axial loads Bending moment	Pipe dimensions Diameter Wall thickness Defect geometry Depth Length Width Shape/ profile	Yield strength Ultimate strength Plasticity/strain hardening Fracture toughness Limiting strain for acceptable performance

The parameters likely to influence the behavior of LTA are applied loadings (operating conditions), vessel geometry, flaw geometry and material characteristics (as listed in Table 4.1). The applied loads include the direct surface traction (internal pressure) and the net section tensile, compressive and bending loads. Vessel geometry, flaw characteristics and material properties directly influence the stress and strain field by controlling the manner in which the damaged area deforms.

4.2. METHODOLOGY FOR PROPOSED LEVEL 2 FITNESS-FOR-SERVICE (FFS) EVALUATIONS

This section discusses the methodology of the proposed Level 2 FFS assessments. Evaluation procedures for spherical and cylindrical shells are recommended based on m_α multiplier, reference volume and variational principle.

4.2.1. Behavior of Local Damage

In the current research, irregular profiles of the flaws are represented by equivalent regular shapes to facilitate the evaluation procedures. For cylindrical shells, a flaw profile is replaced by an equivalent rectangle enclosing the defect with the edges along circumferential and meridian directions of the shell. In the case of spherical shells, it is more advantageous to use an enclosing circular area as illustrated in Figure 4.2. The maximum thickness loss is used in the evaluation of corrosion damage. This implies that the defect has an aspect ratio that is not too different from 1.0 and that the corroded

thickness does not vary widely over the corroded area. For defects with widely varying thicknesses, or highly irregular geometries, we can arrive at similar suitable equivalent properties.

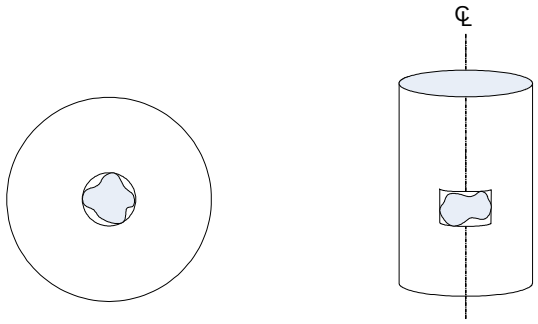

Figure 4.2 (a) Circular equivalent area in sphere (b) Rectangular equivalent area in cylinder

When local damage such as thermal hot spots or corrosion occurs in a component with internal pressure, the damaged region undergoes higher deformations than the undamaged region and the undamaged area acts somewhat like a support to the high bending moments generated in the vicinity of discontinuities. This can result in excessive deformation called “bulging” of the damaged area and the bending moments at the junction are in the direction that restrains the deformation of the softer part.

However, the behavior of corrosion damage and thermal hot spots in pressurized components is slightly different. In the hot spot case, the discrepancy in the deformation between hot and cool regions is due to the reduction of the elastic modulus and yield strength at higher temperature. The hot spot region is softer than the surrounding region and yields before the cooler parts. On the other hand, the difference in the deformations

of the corroded and uncorroded parts is due to the difference in the thicknesses of the two parts. The corroded region is considerably more flexible than the surrounding region.

The behavior of corrosion damage is also different from that of hot spots due to the misalignment of the thickness centerlines of the corroded and uncorroded areas (Figure 4.3). For a pressure vessel with internal corrosion, the mean radius of the corroded area is slightly larger than that of the uncorroded area while for a pressure vessel with external corrosion the mean radius of the corroded area is smaller than that of the uncorroded area. An additional bending moment is introduced due to the thickness misalignment. It is equal to the product of the stretching force at the junction and the eccentricity (the distance between the two centerlines as shown in Figure 4.3).

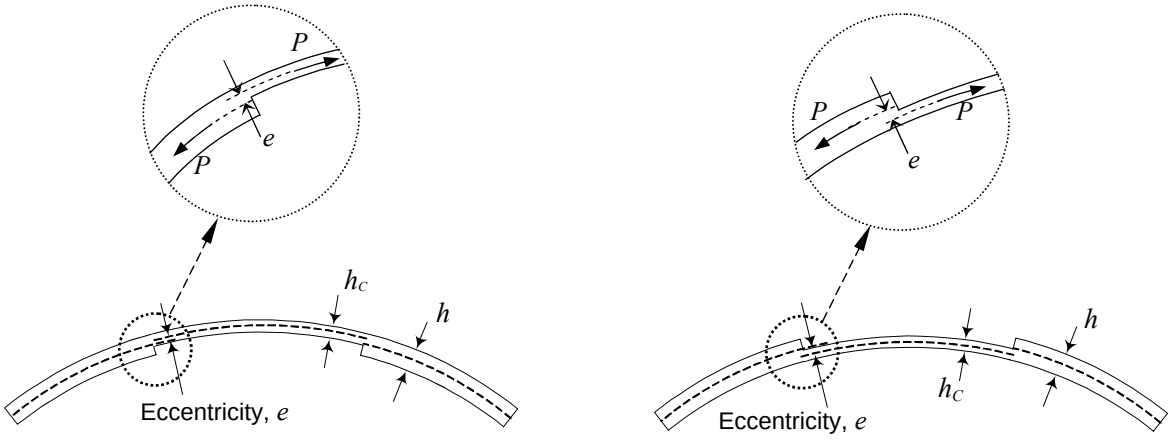

Figure 4.3 Centerlines misalignment in (a) Internal corrosion (b) External corrosion

Excessive plastic deformation in a damaged area can lead to plastic collapse over a localized region of a component. In general, the effects from the discontinuities do not

affect the entire structure but rather only a controlled region. The concept of reference volume is introduced to identify the kinematically active portion of the structure that participates in plastic action. The reference volume prescribes the containment of effects of local stresses and strains acting on the structure.

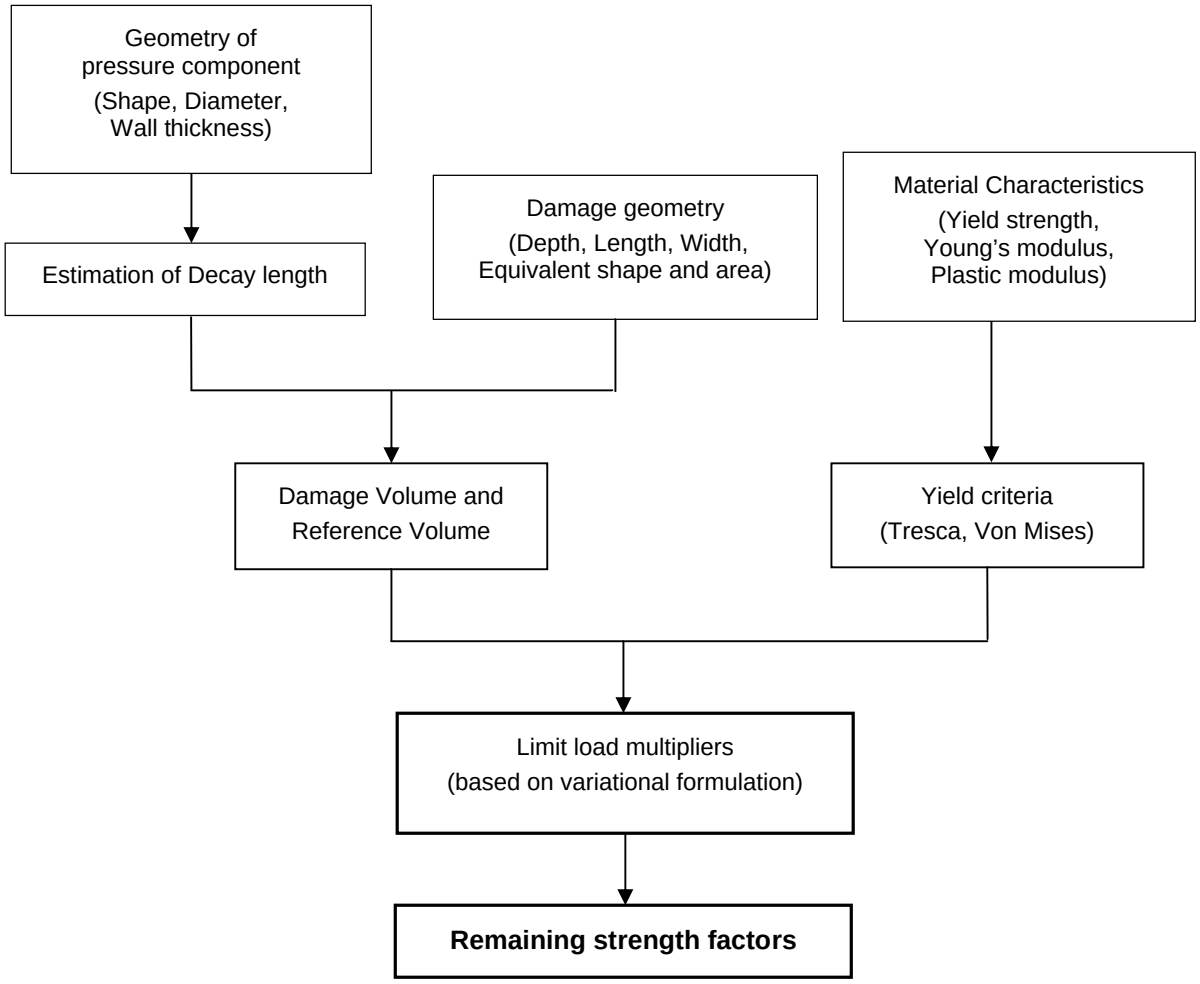

Figure 4.4 Contributing parameters to the proposed Level 2 evaluation methods

In the present research, the reference volume is computed by using the shell decay length. The decay length is determined by the effect of a local force or moment acting on the shell and is defined as the distance from the applied force (or moment) to the point where the effect of the force is dissipated or becomes negligible. The decay length is a characteristic length corresponding to the component geometry, i.e., the shape of the shell surface and its dimensions. Larger decay length generally indicates better energy dissipation of the structure and leads to higher loading capacity whereas smaller decay lengths suggest severe local effects due to the applied forces. Once the decay length associated with the component geometry is obtained, the reference volume can be calculated from the geometric properties of the damage.

A diagram for parameters considered in the proposed Level 2 FFS methodology is shown in Figure 4.4. A key consideration in the determination of RSF is the reference volume estimation and the application of the yield criterion to the RSF calculation.

4.2.2. Assumptions and Failure Criteria

In the current research, the primary loading applied on pressure components is taken as internal pressure. The considered damaged spot is assumed not to interact with any other types of damage, discontinuity or with other nearby corrosion or hot spots. It is also assumed that the corrosion damage is not a crack like flaw. The material is assumed to have sufficient toughness to ensure ductile failure mechanism, i.e., the material inside the thermal hot spot or corrosion damage is assumed to elongate sufficiently prior to failure.

Several kinds of steel are used for the fabrication of pressure vessels depending on the types of applications. These steels have differing strain hardening characteristics. Some of them have significant post yield modulus while others are nearly perfectly plastic immediately after initial yield until a significant amount of plastic strain (like 4-5%) is accumulated beyond which strain hardening may become significant. In order to have a general method for Level 2 estimates, codes often resort to the use of flow stress in place of actual yield stress. This flow stress is higher than the material yield strength. In the present work, this concept is utilized. However, the "flow stress" is simply designated as yield strength in the present work. This implies that beyond the flow stress/ yield strength, the modulus has only a nominal value. The material stress-strain relationship used in finite element analysis is explained in more detail in Chapter 5.

The temperature of the metal is assumed to be between 37.8 °C – 316 °C (100 °F – 600 °F) as appropriate for the different cases that have been studied. Plastic modulus E_T is assumed to be small compared to elastic modulus of the material. For example, at 37.8 °C (100 °F), E_T = 1.38×10^8 Pa (20×10^3 psi) compared to E = 202×10^9 Pa (30×10^6 psi).

The "failure" is assumed to be arrived at when von-Mises membrane strain (strain at mid-surface and not peak strain) at the center of the flaw reaches 1%. Although such materials as carbon steel are known to have much higher strain than 1% at the actual failure state, this criterion is applied to assure the serviceability of the component. This is slightly more conservative than the 2% limit that was used by Sims et al. (1992). Since

the use of flow stress is implied, the strain at failure can be viewed as the average strain between yield and 2% which comes to be nearly 1%. Hence, the use of 1% membrane (centerline) strain in place of 2% strain at the extreme points to define "failure' is justifiable. It must be noted that the 1% membrane (or average) strain is the current industry practice as specified by ASME Boiler and Pressure Vessel Code (Section III Division 1). Clause **T-1310 Limits for Inelastic Strains** states that the maximum accumulated inelastic strain shall not exceed the following values:

(a) strains averaged through the thickness, 1%;

(b) strains at the surface, due to an equivalent linear distribution of strain through the thickness, 2%;

(c) local strains at any point, 5%.

In view of the above, the normal range of materials used in the pressure vessels is covered by the present thesis. However, if the vessels use a high strength steel where is 2% inelastic strain indicates more than 20% increase in the stress beyond yield (1.2 σ_y), a suitable flow stress needs to be used in place of the values used in the current work to make the procedures applicable. An additional failure criterion to control excessive deformation due to the bulging of the component is to limit the out-of-roundness ratio of the component to 1.01. This criterion will be discussed in detail in Section 7.5.

4.2.3. Reference Volume

Typical reference volumes for the equivalent areas as in Figure 4.2 are shown as shaded regions in Figure 4.5. A reference volume is the sum of the volume inside the

damaged spot and the “adjacent volume”. When damage occurs in a pressure component, the entire volume outside the damage does not participate in the failure mechanism. The “adjacent volume” is the effective undamaged volume outside the damaged area that participates in plastic action and will form part of the reference volume.

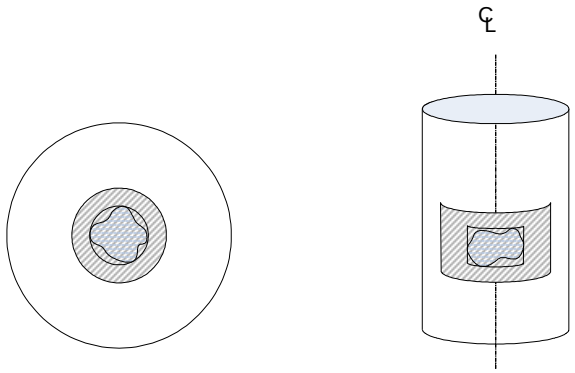

Figure 4.5 Reference volumes in (a) Sphere (or vessel head) (b) Cylinder

The concept of reference volume as discussed above might appear to imply that a material particle that is near the outer edge of the adjacent volume has the same effect as one near the damaged area. However, although the effect from secondary stresses (due to change of thicknesses or thermal stresses) for the two particles is not the same, primary (membrane) stresses of the two particles will be the same. The proposed method considers only primary stresses. More discussion on the concept of the reference volume can be found in Seshadri and Mangalaramanan (1997).

(a) Reference Volume for Spherical Shells

An irregular shape of a hot spot or corrosion damage in a spherical shell is assumed to be represented by an equivalent circular area. For a damaged area identified

through the included angle φ_a in a spherical shell as shown in Figure 4.6, the volume of the damaged area can be calculated as

$$V_D = \pi R_o^2 h_c (1 - \cos \varphi_a) \tag{4.1}$$

where, R_o is the outside radius of the sphere and h_c is the thickness of the damaged area, i.e., the corroded thickness for corrosion damage and the original thickness for hot spot.

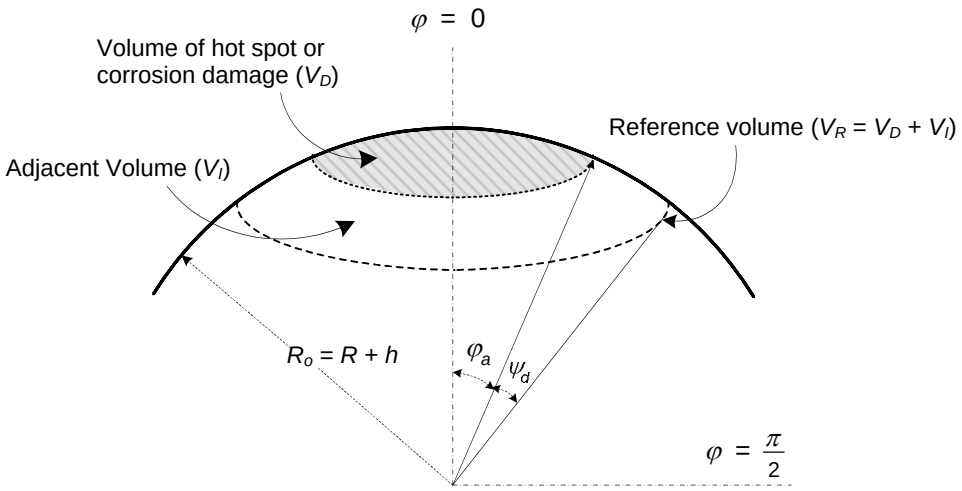

Figure 4.6 Equivalent circular damage and reference volume.

The adjacent volume is defined as the strip volume surrounding the damaged area where the shell might participate in plastic action. If the decay angle where the effects of the discontinuity become negligible is identified, the adjacent volume is

$$V_I = \pi R_o^2 h (\cos \varphi_a - \cos(\varphi_a + \psi_d)) \tag{4.2}$$

where, ψ_d is the decay angle. Derivation of a proposed decay angle in spherical shell is presented Section 6.1.

The reference volume V_R obtained as $V_R = V_D + V_I$ is the total volume of the kinematically active portion of the shell as explained above.

(b) Reference Volume for Cylindrical Shells

An equivalent rectangular shape is utilized to represent an irregular shape of a hot spot or a corroded area in cylindrical shells. For a damaged area of the width 2*a* in circumferential direction and the length 2*b* in longitudinal direction of a cylinder as shown in Figure 4.7, the volume of the damaged spot V_D can be calculated as

$$V_D = 4abh_c \tag{4.3}$$

The adjacent volume is the strip around the damaged volume that participates in plastic action and is bounded by decay lengths of cylindrical shells. Since the extent of decay length in shells is highly dependent on shell curvature, the decay lengths in circumferential and axial directions are different. Therefore, the adjacent volume is given by

$$V_I = 4h\left((x_c + a)(x_l + b) - ab \right) \tag{4.4}$$

where, x_l and x_c are decay lengths of cylindrical shells in axial and circumferential directions, respectively. These decay lengths for cylindrical shells are derived in Section 6.2. As before, the reference volume is the sum of the above volumes or $V_R = V_D + V_I$.

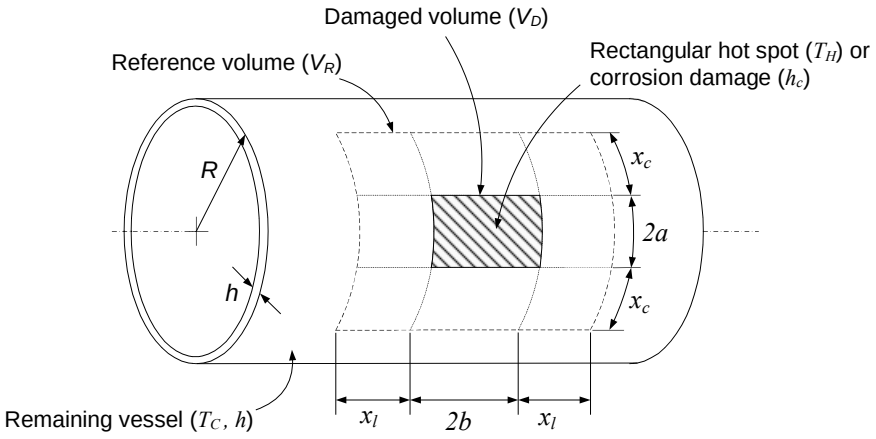

Figure 4.7 Reference volume dimensions for localized damage in cylindrical shell

4.2.4. Equivalent Stress for Thermal Hot Spot and Corrosion Damage

The reference volume is also applied to the calculation of elastic modulus and thermal expansion coefficient of a component with thermal hot spots. The effective elastic modulus and thermal coefficient are used to calculate the elastic thermal stresses and strains due to the temperature change. These are obtained as weighted averages of the volumes corresponding to each temperature zone. Thus, the effective elastic modulus and thermal expansion coefficients can be written as

$$E_{eff} = \frac{E_I V_I + E_D V_D}{V_R} \quad \text{and} \quad \alpha_{eff} = \frac{\alpha_I V_I + \alpha_D V_D}{V_R} \tag{4.5}$$

where, V is volume, E is Young's modulus, α is the coefficient of thermal expansion. The subscripts I, D, and R indicate respectively, initial (or undamaged), damaged and reference zones. The adjacent volume and reference volume are dependent on shell

geometry and can be computed as explained in Section 4.2.3. This is slightly different from the approach used by Seshadri (2004) where a simple mean value was used. This is one of the current research contributions. It must be noted that the hotspot is assumed to have a uniform temperature which is different from that of the adjacent region. In reality, a small transition zone of temperature gradient will be present in the shell near the boundary of the hotspot.

(a) Equivalent Stress in Spherical Shells

For a spherical shell with applied internal pressure, the principal thermo-elastic primary stresses inside a hot spot are the same in the meridianal and tangential directions. They can be calculated as,

$$\sigma_{1,2} = \frac{P_d R_i}{2h} - \frac{E_{eff}\alpha_{eff}\Delta T}{2} \tag{4.6}$$

where, P_d is the design pressure, R_i is the inner radius of the sphere, and $\Delta T = T_H - T_C$ is the temperature change due to loss of refractory lining leading to the formation of hot spot. The effective Young's modulus E_{eff} and the effective thermal coefficient α_{eff} are obtained from Eq. (4.5) The temperature induced effect on the membrane stress in the adjacent volume will be spread over the entire shell and is neglected for the present study.

The von Mises equivalent stress can be expressed as

$$\sigma_e = \sqrt{\sigma_1^2 + \sigma_2^2 - \sigma_1\sigma_2} \tag{4.7}$$

Therefore, the thermo-elastic equivalent stress is $\sigma_e = \sigma_1 = \sigma_2$

For a spherical shell with corrosion damage, the equivalent stresses in the damaged area and the adjacent area are different. The equivalent stress in the undamaged zone, σ_{eI}, and that inside the damaged area, σ_{eD}, are

$$\sigma_{eI} = \frac{P_d R_c}{2h} \quad \text{and} \quad \sigma_{eD} = \frac{P_d R_i}{2h_c} \tag{4.8}$$

where, R_c and h_c are the inner radius and shell thickness of the sphere inside the corrosion damage, respectively

(b) Equivalent Stress in Cylindrical Shells

The principal thermo-elastic membrane stresses of a cylindrical shell subject to internal pressure and temperature change are calculated as,

$$\sigma_1 = \frac{P_d R_i}{h} - \frac{E_{eff}\alpha_{eff}\Delta T}{2} \quad \text{and} \quad \sigma_2 = \frac{P_d R_i}{2h} - \frac{E_{eff}\alpha_{eff}\Delta T}{2} \tag{4.9}$$

The von Mises equivalent stress can then be written as Eq. (4.7).

For corrosion damage in a cylindrical shell, the equivalent stress in the undamaged zone, σ_{eI}, and that inside the damaged area, σ_{eD}, are

$$\sigma_{eI} = \frac{\sqrt{3}P_d R_c}{2h} \quad \text{and} \quad \sigma_{eD} = \frac{\sqrt{3}P_d R_i}{2h_c} \tag{4.10}$$

It can be observed that for similar spherical and cylindrical shells with the same inner radius and thickness, equivalent stress in cylindrical shell is higher than that in spherical shells.

4.2.5. Application of Reference Volume to Mura's Integral Mean of Yield Criterion

From the expression for integral mean of yield criterion Eq. (3.4), the concept of reference volume can be employed as

$$\int_{V_R} \mu^0 \left[f(s_{ij}^{\ 0}) + (\varphi^0)^2 \right] dV \ = \ 0 \tag{4.11}$$

where, the mean of yield criterion is calculated over the reference volume V_R instead of the total volume.

The Tresca and von-Mises yield criteria can be expressed, respectively, as

$$f(s_{ij}^{\ 0}) \ = \ \left| m_d^0 \sigma_e - \sigma_y \right| \ = 0 \tag{4.12a}$$

and

$$f(s_{ij}^{\ 0}) \ = \ [(m_d^0 \sigma_e)^2 - \sigma_y^2] \ = 0 \tag{4.12b}$$

where, m_d^0 is the upper bound limit multiplier for damage component, σ_e is the relevant equivalent stress and σ_y is the appropriate temperature dependent yield strength.

(a) Thermal Hot Spot

The integral mean of yield criterion can be applied to a pressure vessel with local thermal hot spots subject to Tresca yield criterion Eq. (4.12a) assuming the primary stresses to be uniformly distributed within the adjacent volume, V_I, and the hot spot volume, V_D. The flow parameter μ^o is taken as a non-zero constant for all the elements in the model. Hence it drops out of the equation. The integration of Eq. (4.11) leads to

$$\left((m_d^0 \sigma_{eI}^0) - \sigma_{yI}\right) V_I + \left((m_d^0 \sigma_{eD}^0) - \sigma_{yD}\right) V_D = 0 \tag{4.13}$$

where, the suffix *D* refers to the damaged or hot spot region and suffix *I* refers to adjacent volume as explained in Section 4.2.3. Note that the reference volume V_R is the sum of the damaged and adjacent volumes.

If the thickness is constant throughout the reference volume, the effective stresses in both regions are the same and are equal to σ_e. The upper bound limit load multiplier m_d^0 for Tresca criterion can then be obtained by rearranging Eq. (4.13) as,

$$m_d^0 = \frac{\sigma_{yI} V_I + \sigma_{yD} V_D}{\sigma_e V_R} \tag{4.14}$$

Similarly, integration of Eq. (4.11) using von-Mises yield criterion Eq. (4.12b) gives

$$\left((m_d^0 \sigma_e^0)^2 - {\sigma_{yI}}^2\right) V_I + \left((m_d^0 \sigma_e^0)^2 - {\sigma_{yD}}^2\right) V_D = 0 \tag{4.15}$$

Rearrangement of Eq. (4.15) gives the multiplier m_d^0 for von-Mises criterion as

$$m_d^0 = \sqrt{\frac{\sigma_{yI}^2 V_I + \sigma_{yD}^2 V_D}{\sigma_e^2 V_R}} \tag{4.16}$$

Although a uniform stress distribution throughout each volume in the calculation of the multiplier m_d^0 is assumed, this uniform stress is only used to obtain a practical and effective way to calculate approximate lower bound limit load multipliers and does not represent the exact stress distribution in the component. The assumption is justified since the primary stress that leads to limit load is considered as uniform membrane stress for the present case.

(b) Corrosion Damage

For a component containing corroded areas, the integral mean of yield using Tresca criterion can be expressed by integration of Eq. (4.11) as,

$$[(m_d^0 \sigma_{eI}^0) - \sigma_y]\, V_I + [(m_d^0 \sigma_{eD}^0) - \sigma_y]\, V_D = 0 \tag{4.17}$$

In this case, the equivalent stress of the intact portion σ_{eI} is different from the equivalent stress of the corroded portion σ_{eD} as discussed in Section 4.2.4.

The multiplier m_d^0 for corrosion damage using Tresca criterion is

$$m_d^0 = \frac{\sigma_y V_R}{\sigma_{eI}^0 V_I + \sigma_{eD}^0 V_D} \tag{4.18}$$

Von-Mises criterion can be applied to the integral mean of yield in a similar manner. We obtain

$$[(m_d^0\sigma_{eI}^0)^2 - \sigma_y^2]\ V_I + [(m_d^0\sigma_{eD}^0)^2 - \sigma_y^2]\ V_D = 0 \tag{4.19}$$

Therefore, the equation for m_d^0 multiplier for corrosion damage using von-Mises criterion can be written as

$$m_d^0 = \sqrt{\frac{\sigma_y^2 V_R}{\sigma_{eI}^2 V_I + \sigma_{eD}^2 V_D}} \tag{4.20}$$

4.2.6. Remaining Strength Factors (RSF)

The parameter usually employed to identify the acceptance for continued service of a damaged component in FFS assessments is the remaining strength factor (RSF). The RSF of a component containing damage is computed as the ratio of the strength of the damaged component to that of the component before damage. If the calculated RSF is higher than the allowable RSF, the component is allowed to be placed back into service.

Three types of RSF are applied to the proposed methods. The upper bound remaining strength factor RSF_U can be obtained from m_d^0 as

$$RSF_U = \frac{m_d^0}{m_u^0} \tag{4.21}$$

where, $m_u^0 \left(= \sigma_{yI} / \sigma_{eI}\right)$ is the multiplier for undamaged vessel and m_d^0 is determined on the integral mean of yield basis and applicable yield criterion as explained in the previous section using Eqs. (4.14) to (4.20). Since RSF_U is the ratio of an upper bound multiplier of a damaged component to that of the component in the undamaged condition, the RSF is guaranteed to be an upper bound estimate.

The second RSF is calculated based on the improved lower bound multiplier called m_α proposed by Seshadri and Mangalaramanan (1997) as discussed previously in Chapter 3. The remaining strength factor RSF_α is then expressed as,

$$RSF_\alpha = \frac{m_\alpha}{m_u^0} \tag{4.22}$$

Note that in the current research, a finite element analysis is not required to estimate RSF_α since the structure is considered as determinate for obtaining primary stresses in the shell. This is one of the key aspects of the current analysis. This is due to the fact that in spite of the presence of secondary stresses caused by the edge effects, softer or thinner material, etc., the failure is controlled by primary stress, which in this case is membrane tensile stress that can be calculated for determinate conditions.

The third remaining strength factor RSF_L is based on the classical lower bound multiplier m_L and is given by,

$$RSF_L = \frac{m_L}{m_u^o} \tag{4.23}$$

The m_L multiplier is calculated from $m_L = \sigma_{eD} / \sigma_{eI}$ for corrosion damage and from $m_L = \sigma_{yD} / \sigma_{yI}$ for thermal hot spot. This RSF_L is valid, and hence will be used, for all damaged areas larger than the extent of local damage for each shell configuration.

As explained above, the concept of RSF as the ratio of the plastic collapse load of a damaged component to the plastic collapse load of the undamaged component is applied to the evaluation of the acceptability for continued service of a component containing a flaw. The recommended value for the allowable RSF is normally around 0.90 for equipment in process services (Osage, 2001). In the current study, allowable RSF is estimated as the ratio of the required thickness to the pressure vessel thickness in the undamaged state. The required thickness is the minimum thickness required to withstand the applied internal pressure and can be calculated according to applicable standards or design codes. In the present study, it is computed based on Boiler and Pressure Vessel Code (BPVC) Section VIII Division 1 (ASME, 2004).

4.2.7. Local and Global Damage

When corrosion damage or a thermal hot spot occurs in a pressurized component, the overall structural capacity of the component is diminished due to lower strength of the damaged area. However, the remaining strength of the component is not solely dependent on the strength of the damaged area. The neighbouring undamaged area also plays a role in facilitating the severity of the damage via the edge effects near discontinuities. Hence, damage is defined as “local” damage when the edge effects at the discontinuities due to

higher stiffness of the undamaged region have not damped out inside the damage. Beyond the local damage limit, there will be pure membrane stress effect at some place inside the damaged area. Therefore, the extent for local damage can be determined by using the decay lengths of the corresponding shell configuration.

The extent for local damage in a spherical shell can be described by the size of damage covered by an included angle equal to $2\psi_d$ where ψ_d is the decay angle of spherical shell. For cylindrical shells, decay lengths in axial and circumferential directions are different. It is postulated that the extent for local damage in a cylindrical shell depends on the aspect ratio of the equivalent rectangular damaged area. For a damaged area with aspect ratio r (= b/a) equal to the ratio of the axial decay length x_l to the circumferential decay length x_c, the extent of local damage in axial and circumferential directions are equal to the decay length in each direction. For damaged areas with other aspect ratios rather than x_l/x_c, interaction of the damage decay lengths has to be considered.

If a damaged spot is larger than the extent of local damage, it means that pure membrane stress has occurred inside the damaged area and thus the failure is as if a "global" damaged spot has occurred. Therefore, for this case, the classical lower bound remaining strength factor RSF_L is used. This implies that if the damage is large enough, RSF_L governs irrespective of geometry and other considerations.

4.3. CLOSURE

The main factors influencing the behavior of pressurized components containing local damages such as corrosion damage or thermal hot spots are geometries of the damage and the shell and material characteristics. These factors have been considered in the proposed Level 2 assessment based on variation principle and the concept of reference volume. The reference volume identifying the volume participates in plastic action for spherical and cylindrical shells can be determined by using decay lengths of each shell. Effective elastic modulus and effective thermal coefficients are also computed by weight average using the reference volume.

Three remaining strength factors exercised in the current study based on integral mean of yield criterion, m_α-multiplier and classical lower bound multiplier are presented. These remaining strength factors are employed in different circumstances as will be discussed further in Chapter 7. The conditions for a damaged to be called “local” and “global” are the presence of membrane action inside the damaged area in which edge effects from the discontinuity have dissipated and become negligible.

CHAPTER 5

FINITE ELEMENT MODELING

Inelastic strength of the pressurized components with a hot spot or corrosion damage can be determined by using nonlinear finite element analysis (FEA). A detailed inelastic FEA provides fairly accurate estimates but can be very expensive in terms of evaluation time and modeling complication. It is not a tool that a practicing engineer in a plant would use on a daily or weekly basis whenever a maintenance check reveals some possibility of damage. In the current research, the nonlinear FEA is done to validate the recommended remaining strength factor (RSF) values obtained from the proposed evaluation method. In that sense, the proposed method is Level 2 assessment while the nonlinear FEA can be taken as Level 3 technique.

This chapter describes the finite element models of thermal hot spots and corrosion damage in spherical and cylindrical pressure vessels. The chosen element types and material models are validated and samples of typical meshing and results are presented.

5.1. GEOMETRY AND CONSTRAINTS

Two geometries of pressure components are studied in the present research, viz., sphere and cylinder. The symmetries of these components are taken into consideration where applicable.

Figure 5.1 shows geometries and boundary conditions of the models employed in the current research. A quarter sphere with a quarter of circular damaged area on top of the sphere is modeled. Symmetries are applied along the two edges of the model. For cylindrical shell, a rectangular damage of dimensions $2a \times 2b$ (in circumferential and axial directions, respectively) is modeled. Two planes of symmetry are assumed to pass through the center of the damage along the shell parallels and meridians. A spherical cap is also modeled at the cut end of the cylinder to account for the longitudinal stress.

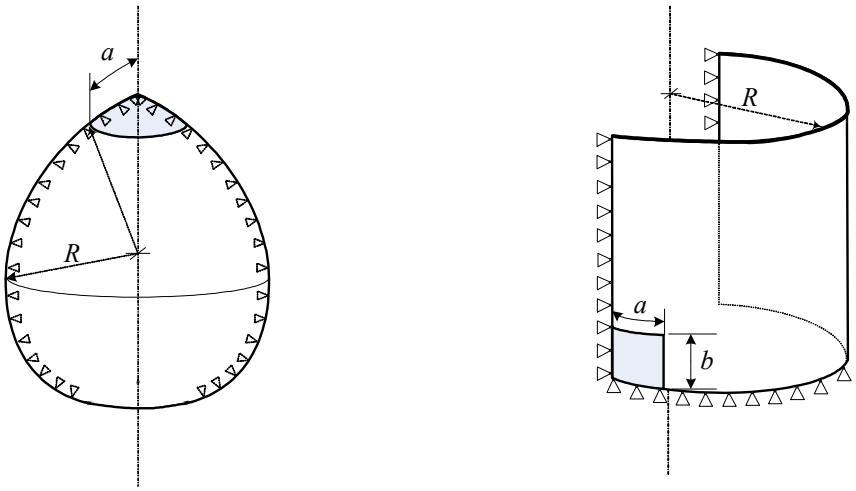

Figure 5.1 Geometries and boundary conditions for finite element analyses (a) Sphere (b) Cylinder.

Different element real constants or material models are assigned to the damaged and undamaged regions in the above models. For corrosion damage, the corrosion spot uses the same material properties as the undamaged part but the element thickness is different. The basis of the current study is based on primary stresses. Since thermal stresses are secondary stresses, thermal analysis is not required in the case of hot spots. The thermal hot spot will only have different material properties (i.e., elastic modulus and yield stress) from the undamaged part. Most structural materials such as steel have lower yield stress at higher temperature. Hence, plastic deformation may occur inside the hot spot even at the design pressure of the pressure vessel.

5.2. FINITE ELEMENT MODEL

Due to the possibility of high bending in the vicinity of the damaged area, shell elements which have rotational degrees of freedom are preferable. Solid elements can be used to model such problems. However, since only translational degrees of freedom are applicable, a number of element divisions through thickness are required in order to accurately represent the bending effects occurring near the edges of damaged portions. This causes the solid-element model to be more expensive in terms of computational time compared with shell-element model and hence is less preferred in the current research.

For the hot spot problem, the finite element models have been constructed by using 8-node structural shell elements (SHELL93) of ANSYS software (Figure 5.2). This element is well suited to model curved shells and has plasticity capability suitable for

material nonlinear analysis. The element has 6 degrees of freedom per node, i.e., translations in *x*, *y* and *z* directions and rotations about the nodal *x*, *y* and *z* axes. An option to store calculated midsurface results (membrane results) in the results file is available in ANSYS. This option to access the correct midsurface results is useful for analyses where averaging the results from top and bottom of the shell elements could sometimes be inappropriate to obtain the midsurface stresses and strains because of the nonlinear material behaviour. The effects of hot spot are simulated by applying the proper material properties (yield stress and modulus of elasticity) consistent with the temperature of the elements in the damaged zone.

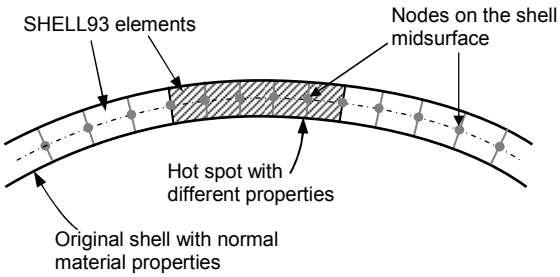

Figure 5.2 The SHELL93 model for thermal hot spot

The metal loss in corroded pressure vessel is modeled by reduced thickness elements in the corrosion zone using 8-node nonlinear layered shell elements SHELL91. The element option for node locations to be at the top, middle or bottom surface of the element (available for this particular shell element in ANSYS) is convenient for modeling different parts of the structure that share the same nodes with different shell thicknesses. At the junction where corroded and uncorroded areas meet, internal corrosion is created

by aligning the outer surfaces of the shell elements in either part while external corrosion is modeled by aligning the inner surfaces of the shell elements. The elements are defined by locating the nodes at the top or bottom surface of the shell instead of at mid-thickness as in the case of hot spot problems. By doing so, the forces and moments are matched at the common nodes as shown in Figure 5.3. Note that the thicknesses of the shells in Figure 5.3 are greatly magnified in order to illustrate the common nodes. The directions of shell normal are verified to ensure the location of common nodes at the top or bottom of the surface.

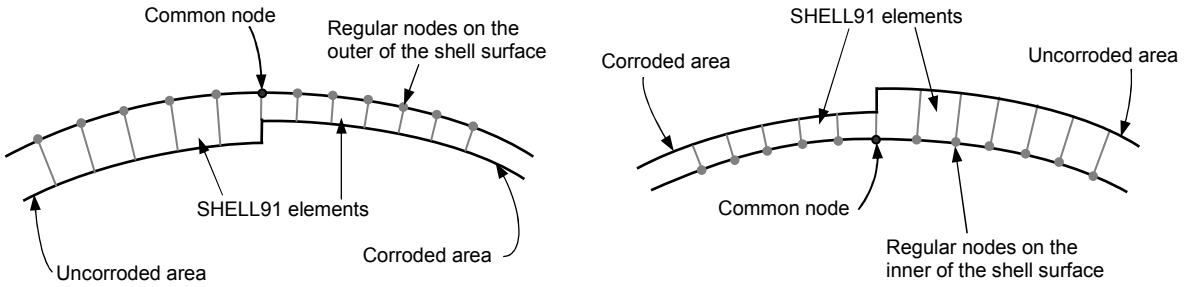

Figure 5.3 Node locations for the SHELL91 model (a) Internal (b) External corrosion

The differential thickness problem can also be tackled by the use of multipoint constraints (MPC). Displacements and rotations of two shell elements (with different shell thicknesses) linked by using MPC elements will be matched. However, in the present study it was not used since SHELL91 element gave satisfactory results. An axisymmetric model has also been used to model spherical shells with circular damage by using 2-D axisymmetric 8-node elements PLANE82. This element has compatible

displacement shapes and is well suited to model curved boundaries. The element has two degrees of freedom per node: translations in the nodal x and y directions. The use of an axisymmetric model can greatly reduce the modeling and analysis time compared to that of an equivalent 3-D model. The results for the same problems using different models are compared and discussed in Sections 5.5.2 and 5.2.3.

A three-dimensional solid modeling of cylindrical components has also been used with solid element SOLID185 in ANSYS. The element is defined by eight nodes having three degrees of freedom at each node - translations in the nodal x, y, and z directions. The element has plasticity capability. Pressures may be input as surface loads on the element faces. As discussed earlier, since solid elements possess only translational degrees of freedom at each node, it is necessary to use an adequate number of elements through the thickness of pressurized components to represent the true stresses especially where high bending occurs such as in the proximity of discontinuity.

All elements are automatically tested for acceptable shape in ANSYS. This testing is performed by computing shape parameters, such as Aspect Ratio, Parallel Deviation, Maximum Corner Angle and Jacobian ratio, which are functions of element geometry, then comparing them to element shape limits. Nothing may be said about an element, one or more warnings may be issued, or it may be rejected with an error. If there are any warnings or error messages, the element models will be re-meshed to eliminate the issue.

In the present research, a mesh convergence study is not explicitly carried out. However, the models have been thoroughly verified by comparing the results for intact

models with known solutions. In addition, the results using different elements (axisymmetric, shell and solid) for the same case of damage have been compared to estimate accuracy of the elastic and inelastic analyses.

5.3. MATERIAL MODEL

It is widely recognized that the design of pipelines and mechanical components based on a limiting elastic stress (or pseudo-elastic stress) may be less economical than that using limiting strain criteria (Walker and Williams, 1995). Structures can be stable and fit-for-purpose even when strained well beyond the yield point. The application of limiting stress criteria for design and strength calculations requires only knowledge of the maximum allowable stress or the specified minimum yield strength (SMYS) of the material whereas strain based design requires more detailed description of material properties or stress-strain relationship.

One of the mathematical formulations broadly used for pipe material is provided by the Ramberg-Osgood formula (Ramberg and Osgood, 1943) given below,

$$\varepsilon = \frac{\sigma}{E} + \frac{\alpha\sigma_0}{E}\left(\frac{\sigma}{\sigma_0}\right)^N \tag{5.1}$$

where, ε is the total strain, σ is the applied stress, E is material modulus, α (plastic yield offset) and N (hardening exponent) are Ramberg-Osgood constants, and σ_0 is the minimum yield stress. It was shown by Walker and Williams (1995) that this model offers well-matched stress-strain curves for pipeline steels.

Table 5.1 Ramberg-Osgood Constants for pipeline and pressure vessel steels

Steel Grade	σ_0 Minimum yield stress (MPa)	ε_0 Yield strain (%)	σ_u Ultimate Tensile Stress (MPa)	ε_u Ultimate Tensile Strain (%)	E Young's Modulus (GPa)	Ramberg-Osgood	
						α Coefficient	N Exponent
API 5L Gr X25	172	0.5	310	34.5	205	4.96	7.49
API 5L Gr X46	317	0.5	434	25.5	205	2.23	13.67
API 5L Gr X70	483	0.5	565	20.0	205	1.13	27.13
A516 Gr. 70	295	0.15	483	21.0	193	1.89	5.84

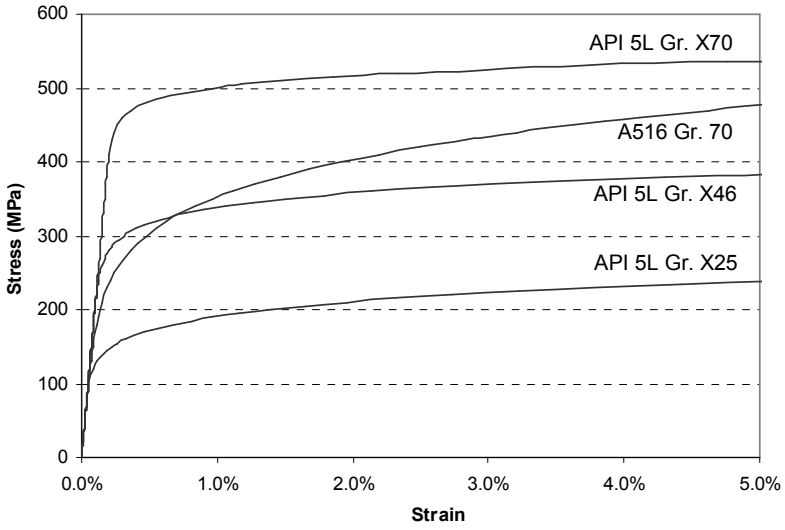

Figure 5.4 Ramberg-Osgood stress-strain relationships for steels

The Ramberg-Osgood constants corresponding to API 5L pipeline steel grades and A 516 pressure vessel plate are shown in Table 5.1 and the stress-strain curves using Ramberg-Osgood formula are shown in Figure 5.4.

It can be seen from Ramberg-Osgood model in Table 5.1 that some strain hardening is present after initial yielding of the material. The ultimate tensile stress for each material is higher than its minimum yield stress by 17% (API 5L X70) to 80% (API 5L X25). Moreover, the ultimate tensile strains are between 20.0% to 34.5% indicating the ductile failure mechanism of pipeline and pressure vessel steel.

Evaluation of a remaining strength factor in the present study assumes a material model almost equivalent to elastic perfectly plastic behavior as shown in Figure 5.5. The Bilinear Kinematic Hardening (BKIN) option in ANSYS, which assumes the total stress range is equal to twice the yield stress is used to represent this material model. This option is suitable for general small-strain use for materials that obey von Mises yield criterion.

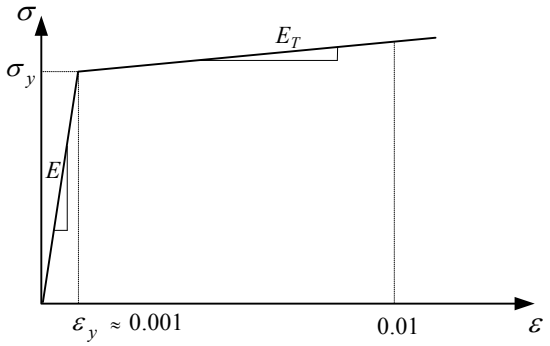

Figure 5.5 Material model for finite element analysis

In Level 2 procedures currently in use (such as modified B31G), the strain hardening aspect is accounted for by the use of flow stress in place of yield stress. This implies that we use an elastic perfectly plastic material which yields at flow stress instead of at the actual material yield point. The calibration for RSF in the current research has also been carried out by adhering to this concept. If we use the flow stress in the proposed calculations, it will automatically account for any strain hardening present in the material. This has been verified by numerical analysis and will be discussed in Section 5.5.1.

API 579 recommends limiting the peak strain at any location of the remaining ligament to 5% when a Level 3 analysis is performed. The limit commonly used in industry is 2% for strains at the surface of shell and 1% for strains averaged through the thickness (ASME, Section III Division 1 Subsection NH). Sims et al. (1992) studied corrosion damage in spheres using the limit for maximum strain inside damaged zone to be 2%. The failure criterion for the present research is taken as von-Mises membrane strain at the center of the damaged area (not peak strain) reaching 1%. Since the study is based on primary stress effects, a 1% limit is justifiable. Although such materials as carbon steel are known to have much higher failure strain than 1% at actual failure rupture, the present criterion is applied to assure the serviceability of the component since excessive deformation in the damaged area can interfere with other functions.

The material used in the current research is SA 516 Grade 55, which is a common carbon steel for pressure vessels. The material properties including modulus of elasticity, thermal coefficients and yield stress for different temperatures are shown in Table 5.2.

Table 5.2 Material Properties for SA 516 Grade 55

Temperature (°F)	100 (37.8 °C)	200 (93.3 °C)	300 (149 °C)	400 (204 °C)	500 (260 °C)	600 (316 °C)
E ($\times 10^6$ psi)	29.3	28.8	28.3	27.7	27.3	26.7
α ($\times 10^{-6}$ in./in./°F)	5.53	5.89	6.26	6.61	6.91	7.17
σ_y (ksi)	30.0	27.3	26.6	25.7	24.5	22.2

The temperature of the metal for the present research is assumed to be between 100 °F (37.8 °C) and 600 °F (316 °C). As mentioned earlier, plastic modulus E_T is assumed to be very small compared to elastic modulus of the material. For example, at temperature 100°F (37.8 °C), E_T is equal to 138 MPa (20 ksi) compared to elastic modulus $E = 202 \times 10^3$ MPa (30×10^3 ksi). If actual strain hardening is higher than the assumed value, flow stress can be used to account for the strain hardening as discussed before. In this case, the stress at 1% strain is equal to 208 MPa (30.2 ksi) or $1.01\sigma_y$. If we use the "flow stress" in place of yield stress, this model will result in a total stress slightly greater than $1.1\sigma_y$ at "failure". Indermohan and Seshadri (2004) used elastic-plastic material model with plastic modulus of 3.45×10^3 MPa (500 ksi) in his finite element analysis, along with limit of 1% strain as in the present study. This leads to yield stress at

1% strain of $1.15\sigma_y$ which can be considered somewhat high and can be unconservative in some cases.

An additional failure criterion to control excessive deformation due to bulging of the component is limiting the out-of-roundness ratio of the component to 1.01 as discussed in Section 6.6.

5.4. SAMPLES OF TYPICAL MESH

Typical meshes of finite element models for spherical and cylindrical pressure vessels using shell elements are shown in Figure 5.6. Higher mesh density has been used inside the damaged area and its neighborhood.

Internal pressure is applied to the pressure components in a series of small incremental steps by using the automatic time stepping feature. This feature responds to plasticity by reducing the load step size after a load step in which a large number of equilibrium iterations were performed or in which a plastic strain increment greater than 15% was encountered. If too large a step was taken, the program bisects the load increment and proceeds using a smaller step size.

Figure 5.7 shows typical bulging that occurs inside a corroded area or hot spot. The membrane strain calculated at midsurface of the shell is obtained at the center of the damage. The inelastic collapse load (pressure) for a component containing hot spot or corrosion corresponds to the time step for which 1% von-Mises strain occurs. Note that as

mentioned earlier, this does not indicate physical collapse. It is merely a limit condition imposed to obtain a limit load. The actual structure may have more reserve strength (due to margin for error in parameters) if excessive strains and serviceability are not a consideration.

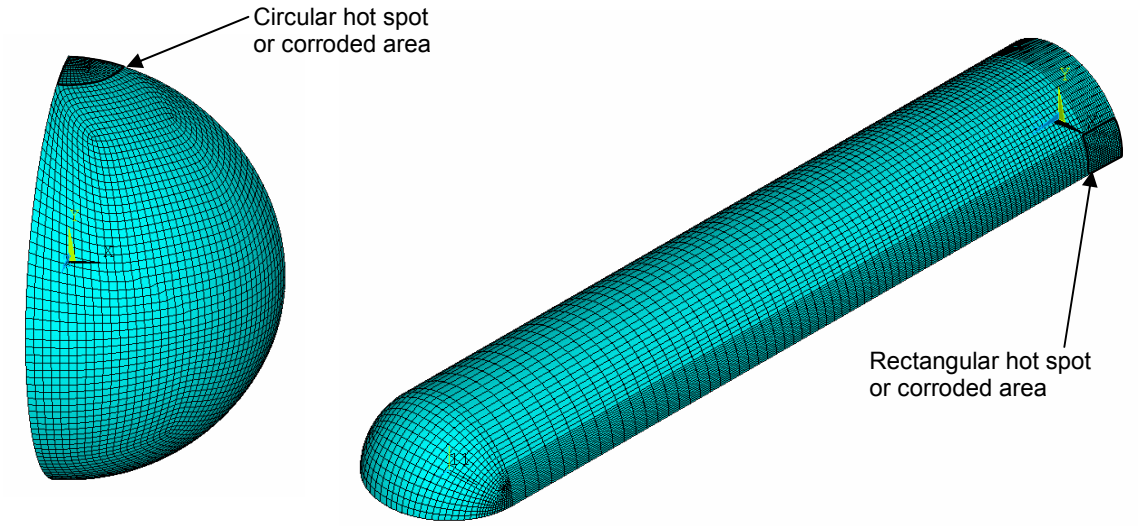

Figure 5.6 Typical meshes for sphere and cylinder

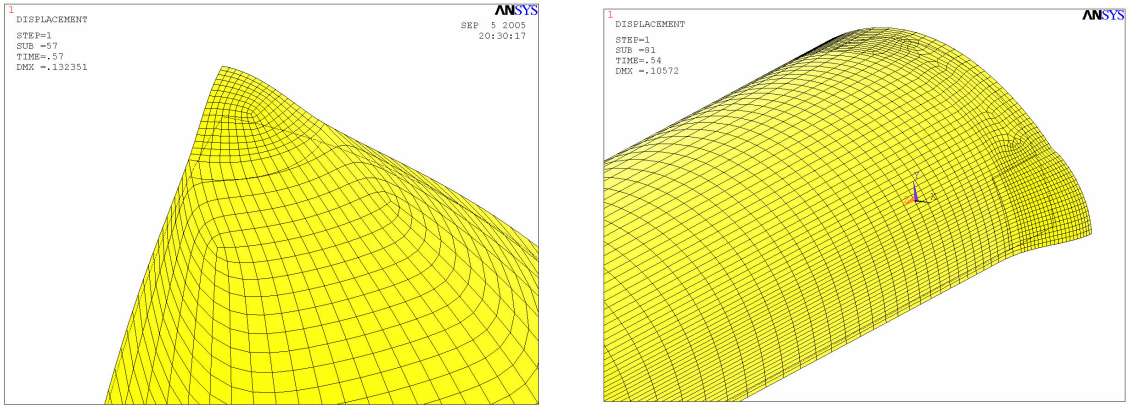

Figure 5.7 Typical bulging in sphere and cylinder with local damage

Typical mesh and bulging in an axisymmetric model for corrosion damage in a sphere are shown in Figure 5.8. The sharp discontinuities at the junction of the corroded and uncorroded areas are replaced by using a fillet to minimize stress concentration at the rim. This is typical of corrosion damage where the thickness usually tapers down from undamaged thickness to the corroded thickness rather than abruptly changing at the junction.

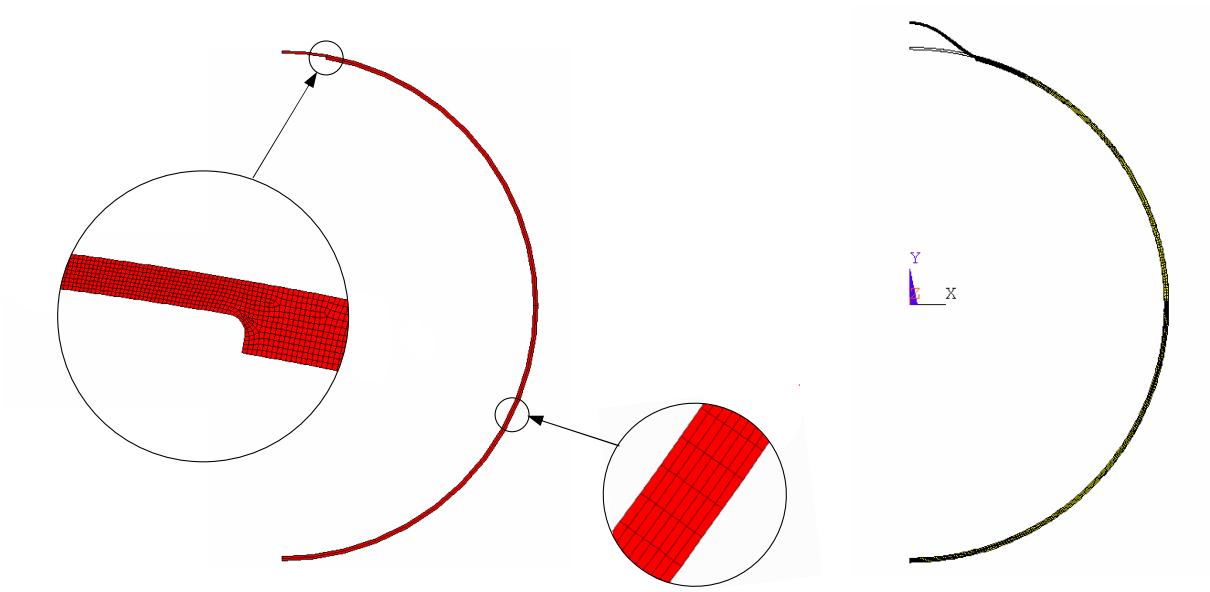

Figure 5.8 (a) Typical mesh (b) Bulging in sphere using axisymmetric elements

Typical 3-D solid models for internal and external corrosion damage in cylinder are shown in Figure 5.9. The mesh is similar to that of the shell model but uses six to ten solid elements through thickness to guarantee proper transmission of bending stresses, if any.

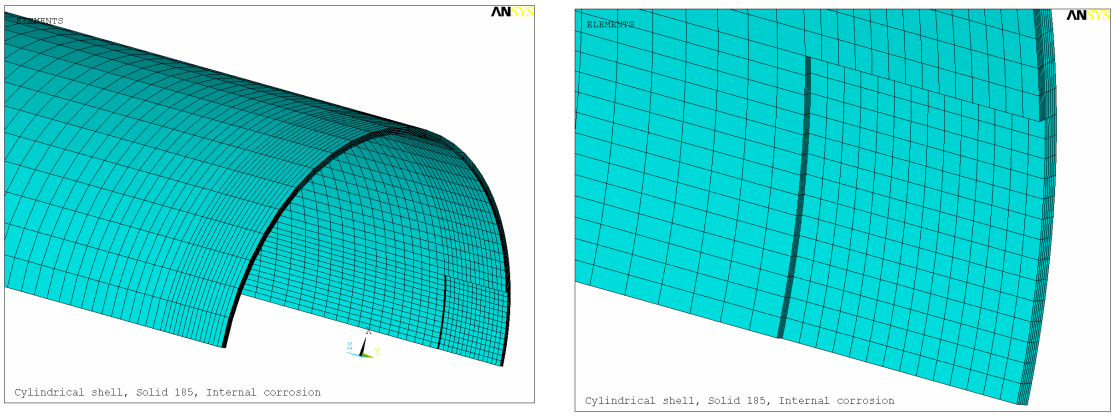

(a)

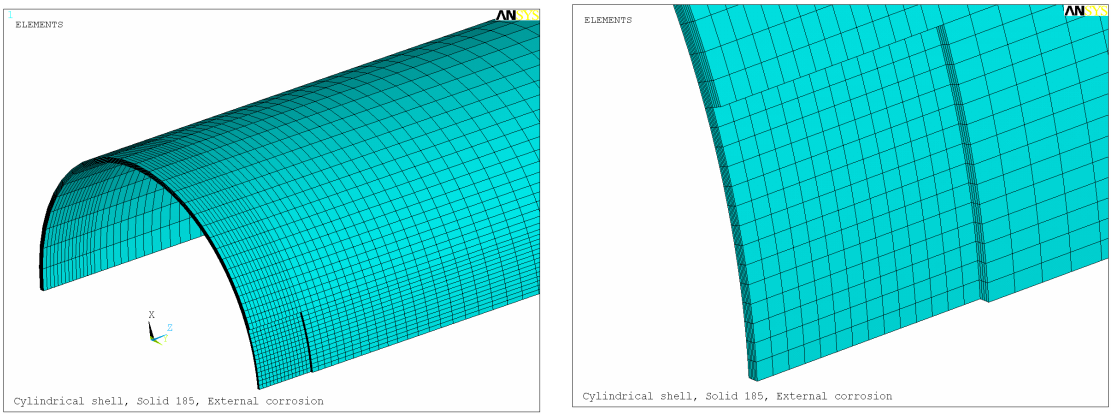

(b)

Figure 5.9 Solid-element models for (a) Internal corrosion (b) External corrosion

5.5. INELASTIC ANALYSIS USING DIFFERENT MODELS

This section discusses inelastic results obtained from different material models and element types. Different material models are employed to verify the use of flow stress to account for strain hardening of the material. Results from FE models using different element types are compared and verified to be similar.

5.5.1. Comparison of Different Material Models

The material model used in FE analysis for the present study is elastic-plastic model with very little strain hardening as explained in Section 5.3. As discussed earlier, strain hardening present in the material is commonly accounted for by the use of flow stress in lieu of yield stress in the calculation procedure. Three different material models are used to verify this concept (Figure 5.10). Model 1 is the elastic-perfectly plastic material model. Model 2 uses flow stress of $1.1\sigma_y$ (similar to that used in ASME B31G) instead of yield stress along with very little post yield strain hardening. Model 3 is a strain hardening similar to that present in the actual material. These models are used to compute the limit pressure for spherical shell with R/h ratio and different damage sizes.

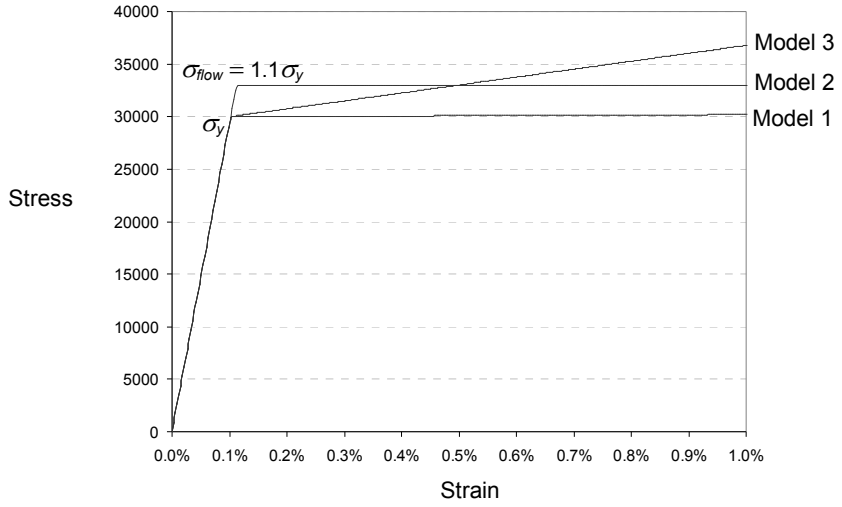

Figure 5.10 Material models using yield stress, flow stress and strain hardening

The limit pressures obtained from the three models are shown in Table 5.3. It can be seen that the limit pressures obtained from FE analysis using model 2 (flow stress

model) and model 3 (strain hardening model) are similar and approximately 1.1 times of those from the model 1 used. Hence, strain hardening present in the material can be accounted for by using the flow stress in the proposed calculations in place of yield stress.

Table 5.3 Comparison of the limit pressures obtained from different material models

R/h	h_c	φ_a	Limit Pressure from model 1, P_1 (psi)	Limit Pressure from model 2		Limit Pressure from model 3	
				P_2 (psi)	P_2/P_1	P_3 (psi)	P_3/P_1
58.4	$h/2$	5°	850	955	1.123	950	1.118
58.4	$2h/3$	12°	733	810	1.105	807	1.101
58.4	$2h/3$	25°	682	751	1.100	751	1.100
20.0	$h/2$	5°	2823	3160	1.119	3167	1.122
20.0	$2h/3$	12°	2605	2860	1.098	2870	1.102

5.5.2. Models for Spherical Shell

The limit pressure for spherical shells with corrosion damage can be obtained from the axisymmetric model using PLANE82 elements or the shell model using SHELL93 elements as explained earlier. The results from both models for corrosion damage of various sizes and remaining thicknesses for spheres are compared in Table 5.4.

Table 5.4 Comparison of limit pressure from PLANE82 axisymmetric model and SHELL91 model for corrosion damage

R/h	h_c	φ_a	Limit pressure		Percent Difference
			PLANE82	SHELL91	
20.0	$5h/6$	5°	2928	2997	2.5 %
20.0	$5h/6$	8°	2790	2826	2.8 %
20.0	$5h/6$	15°	2778	2658	4.0 %
20.0	$h/2$	15°	1671	1620	3.0 %
58.9	$5h/6$	5°	964	985	2.5 %
58.9	$h/2$	5°	734	767	4.6 %
58.9	$h/2$	8°	583	573	1.8 %

It can be seen that both models give comparable results with less than 5% difference which is considered acceptable in numerical analysis.

Similarly, the inelastic results from the PLANE82 axisymmetric model and the SHELL93 model are compared for various sizes of hot spots and temperatures in Table 5.5. The results from both models have difference less than 2.5%. Hence, the axisymmetric models which require less computational effort and are easier to interpret are favorable for both types of damage.

Table 5.5 Comparison of limit pressure from PLANE82 axisymmetric model and SHELL93 model for thermal hot spot damage

R/h	T_h	φ_a	Limit Pressure		Percent Difference
			PLANE82	SHELL93	
20.0	600 °F	8°	2718	2766	1.8 %
20.0	600 °F	12°	2556	2595	1.5 %
20.0	200 °F	12°	2793	2856	2.3 %
58.9	600 °F	5°	965	956	0.9 %
58.9	600 °F	7°	915	910	0.6 %
58.9	200 °F	7°	990	997	0.7%

More comparisons of the results from the two models for other cases are given in Appendix A.

5.5.3. Models for Cylindrical Shell

The limit pressure for cylindrical shells with corrosion damage can be obtained from the shell model using SHELL91 elements with node location option, or the solid element using SOLID185 as explained earlier. The results from the two models for corrosion damage of various sizes, aspect ratios and remaining thicknesses for cylinders are compared in Table 5.7. It can be seen that the results from both models are

comparable. The differences of inelastic results from different models are within 6%. Although the SOLID185 model requires somewhat more computational effort than the SHELL91 model, the modeling is simpler and post-processing procedures are straightforward. Thus, the solid model is employed in the current study of corrosion in cylindrical shells.

Table 5.6 Comparison of the results from inelastic analysis using different models for corrosion damage in cylinders (R/h = 33.6)

h_c	a (in.)	b (in.)	Limit Pressure		Percent Difference
			SHELL91	SOLID185	
$h/2$	5	5	675	658	0.3%
$h/2$	10	10	560	558	2.6%
$2h/3$	10	10	730	725	0.7%
$h/2$	3	9	640	605	5.8%
$h/2$	20	4	671	675	4.7%

5.6. CLOSURE

The present chapter discusses finite element modeling for damage in spherical and cylindrical components. The element models, material models and typical mesh applied to the current study are explained in detail. Finite Element Analysis based on these models is used to determine the "exact" inelastic remaining strength for damaged components. The finite element analyses are regarded as Level 3 assessment and are conducted to verify the effectiveness of the proposed Level 2 evaluation procedures.

CHAPTER 6

DECAY LENGTHS IN SHELLS

This chapter presents the derivation of decay lengths for spherical and cylindrical shells. Decay (or characteristic) length can be estimated by evaluating the effect of a local force (or moment) on the shell configuration. The decay length is defined as the distance from the applied force (or moment) to the point where the effect of the force is almost completely dissipated or becomes negligible. A large decay length generally indicates a large adjacent volume participating in energy dissipation. Thus, if a similar force is applied, the type of structure which possesses larger decay lengths can dissipate a larger amount of energy and therefore has higher loading capacity than that with smaller decay lengths. A small decay length suggests severe local effects due to the applied forces.

Decay lengths for spherical shells will be first investigated based on elastic solutions of shell loaded by concentrated normal force and edge effect bending moments. A conservative decay length will be proposed based on comparison of the effects from both cases for various R/h ratios. For cylindrical shells, a decay length in axial direction is

obtained from solutions to axisymmetric loading while a decay length in circumferential direction is estimated by using solutions to Donnell's differential equations (Donnell,1933) subjected to line load along generator.

It must be noted that the decay lengths studied in the current research are based on elastic analysis. The elastic decay lengths are likely to be smaller than those calculated from plastic analysis due to stress redistribution in structures undergoing plastic deformation. This might lead to an overestimation of the damage severity and thus result in conservative approximation of remaining strength factors. However, results from nonlinear finite element analysis show that the proposed elastic decay lengths are not much different from plastic decay lengths. Hence, the use of elastic analysis for estimating decay lengths, although slightly conservative, is justified. Justification of the proposed decay lengths is discussed in detail in Section 6.3.

6.1. DECAY LENGTHS FOR SPHERICAL SHELLS

The decay lengths (or angles) in spherical shells are approximated from the effects of a concentrated normal force and edge bending moments to the shell (Tantichattanont, 2006a) The decay angles computed in both cases are compared for a range of practical R/h ratios and a conservative decay angle for spherical shell is suggested.

6.1.1. Spherical Shell Loaded with Concentrated Normal Force

Lukasiewicz (1979), among others, has discussed the problem of spherical shells extensively. The shell differential equations in terms of the radial displacement *w* and stress function Φ, take the form:

$$\left(\nabla^2+\frac{2}{R^2}\right)\left[D\left(\nabla^2+\frac{1+\nu}{R^2}\right)w-\frac{1}{R}\left(1-\frac{h^2}{5(1-\nu)}\nabla^2\right)\Phi\right]=\left[1-\frac{(2-\nu)h^2}{10(1-\nu)}\nabla^2\right]P_z$$

$$\left(\nabla^2+\frac{2}{R^2}\right)\left[\frac{1}{Eh}\left(\nabla^2+\frac{1-\nu}{R^2}\right)\Phi+\frac{w}{R}\right]=-\frac{\nu}{2E}\nabla^2 P_z \qquad (6.1)$$

where, *R* is the mean radius, *h* is the shell thickness, ν is the Poisson's ratio, P_z is the component of body forces normal to the shell surface, and *E* is the modulus of elasticity of the material. The flexural rigidity of the shell is expressed as $D = \frac{Eh^3}{12(1-\nu^2)}$, and $\nabla^2=\frac{1}{l^2}\left(\frac{\partial^2}{\partial x^2}+\frac{\partial^2}{\partial y^2}\right)$ is the Laplacian operator in terms of $x=\bar{x}/l$ and $y=\bar{y}/l$, where, *l* is a certain characteristic length.

Consider a spherical shell loaded by a concentrated normal force *P* in the outward normal direction as shown in Figure 6.1. The force can be represented by means of a Fourier integral. The closed form expression for radial displacement *w* is obtained as,

$$w=\frac{Pl^2}{2\pi D}\{f_1+f_2+f_3+f_4\} \qquad (6.2)$$

where, $l = \frac{\sqrt{Rh}}{\sqrt[4]{12(1-\nu^2)}}$ and k_R $(= l^2/R^2)$ is the coefficient characterizing the thinness of the shell, $f_1 = -\text{kei}\, r$, $f_2 = -k_R\left[(1+\nu)\left(\frac{\pi}{2} Y_o(r\sqrt{2k_R}) + \ker r\right) + \frac{1}{2} r \ker' r\right]$, $f_3 = (\eta - \varepsilon)\ker r$, and $f_4 = \frac{\eta}{4} r \ker' r$, r is the distance along x-axis as shown in Figure 6.1, and $Y_o(r\sqrt{2k_R})$ is the Bessel function of the second kind. The functions ker r, kei r are the real and imaginary parts of the Kelvin function, K_ν, stated as $e^{-\nu\pi i/2} K_\nu(ze^{\pi i/4}) =$ $\ker_\nu z$ + $\text{kei}_\nu z$ and $\ker' r$ is the first derivative of ker r with respect to r. For an isotropic shell, $\varepsilon = \frac{\nu h^2}{10(1-\nu)l^2}$, $\eta = \frac{h^2}{5(1-\nu)l^2}$, where, ε and η are coefficients expressing the effects of stress normal to middle surface and the effects of transverse shear deformation, respectively.

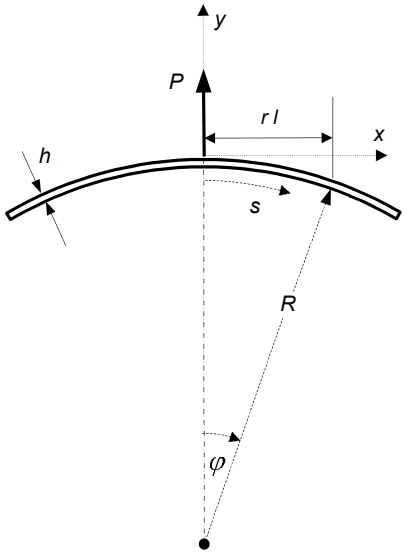

Figure 6.1 A spherical shell subjected to normal concentrated force

The function f_1 in Eq. (6.2) corresponds to Reissner's solution obtained by means of the theory of shallow shells, f_2 presents the result of the use of the complete non-shallow shell equations (6.1a) and (6.1b), and f_3 and f_4 are the effect of transverse shear and normal deformations.

The radial displacement *w* has a peak near the loading point and decays drastically away from this point in an oscillating pattern. The amplitude of *w* in the second and subsequent half waves is considerably smaller compared to that in the first half wave. The decay length, $r_d l$, can be chosen as the distance from the loading point to the first point where zero radial displacement occurs. This location is taken as the characteristic decay location for the current study. It may be noted that other decay locations can be used with slightly varying results, e.g., Seshadri (2004) used the decay location as the point where the amplitude drops to $e^{-\pi} \times$ peak value.

The normalized radial displacement $\overline{w}$ (= $\frac{2\pi w}{P}$) as stated in Eq. (6.2) is then plotted against the nondimensional distance, *r*, for a range of practical *R*/*h* ratios (Figure 6.2). The values of the decay parameter r_d for different *R/h* ratios are shown in Table 6.1. It can be seen that the values of r_d vary from 3.91 to 4.28 for all practical *R/h* values. This range is reasonably narrow. Hence, the conservative value of 3.91 is applied in the derivation below.

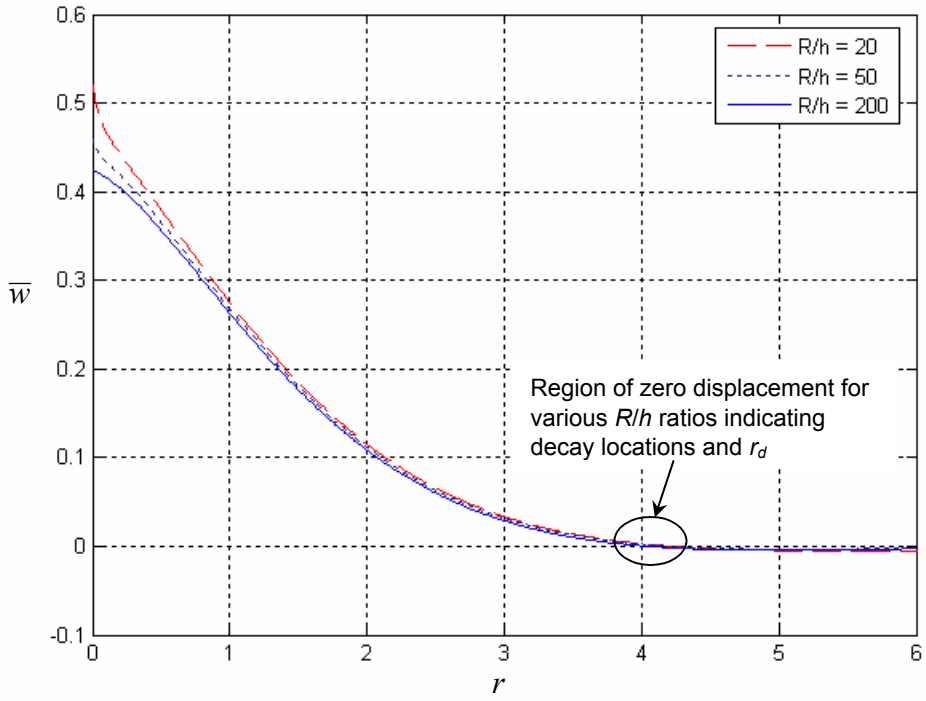

Figure 6.2 Radial displacement for different R/h ratios

Table 6.1 Values of r_d for different R/h ratios

R/h	10	20	30	50	70	100	150	200
r_d	3.91	4.22	4.28	4.25	4.19	4.14	4.08	4.05

For spherical shells, a decay angle gives better perception of the extent of the shell involved in local effects and therefore will be used in lieu of the decay length. From Figure 6.1, the distance along x-axis can be written in terms of the angle to the apex as,

$$rl = R\sin\varphi \tag{6.3}$$

For Poisson's ratio $\nu = 0.3$, the characteristic length l of Eq. (6.2) becomes,

$$l = 0.5501\sqrt{Rh} \tag{6.4}$$

Substitution of $r_d = 3.91$ and l (from Eq. (6.4)) into Eq. (6.3) leads to the expression for the decay angle φ_d for a spherical shell loaded by concentrated normal force as,

$$\varphi_d = \arcsin\left(\frac{r_d l}{R}\right) = \arcsin\left(\frac{2.1454}{\sqrt{R/h}}\right) \tag{6.5}$$

It can be seen from Eq. (6.5) that the elastic decay angle of spherical shell is simply a function of R/h ratio, which specifies the thinness of the shell under consideration. Thin shells have smaller decay angles indicating less amount of energy the structures can absorb when subjected to localized damage.

6.1.2. Edge Rotational Effect on Decay Length

In the subsection above, the decay angle has been computed through the use of a point load on the shell. This simulates the decay in the meridian direction due to the shear at the rim of the hot spot or the corroded area. Similar decay angles can be obtained due to the edge moments along the rim of the damaged area.

In order to simulate the effects of moments along the rim of a hot spot or corroded area, spherical shells subjected to uniform surface pressure p are studied for two cases, viz., edges fixed against translation and rotation, and edges fixed against rotation but not against translation. The actual effect of the edge moments along the rim of the damaged area is likely to be in between the two cases.

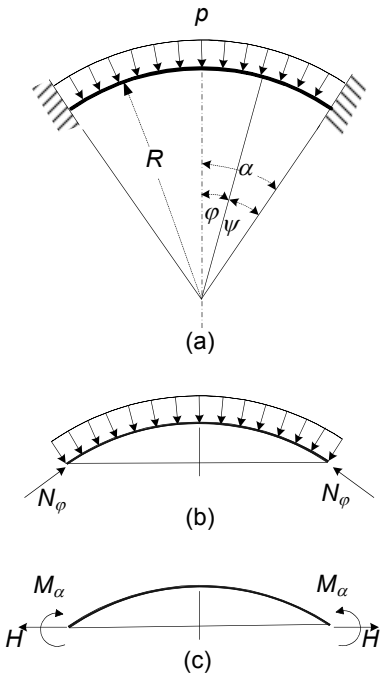

Figure 6.3 (a) A spherical shell with built-in edges subjected to normal pressure (b) Membrane stresses (c) Superposed edge conditions

By applying $r_1 = r_2 = R$ to the operator $L(\cdots)$ as stated in Eq. (2.26) in Chapter 2, Timoshenko (1970) showed that the operator $L(\cdots)$ for a spherical shell of constant thickness becomes

$$L(\cdots) = \frac{1}{R}\left[\frac{d^2(\cdots)}{d\varphi^2} + \cot\varphi\frac{d(\cdots)}{d\varphi} - \cot^2\varphi(\cdots)\right] \tag{6.6}$$

Using Eqs. (2.27), stresses of spherical shells with constant thickness loaded symmetrically with respect to its axis can be described by using two differential equations of the second order as,

$$\frac{d^2Q_\varphi}{d\varphi^2} + \cot\varphi\frac{dQ_\varphi}{d\varphi} - (\cot^2\varphi - \nu)Q_\varphi = EhV$$

$$\frac{d^2V}{d\varphi^2} + \cot\varphi\frac{dV}{d\varphi} - (\cot^2\varphi + \nu)V = -\frac{R^2Q_\varphi}{D} \tag{6.7}$$

where, Q_φ is the shearing force, the angle φ is as shown in Figure 6.3, and V is the angle of rotation of a tangent to a meridian defined by

$$V = \frac{1}{R}\left(v + \frac{dw}{d\varphi}\right) \tag{6.8}$$

where, v and w are displacement components in meridian and radial directions, respectively.

The solutions for Eqs. (6.7) can be estimated by the method of asymptotic integration and a satisfactory approximation for the shearing force can be obtained as,

$$Q_\varphi = Ce^{-\lambda\psi}\sin(\lambda\psi - \gamma) \tag{6.9}$$

where, $\psi = \alpha - \varphi$, α is the angle from the crown to the edge of the sphere, the constants C and γ are to be determined from the edge conditions at $\varphi = \alpha$, and λ is obtained from

$$\lambda^4 = 3(1-\nu^2)\left(\frac{R}{h}\right)^2 \tag{6.10}$$

Since λ is large in the case of thin shells, the derivative of Q_φ is large in comparison with the function itself, and the second derivative is large in comparison with the first. Equation (6.7a) can then be approximated as

$$\frac{d^2 Q_\varphi}{d\varphi^2} = EhV \tag{6.11}$$

Therefore, we obtain the expression for the angle of rotation

$$V = \frac{1}{Eh}\frac{d^2 Q}{d\varphi^2} = -\frac{2\lambda^2}{Eh} Ce^{-\lambda\psi} \cos(\lambda\psi - \gamma) \tag{6.12}$$

The bending moments can be determined as

$$M_\varphi = \frac{D}{R}\frac{dV}{d\varphi} = \frac{R}{\lambda\sqrt{2}} Ce^{-\lambda\psi} \sin\left(\lambda\psi - \gamma + \frac{\pi}{4}\right)$$

$$M_\theta = \nu M_\varphi = \frac{\nu R}{\lambda\sqrt{2}} Ce^{-\lambda\psi} \sin\left(\lambda\psi - \gamma + \frac{\pi}{4}\right) \tag{6.13}$$

In the case of a spherical shell with a built-in edge subjected to a uniform normal pressure p as shown in Figure 6.3a, the membrane force (Figure 6.3b) can be calculated from equilibrium of forces in vertical direction as

$$\pi(R\sin\alpha)^2 p + (\pi R\sin\alpha)(N_\varphi \sin\alpha) = 0 \tag{6.14}$$

This results in uniform compression of the shell

$$N_\varphi = N_\theta = -pR/2 \tag{6.15}$$

The edge of the shell as shown in Figure 6.3b experiences no rotation and undergoes a horizontal displacement

$$\delta = \frac{R\sin\alpha}{Eh}(N_\theta - \nu N_\varphi) = \frac{-pR^2(1-\nu)}{2Eh}\sin\alpha \tag{6.16}$$

The membrane force in Figure 6.3b is superposed with the horizontal forces and the moments uniformly distributed along the edge as shown in Figure 6.3c. These forces and moments are of such magnitude that the corresponding horizontal displacement is equal and opposite to the displacement caused by the membrane compression, and the corresponding rotation of the edge is equal to zero. This leads to,

$$M_\alpha = \frac{-pR^2(1-\nu)}{4\lambda^2}$$

$$H = \frac{2\lambda}{R\sin\alpha}M_\alpha = -\frac{pR(1-\nu)}{2\lambda\sin\alpha} \tag{6.17}$$

The negative signs indicate that M_α and H have directions opposite to those shown in Figure 6.3c. The edge conditions can then be expressed as

$$(M_\varphi)_{\varphi=\alpha} = M_\alpha \quad \text{and} \quad (N_\varphi)_{\varphi=\alpha} = \frac{H}{\cos\alpha} \tag{6.18}$$

Substitution of ψ = 0 into Eqs. (6.9) and (6.13) leads to

$$(M_\varphi)_{\psi=0} = \frac{R}{\lambda\sqrt{2}} C \sin(-\gamma + \frac{\pi}{4}) = \frac{-pR^2(1-\nu)}{4\lambda^2}$$

$$(N_\varphi)_{\psi=0} = \left(-Q_\varphi \cot(\alpha - \psi)\right)_{\psi=0} = -C \cot\alpha \sin\gamma = \frac{pR(1-\nu)}{2\lambda \sin\alpha \cos\alpha} \qquad (6.19)$$

The constants C and γ for spherical shells with built-in edges subjected to uniform pressure p can then be determined by using Eqs. (6.17), (6.18) and (6.19) as

$$C = \frac{-pR(1-\nu)}{2\lambda \cos^2\alpha} \frac{1}{\sin\gamma}$$

and

$$\gamma = \tan^{-1}\left(\frac{1}{1+\cos^2\alpha}\right) \qquad (6.20)$$

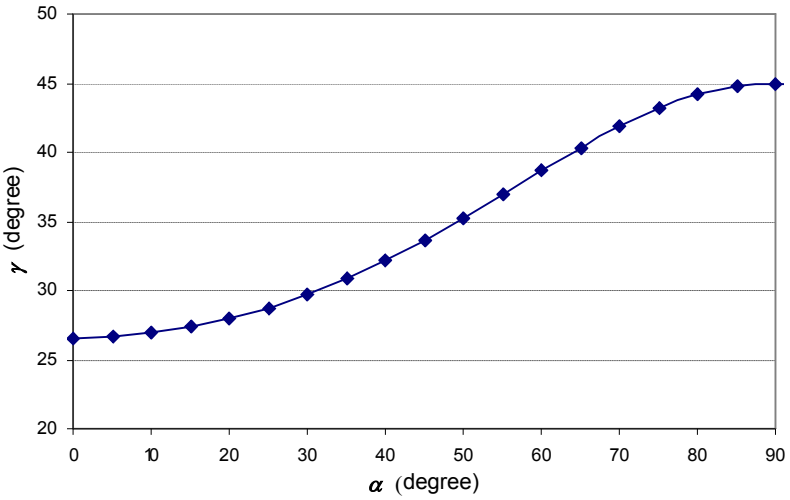

Figure 6.4 The phase shift constant (γ) for angle of fixed-edges (α) ranging from 0° to 90°

It is noticed that the constant C is the magnification factor for functions (6.9) and (6.13), whereas, γ corresponds to the phase shift of the sine function and directly affects

the decay length. For α less than 90°, the angle γ has the value ranging from 26.5° to 45.0° as shown in Figure 6.4.

Similarly, for spherical shells with edge moments where the rotations are restrained and the displacements are allowed, the boundary conditions are

$$(M_\varphi)_{\varphi=\alpha} = M_\alpha \quad \text{and} \quad (N_\varphi)_{\varphi=\alpha} = 0 \tag{6.21}$$

From Eqs. (6.19) and (6.21), the constant γ is equal to zero.

If radial displacements and rotations at the edges of spherical shells are not restrained, the boundary conditions are $(M_\varphi)_{\varphi=\alpha} = 0$ and $(N_\varphi)_{\varphi=\alpha} = H$ and the constant γ is equal to 45°. This is similar to the fixed-fixed case with α = 90°.

In each case, the effects of edge bending moments are considered negligible after the first half sine wave of Eqs. (6.13). This is the same as the angle inside the sine term being equal to $\frac{\pi}{2}$. The angle ψ_1 at which zero moments first occur is

$$\psi_1 = \frac{1}{\lambda}\left(\frac{3\pi}{4} + \gamma\right) \tag{6.22}$$

It can be seen that the decay angle ψ_1 depends on the value of λ, which represents the thinness of the shell, and the angle γ, which is an integration constant satisfied by boundary conditions.

If the damaged spot is very flexible compared to the remaining part, we can assume a sort of fixed support at the damaged area boundary. For this case, the value of γ is given by Eq. (3.20b) $\gamma = \tan^{-1}\left(1/(1+\cos^2\alpha)\right)$. If the damaged spot stiffness is the same as that of the adjacent part, it implies that there is no differential rotation (indicating the presence of rigid connection). For this case, $\gamma = 0$. The actual γ will be between the two extremes.

In the hot spot case, if we assume that the relative stiffness is proportional to the ratio of the Young's moduli of the cold and hot regions, γ can be assumed to vary linearly from that given by $\gamma = \tan^{-1}\left(1/(1+\cos^2\alpha)\right)$ for $E_H/E_C = 0$ to $\gamma = 0$ for $E_H/E_C = 1.0$. It can be shown that for practical values of E_H and E_C, γ values are small. In the case of corrosion damage, the value of γ can vary from 0 to $\frac{\pi}{4}$.depending on the boundary conditions. Therefore, a conservative value of $\gamma = 0$ is assumed for all cases. The decay angle ψ_d can be calculated for $\nu = 0.3$ as,

$$\psi_d = \frac{3\pi}{4\lambda} = \frac{3\pi}{4}\left[\frac{1}{2.73}\left(\frac{h}{R}\right)^2\right]^{1/4} = 1.833\sqrt{\frac{h}{R}} \qquad (6.23)$$

It must be noted that γ and hence ψ_d will have slightly larger values than above if the damaged spot is much more flexible than the adjacent volume.

6.1.3. Comparison of the Decay Angles

The decay angles obtained by using Eqs. (6.5) and (6.23) computed for concentrated loads and edge moments for different *R/h* ratios are plotted in Figure 6.5. Examples of the value of decay angles for some *R*/*h* ratios are also shown in Table 62.

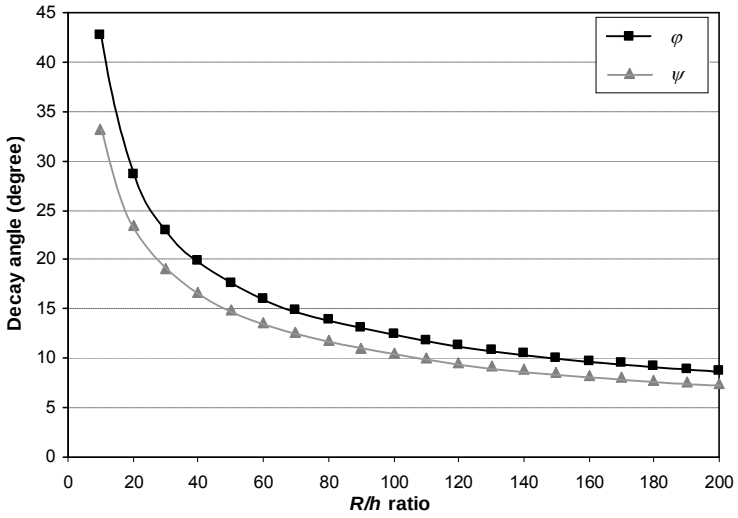

Figure 6.5 The decay angles φ_d and ψ_d for spherical shells of different *R*/*h* ratios

It can be seen that the angle φ_d is only slightly higher than ψ_d for most practical cases. In a real hot spot, the decay length is influenced by both normal loads (pressures) and edge moments at the boundary of hot spots. Therefore, the actual decay angle is likely to be in between φ_d and ψ_d. Conservatively, ψ_d can be used for calculations for Level 2 assessments of decay length since a smaller decay angle would indicate a more adverse effect.

Table 6.2 Decay angles φ_d and ψ_d for different R/h ratios

R/h	20	30	40	50	75	100	200
φ_d (degree)	28.7	23.1	19.8	17.7	14.3	12.4	8.7
ψ_d (degree)	23.5	19.2	17.7	14.9	12.0	10.5	7.4

6.2. DECAY LENGTHS FOR CYLINDRICAL SHELLS

The decay lengths for cylindrical shells in axial and circumferential directions are investigated by using solutions of shells under relevant loading conditions for each case.

6.2.1. Decay Length of Cylindrical Shell in Axial Direction

For circular cylindrical shell subjected to axisymmetric loading, the displacements are independent of the circumferential coordinate *s*. For this case, the expression for radial displacement *w* can be written as (Timoshenko, 1959)

$$\frac{d^4 w}{dx^4} + 4\beta^4 w = 0 \tag{6.24}$$

where, $\beta^4 = \frac{3(1-\nu^2)}{R^2 h^2}$, x is the distance in axial coordinate from the half-length of the cylinder as shown in Figure 6.6 (same as Figure 2.5 repeated here for clarity). Note that

only the homogeneous solution is considered in this case since particular solution is not required for displacement boundary conditions.

The general solution to Eq. (6.24) for radial displacement w can then be written as

$$w = e^{-\beta x}(C_1 \cos \beta x + C_2 \sin \beta x) + e^{\beta x}(C_3 \cos \beta x + C_4 \sin \beta x) \tag{6.25}$$

where, C_1, C_2, C_3 and C_4 are constants obtained from boundary conditions.

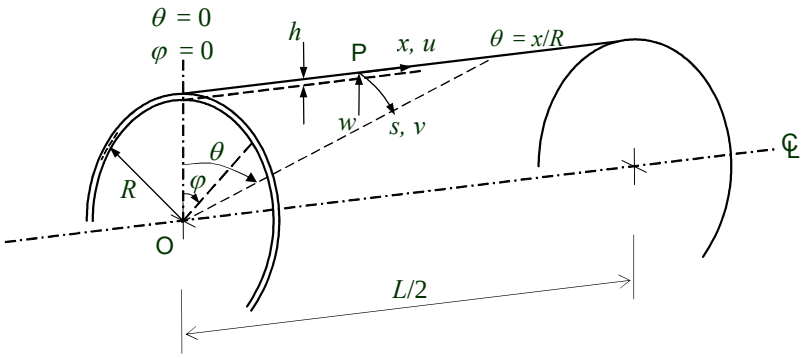

Figure 6.6 Thin Cylindrical Shell

For the displacements to vanish as $x \to \infty$, the constant C_3 and C_4 in Eq. (6.25) must be equal to zero. The constants C_1 and C_2 can be obtained from the symmetry boundary condition, viz., $\frac{dw}{dx} = 0$ at x = 0. Differentiate Eq. (6.25) with respect to x and rearrange the terms, we get $C_1 = C_2$. Hence, the expression for radial displacement is

$$w = C_1 e^{-\beta x}(\cos \beta x + \sin \beta x) \tag{6.26a}$$

or

$$w = \sqrt{2} C_1 e^{-\beta x} \sin\left(\beta x + \frac{\pi}{4}\right) \tag{6.26b}$$

The radial magnitude of the displacement is then described by a descending exponential function with sinusoidal oscillation of period $2\pi/\beta$ as shown in Figure 6.7. Therefore, the magnitude of the radial displacement is bounded by $\sqrt{2}e^{-\beta x}$.

$$x_l = \pi\left[\frac{R^2h^2}{3(1-\nu^2)}\right]^{1/4} \tag{6.26}$$

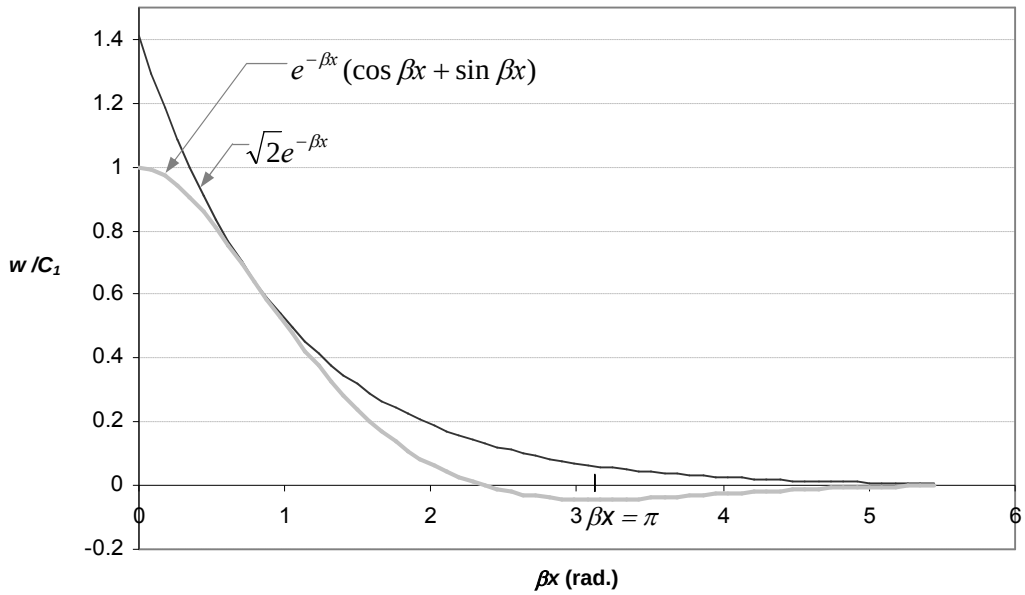

Figure 6.7 Displacement along the axial direction of a cylinder with axisymmetric loading

At some distance away from the origin, the so-called "decay length" or "characteristic length", the displacements will become very small compared to those at the point of the origin and can be considered negligible. The radial displacement diminishes significantly at the distance $x_l = \pi/\beta$ where the bound is $\sqrt{2}e^{-\pi}$ which is 4.3% of that at the point of origin. Therefore, the elastic decay length in longitudinal direction is written as

For general carbon steels used in pressure vessels and piping, taking ν = 0.3, the decay length becomes

$$x_l \approx 2.5\sqrt{Rh} \tag{6.27}$$

Although it was not shown explicitly, this decay length value in the longitudinal direction of cylindrical shells has been incorporated into several Codes at appropriate places. For example, one of the provisions of the API 579 (paragraph 5.4.2.2.d) assessment procedure is the requirement that the locally thinned area (LTA) be located a minimum distance of $L_{msd} = 1.8\sqrt{Dh}$ from the nearest discontinuity where D is the diameter of the shell. This length is essentially equal to $2.5\sqrt{Rh}$ which is the decay length in axial direction for cylinders as derived above.

6.2.2. Decay Length of Cylindrical Shell in Circumferential Direction

Donnell (1933) proposed eighth order governing differential equations for cylindrical shells in which the displacements are decoupled. In the absence of surface loadings, Donnell's equilibrium conditions in a non-dimensional coordinate system are

$$\overline{\nabla}^8\overline{w} + 4k^4\left(\frac{\partial^4\overline{w}}{\partial\theta^4}\right) = 0 \tag{6.28a}$$

$$\overline{\nabla}^4\overline{v} = (2+\nu)\left(\frac{\partial^3\overline{w}}{\partial\theta^2\partial\varphi}\right) + \left(\frac{\partial^3\overline{w}}{\partial\varphi^3}\right) \tag{6.28b}$$

$$\overline{\nabla}^4\overline{u} = \nu\left(\frac{\partial^3\overline{w}}{\partial\theta^3}\right) - \left(\frac{\partial^3\overline{w}}{\partial\theta\,\partial\varphi^2}\right) \tag{6.28c}$$

where, $\overline{\nabla}^2$ is nondimensional Laplace's operator ($\overline{\nabla}^2 = \frac{\partial^2}{\partial\theta^2} + \frac{\partial^2}{\partial\varphi^2}$), the non-dimensional variables are defined as, $\theta = \frac{x}{R}$, $\varphi = \frac{s}{R}$, $\overline{w} = \frac{w}{R}$, $\overline{u} = \frac{u}{R}$, and $\overline{v} = \frac{v}{R}$. The displacements *u*, *v*, and *w* are in axial, circumferential and radial directions as shown in Figure 6.5. The shell characteristic constant *k* is given by $4k^4 = 12\left(1-\nu^2\right)\left(\frac{R}{h}\right)^2$.

Hoff, Kempner and Pohle (1954) suggested closed form solutions to Donnell's equations for the displacements of thin cylindrical shells with radial uniform line load along the generator $\varphi = 0$. The edges $x = \pm L/2$ are assumed to be simply supported, where, *L* is the length of the shell. The simply-supported condition implies that the radial displacement *w* vanishes at the edges. The axial decay length is defined as the distance from the applied force to the location where the effect of the local action dissipates. In other words, the radial displacement at locations further away (in the axial direction) from the origin than the axial decay length will be almost equal to zero. Hence, it is justified to use twice of the axial decay length obtained from Eq. (6.27) as the length of the simply-supported cylinder (or $L = 5\sqrt{Rh}$). This is also confirmed by the length of a cylindrical vessel considered as infinitely long beam suggested by Harvey (1991).

With $-\pi \le \varphi \le \pi$, the solution for radial displacement is assumed in series form as,

$$w_{tot} = w(\varphi) + w(2\pi - \varphi) + w(2\pi + \varphi) + w(4\pi - \varphi) + w(4\pi + \varphi) + \ldots$$

and $$w(\varphi) = Ae^{p\varphi}\cos nx \qquad (6.29)$$

where, $n = m\pi(R/L)$ and m is an odd integer. The constant A and n are assumed to be real while p may be complex. It was shown that the results obtained only from the first term usually have sufficient accuracy. Substitution of w from the latter of Eq. (6.29) into Eq. (6.28a) yields

$$[(p^2 - n^2)^4 + 4k^4n^4]w = 0 \tag{6.30}$$

which must be satisfied identically. Hence,

$$p^2 = n^2 + \sqrt{2}(-1)^{1/4}nk \tag{6.31}$$

Since $\pm i = e^{\pm i\pi/2}$, the fourth root of -1 is $(\sqrt{2}/2)(1-i)$ or $(\sqrt{2}/2)(-1-i)$. Therefore, Eq. (6.31) can be written as

$$\begin{Bmatrix} p_1^2 \\ p_2^2 \end{Bmatrix} = \begin{Bmatrix} n^2 + (1+i)nk \\ n^2 - (1+i)nk \end{Bmatrix} \tag{6.32}$$

where, p_1 and p_2 can be written as $p_1 = -\alpha_1 + i\beta_1$, $p_2 = -\alpha_2 + i\beta_2$, and α_1, α_2, β_1, β_2 are positive real numbers. Substitution of p_1 and p_2 into Eqs. (6.32) and separation of real and imaginary parts gives (Kraus, 1967)

$$\begin{Bmatrix} (\alpha_1^2 - \beta_1^2) + (2\alpha_1\beta_1)i \\ (\alpha_2^2 - \beta_2^2) + (2\alpha_2\beta_2)i \end{Bmatrix} = \begin{Bmatrix} n(n+k) + (nk)i \\ n(n-k) + (nk)i \end{Bmatrix} \tag{6.33}$$

Therefore,

$$\begin{Bmatrix} \alpha_1^2 - \beta_1^2 \\ \alpha_2^2 - \beta_2^2 \end{Bmatrix} = \begin{Bmatrix} n(n+k) \\ n(n-k) \end{Bmatrix} \quad \text{and} \quad \begin{Bmatrix} \beta_1 \\ \beta_2 \end{Bmatrix} = \begin{Bmatrix} nk/2\alpha_1 \\ nk/2\alpha_2 \end{Bmatrix} \tag{6.34}$$

Finally,

$$\begin{Bmatrix} \alpha_1^2 \\ \alpha_2^2 \end{Bmatrix} = \begin{Bmatrix} (n/2)\left\{(n+k) + [(n+k)^2 + k^2]^{1/2}\right\} \\ (n/2)\left\{(n-k) + [(n-k)^2 + k^2]^{1/2}\right\} \end{Bmatrix} \tag{6.35}$$

Note that the conjugate solutions corresponding to the remaining two "fourth roots" of -1, $p_3 = -\alpha_1 - i\beta_1$ and $p_4 = -\alpha_2 - i\beta_2$, are governed by the same relationships as p_1 and p_2. In addition, the positive solution of α_1 and α_2 leads to positive real parts of the exponent p and thus gives displacements which increase without bounds as φ increases.

Equation (6.29) can then be written as

$$\overline{w} = [A_1 e^{-\alpha_1 \varphi} \cos\beta_1\varphi + A_2 e^{-\alpha_1 \varphi} \sin\beta_1\varphi + A_3 e^{-\alpha_2 \varphi} \cos\beta_2\varphi + A_4 e^{-\alpha_2 \varphi} \sin\beta_2\varphi]\cos(n\theta) \tag{6.36}$$

We can plot Eq. (6.36) explicitly to examine the relative influence of α_1 and α_2 for different situations. Figure 6.8 shows the displacement calculated by using the first, second and third harmonics of the series (m = 1, 3 and 5). It can be seen that the second harmonic gives much smaller contribution to the series than the first and the third harmonic is much smaller than the second. Therefore, the radial displacement can be approximately calculated by using only the first harmonic (m = 1).

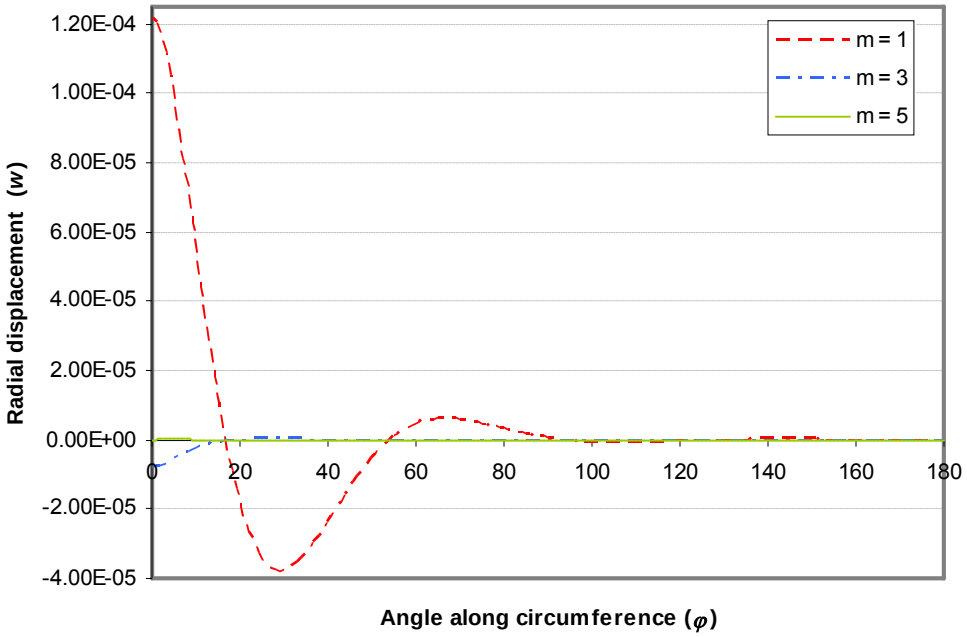

Figure 6.8 Radial displacements obtained by using m = 1, 3 and 5

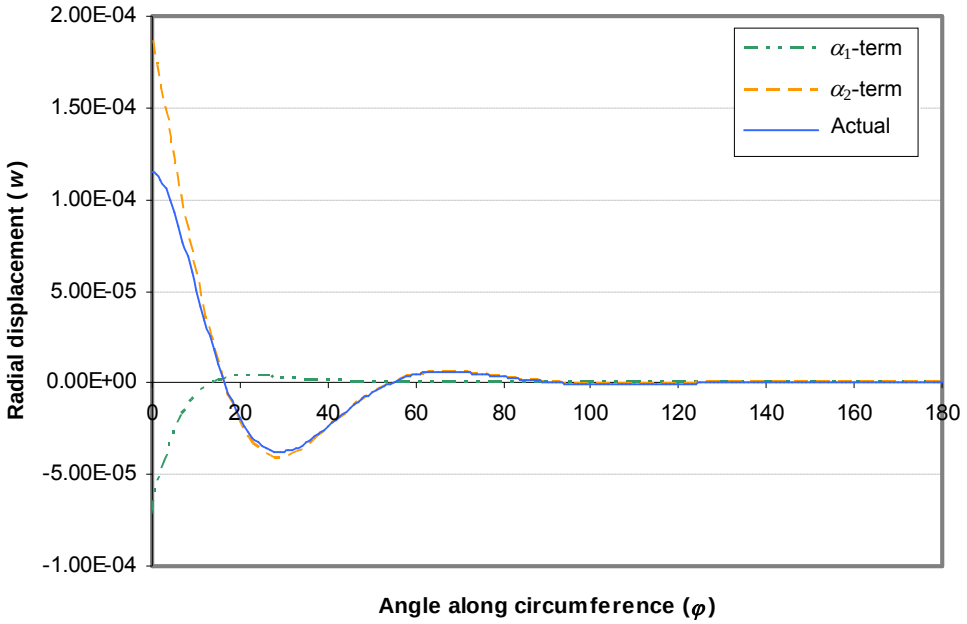

Figure 6.9 Radial displacements obtained from α_1-terms, α_2-terms and all the terms

Figure 6.9 shows the plot of radial displacements computed by using only the α_1-terms (the first and second terms in Eq. (6.36)), only the α_2-terms (the third and fourth terms in Eq. (6.36)), and all the terms in Eq. (6.36). It can be seen that α_2 dominates the displacement pattern. Therefore, only the α_2–terms will be used in the later derivation.

If we consider only the first harmonic (m = 1) and let $L = 5\sqrt{Rh}$ as discussed earlier,

$$n = \frac{m\pi R}{L} = \frac{(1)\pi R}{5\sqrt{Rh}} = 0.6283\sqrt{\frac{R}{h}} \tag{6.37}$$

For ν = 0.3, shell characteristic constant k is

$$k = \sqrt[4]{3(1-0.3^2)\left(\frac{R}{h}\right)^2} = 1.2854\sqrt{\frac{R}{h}} \tag{6.38}$$

Substitution of n and k from Eqs. (6.37) and (6.38) into the second of Eq. (6.35) leads to

$$\alpha_2 = 0.4971\sqrt{\frac{R}{h}} \tag{6.39}$$

Similar to the case of decay length in axial direction, the critical angle φ_c where radial displacement decays considerably is proposed to be at $\varphi_c = \pi/\alpha_2$. The decay length in circumferential direction for cylindrical shell, x_c, can then be calculated from the critical angle φ_c as

$$x_c = \varphi_c R = \pi R/\alpha_2 \approx 6.3\sqrt{Rh} \tag{6.40}$$

It can be seen that the proposed decay length in circumferential direction is much larger than that in longitudinal direction. This may be the result of the curvature of the shell present in the circumferential direction. Justification of the proposed decay lengths in cylindrical shells will be discussed in the following section.

6.3. JUSTIFICATION OF THE PROPOSED DECAY LENGTHS

The decay lengths for spherical and cylindrical shells proposed in the previous sections are justified by performing finite element analysis using ANSYS. The decay lengths (or angles) are taken as the distance from the edge of the damaged area to the location where the local effects dissipate.

6.3.1. Spherical Shells

The elastic decay angle ψ_d for spherical shells as stated in Eq. (6.23) is validated by finite element analyses (FEA) using axisymmetric plane elements based on elastic and elastic-plastic material models Details of FEA modeling are as described in Chapter 5.

The proposed decay angles for *R*/*h* ratios equal to 20 and 58.4 calculated from Eq. (6.23) are 20.3° and 13.2°, respectively. Figures 6.10 and 6.11 show the comparison of the elastic decay angles and the equivalent stress and strain distributions and the radial displacements from elastic analyses for different cases of corrosion damage in spheres

subject to internal pressure. The stress-strain curve is assumed to be linear with elastic modulus equal to 202×10^9 Pa (30×10^6 psi).

Due to high stress concentration at the discontinuity, the parts that experience high local bending stresses can not sometimes be easily differentiated from the adjoining parts using the contour plot for stress and strain distributions (Figure 6.10). However, the local effects can also be identified by using the elastic radial displacement contours (Figure 6.11). It can be seen that the decay angle ψ_d as proposed in Eq. (6.23) is sufficient to enclose most of the local effects due to damage.

Figures 6.12 and 6.13 illustrate von-Mises stress distribution obtained from nonlinear FEA for spherical shells with different cases of corroded area and thermal hot spot based on elastic-plastic material model. The operating temperature is assumed to be 100 °F. The material properties are as given in Table 5.2 in Chapter 5. The plots shown are at the load step in which von-Mises membrane strain at the crown of the sphere is 1% (failure criterion for serviceability used in the present research).

Although the deformed shapes for inelastic analyses in Figures 6.12 and 6.13 seem to experience less deformation in the undamaged part than that for elastic cases (Figures 6.10 and 6.11), this is merely due to scale effect. For inelastic analysis, the displacement at the crown is much larger than that for elastic analysis. Therefore, by proportion, the displacements at the remaining parts of the shell merely appear to be small for the inelastic cases.

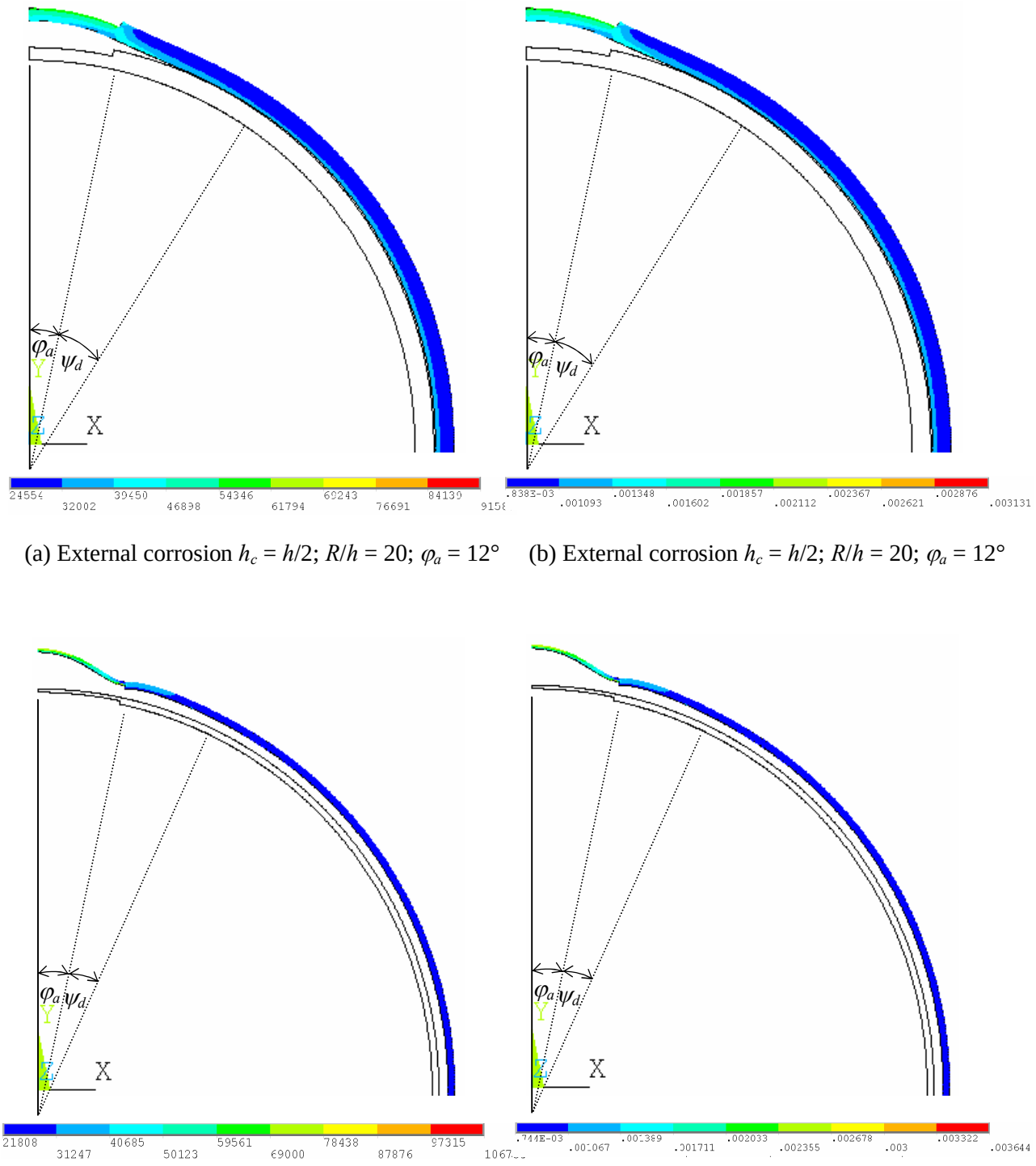

(a) External corrosion $h_c = h/2$; $R/h = 20$; $\varphi_a = 12°$ (b) External corrosion $h_c = h/2$; $R/h = 20$; $\varphi_a = 12°$

(c) Internal corrosion $h_c = h/2$; $R/h = 58.4$; $\varphi_a = 12°$ (d) Internal corrosion $h_c = h/2$; $R/h = 58.4$; $\varphi_a = 12°$

Figure 6.10 Elastic equivalent stress and strain distributions for corroded spherical shells with $R/h = 20$ and 58.4 subject to internal pressure

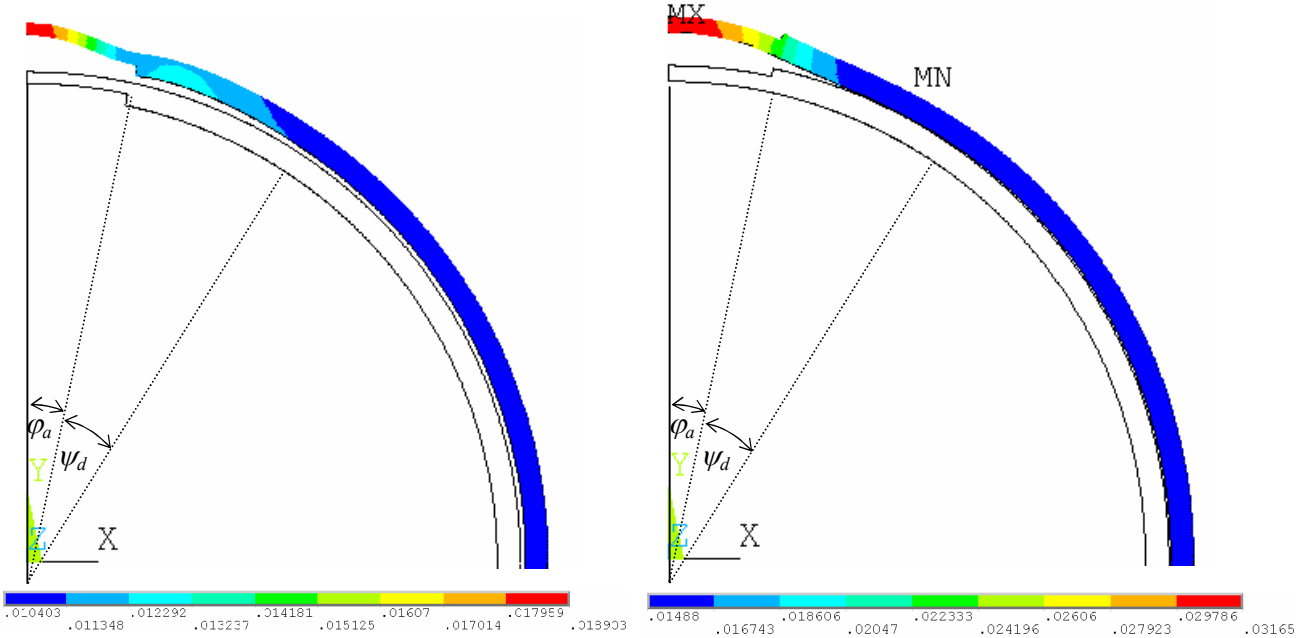

(a) Internal corrosion $h_c = h/2$; $R/h = 20.0$; $\varphi_a = 12°$ (b) External corrosion $h_c = 2h/3$; $R/h = 20.0$; $\varphi_a = 12°$

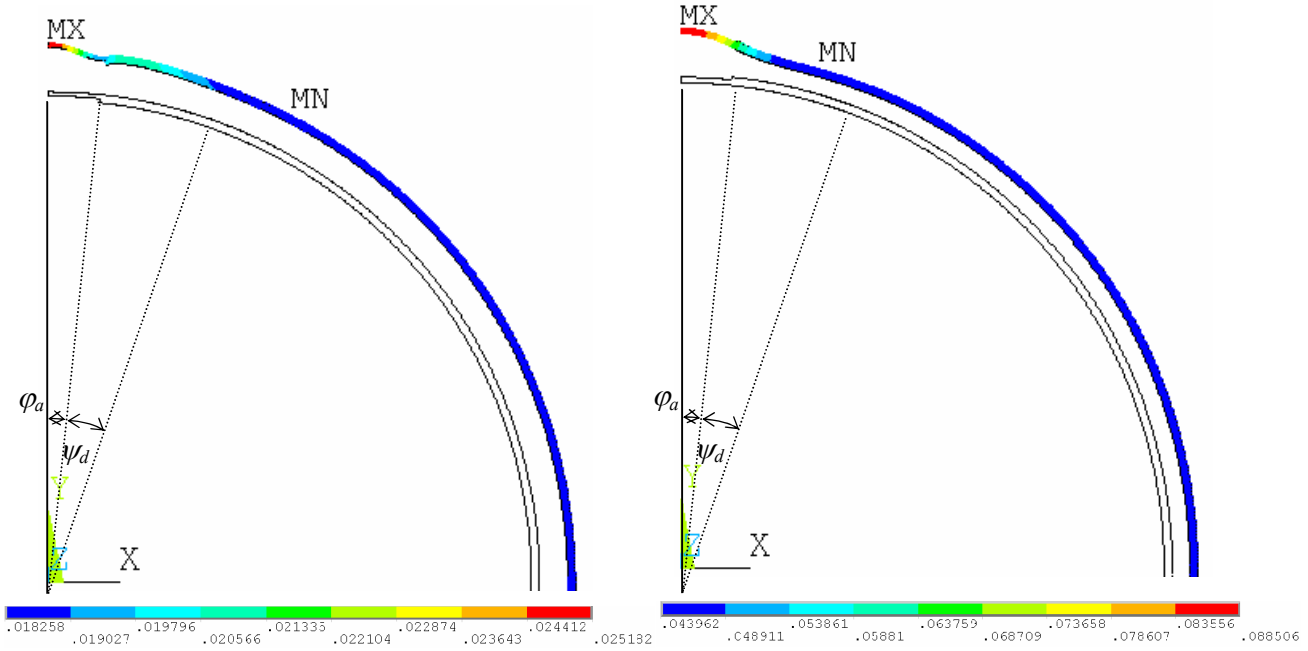

(c) Internal corrosion $h_c = h/2$; $R/h = 58.4$; $\varphi_a = 6°$ (d) External corrosion $h_c = 2h/3$; $R/h = 58.4$; $\varphi_a = 6°$

Figure 6.11 Elastic radial displacement distributions for corroded spherical shells with with $R/h = 20$ and 58.4 subject to internal pressure

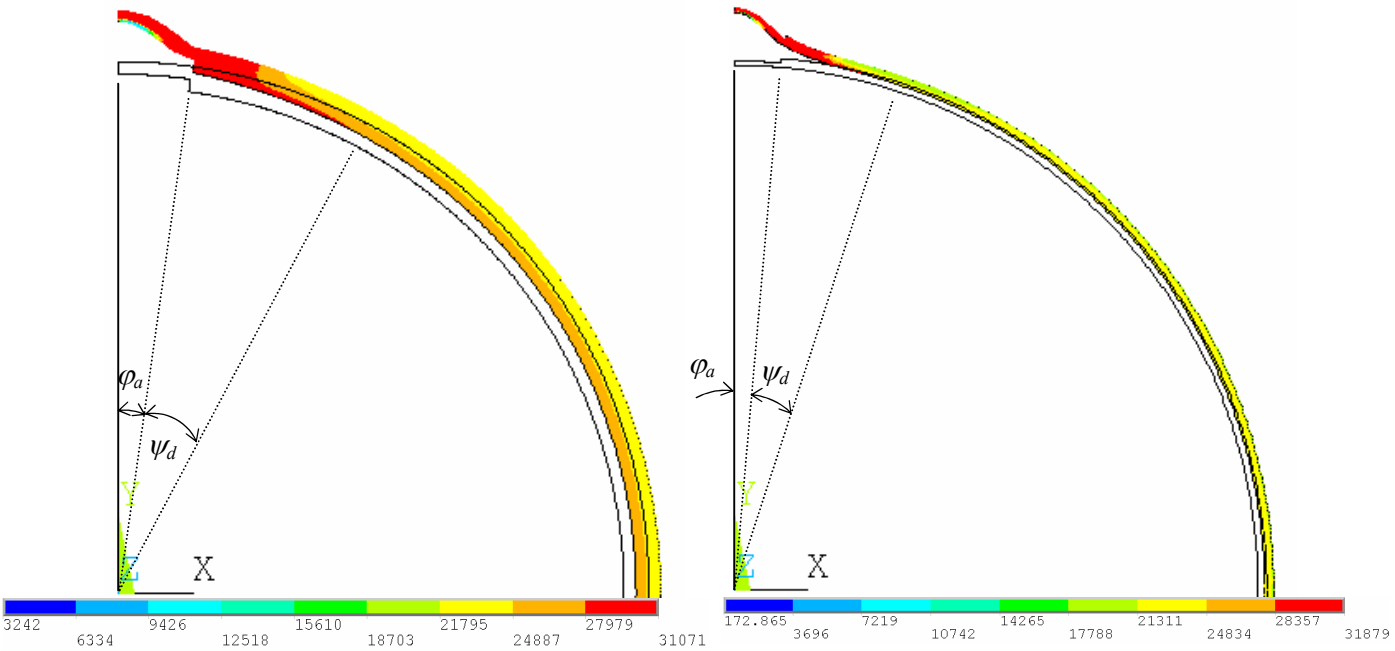

(a) Internal corrosion $h_c = h/2$; $R/h = 20$; $\varphi_a = 8°$ (b) External corrosion $h_c = h/2$; $R/h = 58.4$; $\varphi_a = 5°$

Figure 6.12 Inelastic equivalent stress distribution distributions for corroded spherical shells with $R/h = 20$ and 58.4 subject to internal pressure

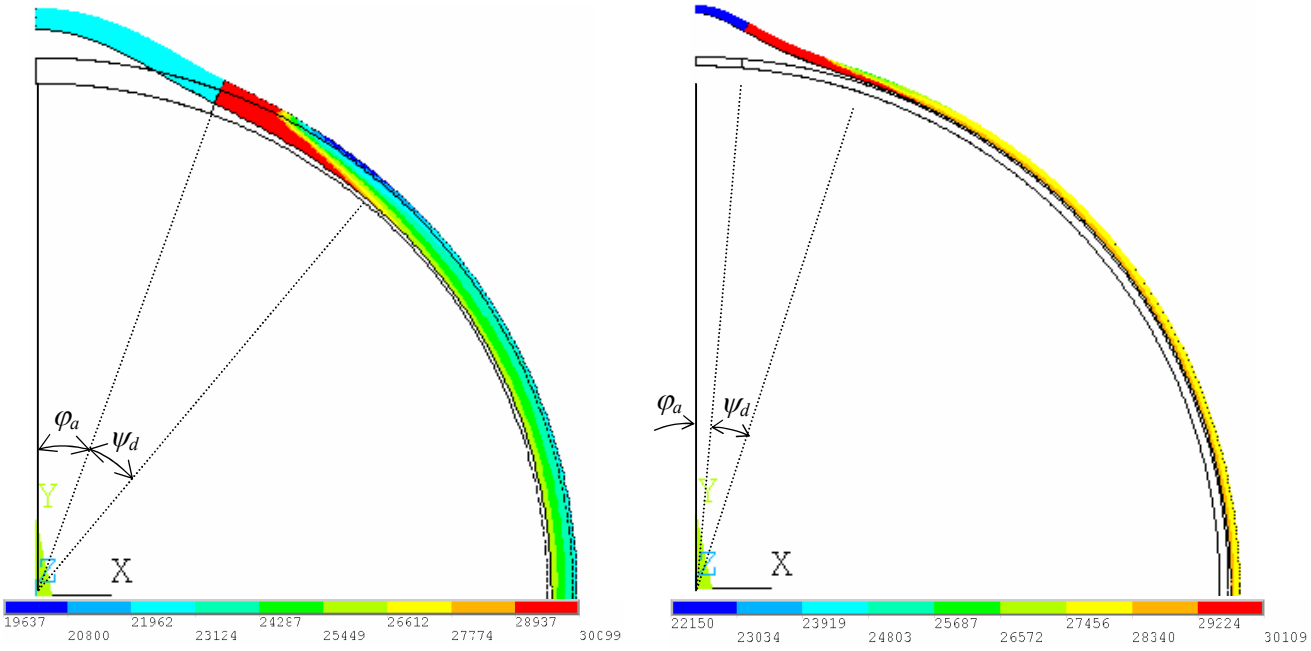

(a) $R/h = 20$; $\varphi_a = 20°$ (b) $R/h = 58.4$; $\varphi_a = 5°$

Figure 6.13 Inelastic equivalent stress distributions for spherical shells with a thermal hot spot ($T_h = 600$ °F) subject to internal pressure

It can be seen that the plastic decay angle obtained from FEA is less than the proposed elastic decay angle for both corrosion damage and hot spot cases. Moreover, it is observed that the effect from bending action seems to decay more rapidly for large damaged spots than smaller damages. The difference in decay angles of small and large damaged spots may be the result of different mechanisms of the shells. It is observed from the FEA results that shells with highly localized damage tend to open up rather than forming a bulge. The decay angle for this behavior is larger than that for bulging. These types of shell behavior will be further investigated in Chapter 7 and 8.

6.3.2. Cylindrical Shells

The decay lengths in axial and circumferential directions calculated by using Eqs. (6.27) and (6.40), respectively, are verified using the results obtained from finite element analysis.

Cylinders with inner radius R_i = 53.3 cm (21 in.) are used. Decay lengths in the axial direction x_l are calculated by using Eq. (6.27) and those in the circumferential direction x_c are obtained from Eq. (6.40). A simply-supported cylinder subject to uniform ring load is used to validate the derived decay length in axial direction (x_l) whereas a uniformly distributed line load along the generator is applied to verify the decay length in the circumferential direction (x_c). Figure 6.14 shows radial displacements of the cylinders from the two models for R/h ratio of 60, 32.6 and 20. It can be seen that the derived decay lengths are justifiable.

Axial direction

Circumferential direction

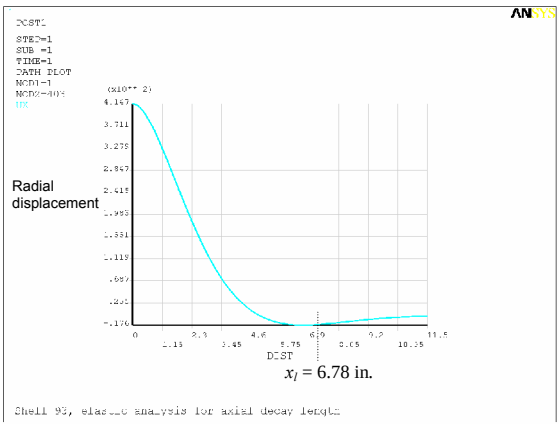

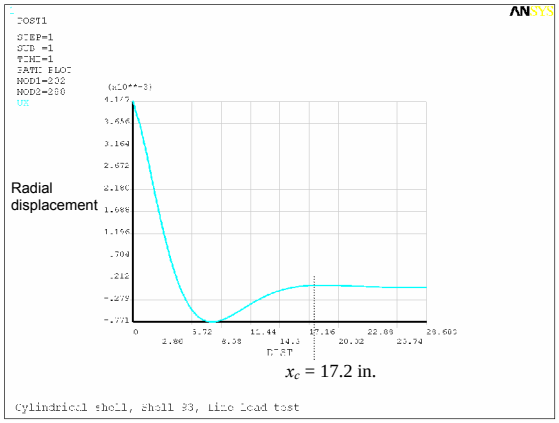

(a) R/h = 60

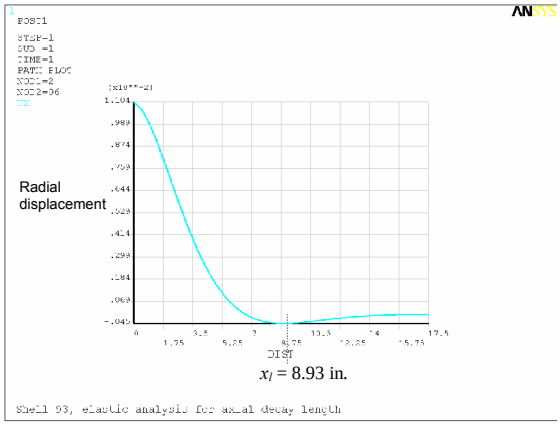

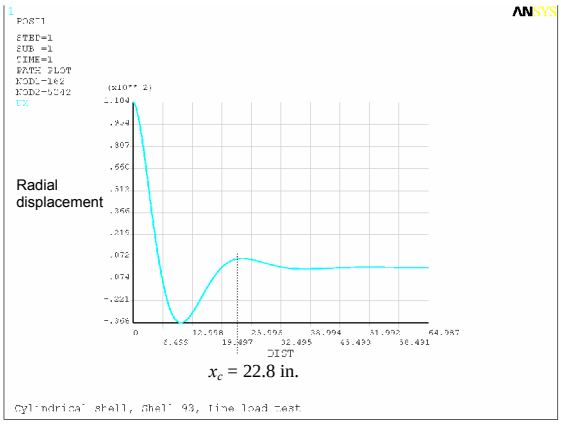

(b) R/h = 32.6

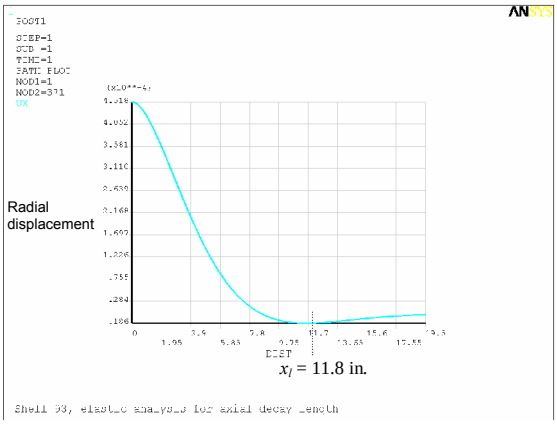

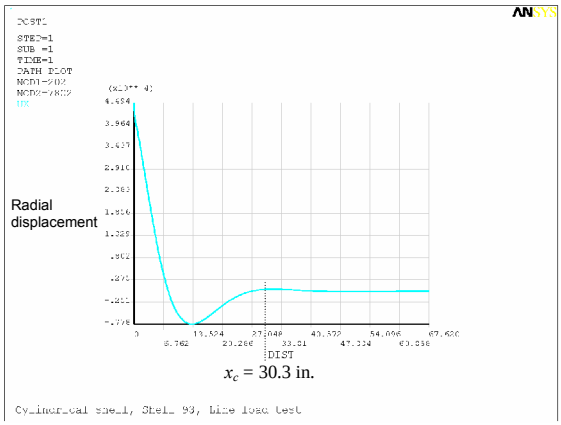

(c) R/h = 20

Figure 6.14 Decay lengths due to local force in the axial and circumferential directions

An elastic analysis is carried out to study decay lengths due to the effects of damaged area in cylinders. The damaged areas are assumed to be rectangular ($2a \times 2b$). Equivalent stress and strain distributions along the paths passing through the middle of rectangular damaged areas in circumferential ($\theta = 0$) and axial ($\varphi = 0$) directions of the cylinders are then plotted and compared with theoretical decay lengths from elastic solutions. Figure 6.14 shows that elastic decay lengths for local damages such as corroded area obtained from FEA are comparable with the theoretical decay lengths.

Inelastic analyses are then performed on similar cylindrical shells with hot spot or corrosion damage of various sizes using elastic-plastic material model. Examples of plastic decay lengths for different cases of hot spots and corrosion damage are shown in Figures 6.15 to 6.18. It can be seen that the proposed decay lengths are reasonably conservative for both elastic and inelastic analyses. The estimations are proportionately similar for x_c and x_l. I may be noted that the displacements shown here include the primary displacements which will be present even if the shell is not damaged. These displacements will vary depending on the support point provided in the FE model. For this reason, the displacements shown in, e.g., Figure 6.17 may appear to be significant even beyond the end of decay length location. However, the appropriateness of the computed decay length can still be seen from the strain distribution diagrams.

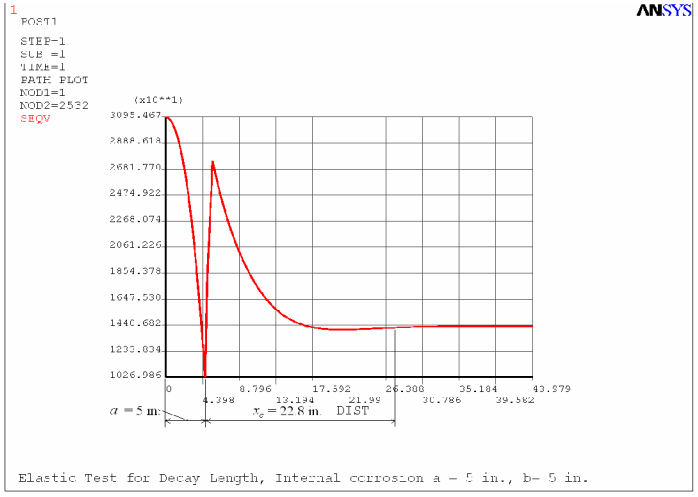

(a) Equivalent stress distribution along circumferential direction ($\theta = 0$)

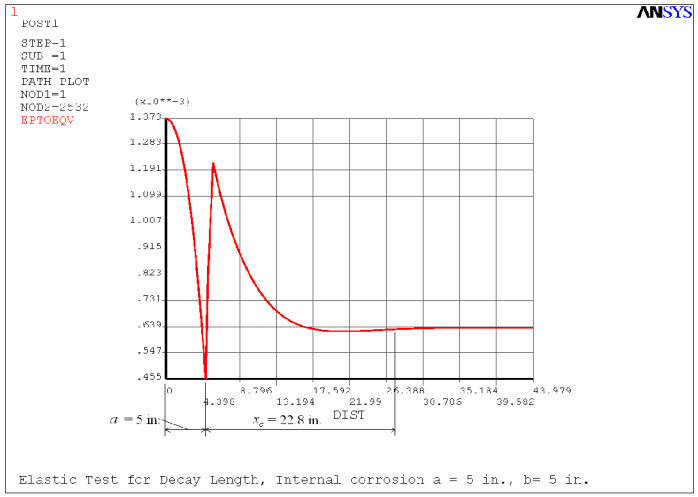

(b) Equivalent strain distribution along circumferential direction ($\theta = 0$)

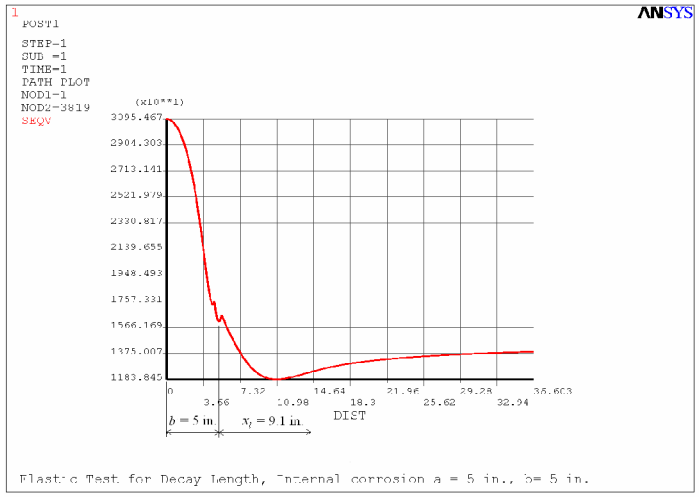

(c) Equivalent stress distribution along axial direction ($\varphi = 0$)

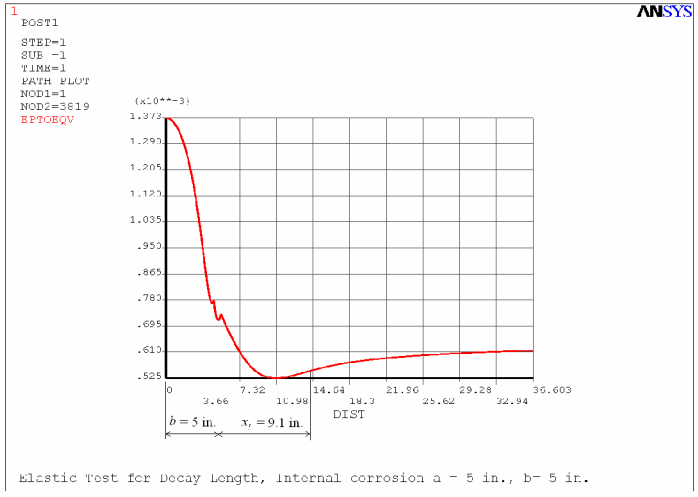

(d) Equivalent strain distribution along axial direction ($\varphi = 0$)

Figure 6.15 Elastic decay lengths for cylindrical shell with R/h ratio 32.6 with internal corrosion $a = b$ = 12.7 cm

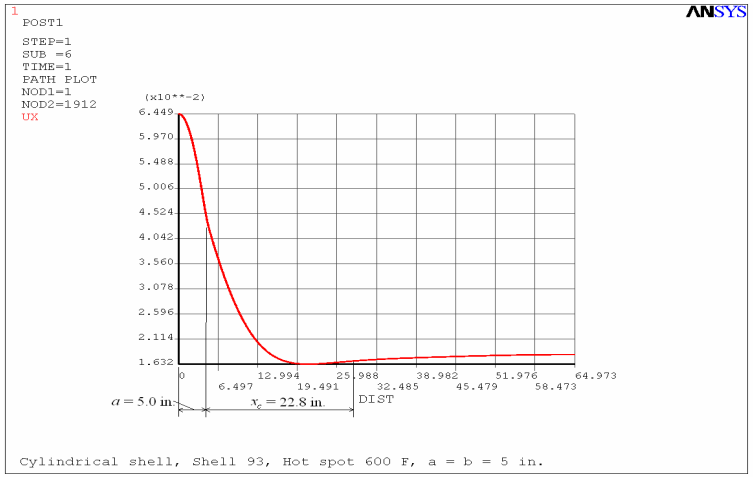

(a) Along circumferential direction ($\theta = 0$); $a = b$ = 12.7 cm

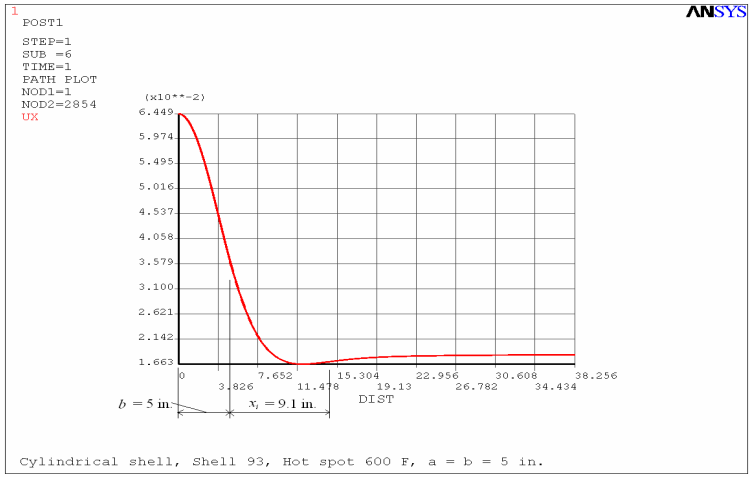

(b) Along axial direction ($\varphi = 0$);$a = b$ = 12.7 cm

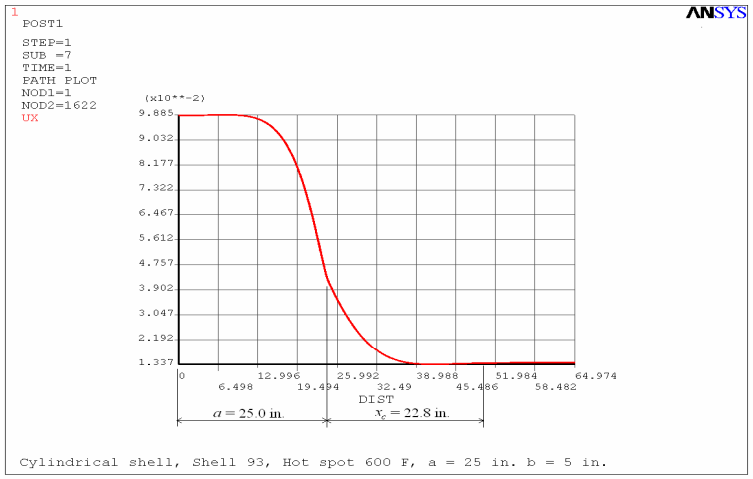

(c) Along circumferential direction (θ =0); a = 63.5 cm, b = 12.7 cm

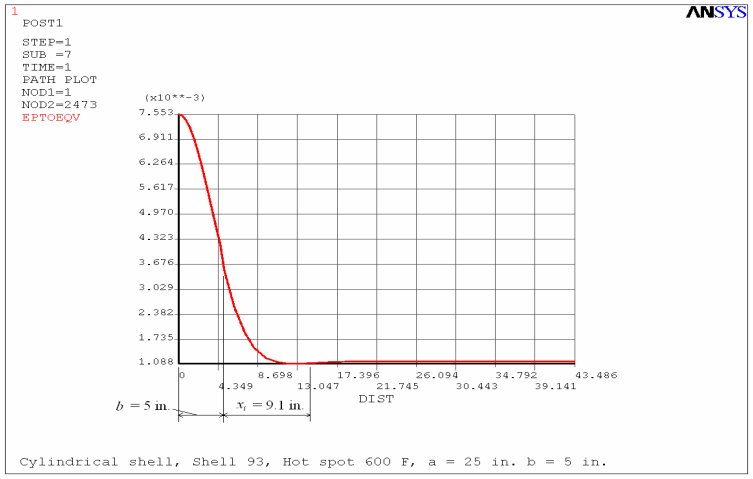

(d) Along axial direction ($\varphi = 0$)); a = 63.5 cm, b = 12.7 cm

Figure 6.16 Radial displacement distributions and decay lengths for cylindrical shell R/h ratio 32.6 with hot spot size 2a x 2b at 316ºC

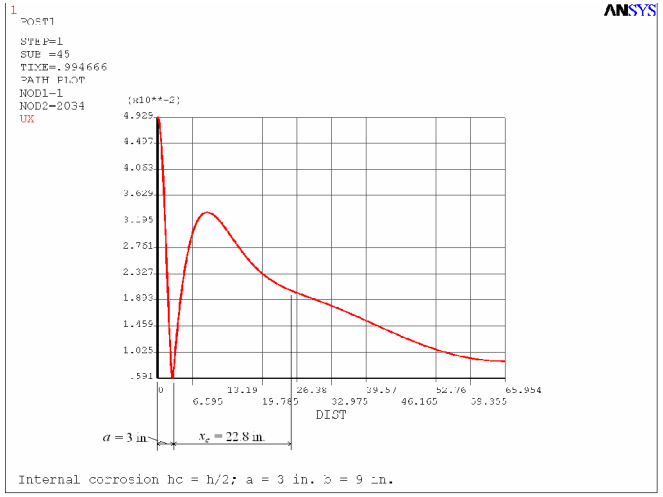

(a) Radial displacement along $\theta = 0$

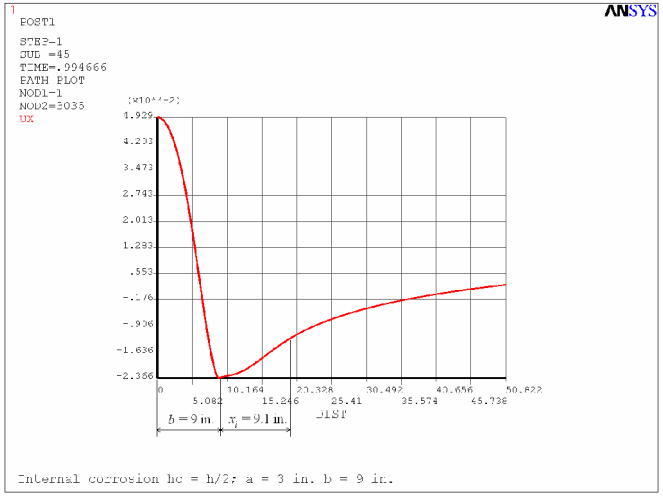

(b) Radial displacement along $\varphi = 0$

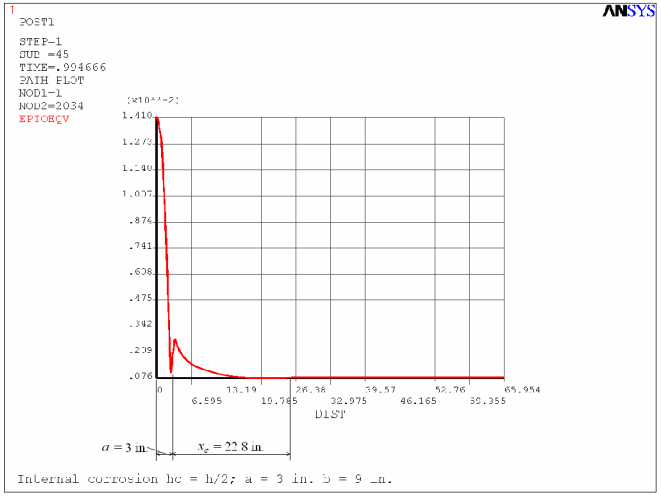

(c) Equivalent strain distribution along $\theta = 0$

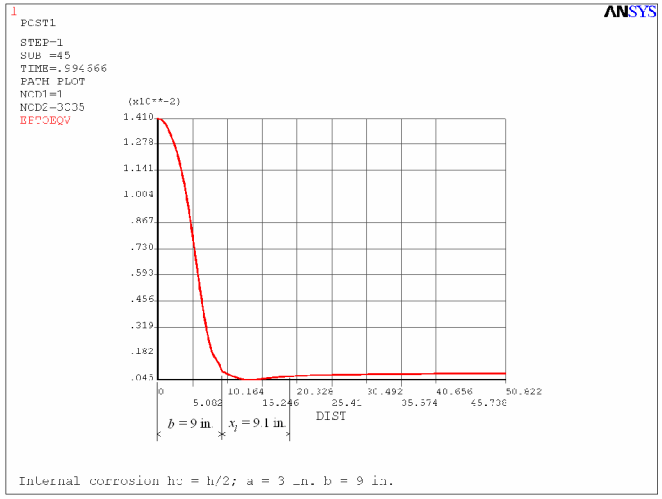

(d) Equivalent strain distribution along $\varphi = 0$

Figure 6.17 Results for internal corrosion of the size 2*a* x 2*b* (*a* = 7.6 cm and *b* = 22.9 cm) in cylindrical shell *R*/*h* ratio 32.6

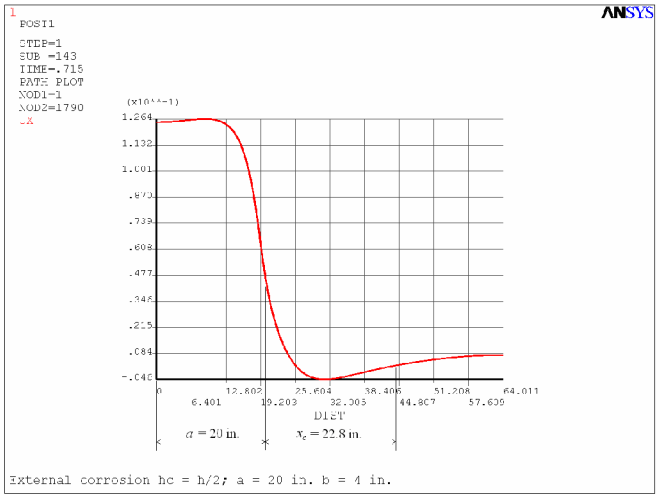

(a) Radial displacement along $\theta = 0$

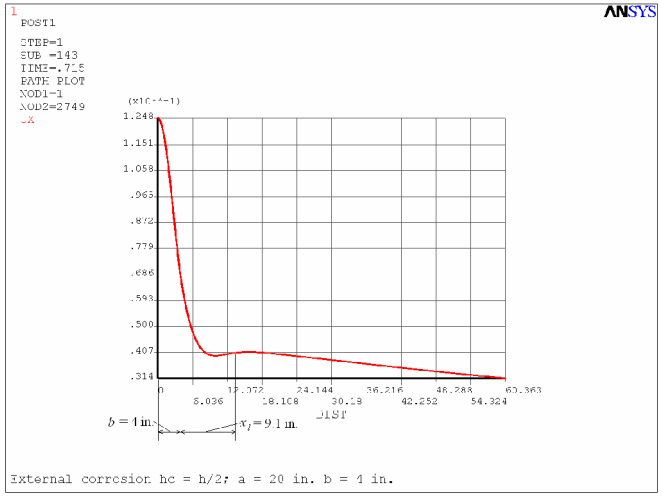

(b) Radial displacement long $\varphi = 0$

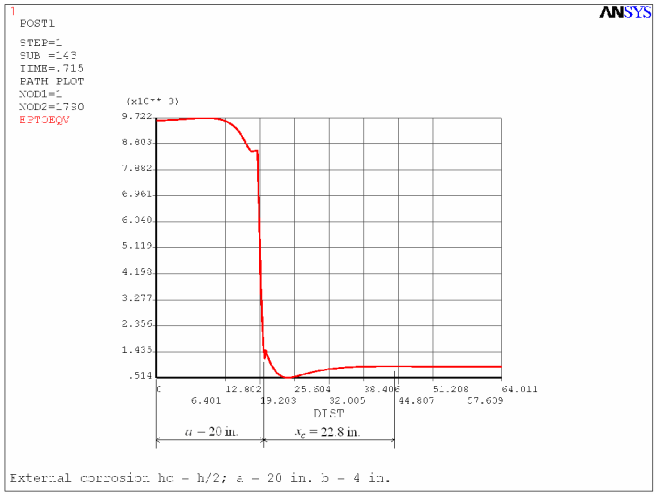

(c) Equivalent strain distribution along $\theta = 0$

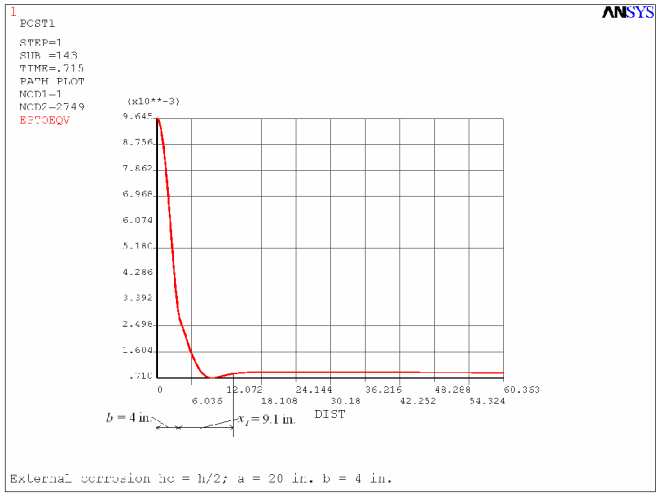

(d) Equivalent strain distribution along $\varphi = 0$

Figure 6.18 Results for external corrosion of the size 2*a* x 2*b* (*a* = 50.8 cm and *b* = 10.2 cm) in cylindrical shell *R*/*h* ratio 32.6

6.4. COMPARISON OF THE PROPOSED DECAY LENGTHS

In all problems of interest in the present research, the distance to which the effects of local action extend is defined by a decay angle (or length). For spheres, this angle is presented in Eq. (6.23). From this decay angle, the decay length for spherical shell, x_s, is obtained as

$$x_s = 1.83\sqrt{Rh} \tag{6.42}$$

The decay lengths of cylindrical shell in axial and circumferential directions are derived in Eqs. (6.26) and (6.40) as, $2.5\sqrt{Rh}$ and $6.3\sqrt{Rh}$, respectively.

The decay length for a sphere is less than that for a cylinder of the same radius and thickness. This is because spheres have double curvature compared to the single curvature of cylinders. Deformations in a sphere are dissipated much more rapidly than those in a cylinder. Thus, the effects from damaged spots in spheres are much more localized and hence have an adverse effect compared to those in cylinders. It is also evident that the effects of local action are different in the axial and circumferential directions for cylinders. The decay length in the axial direction of a cylinder is 40% of that in circumferential direction indicating the greater severity of axial damage. This is perhaps an indication that the decay length is influenced heavily by the curvature in the perpendicular direction. For the decay length along the length of cylinder, the curvature in the circumferential direction is high whereas for the decay length in the circumferential

direction, the curvature in the perpendicular direction is zero. The curvature in the perpendicular direction is similar to the subgrade modulus in a problem involving beam-on-elastic foundation. The more the curvature, the stiffer the subgrade modulus and faster the decay of the displacements. It implies that the decay length in the longitudinal direction will be much smaller than that in the circumferential direction.

Seshadri (2004) derived a decay length in the circumferential direction of cylindrical shells as $6.1(R^3h)^{1/4}$ using a slightly different set of assumptions. However, the decay length proposed in the present work is a function of $\sqrt{Rh}$ similar to the well-known value for longitudinal direction and hence is adopted here.

6.5. APPLICATIONS OF DECAY LENGTHS

When a corroded area or a thermal hot spot occurs in a pressure vessel, local bending and shear actions will take place at the perimeter of the discontinuity. The decay lengths can be used to identify the kinematically active portion of the structure that participates in plastic action. The so-called reference volume prescribes the containment of local effects acting on the structure. Details in calculations of reference volume for spherical and cylindrical shells are presented in Chapter 4.

As discussed earlier, damage is defined as “local” when the edge effects at the discontinuities have not damped out inside the damage and the pure membrane stress effect does not occur at any place inside the damaged area. Therefore, the extent of “local” damage can be defined by using the decay lengths. This also implies that

interaction between two spots of local damage will not occur if the distance between the outer edges of the damaged areas is at least equal to twice the decay length. For spherical shell, two locally damaged areas which are at least $2\psi_d$ apart from each other will not interact and the effects of the damage to the shell integrity can be treated separately. For cylindrical shells, the decay lengths in the axial and circumferential directions are different. The extent of local damage and interaction are likely to be affected by the effects from both directions. These aspects will be investigated further in Chapter 8.

6.6. CLOSURE

The decay lengths in spherical and cylindrical shells are proposed based on elastic solutions to local forces or edge effects around damaged areas. The proposed elastic decay lengths are shown to be applied in plastic analysis by using results obtained from finite element analyses. It was also shown that decay lengths in shells with small curvature are likely to be larger than shells with large curvature. This implies that small-curvature shells can dissipate the energy better and thus be able to tolerate larger extents of damage. The decay lengths as proposed in this chapter will be utilized in calculation of the reference volume and the extent of local damage.

CHAPTER 7

RECOMMENDATIONS FOR REMAINING STRENGTH FACTORS OF SPHERICAL SHELLS

This chapter proposes Level 2 structural integrity or Fitness-for-Service (FFS) assessments for spherical pressure vessels containing damage due to corrosion or thermal hot spots. As discussed earlier, the parameter generally used to quantify the acceptability (for continued service) of a structure with such damaged areas is the remaining strength factor (RSF). It can be computed as the ratio of the limit loads of the component with and without damage. Three possible methods for RSF estimation are suggested. Each format contains different cases based on the size of the damaged area. An approach to estimate "bulging" deformation using geometric properties of the shell is also explained.

7.1. LOCAL AND GLOBAL DAMAGE IN SPHERICAL SHELL

In the current research, it is postulated that there is a certain size of damage below which the damage can be identified as "local." Damage larger than this limit can be

deemed "global." For global damages, the remaining strength will be "as if" the damage extends to the entire component. In other words, beyond a limiting size the damage behaves as if it is a global damage.

As explained in Chapter 6, the local damage limit is defined as the maximum size of damage beyond which a pure equilibrium stress occurs at some place inside the damaged area. This extent can be obtained by using the decay angle (or decay length).

The decay angle ψ_d for a spherical shell is proposed in Eq. (6.23) as (Tantichattanont, 2006a),

$$\psi_d = 1.83\sqrt{h/R_i} \tag{7.1}$$

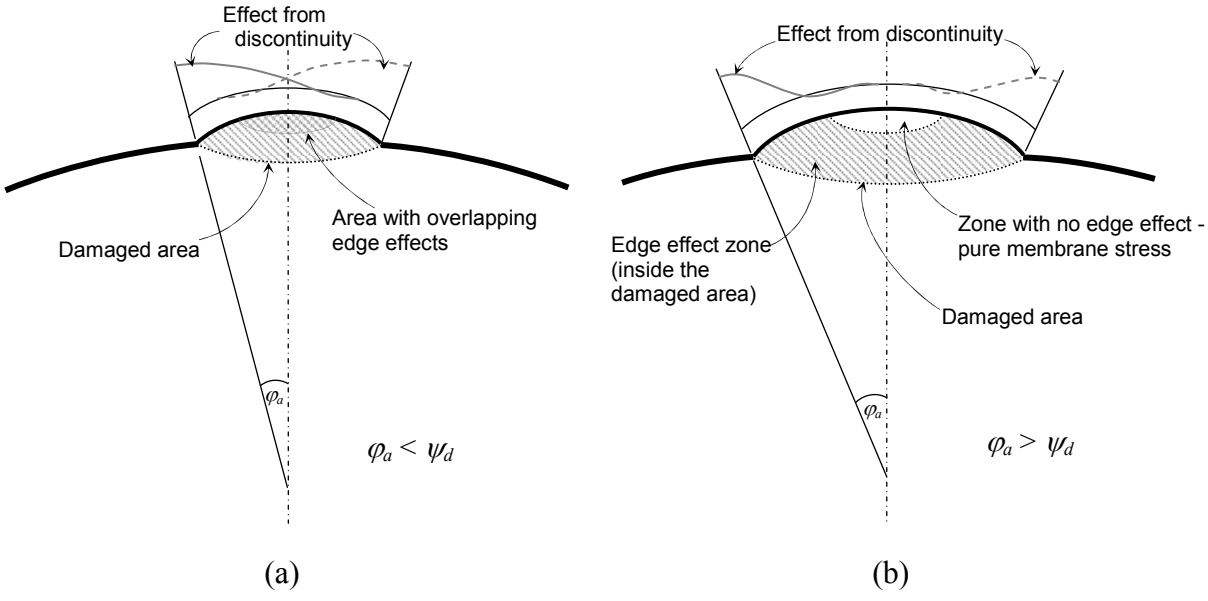

Figure 7.1 (a) Overlapping edge effect region in a local damage (b) Pure equilibrium stress region inside a "global" size damage

If the angle φ_a defining the size of the actual damaged spot is smaller than the limit ψ_d, it means that the effects from discontinuities at the edge of the hot spot or corroded area have not yet damped out inside the damaged area and there is an area of overlapping edge effects (Figure 7.1a). On the other hand, if the angle φ_a is larger than ψ_d, there is a certain area within the hot spot where the edge effects from discontinuities have dissipated and hence the area is in pure membrane action defined by equilibrium stresses alone (Figure 7.1b).

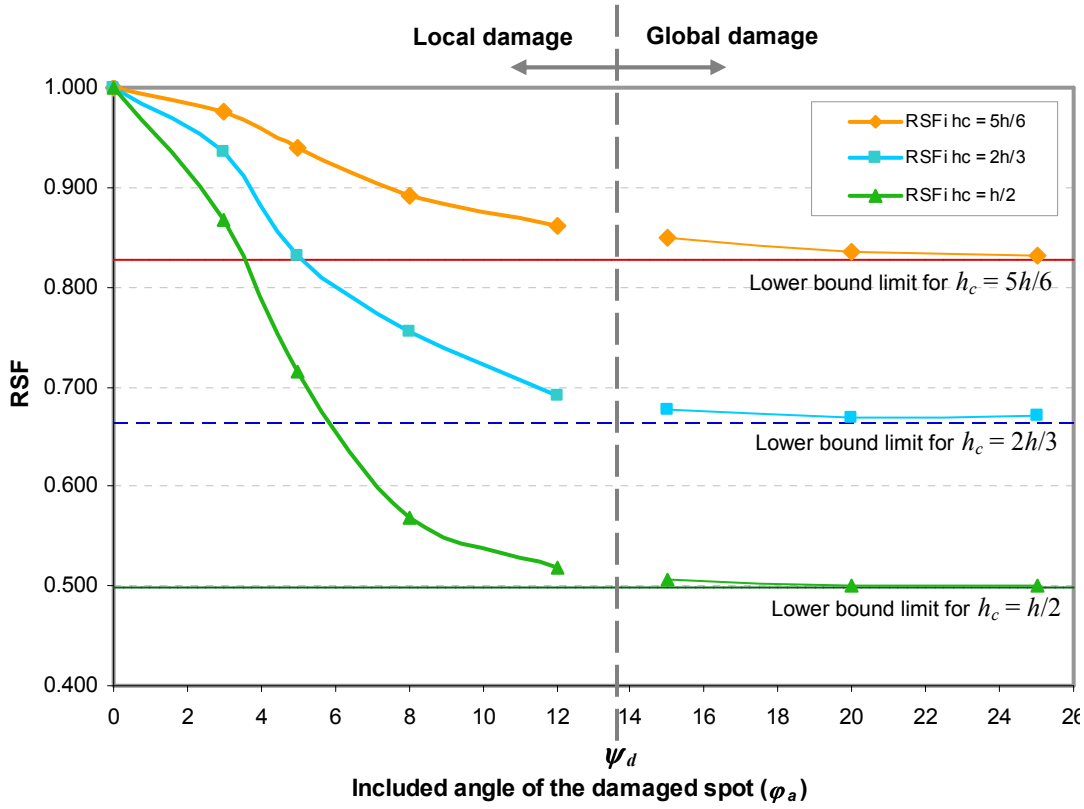

Figure 7.2 An example of comparison between RSF_i and lower bound limits for local and global corrosion damage in a spherical shell (R/h = 58.4)

This area will accordingly fail in pure membrane action controlled by the yield stress of the hot region in the case of hot spot, or the remaining thickness in the case of corrosion damage. Hence for this case, we can deduce that even if the damaged spot is larger than the extent of "local" damage, the failure is "as if" a "global" damaged spot has occurred. It must be noted that this extent may not be defined sharply in practice. In addition, the actual structure would in all likelihood have other reserve strengths. "Failure" here is simply indicative of the limit criterion being surpassed. For this case, RSF_L (where the damaged area extends over the whole component) is the governing value.

Figure 7.2 shows an example of inelastic RSF (RSF_i) obtained from finite element analysis for internal corrosion damage in a spherical shell with R/h of 58.4. The corrosion damage is studied for three different remaining thicknesses h_c equal to $5h/6$, $2h/3$ and $h/2$ (shown as diamond, square and triangular markers, respectively), where, h is the uncorroded thickness. The horizontal lines in the graph indicate the lower bound RSF_L for different h_c. The RSFs are plotted against the included angle of the corroded area, φ_a. In this particular case, the decay angle ψ_d calculated by using Eq. (7.1) is 13.9^o. A damaged area with φ_a less than this decay angle ψ_d can be called "local" damage whereas a damaged area with φ_a larger than this extent can be called "global" damage. It can be seen from the graph that the values of inelastic RSF_i for global damage are converging to RSF_L.

Note that the value of RSF_L in Figure 7.2 is slightly smaller than h_c/h since it is calculated by the ratio of equivalent membrane stress in the undamaged zone σ_{eI} ($= pR_i/h$) and the equivalent membrane stress inside the corroded area σ_{eD} ($= pR_{ic}/h_c$), where, R_{ic} is the inner radius of the sphere inside the corroded part which is slightly larger than the original inner radius R_i in the case of internal corrosion. Hence, the lower bound limit or the RSF_L, obtained as $\frac{R_i}{R_{ic}}\left(\frac{h_c}{h}\right)$, is slightly smaller than h_c/h.

The above observation (that inelastic strength converges to that indicated by RSF_L for large damage spots) is also valid for other cases of corrosion damage and hot spot in spherical shells. More results supporting this are shown in the following sections. Details on FEA modeling used to determine RSF_i are discussed in Chapter 5.

7.2. RECOMMENDATION FOR SPHERICAL SHELLS – METHOD I

Thus far in the present study, different concepts and scenarios for calculating the strength of the damaged components is discussed. These include the concepts of reference volume, decay length, limit loads based on the m_α-method, lower bound limit loads, remaining strength factors, etc. While RSF_α, RSF_L, and others are ways of estimating the remaining strength factors for specific situations, they do not necessarily apply for all ranges of parameters as explained earlier. These are limited in their applicability by

factors such as decay length. All these concepts are brought together in the following sections to arrive at comprehensive recommendations for estimating RSF of pressure components. The recommendations will be applicable for different ranges of parameters. Three alternative strategies are recommended as Methods I, II and III (Tantichattanont, 2006b).. In all these methods, the damaged area is assumed to be replaced by an equivalent circular spot. The size of the damaged area is represented by an included angle φ_a.

In recommended Method I, the remaining strength factor RSF_α is taken to provide a lower bound approximation for the component with small local damage where decay lengths from opposite ends overlap significantly at the middle of the damaged zone. For large spots where the decay lengths do no overlap at all, RSF_L (Eq. 4.23) is applicable as explained earlier. A linear interpolation between RSF_α and RSF_L is assumed for intermediate size local corroded spots. The transition angle from small to intermediate damaged spots is suggested as the location where the direction of curvature of the bending moment expression changes. This is equal to one-third of the decay angle and can be given as,

$$\psi_L = \frac{\pi}{4\lambda} \tag{7.2}$$

Figure 7.3 summarizes this recommendation which is identified as $RSF_{r\text{-}1}$. The relevant equations for Method I (for a spherical pressure vessel containing a corroded area or a hot spot) are listed below.

For $\varphi_a \le \psi_L$, $RSF_{r-1} = RSF_\alpha$

For $\psi_L < \varphi_a \le \psi_d$, $RSF_{r-1} = (1.5 - 0.637\lambda\varphi_a)RSF_{\alpha \text{ at } \psi_L} + (0.637\lambda\varphi_a - 0.5)RSF_L$ (7.3)

For $\varphi_a > \psi_d$, $RSF_{r-1} = RSF_L$

where, $\lambda^4 = 3(1-\nu^2)(R/h)^2$.

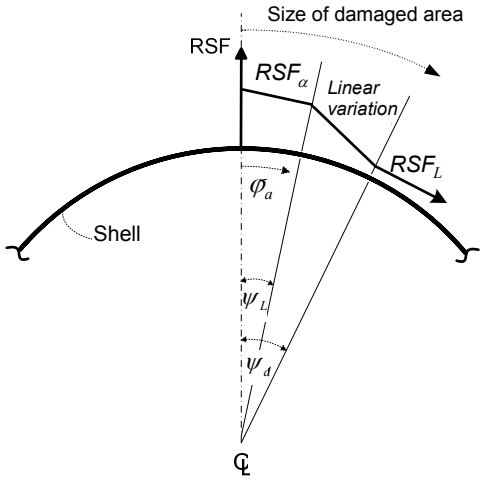

Figure 7.3 Method I Recommendation: RSF_{r-1} for various sizes of damaged areas in spherical shells

Different cases of damaged areas (corrosion or hot spots), remaining thickness and temperatures have been studied to evaluate the effectiveness of the proposed recommendation. An inelastic Finite Element Analysis is performed using ANSYS to determine the inelastic strength. The inelastic RSF_i is calculated from the ratio of the internal pressure that causes a maximum of 1% average strain (in the hot spot) and the limit pressure of undamaged sphere (not design pressure). The models used for FEA are described in Chapter 5.

Table 7.1 RSF for a corroded spherical shell (R/h = 58.9) with remaining thickness 5h/6

φ_a	RSF_U	RSF_α	RSF_L	$RSF_{r\text{-}1}$	$RSF_{i\text{-}external}$	$RSF_{i\text{-}internal}$
3°	0.994	0.927	0.827	0.927	0.975	0.993
5°	0.986	0.923	0.827	0.920	0.939	0.983
8°	0.973	0.917	0.827	0.889	0.891	0.949
12°	0.958	0.909	0.827	0.847	0.862	0.896
15°	0.947	0.904	0.827	0.827	0.849	0.867
20°	0.932	0.895	0.827	0.827	0.835	0.842
25°	0.920	0.889	0.827	0.827	0.832	0.834

Tables 7.1, 7.2 and 7.3 show RSF according to Method I for various sizes of external and internal corrosion damage in a spherical shell (R/h ratio 58.9, inner radius 21.9 in.) with the remaining thickness inside the corroded area equal to 5h/6, 2h/3 and h/2, respectively. It can be concluded from these results that the upper bound RSF_U offers close upper bound approximations for all the cases. The RSF_U estimations are closer to "exact" inelastic RSF_i in the cases where the damaged area is small and the corroded thickness is not much different from the original undamaged thickness. The recommended $RSF_{r\text{-}1}$ can bee seen to offer lower bound estimations for all the cases.

Table 7.2 RSF for a corroded spherical shell (R/h = 58.9) with remaining thickness 2h/3

φ_a	RSF_U	RSF_α	RSF_L	$RSF_{r\text{-}1}$	$RSF_{i\text{-}external}$	$RSF_{i\text{-}internal}$
3°	0.987	0.807	0.663	0.807	0.935	0.976
5°	0.971	0.803	0.663	0.799	0.832	0.949
8°	0.945	0.797	0.663	0.753	0.754	0.811
12°	0.913	0.788	0.663	0.692	0.692	0.714
15°	0.882	0.782	0.663	0.663	0.678	0.687
20°	0.863	0.771	0.663	0.663	0.669	0.672
25°	0.840	0.762	0.663	0.663	0.671	0.664

Table 7.3 RSF for a corroded spherical shell (R/h = 58.9) with remaining thickness h/2

φ_a	RSF_U	RSF_α	RSF_L	$RSF_{r\text{-}1}$	$RSF_{i\text{-}external}$	$RSF_{i\text{-}internal}$
3°	0.976	0.608	0.498	0.608	0.868	0.967
5°	0.949	0.612	0.498	0.607	0.715	0.828
8°	0.906	0.617	0.498	0.569	0.568	0.592
12°	0.854	0.618.	0.498	0.521	0.518	0.526
15°	0.822	0.617	0.498	0.498	0.507	0.508
20°	0.777	0.612	0.498	0.498	0.501	0.503
25°	0.743	0.606	0.498	0.498	0.499	0.497

These results plotted against the included angle of the shell are shown in Figure 7.4. The solid and hollow markers are inelastic RSF_i for internal and external corrosion, respectively. The solid lines represent the lines for the recommended $RSF_{r\text{-}1}$. It can be seen that the recommended $RSF_{r\text{-}1}$ provide close lower bound RSF approximation for this sphere. The study is extended to a thicker spherical shell with R/h ratio of 20 (the same inner radius as before). A similar plot for various sizes of external and internal corrosion damage with the remaining thicknesses of $5h/6$, $2h/3$ and $h/2$ is shown in Figure 7.5. Tabulated results for these cases are shown in Appendix A. It can be seen from Figure 7.5, that Method I gives a lower bound result in comparison with inelastic analysis. For damaged spots with included angles larger than ψ_d (or "global" damages), RSF_i are equal to RSF_L as discussed before. However, it is observed that there is higher conservatism in the recommended $RSF_{r\text{-}1}$ estimation in the cases of highly localized damage especially when there is high thickness loss.

Similar spherical shells with the same R/h ratios of 58.9 and 20.0 are also studied for thermal hot spots. The RSF for the spherical shell R/h ratio of 20.0 with thermal hot spot temperatures 93.3 °C, 204 °C and 316 °C are shown in Tables 7.4, 7.5 and 7.6, respectively. As before, the RSF_U gives upper bound estimates whereas the $RSF_{r\text{-}1}$ offers lower bound values for all the cases.

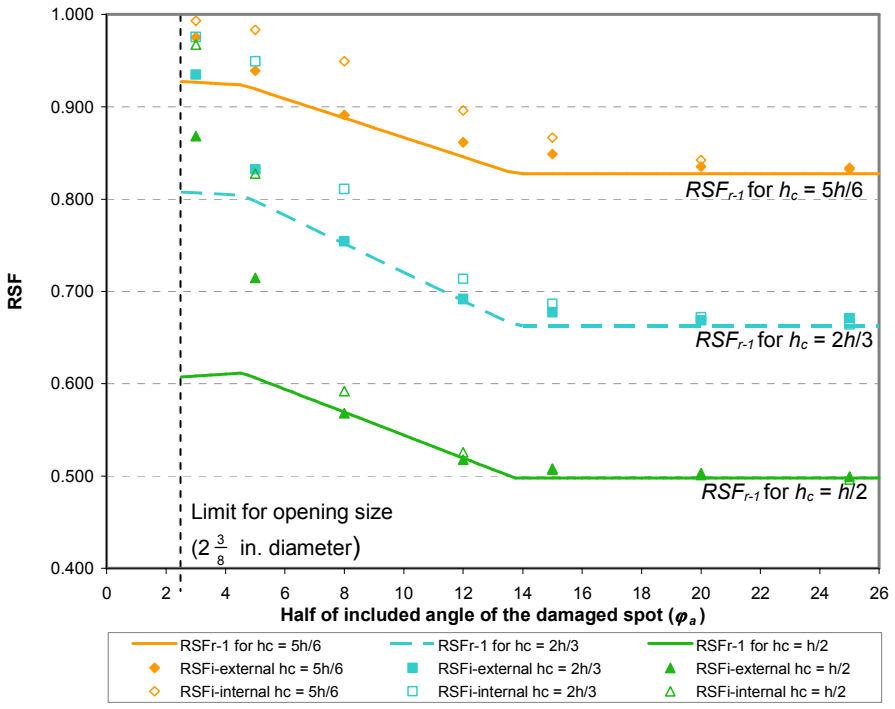

Figure 7.4 Comparison of Method I RSF_{r-1} and inelastic RSF_i for corrosion damage in spherical shell with R/h ratio 58.9

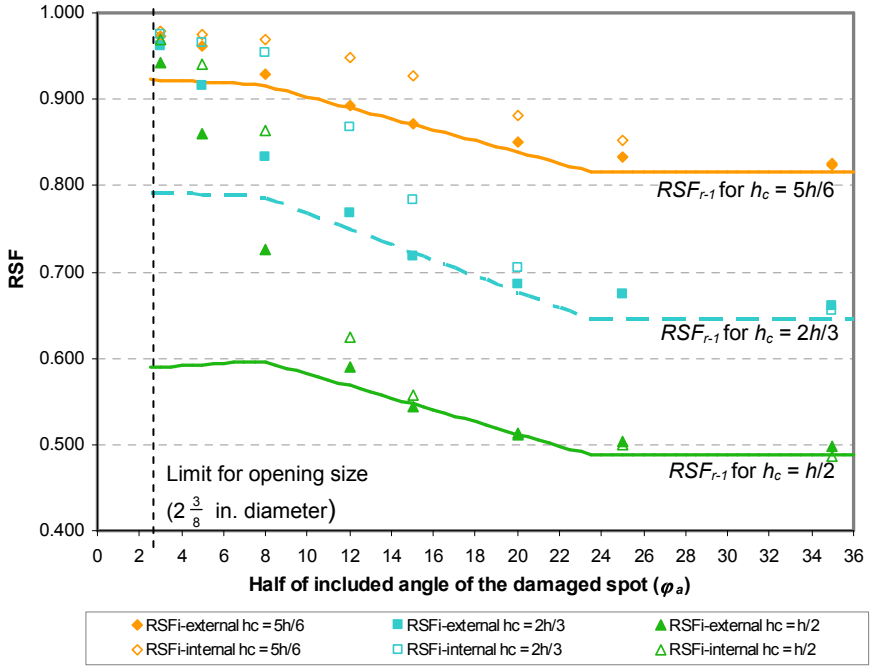

Figure 7.5 Comparison of Method I RSF_{r-1} and inelastic RSF_i for corrosion damage in spherical shell with R/h ratio 20

Table 7.4 RSF for a spherical shell with a 93.3 °C (200 °F) thermal hot spot (R/h = 20)

Case No.	φ_a	RSF_U	RSF_α	RSF_L	$RSF_{r\text{-}1}$	$RSF_{inelastic}$
1	8°	0.994	0.965	0.910	0.964	0.967
2	12°	0.990	0.962	0.910	0.950	0.952
3	18°	0.983	0.958	0.910	0.929	0.931
4	22°	0.979	0.956	0.910	0.914	0.919
5	25°	0.976	0.954	0.910	0.910	0.913

Table 7.5 RSF for a spherical shell with a 204°C (400 °F) thermal hot spot (R/h =20**)**

Case No.	φ_a	RSF_U	RSF_α	RSF_L	$RSF_{r\text{-}1}$	$RSF_{inelastic}$
1	8°	0.991	0.940	0.857	0.939	0.957
2	12°	0.984	0.936	0.857	0.917	0.932
3	18°	0.973	0.930	0.857	0.885	0.895
4	22°	0.967	0.927	0.857	0.863	0.875
5	25°	0.962	0.924	0.857	0.857	0.865

Table 7.6 RSF for a spherical shell with a 316°C (600 °F) thermal hot spot (R/h =20)

Case No.	φ_a	RSF_U	RSF_α	RSF_L	$RSF_{r\text{-}1}$	$RSF_{inelastic}$
1	8°	0.985	0.869	0.740	0.867	0.922
2	12°	0.973	0.864	0.740	0.833	0.865
3	18°	0.954	0.857	0.740	0.783	0.795
4	22°	0.943	0.853	0.740	0.750	0.767
5	25°	0.934	0.849	0.740	0.740	0.745

Figures 7.6 and 7.7 compare the recommended RSF_{r-1} and the inelastic RSF_i for thermal hot spots in spherical shells (inner radius 21 in.) with R/h ratios equal to 20.0 and 58.9, respectively. The same trend as in the case of corrosion damage can be observed. Samples of detailed calculation of RSF_{r-1} are presented in Section 7.6.

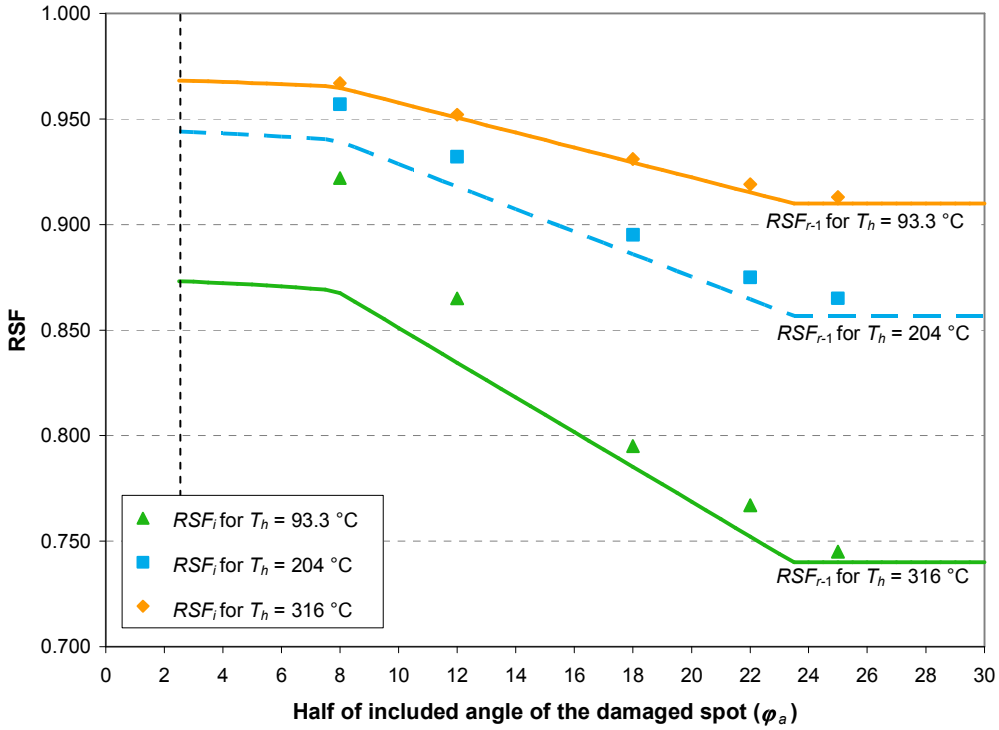

Figure 7.6 Comparison of Method I RSF_{r-1} and inelastic RSF_i for thermal hot spots in spherical shell with R/h ratio 20

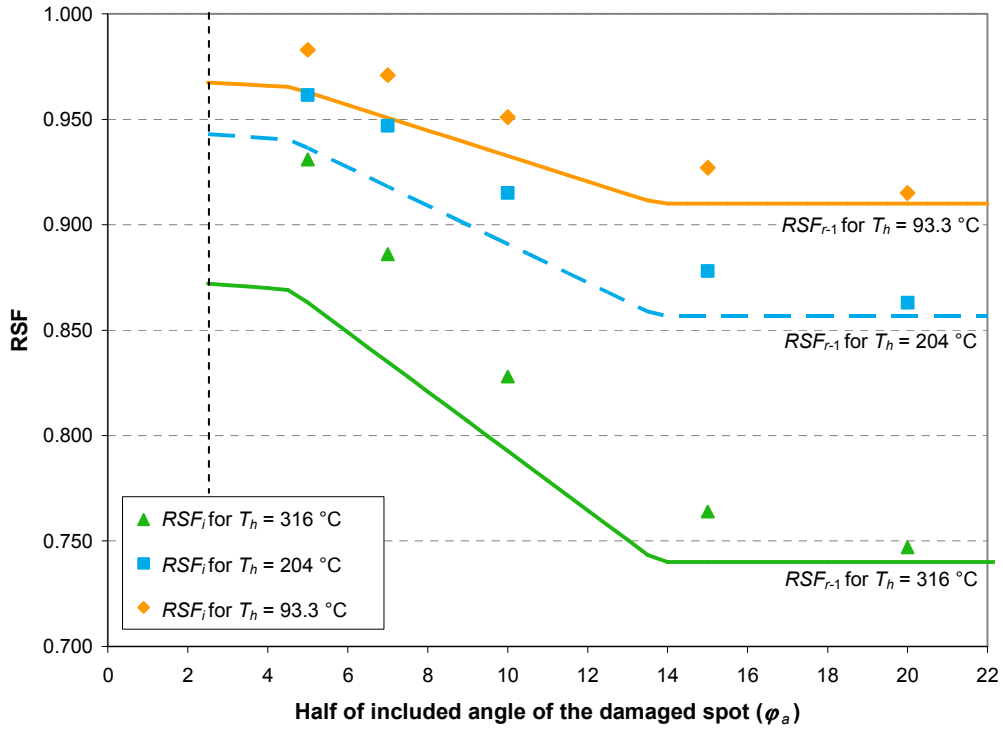

Figure 7.7 Comparison of Method I RSF_{r-1} and inelastic RSF_i for thermal hot spots in spherical shell with R/h ratio 58.9

From the above, it can be concluded that for all cases of R/h ratios, remaining corroded thickness and practical hot spot temperatures, RSF_{r-1} provide good lower bound approximation. For spherical shells containing damaged spots with large included angles, the remaining strength factors obtained from finite element analyses are shown to be constant and are equal to RSF_L indicating the dominance of primary membrane effects as discussed earlier. The "local" damaged-spot limit defined by the angle ψ_d as indicated by Eq. (7.1) is slightly on the conservative side. For very small damaged areas, the failure is less influenced by the decay length compared to the stretching action. The stretching decay lengths are likely to be larger than those of bending action thus indicating a more diffused effect resulting in higher RSF. In that sense, for very small damaged spots the RSF as computed above from RSF_α will be conservative. This is also confirmed by the results of FEA.

Although the proposed (Method I) approach provides lower bound approximation to the problems of interest, the results for very small damaged areas can be fairly conservative compared with FEA results. The value of RSF_α does not converge to unity when there is no damage. For spherical shell with highly localized corroded area or hot spots, the effects of stretching membrane action govern the shell behavior and the decay angle ψ_d is sometimes significantly underestimated. Since a small decay angle indicates an adverse effect, this leads to an overestimation of the effect on the components containing small corroded areas. This usually does not give a problem since very small corrosion spots can simply be ignored. This also depends on how much margin the shell

has. For pressure vessels over $\frac{3}{8}$ in. in thickness (ASME, Part UG-36 Section VIII Division 1) allows $2\frac{3}{8}$ in. diameter opening without reinforcement. This dimension is shown as dashed lines in Figs. 7.4 and 7.7. This opening size may appear to be large for the examples shown above. However, for shells with larger inner radius, this is merely a small size and the dashed lines will be closer to the *y*-axes. Therefore, RSF_{r-1} for very small damages, although fairly conservative, is not of much practical use. Thus, if the conservatism present in the use of RSF_{r-1} for very small damage spots is acceptable, Method I can be adopted for regular use. However, if it is not acceptable, a second alternative recommendation in the form of RSF_{r-2} is proposed. This is based on an approximate calculation of the crossover limit or the threshold between bending and stretching decay angles.

7.3. RECOMMENDATION FOR SPHERICAL SHELLS - METHOD II

7.3.1. Membrane and Bending Effects due to Local Damage

The decay angle of spherical shell calculated as suggested in Chapter 6 is based on applied local loads (shear and moment) acting on the shell. When a shell is subjected to a pure stretching membrane action, the decay angle is not the same. Owing to the nature of shell behavior, the decay length due to membrane action is much larger than that due to bulging action (Tantichattanont, 2006b)..

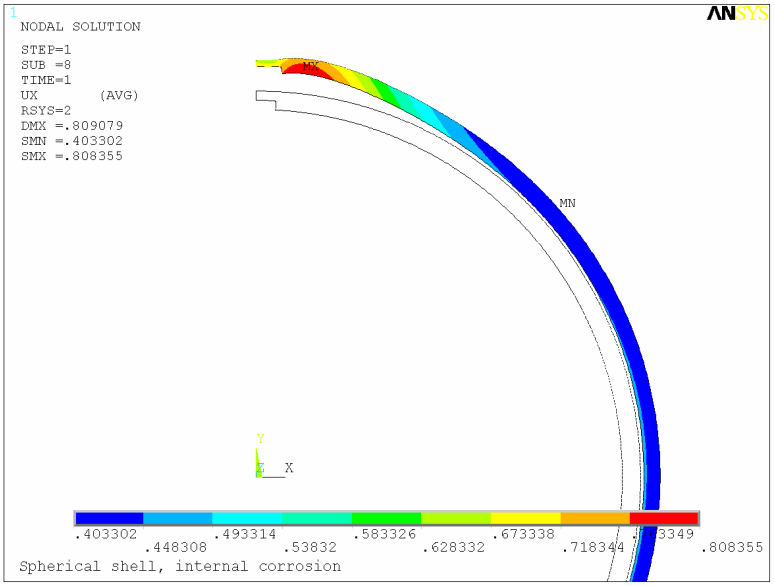

Figure 7.8 Dominance of stretching effect in spherical shell with corrosion damage

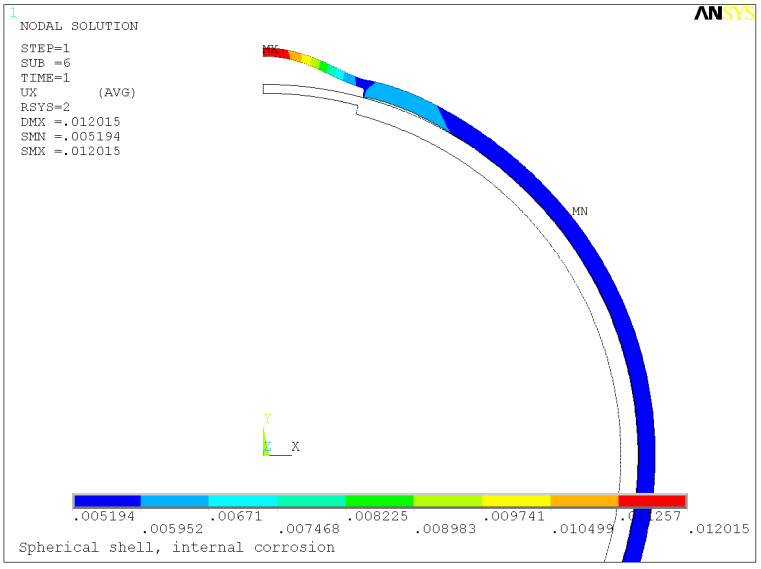

Figure 7.9 Typical bulging of damaged area

For highly localized damaged areas, the effects of membrane action dominate the behaviour of the damaged and surrounding areas. For larger sizes of damaged area, the effects of bending action compared to those of stretching action are increased. At a certain size of damaged spot, a crossover from dominance of the stretching effects to dominance of the bending effects occurs. Membrane action causes the shell to stretch out such that the damaged area becomes flat like the membrane of a musical drum whereas bending action causes the shell to "bulge" or deform in radial (out-of-plane) direction

Results from inelastic finite element analyses illustrate this behavior. The damaged area is stretched and tries to "open up" the surrounding shell rather than becoming a bulge. Figure 7.8 shows an example of the "open up" behaviour and the effect of stretching action in shells with a small damaged area.

For larger sizes of damage, the effects of bulging action compared to those due to membrane action are increased. Eventually, at a certain size of hot spot or corrosion damage, a "crossover" from dominance of the stretching effects to dominance of bulging behaviour occurs. An example of bulging in spherical shell is shown in Figure 7.9.

The behavior of the surrounding region in the two figures 7.8 and 7.9 is different (Figure 7.10). The absence of bulging in Figure 7.8 is partly due to the plastic rotation at the edge of damage similar to the formation of a plastic hinge. The size of a damaged area defining the threshold of dominance of membrane effects for spherical shell is discussed in the following section.

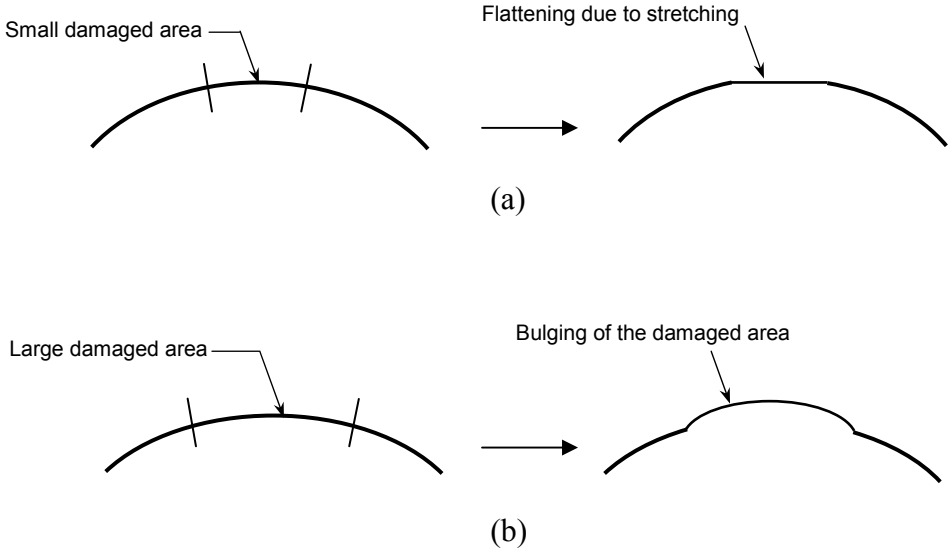

Figure 7.10 Shell behaviors for different sizes of damaged area (a) Open-up behavior (b) Bulging behavior

7.3.2. Threshold to Dominance of Membrane Effects for Spherical Shell

Consider the limit state when "plastic hinges" are formed around the circular damaged area as shown in Figure 7.11. If the damaged spot is not too large, the curved shell can be approximately considered to be a circular flat plate (Figure 7.12a). For a segment of a unit perimeter "cut out" of the circular plate (Figure 7.12b), the edge moment can be calculated by assuming that the undamaged zone is much more rigid than the damaged part.

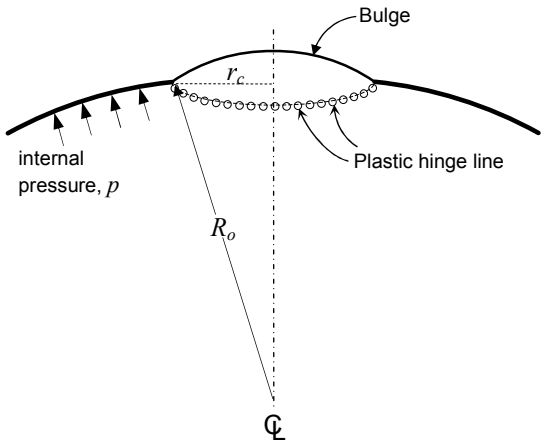

Figure 7.11 Formation of "plastic hinges" along the edge of a circular corroded area

Figure 7.12 (a) Top view of a circular corroded area (b) Unit perimeter segment

The edge moments due to the applied internal pressure, M, can be approximately computed by the resultant force F and the average lever arm measured from the edge of the damaged area (Figure7.12b) as

$$M = p(\Delta A) \cdot \frac{r_c}{3} \tag{7.4}$$

where, p is the applied internal pressure, ΔA is the area of the segment under consideration, and r_c is the radius of the nearly-flat damaged zone.

The area ΔA for a unit length of perimeter is computed as,

$$\frac{\Delta A}{\pi r_c^2} = \frac{1}{2\pi r_c} \quad \text{or} \quad \Delta A = \frac{r_c}{2} \tag{7.5}$$

The plastic moment capacity of the cross section for a unit perimeter segment (Figure 7.13) is

$$M_p = \frac{\sigma_y h_c^{\,2}}{4} \tag{7.6}$$

where, M_p is the plastic moment of the section, σ_y is material yield stress, h_c is the thickness inside the damaged area. In the case of hot spot, the thickness h_c is the same as the original shell thickness h.

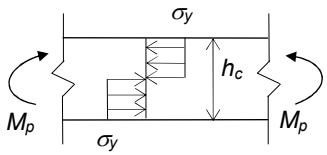

Figure 7.13 Plastic moment capacity of a cross section

The pressure that initiates plastic flow at the edge of the damaged area can then be calculated by equating the moments from Eqs. (7.4) and (7.6). as

$$p\left(\frac{r_c}{2}\right)\cdot\frac{r_c}{3} = \frac{\sigma_y h_c^{\,2}}{4} \tag{7.7}$$

Equation (7.7) leads to the expression for the crossover pressure for a spherical shell, p_s^* as

$$p_s^* = \frac{3}{2}\sigma_y \left(\frac{h_c}{r_c}\right)^2 \tag{7.8}$$

For a given radius of the damaged area r_c, the pressure p_s^* defining the threshold to dominance of membrane action can be calculated. This pressure is a function of material yield stress, remaining thickness and the size of the damaged spot. It is postulated that if the design pressure P_d is smaller than p_s^*, stretching action dominates the behavior of the damage and the decay angle is expected to be larger than the decay angle based on bending effect ψ_d proposed in Eq. (7.1). If the design pressure is larger than p_s^*, bending action dominates the damage behavior and the decay angle ψ_d can be applied for the remaining strength factor calculation.

Rearrangement of Eq. (7.8) leads to the radius of the circular damaged area that defines the threshold between dominance of membrane and bending effects as

$$r_c = h_c \sqrt{\frac{3\sigma_y}{2p_s^*}} \tag{7.9}$$

Membrane action will dominate the behavior of a pressure vessel with a damaged area of radius smaller than r_c, whereas bulging action dominates the behavior of a larger damaged area.

By introducing some safety factor to the calculation above, the threshold angle to the dominance of membrane effect can be given by,

$$\varphi^* = f^* \frac{h_c}{R_o}\sqrt{\frac{3\sigma_y}{2P_d}} \tag{7.10}$$

where, φ^* $(= r_d^* R_o)$ is the included angle of damaged spot at the threshold, r_d^* is the radius of the circle of the damaged spot at the threshold and f^* is an empirical safety factor included to account for the approximation introduced in deriving p^*.

In the present research, the value of f^* is chosen conservatively as 0.5. It can be shown that a slightly larger value of the factor does not significantly alter RSF calculation. Note that the derivation of the above limit is approximate. In reality, the two actions (stretching and bulging) are both present to some extent regardless of the size of the damaged area.

7.3.3. Recommendation and Results

Based on the previous discussion about the demarcation between stretching and bulging, the second recommendation (Method II) RSF_{r-2}, can be determined as shown in Figure7.14.

First, the RSF_α at angle defining the threshold to dominance of membrane effect φ^* is calculated. For small damaged spots where, $\varphi_a < \varphi^*$, RSF_{r-2} is computed by linear interpolation of the known RSF equaling unity at $\varphi_a = 0$ (no damage) and RSF_α at angle

φ^*. For intermediate sized damaged spots where $\varphi^* < \varphi_a < \psi_d$, a linear transition from RSF_α at angle φ^* to RSF_L at angle ψ_d is applied. For large damaged spots with $\varphi_a > \psi_d$, RSF_L is used as in the case of Method I.

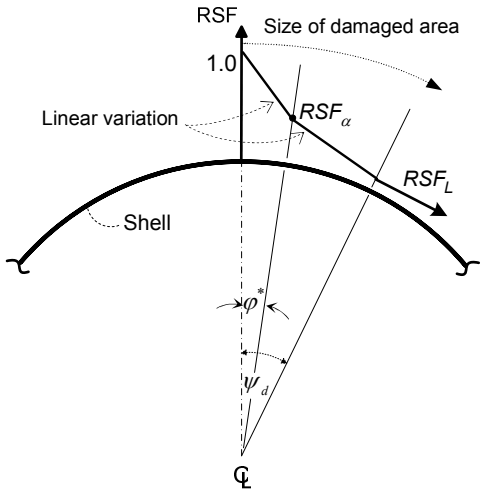

Figure 7.14 Method II Recommendation: RSF_{r-2} for various sizes of damaged areas in spherical shells

In summary, the second recommendation (Method II) for the remaining strength factor (RSF_{r-2}) for a spherical component with a corroded area or a hot spot can be computed as below.

For $\varphi_a \le \varphi^*$, $\quad RSF_{r-2} = 1 - (1 - RSF_\alpha^*)(\varphi_a / \varphi^*)$

For $\varphi^* < \varphi_a \le \psi_d$, $\quad RSF_{r-2} = RSF_\alpha^* - \dfrac{RSF_L - RSF_\alpha^*}{\psi_d - \varphi^*}(\varphi^* - \varphi_a)$ (7.11)

For $\varphi_a > \psi_d$, $\quad RSF_{r-2} = RSF_L$

where, RSF_{α}^{*} is RSF_{α} at angle φ^{*}.

Some samples of comparisons of the Method II recommended RSF_{r-2} and inelastic RSF_{i} for various cases of corrosion and hot spot damage in spherical shells are illustrated in Figures 7.15 and 7.16.

It must be noted that for the purpose of plotting the curve for RSF_{r-2}, the design pressure must be specified in order to calculate the angle φ^{*}. For the graphs as shown below, the design pressures are computed by using the maximum internal pressure that can be sustained by the shell, i.e., the design pressures in these figures are back-calculated from the formula for design thickness. The actual design pressures will be lower than those that are back calculated and hence the actual curves will be less conservative than those shown in the figures. The RSF_{r-2} is shown to provide lower bound approximations for all the cases studied and reduce the conservatism present in RSF_{r-1} for highly localized damage.

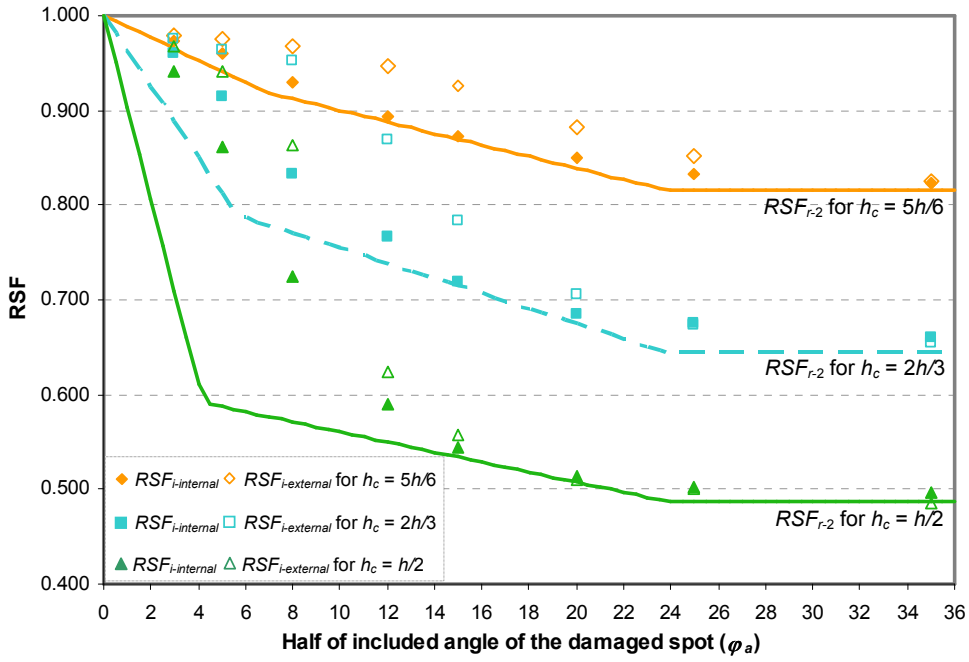

Figure 7.15 Comparison of RSF_{r-2} and RSF_i for internal and external corrosion in spherical shells with R/h ratio = 20

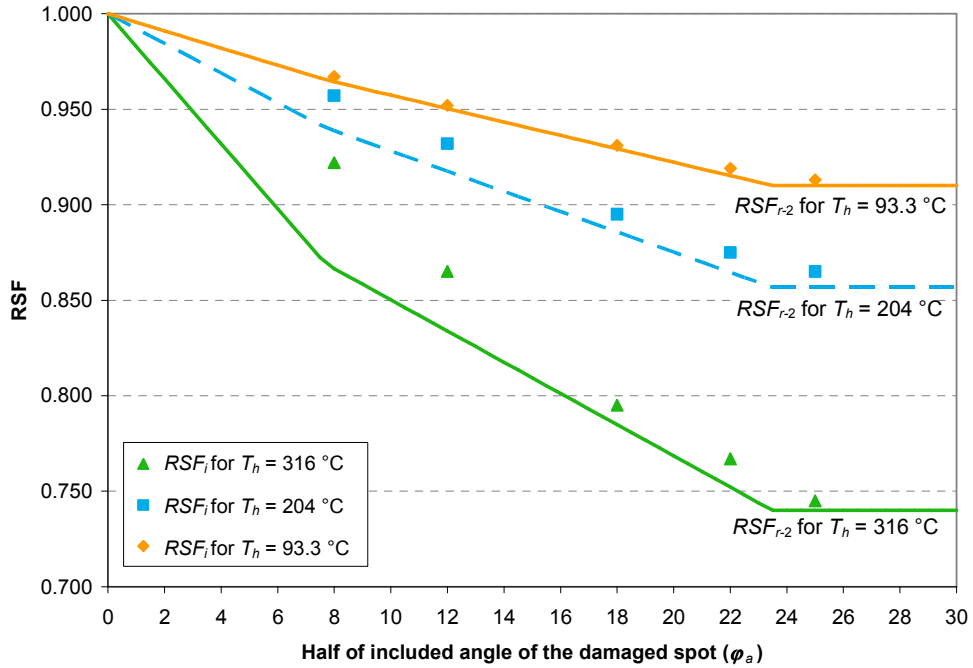

Figure 7.16 Comparison of RSF_{r-2} and RSF_i for thermal hot spots in spherical shells with R/h ratio = 20

7.4. RECOMMENDATION FOR SPHERICAL SHELLS – METHOD III

As it can be seen that both Method I and II presented above have phenomenological and intuitive basis and are grounded in variational formulation in the form of m_α calculation, etc. They are both lower bound estimates. However, both the recommendations employ linear transitions and have a kink at the changeover points. A third recommendation is provided if the user likes to avoid these issues. This method (III) uses RSF_L for large corroded areas as in the case of the other two recommendations. For smaller corrosion areas, a parabolic transition is employed between the limits of $RSF_{r\text{-}3}$ = 1 at $\varphi_a = 0$ and $RSF_{r\text{-}3} = RSF_L$ at $\varphi_a = \psi_d$ (as shown in Figure 7.17).

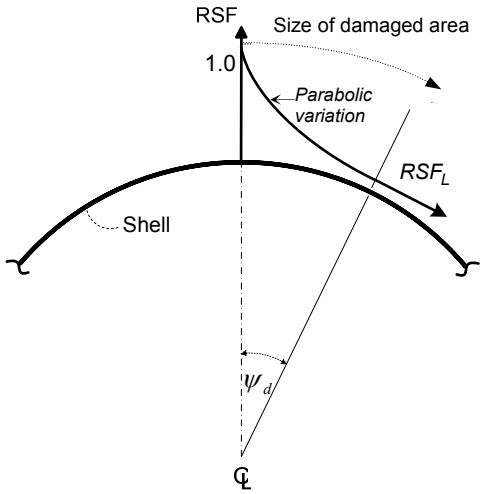

Figure 7.17 Method III Recommendation: RSF_{r-3} for various sizes of damaged areas in spherical shells

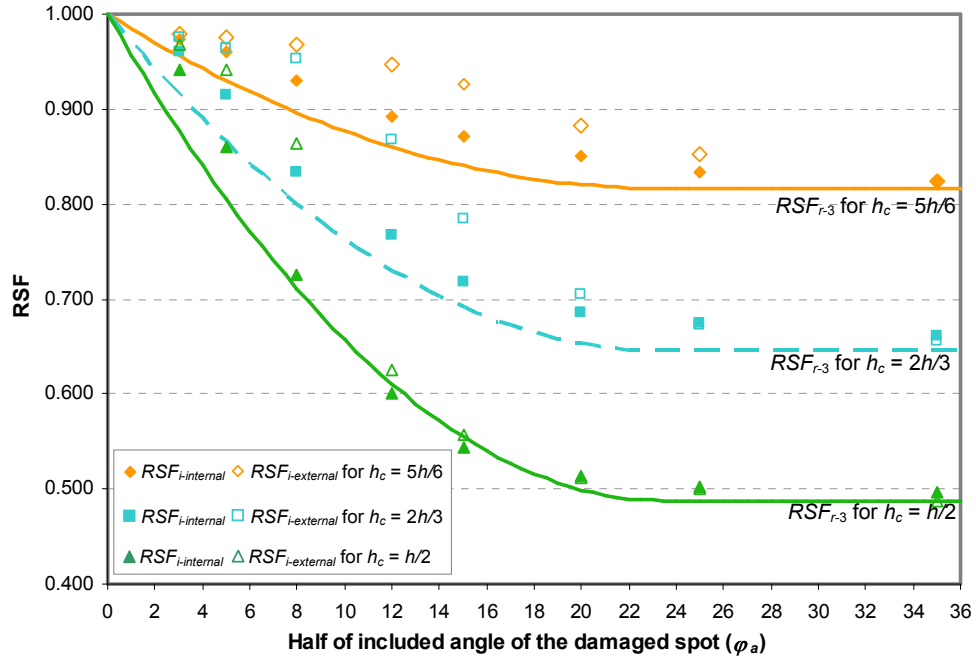

Figure 7.18 Comparison of RSF_{r-3} and RSF_i for internal and external corrosion in spherical shells with R/h ratio = 20

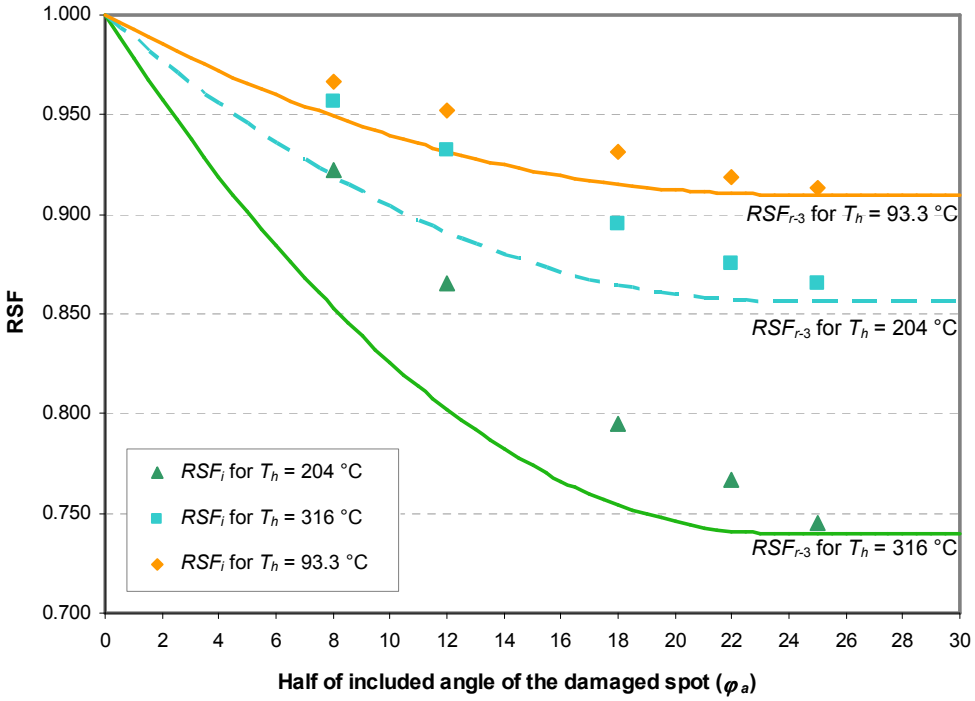

Figure 7.19 Comparison of RSF_{r-3} and RSF_i for thermal hot spots in a spherical shell with R/h ratio = 20

The function for RSF_{r-3} can be expressed as below:

$$\text{For } \varphi_a \le \psi_d, \quad RSF_{r-3} = \frac{1 - RSF_L}{\psi_d^2}\varphi_a^2 - \frac{2\left(1 - RSF_L\right)}{\psi_d}\varphi_a + 1$$

$$\text{For } \varphi_a > \psi_d, \quad RSF_{r-3} = RSF_L \tag{7.12}$$

It must be noted that Method III is simpler than the previous two. However, it is also less grounded in theoretical considerations compared to the first two recommendations.

Figures 7.18 and 7.19 show some examples of RSF_{r-3} compared with inelastic RSF_i from FEA for spheres (R/h = 20) with corrosion damage and thermal hot spots, respectively. It can be seen that RSF_{r-3} gives close lower bound approximates to almost all of the cases. Numerical results and additional graphs are provided in Appendix A.

7.5. DISTORTION DUE TO BULGING

Deformation due to damaged spots could result in bulging of the component. Bulging is the local inward or outward deviation from the original geometry. Strain due to bulging and the included angle (Seshadri, 2004) of the bulge can be shown to be,

$$\varepsilon_b = \frac{R_b\varphi_b - R_o\varphi_a}{R_o\varphi_a} \quad \text{and} \quad \varphi_b = \arcsin\left(\frac{R_o \sin\varphi_a}{R_b}\right) \tag{7.13}$$

where, ε_b is the maximum membrane strain in the bulge, and R_o is the outside radius of the shell. The angle φ_a is the included angle of the corrosion or hot spot area and R_b and φ_b are the radius and angle of the bulge as shown in Figure 7.20.

By limiting ε_b to 1%, we can find R_b and φ_b from Eq. (7.13). Radial displacement of the assumed spherical bulge δ_b is then given by

$$\delta_b = (R_b - \delta_o) - \sqrt{R_b^2 - (R_o \sin\varphi_a)^2} \tag{7.14}$$

where, $\delta_o = (1 - \cos\varphi_a) R_o$.

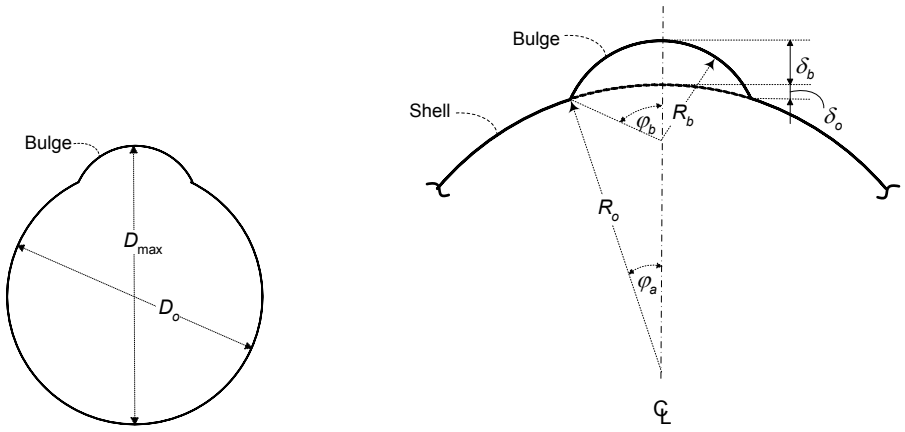

Figure 7.20 Idealized bulging geometry

The out-of-roundness ratio is computed as the ratio of the maximum diameter of the component due to bulging $D_{\max} (= D_o + \delta_b)$, and the original diameter of the component D_o, as shown in Figure 7.20. If the out-of-roundness ratio exceeds a certain

recommended value, RSF_r should be taken as RSF_L. This will be an additional limit criterion for the shell based on excessive deformation.

7.6. ILLUSTRATIVE EXAMPLE

The following example is given to demonstrate the proposed Level 2 integrity assessment methods for a sphere under internal pressure. The values given in the parentheses are in SI units.

ASTM Material	:	SA 516 Grade 55
Shell Inside Radius (R_i)	:	21.9 in. (556 mm)
Operating Pressure	:	250 psi (1.72 MPa)
Design Pressure (P_d)	:	390 psi (2.69 MPa)
Operating Temperature	:	90 °F (32.2 °C)
Design Temperature	:	100 °F (37.8 °C)
Corrosion Allowance (CA)	:	1/16 in (1.59 mm)
Joint Efficiency (E_j)	:	1.0

7.6.1. Required Thickness Calculation

Design thickness, h_d, for spherical shell can be determined as (Bednar, 1985):

$$h_d = \frac{P_d R_i}{2SE_j - 0.2P_d} = 0.313 \text{ in. } (7.95 \text{ mm})$$

Required shell thickness is $h = h_d + CA = 0.375$ in. (9.53 mm)

Therefore, a 3/8 in. wall thickness is specified.

The allowable RSF can be expressed as $RSF^* = h_d/h = 0.835$. Note that this RSF^* is based on design requirements.

Outside radius of the sphere, $R_o = 22.275$ in. (566 mm)

In this case, R/h ratio is 58.9.

The decay angle of spherical shells is calculated from Eq. (7.1), $\psi_d = 13.7°$.

7.6.2. Recommended RSF_r for Corrosion Damage

For the following demonstration for corrosion damage, the thickness loss inside the corroded area is assumed to be equal to $h/6 = 1/16$ in. (1.59 mm). For internal corrosion, the inner radius of the shell inside the corroded spot R_c becomes 21.963 in. (558 mm) and the remaining thickness h_c is 5/16 in. (7.94 mm)

The extent of the corroded spot are defined with $\varphi_a = 8.0°$.

From Eq. (7.2), $\psi_L = 4.6°$.

Since $\psi_L < \varphi_a \leq \psi_d$, this is the case of intermediate corroded spot. $RSF_{r\text{-}1}$ is calculated from the second of Eq. (7.3) and $RSF_{r\text{-}3}$ is calculated from the first of Eq. (7.12).

The angle for reference volume is $\varphi_R = \varphi_a + \psi_d = 21.7°$

From Eq. (4.1), Corroded Volume $V_D = \pi R_o^2 h_c(1-\cos\varphi_a) = 9.481$ in^3 (1.554×10^4 mm^3)

From Eq. (4.2), adjacent Volume $V_I = \pi R_o^2 h(\cos\varphi_a - \cos(\varphi_a+\psi_d)) = 67.43$ in^3 (1.105×10^6 mm^3)

Reference Volume $V_R = V_D + V_I = 76.91$ in^3 (1.260×10^6 mm^3)

The yield stress of carbon steel at a temperature of 100 °F (37.8 °C) is 30 ksi (207 MPa)

The primary stress of the undamaged shell is $\sigma_{eI} = P_d R_i/2h = 11.4$ ksi (78.6 MPa)

The primary membrane stress inside the corroded spot is $\sigma_{eD} = P_d R_c/2h_c = 13.8$ ksi (96.1 MPa)

Comparing with σ_y, σ_{eI} and σ_{eD} indicate that there is no general yielding through membrane action. It must be noted that σ_{eI} and σ_{eD} need not be computed to estimate RSF values although it serves a useful purpose to compare with σ_y.

Using the above, $m_u^0 = \sigma_y / \sigma_{eI} = 2.620$ and $m_L = \sigma_y/\sigma_{eD} = 2.177$.

From Eq. (6.14), $RSF_L = m_L / m_u^0 = 0.831$

The RSF_U and RSF_α can be calculated for on Tresca and von Mises yield criteria.

Tresca criterion:

From Eq. (4.18), $m_d^0 = \dfrac{\sigma_y V_R}{\sigma_{eI}^0 V_I + \sigma_{eD}^0 V_D} = 2.556.$

From Eq. (4.21), $RSF_U = m_d^0 / m_u^0 = 0.976$.

$$Z = \frac{m_d^0}{m_L} = 1.174.$$

From Eq. (3.19), $m_\alpha = 2.408$.

From Eq. (4.22), $RSF_\alpha = m_\alpha / m_u^0 = 0.919$.

Von Mises criterion:

From Eq. (4.20), $m_d^0 = \sqrt{\frac{\sigma_y^2 V_R}{\sigma_{eI}^2 V_I + \sigma_{eD}^2 V_D}} = 2.551$

From Eq. (4.21), $RSF_U = m_d^0 / m_u^0 = 0.974$.

$$Z = \frac{m_d^0}{m_L} = 1.171.$$

From Eq. (3.19), $m_\alpha = 2.406$.

From Eq. (4.22), $RSF_\alpha = m_\alpha / m_u^0 = 0.918$.

Similarly, RSF_α calculated using the angle $\varphi = \psi_L$ is 0.926.

From the second of Eq. (7.3), $RSF_{r\text{-}1} = 0.887$

From Eq. (7.10), the angle $\varphi^* = 4.4°$. Thus, RSF_α at the angle φ^* is 0.926. Linear interpolation from RSF_α at the angle φ^* and RSF_L at the angle ψ_d using the third of Eq. (7.11) gives $RSF_{r\text{-}2} = 0.887$.

From the first of Eq. (7.12), $RSF_{r\text{-}3} = 0.857$

If the maximum strain in the bulge ε_b is 1%, from Eqs. (7.13), R_b = 12 in. (305 mm) and φ_b = 15.0°.

From Eq. (7.14), δ_b = 0.191 in. (4.85 mm). This corresponding value from inelastic analysis is 0.082 in. (2.08 mm). The MATLAB files used in calculation of δ_b are given in Appendix B (along with spreadsheet files in the CD).

Thus, $r_{out\text{-}of\text{-}roundness} = (D_o + \delta_b)/D_o = 1.004 \leq 1.01$.

7.6.3. Recommended RSF_r for Thermal Hot spot Damage

For the following example for thermal hot spot evaluation, hot spot temperature is assumed as 400 °F (204 °C).

The dimensions of the hot spot are defined with φ_a = 10.0°.

From Eq. (7.2), ψ_L = 4.6°.

Since $\psi_L < \varphi_a \leq \psi_d$, this is the case of intermediate hot spot. $RSF_{r\text{-}1}$ is again calculated from the second of Eq. (7.3) and $RSF_{r\text{-}3}$ is calculated from the first of Eq. (7.12).

The angle for reference volume is $\varphi_R = \varphi_a + \psi_d$ = 23.7°.

From Eq. (4.1), Hot spot Volume $V_D = \pi R_o^2 h(1\text{-}\cos\varphi_a)$ = 17.76 in^3 (2.91×10^5 mm^3).

From Eq. (4.2), Adjacent Volume $V_I = \pi R_o^2 h(\cos\varphi_a - \cos(\varphi_a+\psi_d))$ = 80.71 in^3 (1.32×10^5 mm^3).

Reference Volume $V_R = V_D + V_I = 98.472$ in^3 (1.61×10^5 mm^3).

The yield stress of steel at a temperature of 100 °F (37.8 °C) is 30 ksi (207 MPa)

The yield stress of steel at the hot spot temperature of 400 °F (204 °C) is 25.7 ksi (177 MPa)

The thermo-elastic primary stress of the shell is calculated as $\sigma_e = p_d R_i/2h - E\alpha\Delta T/2 =$ 14.0 ksi (96.5 M Pa)

Using the above, $m_u^0 \doteq \sigma_{yc.}/\sigma_e = 2.149$ and $m_L \doteq \sigma_{yh.}/\sigma_e = 1.841$.

From Eq. (6.14), $RSF_L = m_L / m_u^0 = 0.857$.

Tresca criterion:

From Eq (4.14), $m_d^0 = \dfrac{\sigma_{yI} V_I + \sigma_{yD} V_D}{\sigma_e V_R} = 2.09$

From Eq. (4.21), $RSF_U = m_d^0 / m_u^0 = 0.974$.

$Z = \dfrac{m_d^0}{m_L} = 1.137$.

From Eq. (3.19), $m_\alpha = 2.000$.

From Eq. (4.22), $RSF_\alpha = m_d^0 / m_u^0 = 0.931$.

Von Mises criterion:

From Eq. (4.16), $m_d^0 = \sqrt{\dfrac{\sigma_{yI}^2 V_I + \sigma_{yD}^2 V_D}{\sigma_e^2 V_R}} = 2.096$

From Eq. (4.21), $RSF_U = m_d^0 / m_u^0 = 0.976$.

$$Z = \frac{m_d^0}{m_L} = 1.139.$$

Similarly, RSF_α calculated using the angle $\varphi = \psi_L$ is RSF_α at the angle $\psi_L = 0.940$.

From the second of Eq. (7.3), $RSF_{r\text{-}1} = 0.890$

From Eq. (7.10), the angle $\varphi^* = 4.4°$. Thus, RSF_α at the angle φ^* is 0.926. Linear interpolation from RSF_α at the angle φ^* and RSF_L at the angle ψ_d using the third of Eq. (7.11) gives $RSF_{r\text{-}2} = 0.892$.

From the first of Eq. (7.12), $RSF_{r\text{-}3} = 0.867$

If the maximum strain in the bulge ε_b is 1%, from Eqs. (7.13), $R_b = 13.095$ in.(333 mm) and $\varphi_b = 17.2°$.

From Eq. (7.14), $\delta_b = 0.246$ in. (6.25 mm). This corresponding value from inelastic analysis is 0.091 in. (2.31 mm). The MATLAB files used in calculation of δ_b are in Appendix B (spreadsheet files are in the CD).

Thus, $r_{out\text{-}of\text{-}roundness} = (D_o + \delta_b)/D_o = 1.006 \leq 1.01$.

7.6.4. Comparison with Nonlinear (Level 3) Analysis

To verify the above recommendation, the inelastic remaining strength factor RSF_i is calculated from the ratio of the internal pressure that causes 1% von-Mises membrane

strain in the damaged region to the limit pressure of the undamaged sphere. For the examples given above, RSF_i is 0.949 and 0.915 for corrosion damage and hot spot, respectively. It can be seen that all three recommendations of the current study provide lower bound RSF approximations compared to the inelastic results. Thus, the recommended RSF are acceptable and conservative.

It may be noted that an improved estimate of the mobilized reference volume might yield a better prediction. However, the aim of the present study is to give the practicing engineers a simple yet effective Level 2 method of obtaining the remaining strength factor without recourse to a detailed study.

7.7. DISCUSSION

7.7.1. Comparison of the Three Methods

The three recommended RSF as proposed above and the inelastic RSF are compared. Some sample plots of spheres with R/h ratio 58.9 for corroded thickness $5h/6$ and $h/2$ are shown in Figures 7.21 and 7.22, respectively. Examples of numerical data are shown in Table 7.7.

It can be seen that all three recommended methods offer the same RSF for large damages. For large damages, the results are very close to the Level 3 inelastic RSF. For highly localized damages, RSF_{r-2} and RSF_{r-3} provide closer approximations than RSF_{r-1} as discussed earlier. In most cases, RSF_{r-1} and RSF_{r-2} give better RSF estimate for

damages of intermediate size than RSF_{r-3} (Figure 7.21). However, in some cases particularly when the depth of corrosion is large, RSF_{r-3} can provide the closest recommendation to the inelastic RSF compared to the other two (Figure 7.22). Note that all the three proposed methods are shown to provide a lower bound estimation compared to inelastic FEA results. The first method is more theoretically grounded than the other two but can overestimate the adverse effect for very small damaged areas. In general, the second method RSF_{r-2} gives closer RSF estimation than the first recommendation. The third method can be used with the least amount of calculation among the three. The users can choose one of the three methods depending on their preference for rigor and the amount of computation (Tantichattanont, 2006c)..

Table 7.7 Comparison of the three methods with inelastic analysis of a sphere (R/h =58.9, corroded thickness $h/2$)

φ_a	RSF_U	RSF_{r-1}	RSF_{r-2}	RSF_{r-3}	$RSF_{inelastic}^{internal}$
3°	0.970	0.606	0.602	0.778	0.863
5°	0.936	0.594	0.578	0.665	0.715
8°	0.887	0.551	0.542	0.550	0.568
12°	0.831	0.496	0.496	0.496	0.518
15°	0.831	0.496	0.496	0.496	0.507
20°	0.797	0.496	0.496	0.496	0.501

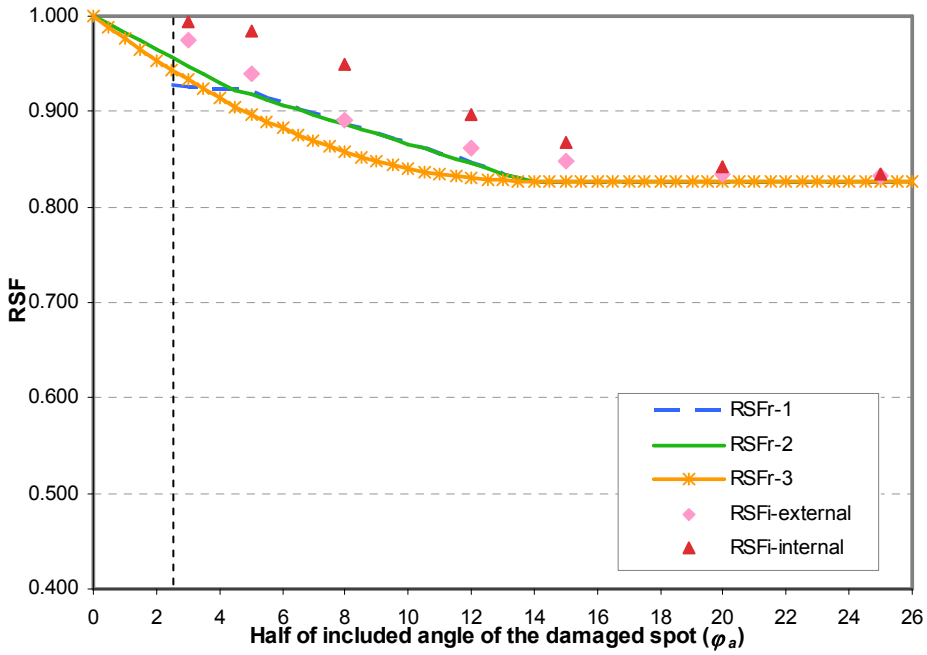

Figure 7.21 Comparison of the three RSF recommendations for spherical shells (R/h ratio = 58.9, corroded thickness $h_c = 5h/6$)

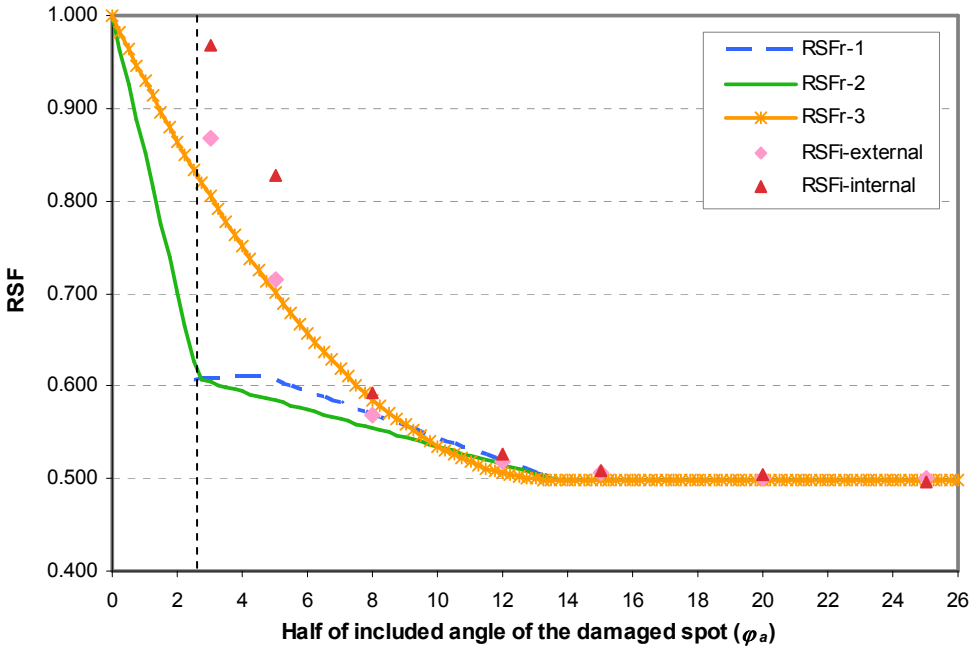

Figure 7.22 Comparison of the three RSF recommendations for spherical shells (R/h ratio = 58.9, corroded thickness $h_c = h/2$)

7.7.2. Effect of *R*/*h* ratio and Inner Radius

Since the recommended RSF in the current study depends on the *R*/*h* ratio rather than the exact values of *R* and *h*, an inelastic finite element analysis of another smaller sphere with *R*/*h* ratio of 20 but the shell inner radius of 7.5 in. is also studied for corrosion damage. The comparison between these results is shown in Table 7.8. As expected, the two spheres possess similar remaining strength for all the cases.

Table 7.8 Comparison of the RSF_i for spheres *R*/*h* ratio 20 with different inner radius

h_c	φ_a	RSF_i		Percent Difference
		R_i = 21.9 in.	R_i = 7.5 in.	
5*h*/6	5°	0.976	0.975	0.1%
5*h*/6	8°	0.969	0.968	0.1%
5*h*/6	12°	0.947	0.947	0.0%
2*h*/3	5°	0.953	0.930	2.3%
2*h*/3	8°	0.868	0.838	0.9%
h/2	5°	0.941	0.941	0.0%
h/2	12°	0.625	0.614	1.8%

Unlike RSF recommendation in the present study, Sims, et al. (1992) suggest an empirical equation for the remaining strength of spherical shells containing LTA's be independent of R/h ratio. However, FEA results show an effect of R/h ratios on RSF values. Table 7.9 compares inelastic RSF for damaged areas with the same ratio of corroded thickness to original thickness (h_c/h) and the same included angle (φ_a) for spheres with R/h ratios of 20 and 58.9. The shell inner radius for both cases is 21.9 in.

Table 7.9 Comparison of RSF_i for spheres with R/h ratios 20 and 58.9

h_c	φ_a	RSF_i		Percent Difference
		$R/h = 20$	$R/h = 58.9$	
$5h/6$	5°	0.976	0.983	0.7%
$5h/6$	15°	0.926	0.842	9.0%
$2h/3$	8°	0.953	0.867	14.9%
$2h/3$	15°	0.784	0.687	12.4%
$h/2$	5°	0.941	0.828	12.0%
$h/2$	12°	0.625	0.526	15.8%
$h/2$	20°	0.511	0.503	1.6%

It can be seen that although RSF for the two cases are not much different for very small damage, the discrepancies are much larger when the damages are more severe. In most cases, RSF for spherical shells with larger R/h ratio (thinner shells) are less than those for spheres with smaller R/h ratio (thicker shells). This can be explained as the effect of a smaller decay angle and more contained effects from local damage in thin shells. For damaged areas with very large included angle, the damage is considered "global" and RSFs are converging to RSF_L (= h_c/h) as discussed before. Hence, the differences between the two cases are small for very large damages. For intermediate size damages, the difference in RSF for thinner and thicker shells can be significant as shown in the table.

7.7.3. Shape Independence Feature of RSF

It can be seen that the three remaining strength factors used in the present research, i.e., RSF_U, RSF_α and RSF_L (as defined by Eqs. (4.21), (4.22) and (4.23), respectively) are non-dimensional. They only depend on the ratios of physical parameters and not on actual values. Hence, the theory for the calculation of RSF is very likely common to all shapes and sizes of pressure vessels provided that a few necessary adjustments are made to the parameters, e.g., the decay length along the generator for a cone will include the term *sin(*β*)*, where β is the angle of the side with the base.

The shape influences the equivalent primary stress. For example, calculation of equivalent stress σ_e will use $P_d R_i / 2h$ for spheres and $\sqrt{3} P_d R_i / 2h$ for cylinders. The

individual load factors m_u^0, m_L, etc., are all inversely proportional to σ_e for any given pressure. The RSFs, however, are ratios of these load factors. Thus, the RSFs are not directly dependent on the shape induced primary stress σ_e. This can be easily verified. Therefore, the RSF for any pressure vessel is only a function of the geometrical and material property ratios for a given situation and are independent of the actual applied (or operating) load. The shape, of course, influences the decay length and hence the reference volume. But, for the same volume ratio, the formulas (and values) of RSF_U, RSF_α and RSF_L are identical for a sphere and a cylinder. It can be postulated that for other types of geometries, we can use the same argument and obtain a simplified level 2 estimation of RSF. This could be a key conclusion of the present research.

In terms of property ratios, we can express RSF for pressure vessels containing hot spots as below. Let $r_V = V_D / V_I$, $r_\sigma = \sigma_{yD} / \sigma_{yI}$, and $r_\alpha = \sqrt{\dfrac{1 + r_\sigma^2 r_V}{1 + r_V}}$. Then,

$$
\begin{aligned}
Z &= r_\alpha / r_\sigma \\
RSF_U &= r_\alpha \\
RSF_\alpha &= 2 r_\alpha \left[\frac{2Z^2 + \sqrt{Z(Z-1)^2 (1+\sqrt{2}-Z)(Z-1+\sqrt{2})}}{(Z^2 + 2 - \sqrt{5})(Z^2 + 2 + \sqrt{5})} \right] \\
RSF_L &= r_\sigma .
\end{aligned}
\tag{7.15}
$$

The non-dimensional ratios for corrosion similar to those for hot spots become $r_V = V_I / V_D$, $r_\sigma = \sigma_{eI} / \sigma_{eD}$, and $r_\alpha = \sqrt{\frac{1+r_V}{1+r_\sigma^2 r_V}}$. However, the RSF formulas in Eqs. (7.15) remain the same for corrosion as well.

Note that since internal pressure is considered as the only primary load, the equivalent stresses in the corroded and uncorroded areas (σ_{eD} and σ_{eI}) are calculated as $PR_i/2h$ and $PR_C/2h_C$, respectively, where, R_C is the inner radius of the corroded segment of the component and h_C is the remaining thickness of the corroded area or the original thickness for hotspot problems. Hence, the ratio r_σ here equals to $\frac{h_c/h}{R_i/R_c}$ which depends only on the geometry of the component and the damaged area and not the actual applied load.

For corrosion damage, it can also be observed that since the inner radius R_c of a pressure vessel containing external corrosion is the same as the uncorroded inner radius R_i , r_σ will only be the ratio of the remaining thickness and the uncorroded thickness. However, R_c is slightly larger than R_i for pressure components with internal corrosion. Thus, r_σ and consequently RSF_L for internal corrosion will be slightly less than that for external corrosion for the same thickness loss. In thin shells, this difference is not prominent and hence the more conservative RSF calculation assuming internal corrosion has been presented in the current study.

7.8. SUMMARY

The main factors influencing the remaining strength factors of pressurized components containing local damages such as corrosion or thermal hot spots are: the size of the damage, shell geometry and material characteristics. These factors have been considered in the Level 2 assessments recommended in this chapter. A decay angle for spherical shells based on edge effects is defined. It gives the extent of what can be called as 'local' damage. Various aspects of these edge effects have been discussed using shell theory and simplified analysis. Three alternative methods (recommendations) are proposed using the concept of reference volume in conjunction with a variational formulation to assess limit strength. These recommendations will be the basis of RSF evaluation in cylindrical shells.

For corroded areas or hot spots larger than the local damage limit, the lower bound remaining strength factor RSF_L is used in all the three methods. For very small damaged spots, the recommendations involve using the m_α-multiplier and integral mean of yield criterion or a transition between two limit points. For intermediate size damaged spots, a linear or parabolic transition is shown to work well.

The first recommendation is more conservative than the others for very small damaged spots but is also more theoretically grounded. The second recommendation involves a simplified analysis to identify the threshold between dominance of stretching and bending effects. It uses a linear transition between applicable points and uses the

m_α - multiplier for the intermediate limit. Third recommendation involves a simple parabolic transition between the zero damage case and the limiting case for large damages.

All the three proposed recommendations are verified to provide good lower bound estimation compared to inelastic FEA results. The users can choose one of the three methods depending on their need or preference for rigor and the amount of computation. Excessive deformation in bulging is also prevented by limiting the out-of-roundness ratio of the shell to 1.01. Approximate equations for estimating the bulging displacement are provided.

CHAPTER 8

RECOMMENDATIONS FOR REMAINING STRENGTH FACTORS OF CYLINDRICAL SHELLS

The present chapter proposes Level 2 Fitness-for-Service (FFS) assessment procedures for cylindrical pressure vessels with corrosion damage or thermal hot spots. The extent of "local" damage in cylindrical shells and interactions of damage effects in the circumferential and axial directions of the shells are discussed based on elastic decay lengths.

Three methods for assessment of spheres were proposed in Chapter 7. These are used in the present chapter as the basis of the recommendations for similar problems in cylindrical shells. The effectiveness of the recommendations is verified through illustrative examples and comparison with results from Level 3 inelastic finite element analysis.

8.1. LOCAL DAMAGE AND INTERACTION EQUATIONS

The size of "local damage" in a cylindrical shell can be suggested on lines similar to those proposed for spheres in Chapter 7. Damage can be called "local" when the edge effect from the undamaged region has not yet dissipated inside the damaged area thus preventing pure membrane stress from occurring anywhere inside the damaged zone. Damage larger than the limit for "local" is identified as "global" damage.

As in the case of spheres, decay lengths of cylinders proposed in Chapter 6 can be used to define the extent for local damage. However, unlike the case for spheres, where the damaged zone is assumed to be circular, the cylinder damages can be anywhere between a perfect square and very long and narrow rectangle. For narrow rectangles, the edge effects in the narrow direction interfere with those in the length direction. Interaction of such effects in circumferential and axial directions is investigated and discussed in detail in Section 8.1.2. The proposed interaction curves for different aspect ratios of damaged area are verified by comparison with inelastic results.

8.1.1. Local Damage Limit

Typical damaged zones in cylinder are assumed to be rectangles $2a \times 2b$, where a and b are half of the damaged area dimensions measured along circumferential and axial direction, respectively. If damaged zones are not exactly rectangular, equivalent rectangles bounding around damage are assumed.

As discussed in Chapter 6, elastic decay lengths in axial and circumferential directions (x_l and x_c, respectively) are calculated as given below

$$x_l \approx 2.5\sqrt{Rh} \qquad \text{and} \qquad x_c = 6.3\sqrt{Rh} \tag{8.1}$$

It is postulated that if the size of the damage is smaller than $2x_c \times 2x_l$, there will be no pure membrane action at any point inside the damage. If the damage is slightly larger than $2x_c \times 2x_l$, pure membrane stress will occur at the centre of the damaged area. This can be called as "global" damage. The behaviour then is "as if" the damage extends over the entire cylinder.

Note that since the effect from the discontinuity in the circumferential direction dissipates at the distance x_c inside the damage as well as outside the damage, for both effects not to interact, the distance $2x_c$ cannot be larger than half of the cylinder perimeter or $2(6.3\sqrt{Rh}) \leq \pi R$. Hence, the proposed x_c is valid for only cylinders with R/h greater than 16. For cylinders with R/h ratio less than 16, interaction will occur. This effect is outside the scope of the current study.

8.1.2. Interaction of Damage in Axial and Circumferential Directions

Different damage sizes yield different RSF for the pressure vessel. The proposed Level 2 methods for RSF indicate that RSF gradually decreases with increase in damage size until it reaches a "global" size damage. In sphere, the size of the damage is simply defined by the central included angle. However, in the case of the cylinder the damage

defined by both *a* and *b*. If *a* is large, the edge effects in the circumferential direction will not play any role in the RSF. However, if *b* is not large, the edge effects still influence the RSF. A similar effect is observed if *a* is small and *b* is large. There is a definite interaction between *a* and *b* in defining the extent of damage and its influence on the calculation of RSF. We need to have a single parameter to characterize the severity of damage instead of two values *a* and *b*. Such interaction curves are common when more than one parameter (or effect) influences "failure" or limit criterion simultaneously. For example, if a column is subject to axial load only, the limit criterion is given as $C_f \le C_r$, where, C_f is the applied compressive force and C_r is the compressive resistance. If the same member is subject to bending moment only, its limit criterion is given by $M_f \le M_r$, where M_f is the applied moment and M_r is the moment resistance. It is well known that if a certain C_f ($\le C_r$) and some other M_f ($\le M_r$) are both present, the failure criterion is not a single point but is instead given by an interaction curve defined as $\frac{C_f}{C_r} + U\frac{M_f}{M_r} \le 1$, where *U* is an amplification factor. The left hand side of the above equation presents a single factor for the combined effect of axial force and moment which will have a single limiting value (1.0). Similar logic is used here to estimate the interaction between decay lengths in axial and circumferential directions of a cylinder.

Interaction in axial and circumferential directions for damages with aspect ratios (b/a) other than x_c/x_l is investigated by proposing linear or elliptic interaction curves. Linear and elliptic interaction curves are simple to calculate and have been effectively used in many areas. Any of these interaction curves need to pass through the point

(x_l, x_c) . Figure 8.1 shows an example of such interaction curves for a particular cylindrical shell with inner radius of 21.0 in.(533 mm) and wall thickness of 0.625 in. (15.9 mm). For this cylinder, the decay length in the axial direction, x_l, is 9.1 in.(232 mm) and the decay length in the circumferential direction, x_c, is 22.8 in. (579 mm). Corroded areas or thermal hot spots with dimensions inside the area enclosed by an interaction curve might be considered "local" damage. Any damage with dimensions outside this bound might be regarded as "global" damage.

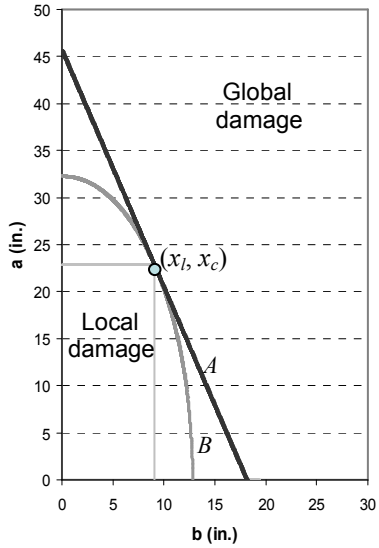

Figure 8.1 Linear and elliptic interaction curves

Equation for linear interaction curves can be written in the form,

$$\alpha \frac{b}{x_l} + (1-\alpha)\frac{a}{x_c} = 1.0 \tag{8.2}$$

where, α is a slope parameter varying from 0 to 1. The larger the parameter α, the steeper the line. It can be seen from Figure 8.2 that the local damage limit depends on the value of parameter α and the aspect ratio of the damaged area.

For each b/a ratio (= r), the limits for local damage based on linear interaction curves (defined by $a_{L,linear}$ and $b_{L,linear}$) can be calculated by substitution of $b = a \times r$ into Eq. (8.2). This gives

$$a_{L,linear} = \frac{x_c x_l}{\alpha r x_c + (1-\alpha) x_l} \quad \text{and} \quad b_{L,linear} = a_{L,linear} r \tag{8.3}$$

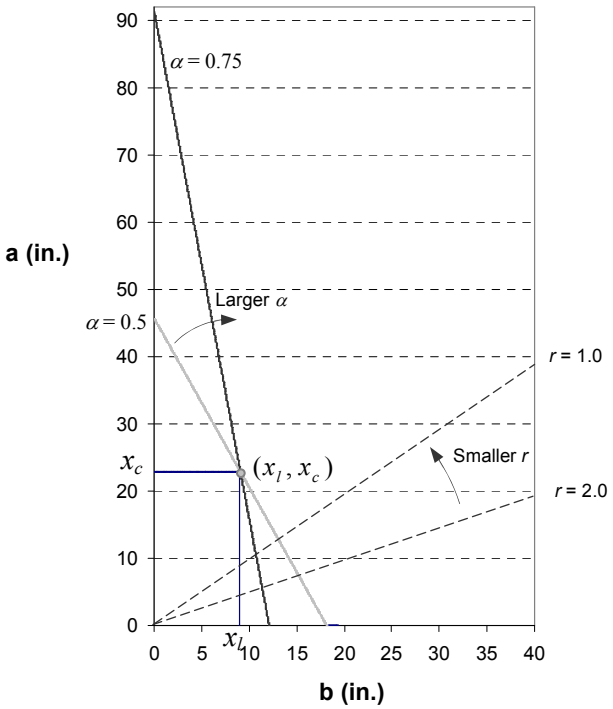

Figure 8.2 Extent for local damage for different values of slope parameter α.

The local damage limits based on elliptic interaction curves can also be calculated in a similar manner. Equations for elliptic interaction curves are in the form,

$$\beta\left(\frac{b}{x_l}\right)^2 + (1-\beta)\left(\frac{a}{x_c}\right)^2 = 1.0 \tag{8.4}$$

where, β is a parameter varying from 0 to 1. The local damage limit $a_{L,ellipstic}$ and $b_{L,elliptic}$ can be computed as

$$a_{L,elliptic} = \frac{x_c x_l}{\sqrt{\beta r^2 x_c^2 + (1-\beta)x_l^2}} \quad \text{and} \quad b_{L,ellliptic} = a_{L,elliptic} r \tag{8.5}$$

Figure 8.3 shows examples of the local damage limits calculated for linear and elliptic interaction curves for different cases.

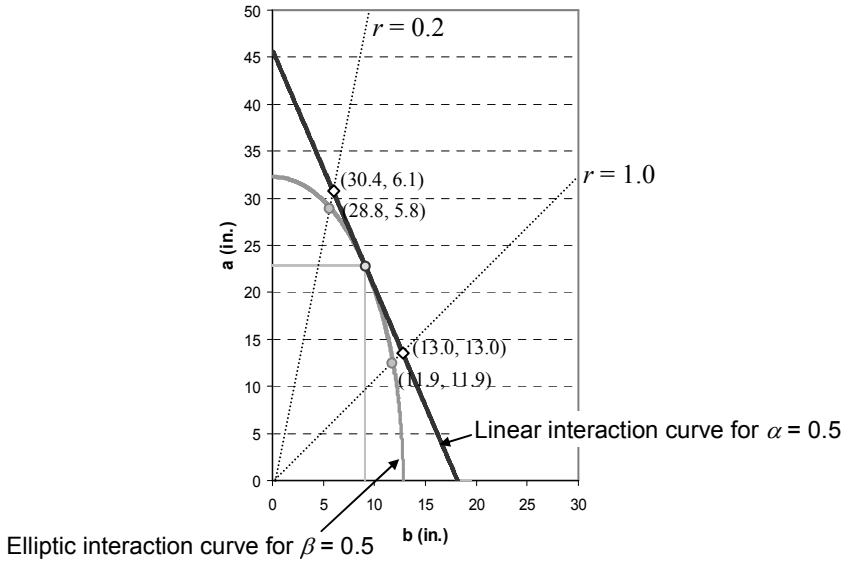

Figure 8.3 Examples of local damage limit for r = 1 and r = 0.2

The extents for local damage obtained from linear and elliptic envelopes are then investigated by comparison with inelastic RSF_i from FEA and with RSF_L for thermal hot spots or corrosion damage with different damage sizes and aspect ratios. The value of RSF_i generally decreases as the size of the damage increases until it converges to the value RSF_L. for damage sizes equal to or greater than the "local" damage limit.

It was observed that linear interaction curves give better estimations of the local damage limit than elliptic interaction curves for all the cases studied. Comparison of linear interaction curves with different slope parameters suggests an optimal value of $\alpha =$ 0.75. Therefore, the linear interaction curve with $\alpha = 0.75$ will be used in the FFS evaluation of cylindrical shells in the current research. Verification for this recommendation will be given in Section 8.7.2 where it is more appropriate. Note that the straight line interaction curve is likely valid only for damaged area shapes with reasonable aspect ratios and may not work for very narrow and very long damaged areas.

The equation for the proposed linear interaction curve for damage in cylindrical shells is given by,

$$\frac{3b}{4x_l} + \frac{a}{4x_c} = 1.0 \tag{8.6}$$

Hence, the extent for the local damage limit is calculated as,

$$a_L = \frac{4x_c x_l}{3rx_c + x_l} \quad \text{and} \quad b_L = a_L r \tag{8.7}$$

8.2. METHOD I FOR REMAINING STRENGTH FACTOR CALCULATION FOR CYLINDRICAL SHELLS

In the following discussion, three different methods for calculation of remaining strength factors (RSF) for cylindrical shells are proposed. These are similar to those for spherical shells. In each of the recommended methods, the size of "local" damage limit is calculated by using Eq. (8.7). For damage larger than this extent, the recommended RSF is equal to RSF_L. Interaction of damaged spots can be neglected when the distance between the outer edges of the damaged areas is more than the extent a_L in the axial direction and b_L in the circumferential direction.

The first recommended remaining strength factor $RSF_{r\text{-}1}$ is shown in Figure. 8.4. The x-axis is plotted by using a normalized variable ξ, calculated as,

$$\xi = \frac{a}{4x_c} + \frac{3b}{4x_l} \tag{8.8}$$

This parameter is equal to zero when there is no damage ($a = b = 0$). At the local damage limit $a = a_L$ and $b = b_L$, ξ, equals to unity. A value of ξ more than unity indicates "global" damage.

Similar to those for spherical shells, the recommended $RSF_{r\text{-}1}$ has three parts corresponding to the sizes of corroded areas or hot spots. The remaining strength factor RSF_α provides a lower bound approximation for the component with small local damaged spots. For global damaged spots larger than the extent as stated in Eq. (8.7), which gives ξ

greater than 1, RSF_L is applicable. A linear interpolation between RSF_α and RSF_L can be used for local damaged spots of intermediate size. The transition size from small to intermediate damaged spots is suggested as

$$a_T = \frac{a_L}{3} = \frac{4x_c x_l}{9rx_c + 3x_l} \quad \text{and} \quad b_T = a_T r \tag{8.9}$$

or in terms of the normalized variable, $\xi_T = 1/3$. This is similar to the transition angle for spherical shell ψ_L, which is also proposed to be one-third of the decay angle ψ_d.

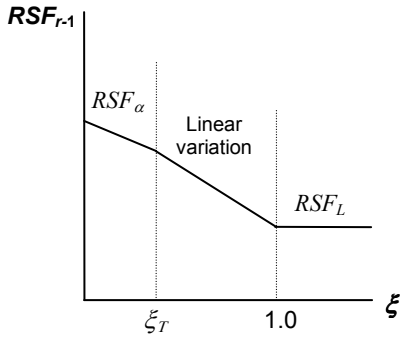

Figure 8.4 Method I recommendation: RSF_{r-1} for various sizes of damaged areas in cylindrical shells

In summary, the first recommended method for the remaining strength factor RSF_{r-1} for cylindrical shells can be calculated as below.

For $\xi \le \xi_T$, $\quad RSF_{r-1} = RSF_\alpha$

For $\xi_T < \xi \le 1$, $\quad RSF_{r-1} = RSF_{\alpha \text{ at } \xi_T} - 1.5(RSF_{\alpha \text{ at } \xi_T} - RSF_L)(\xi - \xi_T)$ (8.10)

For $\xi > 1$, $\quad RSF_{r-1} = RSF_L$

As will be shown later in Section 8.7, RSF_{r-1} provides a lower bound approximation in the evaluation of corrosion damage and thermal hot spots in cylinders compared with inelastic FEA results. As explained in the case of spherical shell, the results for damaged spots of very small sizes are fairly conservative due to the difference of decay lengths for stretching and bulging actions. To reduce this conservatism, the second recommended method based on the threshold to dominance of membrane action is proposed.

8.3. METHOD II FOR REMAINING STRENGTH FACTOR CALCULATION FOR CYLINDRICAL SHELLS

8.3.1. Threshold to Dominance of Stretching Effects for Cylindrical Shells

Similar to the behavior of spherical shells with local damage as discussed in Chapter 7, results from inelastic finite element analyses indicate that the effects of stretching action dominate the behaviour inside the damaged area if damaged spots are very small in size. The damaged area is stretched and tries to open up (Figure 8.5). Note that even for small damage, there may be bulging. However, this will be largely outside the damaged zone. For this dominance of stretching action, the decay length and thus the reference volume are different from those due to bulging action. In Figure 8.5, the decay length extends far outside the boundary of the damage itself.

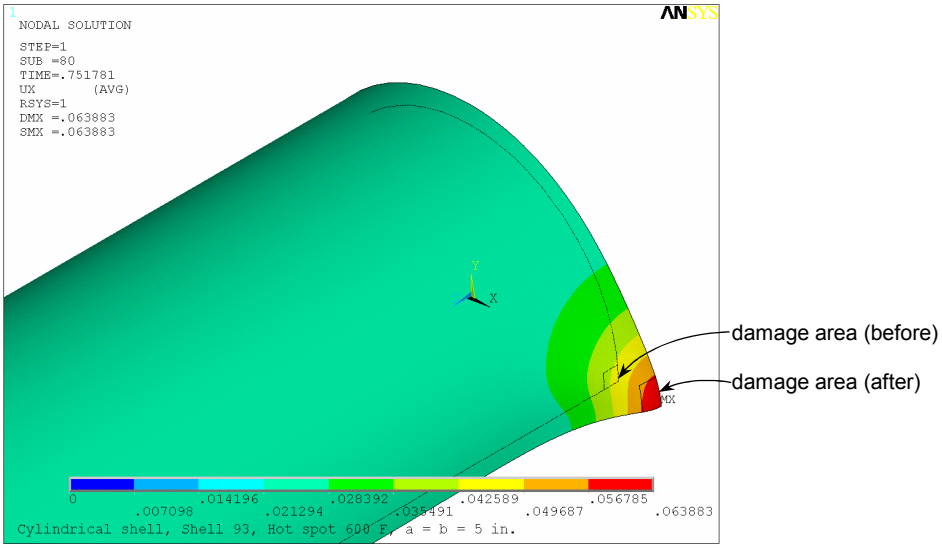

Figure 8.5 Dominance of stretching effect in a cylinder with small damaged spot

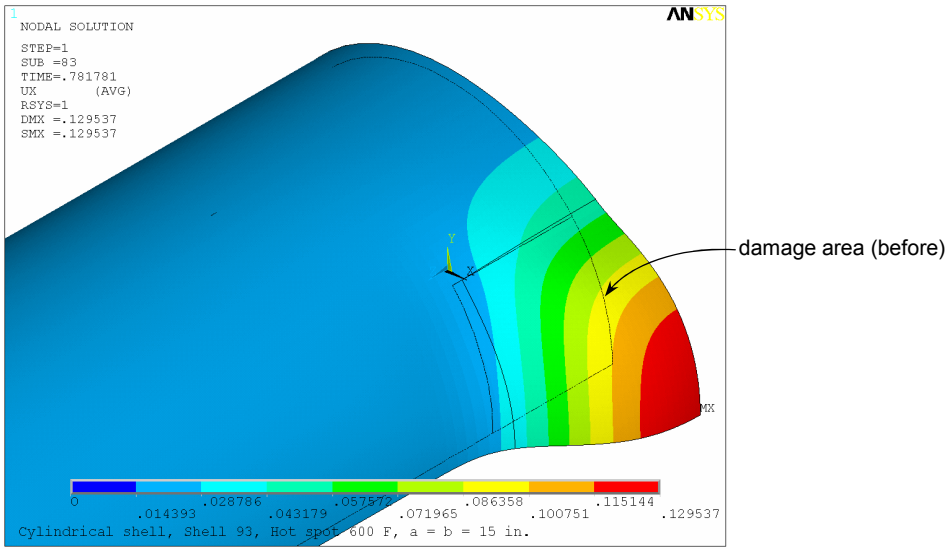

Figure 8.6 Typical bulging in cylindrical shell

For larger sizes of damaged spots, the effects of bulging action compared to those of stretching action are increased. Typical bulging in a cylinder with a large rectangular damaged area is shown in Figure 8.6. As can be seen, the bulging effects inside the damaged area are a lot more pronounced compared to those inside small damage areas. Also, the decay length of bulging does not extend much beyond the damage boundary as compared to the case with small damage. The size of damaged area defining the threshold of dominance of stretching effects for cylindrical shell is discussed below.

The mechanism of a cylindrical shell containing a rectangular corroded area or thermal hot spot is postulated to be similar to that of a fixed plate with UDL. If the damaged spot is not too large, the curved shell can be approximately considered to be a flat plate. Plastic hinge lines are formed at the edges and inside the damaged area as shown in Figure 8.7. The limit pressure for the equivalent plate can be calculated by assuming that the undamaged zone is much more rigid than the hot zone or corroded area.

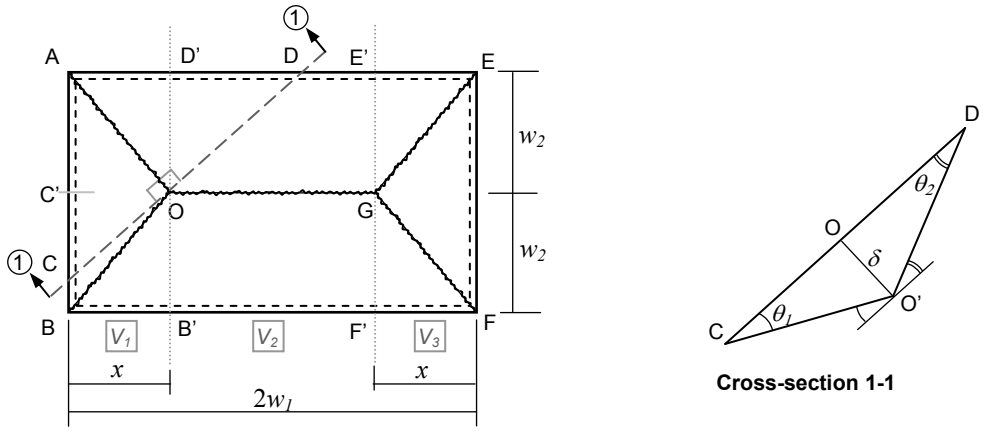

Figure 8.7 Yield line mechanism of an approximate rectangular flat plate

The load required to initiate plastic hinge mechanism can be calculated by equating the external work done by the applied pressure and the internal work done by plastic moments along the yield lines. The results for standard cases can be obtained using the well known yield line theory (Johansen, 1972). This theory is heavily used for concrete slabs, metal plates and a variety of other applications (Thakkar, 2006; Morris, 1988; Baumann, 1985). It is an upper bound method. The limit load is computed in terms of a geometrical parameter such as the location of yield line. This parameter is used to minimize the limit load expression to obtain the 'exact' limit load. Variational formulations for finding limit loads of plats using secant rigidity is developed by Bolar and Adluri (2005). The work uses techniques similar to m_a method and derived limit loads by avoiding full nonlinear analysis and contains extensive examples and theoretical development (see, Bolar, 2002).

The external work from the applied internal pressure p to deflect the line OG of the flat plate by a distance δ is given by the product of the pressure p and the volume of the inverted rectangular pyramid formed by the displaced plate. Assume that point O moves to O' as a result of the displacement.

The total volume of the pyramid is divided into 3 parts, from AB to $\mathrm{D}'\mathrm{B}'$ (V_1), from $\mathrm{D}'\mathrm{B}'$ to $\mathrm{E}'\mathrm{F}'$ (V_2), and from $\mathrm{E}'\mathrm{F}'$ to EF (V_3). The volumes V_1 and V_3 together form a pyramid of single vertex with a base $2w_2 \times 2x$ and a height δ with a volume of $(2w_2)(2x)\delta/3$. Volume V_2 is calculated by the product of the area $\mathrm{D}'\mathrm{B}'\mathrm{O}'$ and the length OG as $\frac{\delta(2w_2)}{2}(2w_1 - 2x)$. Therefore, the external work is given by,

$$W_{ext} = p\delta\left[\frac{4}{3}w_2 x + 2w_2(w_1 - x)\right] \tag{8.11}$$

The length of line AO, L_{AO}, is $\sqrt{x^2 + {w_2}^2}$. The length of line OC, L_{OC}, is calculated by,

$$\tan(\angle OAC') = \frac{x}{w_2} = \tan(\angle OAC) = \frac{L_{OC}}{L_{AO}}$$

$$\therefore L_{OC} = \frac{x}{w_2}\sqrt{x^2 + {w_2}^2} \tag{8.12}$$

The angle OCO' is

$$\angle OCO' \cong \tan(\angle OCO') = \frac{\delta}{L_{OC}} = \frac{\delta w_2}{x\sqrt{x^2 + {w_2}^2}} \tag{8.13a}$$

Similarly, the length of line OD is $L_{OD} = \frac{w_2}{x}\sqrt{x^2 + {w_2}^2}$ and the angle ODO' is

$$\angle ODO' \cong \tan(\angle ODO') = \frac{\delta}{L_{OD}} = \frac{\delta x}{w_2\sqrt{x^2 + {w_2}^2}} \tag{8.13b}$$

For work done along diagonal lines, line AO is considered. Internal dissipation along line AO can be expressed as

$$W_{\text{int}-AO} = M_p \cdot L_{AO}(\angle OCO' + \angle ODO') = M_p\left(\frac{w_2}{x} + \frac{x}{w_2}\right)\delta \tag{8.14}$$

where, M_p is the plastic moment per unit length of the section. Internal work done by plastic moment along line BO, EG and FG can be calculated in a similar manner. Therefore, total internal dissipation along all diagonal lines is $4M_p\left(\frac{w_2}{x}+\frac{x}{w_3}\right)\delta$.

For lines AE and BF along the longer side, internal dissipation can be written as

$$W_{\text{int}-AE,BF} = 2\cdot M_p \cdot L_{AE}(\angle OD'O') = 2M_p \frac{2w_1}{w_2}\delta \tag{8.15}$$

Internal work done along line OG is

$$W_{\text{int}-OG} = 2\cdot M_p \cdot L_{OG}(\angle OD'O') = 2M_p \frac{2w_1-2x}{w_2}\delta \tag{8.16}$$

For line AB and EF along the shorter side, internal dissipation is

$$W_{\text{int}-AB,EF} = 2\cdot M_p \cdot L_{AB}(\angle OC'O') = 2M_p \frac{2w_2}{x}\delta \tag{8.17}$$

Therefore, total internal work done by plastic moments is

$$W_{\text{int}-total} = M_p\delta\left[4\left(\frac{w_2}{x}+\frac{x}{w_2}\right)+\frac{4w_1}{w_2}+4\frac{w_1-x}{w_2}+4\frac{w_2}{x}\right] \tag{8.18}$$

Equating the total internal work done expression, Eq. (8.18), to the external work done Eq. (8.11) gives

$$M_p\delta\left[4\left(\frac{w_2}{x}+\frac{x}{w_2}\right)+\frac{4w_1}{w_2}+4\frac{w_1-x}{w_2}+4\frac{w_2}{x}\right] = p\delta\left[4\frac{w_2x}{3}+2w_2(w_1-x)\right] \tag{8.19}$$

Rearrangement of Eq. (8.19) gives the expression for the limit pressure that initiates plastic moment

$$p_{\lim} = 12\frac{w_1 x + {w_2}^2}{w_2 x(3w_1 w_2 - w_2 x)} M_p \tag{8.20}$$

Varying the value of x to obtain the minimum value of $p_{\lim}$,

$$\frac{\partial p}{\partial x} = 12M_p \frac{w_1(w_2 x(3w_1 w_2 - w_2 x)) - (w_1 x + {w_2}^2)(3w_1 {w_2}^2 - 2{w_2}^2 x)}{{w_2}^2 x^2 (3w_1 w_2 - w_2 x)^2} = 0$$

or

$$w_1 {w_2}^2 x^2 + 2{w_2}^4 x - 3w_1 {w_2}^4 = 0 \tag{8.21}$$

Therefore,

$$x = \frac{-{w_2}^2 + w_2\sqrt{{w_2}^2 + 3{w_1}^2}}{w_1} \tag{8.22}$$

The plate is assumed to be made of elastic-perfectly plastic material with a yield stress σ_y. The plastic moment capacity of the cross section M_p can be written in terms of the shell thickness h. For a unit length, $M_p = \sigma_y h^2 / 4$. Therefore, the pressure for plastic hinge lines to occur is calculated by

$$p_c^* = 3\sigma_y h^2 \frac{w_1 x + {w_2}^2}{w_2 x(3w_1 w_2 - w_2 x)} \tag{8.23}$$

where, p_c^* is the internal pressure for which plastic hinges are initiated. As before, it is postulated that if the applied internal pressure of a cylinder is less than or equal to p_c^*

determined by using Eq. (8.23), stretching effect dominates the behaviour of the damaged shell whereas if the applied internal pressure is more than p_c^*, bulging effect is dominant.

For the damaged area with aspect ratio r (= b/a), substitution of design pressure P_d into Eq. (8.23) gives,

$$\text{for } a > b, \qquad P_d = \frac{3\sigma_y h^2\left(x + ar^2\right)}{3a^2r^2x - ar^2x^2}, \qquad \text{where } x = ar\sqrt{r^2+3} - ar^2 \tag{8.24a}$$

$$\text{for } a < b, \qquad P_d = \frac{3\sigma_y h^2\left(rx + a\right)}{3a^2rx - ax^2}, \qquad \text{where } x = \frac{1}{r}\left(a\sqrt{1+3r^2} - a\right) \tag{8.24b}$$

Equations (8.24) can be used to determine the dimensions ($2a^* \times 2b^*$) of a damaged area in a cylindrical shell that identify the threshold of dominance of stretching action. If the damaged area is smaller than this limit, stretching effect dominates the shell behaviour and the shell tries to open-up instead of bulging. Bulging will dominate the behaviour of cylindrical pressure vessels with damaged areas larger than this limit.

In the form of the normalized variable ξ, the threshold to dominance of stretching effect is,

$$\xi^* = f^*\left(\frac{a^*}{4x_c} + \frac{3b^*}{4x_l}\right) \tag{8.25}$$

where, f^* is an empirical safety factor included to account for the approximation introduced in deriving p_c^*. In the present research, the value of f^* is chosen conservatively as 0.6.

8.3.2. Calculation Procedures for the Method II

The second recommended $RSF_{r\text{-}2}$ can be determined from the threshold to dominance of membrane effects, as shown in Figure 8.8. First, the RSF_α at $\xi = \xi^*$ is calculated. For small damaged spots where, $\xi < \xi^*$, $RSF_{r\text{-}2}$ is computed by linear interpolation of the known RSF of unity at $\xi = 0$ (no damage) and RSF_α at $\xi = \xi^*$. For intermediate size of the damaged areas where, $\xi^* < \xi \leq 1$, a linear variation from RSF_α at $\xi = \xi^*$ to RSF_L at $\xi = 1$ is applied. For "global" damage sizes in which $\xi > 1$, RSF_L is used.

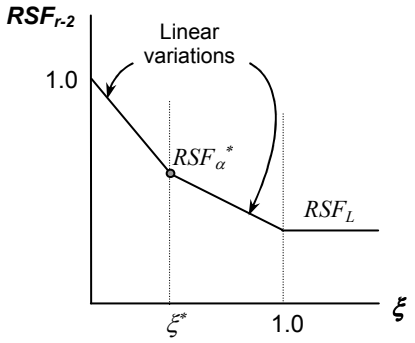

Figure 8.8 Method II Recommendation: RSF_{r-2} for cylindrical shells

In summary, the method II recommendation $RSF_{r\text{-}2}$ for cylindrical shells with corroded areas or thermal hot spots can be calculated as below.

For $\xi \leq \xi^*$, $\quad RSF_{r\text{-}2} = 1 - (1 - RSF_\alpha^*)(\xi / \xi^*)$

For $\xi^* < \xi \leq 1$, $\quad RSF_{r\text{-}2} = RSF_\alpha^* - (RSF_\alpha^* - RSF_L)(\xi - \xi^*)/(1 - \xi^*)$ (8.26)

For $\xi > 1$, $RSF_{r\text{-}2} = RSF_L$

The second recommended $RSF_{r\text{-}2}$ can be shown to provide less conservative RSF than $RSF_{r\text{-}1}$ especially for highly localized damaged areas.

8.4. METHOD III FOR REMAINING STRENGTH FACTOR FOR CYLINDRICAL SHELLS

As in the case of spherical shell, the third recommended approach is provided to avoid abrupt change at the changeover points of the first and second recommended methods. For local damaged areas, a parabolic variation is employed between the limits of $RSF_{r\text{-}3}$ equal to unity at $\xi = 0$, and $RSF_{r\text{-}3} = RSF_L$ at $\xi = 1$ as shown in Figure 8.11. For global damaged areas ($\xi > 1$), RSF_L is used.

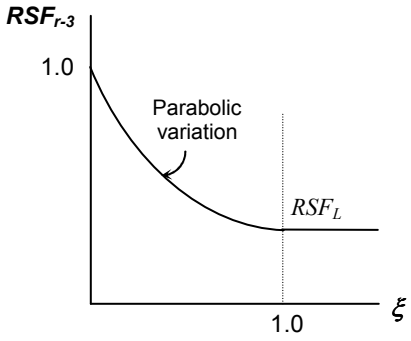

Figure 8.9 Method III Recommendation: RSF_{r-3} for cylindrical shells

The expressions for $RSF_{r\text{-}3}$ can be written as below.

For $\xi \leq 1$, $RSF_{r\text{-}3} = (1 - RSF_L)(\xi^2 - 2\xi) + 1$

For $\xi > 1$, $RSF_{r\text{-}3} = RSF_L$ (8.27)

Obviously, this recommendation is less rigorous in theoretical background compared to Methods I and II. However, it is simpler to use.

8.5. DISTORTION DUE TO BULGING

An additional limit criterion for the shell is based on excessive deformation due to bulging inside the damaged area of the component. If the damaged area is not too large, the bulge is assumed to be an inscribed ellipsoid given in Cartesian coordinate by (Fig. 8.10)

$$\frac{x^2}{a^2} + \frac{y^2}{b^2} + \frac{z^2}{c^2} = 1 \tag{8.28}$$

where, c is the bulging displacement at the center of the damaged area. Surface area of half of the ellipsoid is computed by Knud Thomsen's formula (Tee, 2005) as,

$$S(a,b,c) = \pi\left(a^\gamma b^\gamma + a^\gamma c^\gamma + b^\gamma c^\gamma\right)^{1/\gamma} \tag{8.29}$$

where, $\gamma = \ln(3)/\ln(2)$.

Therefore, strain due to bulging is given by

$$\varepsilon_b \approx \frac{S(a,b,c) - \pi ab}{\pi ab} \tag{8.30}$$

where, ε_b is the average membrane strain in the entire bulge. The inelastic limiting membrane strain for crown point is 1%. Hence, radial displacement of the assumed bulge, c, is calculated as

$$c = \left[\frac{(1.01ab)^{\gamma} - a^{\gamma} b^{\gamma}}{a^{\gamma} + b^{\gamma}} \right]^{1/\gamma} \tag{8.31}$$

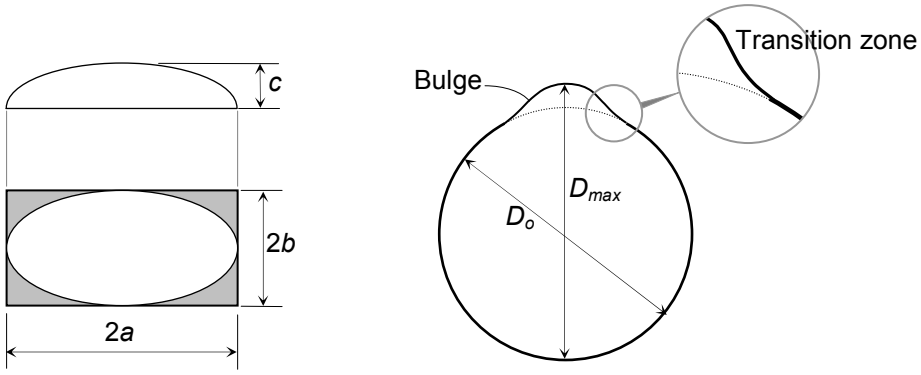

Figure 8.10 Idealized bulging geometry for rectangular damage

The out-of-roundness ratio is computed as the ratio of the maximum diameter of the circular cylinder due to bulging (= $D_o + \bar{c}$), and the original diameter of the cylinder Do. If the out-of-roundness ratio exceeds a certain recommended value (equal to 1.01 in the current study), RSF_r should be taken as RSF_L.

Note that since the stiffness of the undamaged shell is higher than that of the damaged area, the undamaged portion acts like a support to the damaged area. The edge moments at the rim of the damaged spot cause “transition zone” where there is reversal of bulge curvature (Fig. 8.10). A better estimation of bulging displacement can be achieved

by using “effective” dimensions of the ellipsoid depending on differential stiffness of the two parts.

8.6. ILLUSTRATIVE EXAMPLE

The following example is given to demonstrate the proposed Level 2 integrity assessment methods for a cylinder under internal pressure. The values given in the parentheses are in SI units.

ASTM Material	:	SA 516 Grade 55
Shell Inside Radius (R_i)	:	33.0 in. (838 mm)
Shell Overall Length (L)	:	400 in. (10160 mm)
Operating Pressure	:	180 psig (1.24 MPa)
Design Pressure (P_d)	:	220 psi (1.52 MPa)
Operating Temperature	:	90 °F (32.2 °C)
Design Temperature	:	100 °F (37.8 °C)
Allowable stress (S)	:	13700 psi (94.5 MPa)
Corrosion Allowance (CA)	:	1/16 in. (1.59 mm)
Joint Efficiency (E_j)	:	1.0

8.6.1. Required Thickness Calculation

Design thickness, h_d, for spherical shell can be determined as (Bednar, 1985):

$$h_d = \frac{P_d R_i}{SE_j - 0.6P_d} = 0.536 \text{ in. } (13.6 \text{ mm})$$

Required shell thickness is $h = h_d + CA = 0.599$ in. (15.2 mm)

Therefore, a 5/8 in. wall thickness is specified.

The allowable RSF can be expressed as $RSF^* = h_d/h = 0.895$. Note that this RSF^* is based on design requirements.

Outside radius of the sphere, $R_o = 33.625$ in.(854 mm)

In this case, R/h ratio is 52.8.

The decay length in axial direction of a cylindrical shell is calculated from the first of Eq. (8.1), $x_l = 11.5$ in. (291 mm)

The decay length in circumferential direction of a cylindrical shell is calculated from the latter of Eq. (8.1), $x_c = 28.9$ in. (734 mm)

8.6.2. Recommended RSF_r for Corrosion Damage

For the following demonstration for corrosion damage, the depth of thickness loss inside the corroded area is assumed to be equal to $h/3 = 0.208$ in. (5.3 mm). For internal corrosion, the inner radius of the shell inside the corroded spot R_c becomes 33.42 in. (849 mm) and the remaining thickness h_c is 0.417 in.(10.6 mm).

The circumferential extent of corrosion ($2a$) is 10 in. (254 mm)

The longitudinal extent of corrosion ($2b$) is 10 in. (254 mm)

Aspect ratio of the damaged area is $r = b/a = 1.0$

From Eq. (8.8), the dimensions of the damaged area is defined by the normalized variable $\xi = 0.370$.

Since $\xi_T < \xi \leq 1$, this is the case of intermediate corroded spot. $RSF_{r\text{-}1}$ is calculated from the second of Eq. (8.10) and $RSF_{r\text{-}3}$ is calculated from the first of Eq. (8.27).

From Eq. (4.3), Corroded Volume $V_D = 4abh_c = 41.67$ in^3 (6.827 x 10^5 mm^3)

From Eq. (4.4), Adjacent Volume $V_I = 4h\big((x_c + a)(x_l + b) - ab\big) = 1332$ in^3 (2.182 x 10^7 mm^3)

Reference Volume $V_R = V_D + V_I = 1373$ in^3 (2.251 x 10^7 mm^3)

The yield stress of steel at a temperature of 100 °F (37.8 °C) is 30 ksi (207 MPa)

The principal stresses of the undamaged shell are $\sigma_{1I} = P_d R_i/h = 11616$ psi (80.1 MPa) and $\sigma_{2I} = P_d R_i/2h = 5808$ psi (40.0 MPa). Therefore, the equivalent stress of the undamaged shell (σ_{eI}) is calculated from $\sigma_{eI} = \sqrt{\sigma_{1I}^2 + \sigma_{2I}^2 - \sigma_{1I}\sigma_{2I}}$, = 10060 psi (69.4 MPa)

The principal stresses inside the corroded spot are $\sigma_{1D} = P_d R_c/h_c$ = 17643 psi (122 MPa) and $\sigma_{2I} = P_d R_c/2h_c$ = 8821 psi (60.8 MPa). Similarly, the equivalent stress of inside the corrosion damage (σ_{eD}) is 15279 psi (105 MPa)

Using the above, $m_u^0 = \sigma_y / \sigma_{eI} = 2.982$ and $m_L = \sigma_y / \sigma_{eD} = 1.976$.

From Eq. (4.23), $RSF_L = m_L / m_u^0 = 0.663$.

The RSF_U and RSF_α can be calculated for Tresca and von Mises yield criteria.

Tresca criterion:

From Eq. (4.18), $m_d^0 = \dfrac{\sigma_y V_R}{\sigma_{eI}^0 V_I + \sigma_{eD}^0 V_D} = 2.937$.

From Eq. (4.21), $RSF_U = m_d^0 / m_u^0 = 0.985$.

$Z = \dfrac{m_d^0}{m_L} = 1.487$.

From Eq. (3.19), m_α =2.404.

From Eq. (4.22), $RSF_\alpha = m_\alpha / m_u^0 = 0.806$.

Von Mises criterion:

From Eq. (4.20), $m_d^0 = \sqrt{\dfrac{\sigma_y^2 V_R}{\sigma_{eI}^2 V_I + \sigma_{eD}^2 V_D}} = 2.926$

From Eq. (4.21), $RSF_U = m_d^0 / m_u^0 = 0.981$.

$Z = \frac{m_d^0}{m_L} = 1.481.$

From Eq. (3.19), m_α =2.402.

From Eq. (4.22), $RSF_\alpha = m_\alpha / m_u^0 = 0.805$.

Similarly, RSF_α calculated at the transition $\xi = \xi_T$ is 0.806.

From the second of Eq. (7.3), $RSF_{r\text{-}1} = 0.793$

From Eq. (8.24), $a^* = 2.93$ in. From Eq. (8.25), the variable $\xi^* = 0.217$. Thus, RSF_α at $\xi = \xi^*$ is 0.808. Linear interpolation from RSF_α at $\xi = \xi^*$ and RSF_L at $\xi = 1$ using the second of Eq. (8.26) gives $RSF_{r\text{-}2} = 0.779$.

From the first of Eq. (8.31), $RSF_{r\text{-}3} = 0.796$

From Eqs. (8.31), $c = 0.236$ in.

Thus, $r_{out\text{-}of\text{-}roundness} = (D_o + \delta_b)/D_o = 1.004 \leq 1.01$.

8.6.3. Recommended RSF_r for Thermal Hot spot Damage

For the following example for thermal hot spot evaluation, hot spot temperature is assumed as 400 °F (204 °C).

The dimensions of the hot spot are $2a$ x $2b$ = 10 x 10 in^2 (25.4 x 25.4 mm^2) Aspect ratio of the damaged area is $r = b/a = 1.0$

From Eq. (8.8), the dimensions of the damaged area is defined by the normalized variable $\xi = 0.370$.

Since $\xi_T < \xi \leq 1$, this is the case of intermediate hot spot. $RSF_{r\text{-}1}$ is calculated from the second of Eq. (8.9) and $RSF_{r\text{-}3}$ is calculated from the first of Eq. (8.27).

From Eq. (4.3), Hot Spot Volume $V_D = 4abh = 62.50$ in^3 (1.024×10^6 mm^3)

From Eq. (4.4), Adjacent Volume $V_I = 4h\left((x_c + a)(x_l + b) - ab \right) = 1332.0$ in^3 (2.182×10^6 mm^3)

Reference Volume $V_R = V_D + V_I = 1394.3$ in^3 (2.285×10^7 mm^3)

The yield stress of steel at a temperature of 100 °F (37.8 °C) is 30 ksi (207 MPa)

The yield stress of steel at the hot spot temperature of 400 °F (204 °C) is 25700 psi (177 MPa)

The effective elastic modulus and thermal coefficient are obtained from Eq. (4.5) as

$E_{eff} = \dfrac{E_I V_I + E_D V_D}{V_R} = 29.2 \times 10^6$ psi and $\alpha_{eff} = \dfrac{\alpha_I V_I + \alpha_D V_D}{V_R} = 5.578 \times 10^{-6}$ in./in./°F.

The thermo-elastic principal stresses inside the hot spot are calculated from Eqs. (4.9) as

$\sigma_1 = \dfrac{P_d R_i}{h} - \dfrac{E_{eff}\alpha_{eff}\Delta T}{2}$ = -18649 psi (129 MPa) and $\sigma_2 = \dfrac{P_d R_i}{2h} - \dfrac{E_{eff}\alpha_{eff}\Delta T}{2}$ = -12841 psi (88.5 MPa). The equivalent stress is 16529 psi (114 MPa).

Using the above, $m_u^0 = \sigma_{yc} / \sigma_e = 1.815$ and $m_L = \sigma_{yh} / \sigma_e = 1.555$.

From Eq. (4.23), $RSF_L = m_L / m_u^0 = 0.857$.

Tresca criterion:

From Eq (4.14), $m_d^0 = \dfrac{\sigma_{yI}V_I + \sigma_{yD}V_D}{\sigma_e V_R} = 1.803$

From Eq. (4.21), $RSF_U = m_d^0 / m_u^0 = 0.994$.

$Z = \dfrac{m_d^0}{m_L} = 1.160.$

From Eq. (3.19), m_α =1.708.

From Eq. (4.22), $RSF_\alpha = 0.941$.

Von Mises criterion:

From Eq. (4.16), $m_d^0 = \sqrt{\dfrac{\sigma_{yI}^2 V_I + \sigma_{yD}^2 V_D}{\sigma_e^2 V_R}} = 1.804$

From Eq. (4.21), $RSF_U = m_d^0 / m_u^0$ =0.994.

$Z = \dfrac{m_d^0}{m_L} = 1.160.$

From Eq. (3.19), m_α =1.709.

From Eq. (4.22), $RSF_\alpha = m_d^0 / m_u^0 = 0.942$.

Similarly, RSF_α calculated at the transition $\xi = \xi_T$ is 0.871.

From the second of Eq. (7.3), $RSF_{r\text{-}I} = 0.841$

From Eq. (8.24), a^* = 4.07 in. From Eq. (8.25), the variable ξ^* = 0.301. Thus, RSF_α at $\xi = \xi^*$ is 0.942. Linear interpolation from RSF_α at $\xi = \xi^*$ and RSF_L at $\xi = 1$ using the second of Eq. (8.30) gives $RSF_{r\text{-}2}$ = 0.934.

From the first of Eq. (8.31), $RSF_{r\text{-}3}$ = 0.913

From Eqs. (8.31), c = 0.236 in.

Thus, $r_{out\text{-}of\text{-}roundness}$ = 1.004 $\leq$ 1.01.

8.6.4. Comparison with Nonlinear (Level 3) Analysis

The inelastic remaining strength factor RSF_i is calculated from the ratio of the internal pressure that causes 1% von-Mises membrane strain in the damaged region to the limit pressure of the undamaged cylinder. For the examples given above, RSF_i are 0.859 and 0.938 for corrosion damage and thermal hot spot, respectively. Bulging displacements at the center of the damaged spot from inelastic analysis for corrosion damage and hot spot are 0.160 in. and 0.173 in., respectively. It can be seen that all three recommendations of the current study provide lower bound RSF approximations compared to the inelastic results. Thus, the recommended RSF are acceptable and conservative.

8.7. DISCUSSION

8.7.1. Comparison of RSF from the Three Methods

An analysis is carried out to evaluate the effectiveness of the proposed Level 2 methods for cylindrical shells with different damaged conditions. For corrosion damage, the methods are applied to internal and external corrosion with different damaged sizes, aspect ratios and remaining thicknesses. Examples of numerical data for comparison of RSF obtained from the three recommended methods and inelastic finite element analysis for cylindrical shells with inner radius 21.0 in. and R/h ratio of 33.6 are shown in Tables 8.1 and 8.2. Additional numerical results are given in Appendix A.

Table 8.1 Comparison of RSF from the three recommended methods and inelastic analysis for corrosion damage in a cylinder (R/h =33.6, $h_c = h/2$, r = 1.0)

a (in.)	b (in.)	RSF_U	RSF_{r-1}	RSF_{r-2}	RSF_{r-3}	$RSF_{inelastic}^{external}$
1.0	1.0	0.997	0.596	0.785	0.908	0.965
2.5	2.5	0.984	0.599	0.590	0.787	0.813
3.5	3.5	0.972	0.596	0.577	0.718	0.712
5.0	5.0	0.953	0.574	0.559	0.632	0.630
10.0	10.0	0.888	0.500	0.499	0.494	0.520
12.5	12.5	0.860	0.492	0.492	0.492	0.512

Table 8.2 Comparison of RSF from the three recommended methods and inelastic analysis for hot spot damage in a cylinder (R/h =33.6, T_h = 600 °F, r = 0.2)

a (in.)	b (in.)	RSF_U	RSF_{r-1}	RSF_{r-2}	RSF_{r-3}	$RSF_{inelastic}$
5	1	0.996	0.873	0.938	0.932	0.978
10	2	0.988	0.871	0.876	0.875	0.920
15	3	0.980	0.859	0.847	0.828	0.878
20	4	0.971	0.830	0.821	0.791	0.842
25	5	0.964	0.802	0.795	0.764	0.813
32	6.4	0.955	0.762	0.760	0.743	0.776

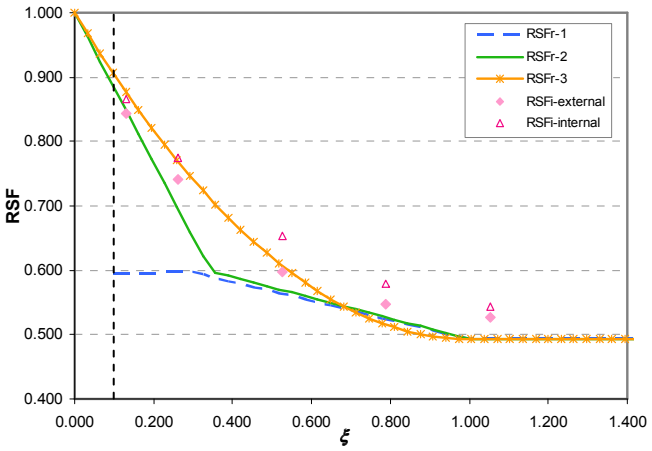

(a) $r = 3.0$; $h_c = h/2$

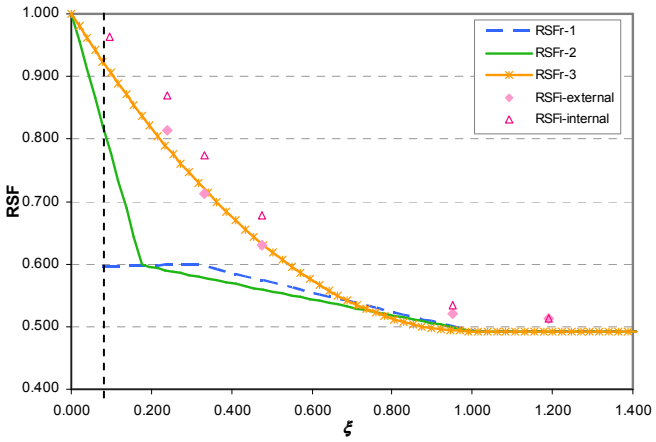

(b) $r = 1.0$; $h_c = h/2$

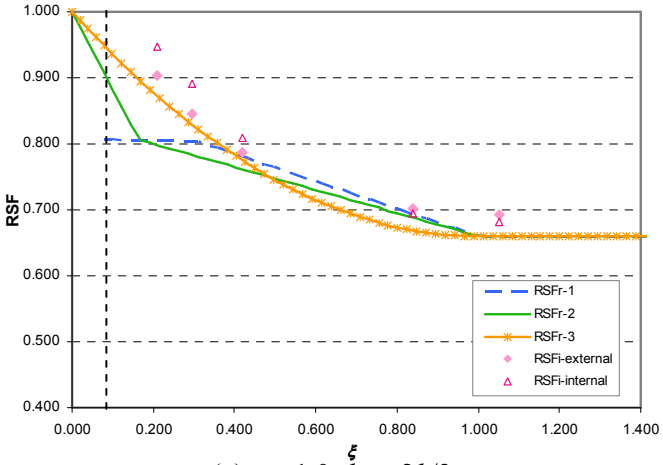

(c) $r = 1.0$; $h_c = 2h/3$

Figure 8.101 Comparison of RSF_r and RSF_i for cylindrical shells (R/h ratio = 33.6) with corrosion damage

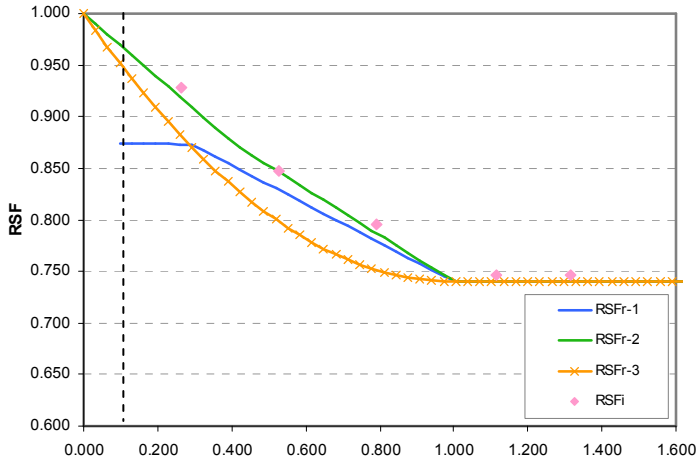

(a) $r \frac{\xi}{=} 3.0$

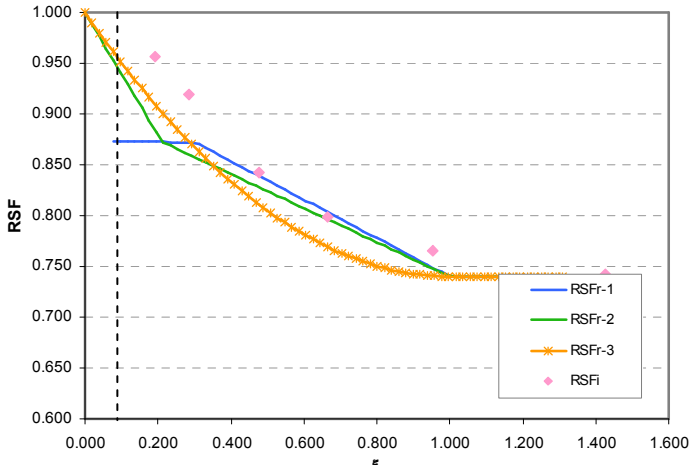

(b) $r \frac{\xi}{=} 1.0$

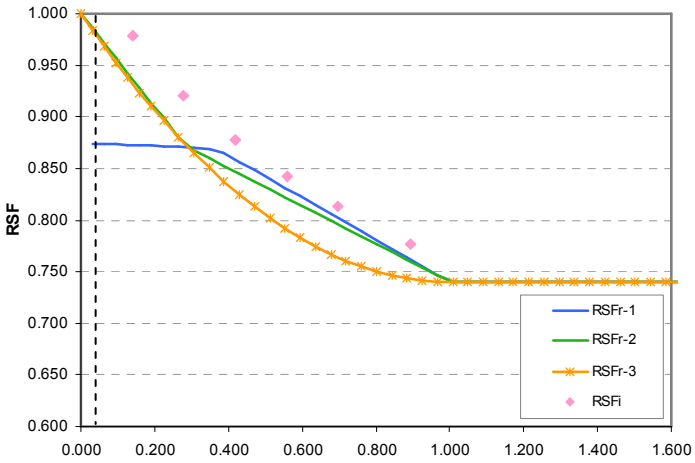

(c) $r \frac{\xi}{=} 0.2$

Figure 8.112 Comparison of RSF_r and RSF_i for a cylindrical shell R/h ratio = 33.6 with thermal hot spots T_H = 316 °C

Figure 8.11 compares the recommended RSF_{r-1}, RSF_{r-2}, RSF_{r-3} and the inelastic RSF_i for corrosion damage with remaining corroded thicknesses of *2h/3* and *h/2* and damage area aspect ratio *r* of 3.0 and 1.0. The RSF are plotted against the normalized variable defining the size of the damaged area, ξ. Figure 8.12 shows similar comparisons for a cylinder with thermal hot spots of aspect ratios 1.0 and 0.2. It can be seen that all three recommended methods offer good lower bound approximations compared to inelastic FEA results. Note that vertical dashed lines in Figs 8.11 and 8.12 indicate the allowable opening size of $2\frac{3}{8}$ in (along the diagonal of rectangular damaged areas) without reinforcement as in the case of spherical shells.

Similar to the recommendation for spherical shells, the three methods give the same remaining strength factor for "global" damages. The RSF for global damage is almost the same as the inelastic RSF.

The first method is more theoretically grounded than the other two but can overestimate the damage severity for very small damaged area. The second method in which the threshold to dominance of stretching effect is taken into consideration provides closer estimations of RSF for highly localized damage than RSF_{r-1}. The RSF from the first and second recommended methods are also shown to give better estimate for intermediate size than RSF from the third method. The third recommended RSF_{r-3} is less theoretically grounded but has advantages in providing a smooth curve with no abrupt change as well as in the simplification of calculation procedures compared to the other

two methods. The users can choose one of the three recommendations depending on their preference.

8.7.2. Verification of the Proposed Interaction Curve

In the current research, interaction curves are used to calculate the extent of local damage in cylindrical shells as discussed in Section 8.1. Linear and elliptic interaction curves are studied and the interaction curve for damage in cylindrical shells is proposed to be a linear line with slope diameter $\alpha = 0.75$.

The recommendation is verified by comparison of the method III recommendation $RSF_{r\text{-}3}$ and inelastic RSF_i from FEA. The RSF_{r-3} are plotted against the normalized parameter for each curve. Different cases of damage type and aspect ratio of damaged area (from r = 0.2 to r = 5.0) are studied for linear interaction curve with $\alpha = 0.5$ and elliptic interaction curve with $\beta = 0.5$.

Some examples of comparison for r = 1.0 and r = 0.2 are shown in Figures 8.13 and 8.14. The normalized variables for linear interaction curve is calculated by the left-hand side of Eq. (8.2) as

$$\eta_\alpha = \alpha \frac{b}{x_l} + (1-\alpha)\frac{a}{x_c} \tag{8.28}$$

For each value of α, the parameter η is different. By changing α, we can study the best possible alternative η to represent RSF curve. Several different values of α (and hence

η_α) were examined to get a good fit. Note that $\eta_\alpha = 1$ indicates the limit of local damage for each value of α and $\eta_{0.75}$ is the same as the recommended variable ξ.

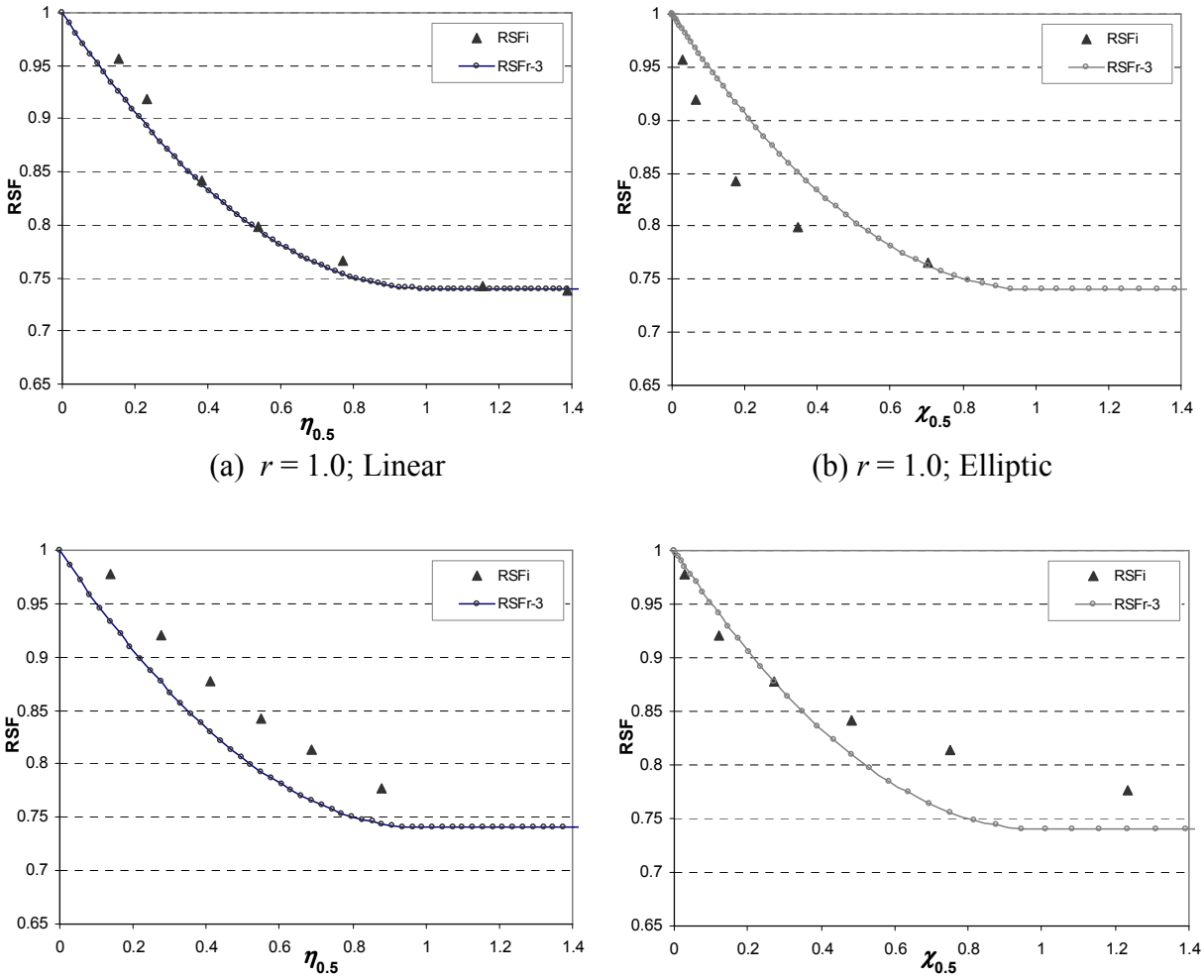

(a) $r = 1.0$; Linear (b) $r = 1.0$; Elliptic

(c) $r = 0.2$; Linear (d) $r = 0.2$; Elliptic

Figure 8.123 Comparison of RSF_i and RSF_{r-3} using linear and elliptic interaction curves for a cylinder (R/h = 32.6) with thermal hot spots of different aspect ratios

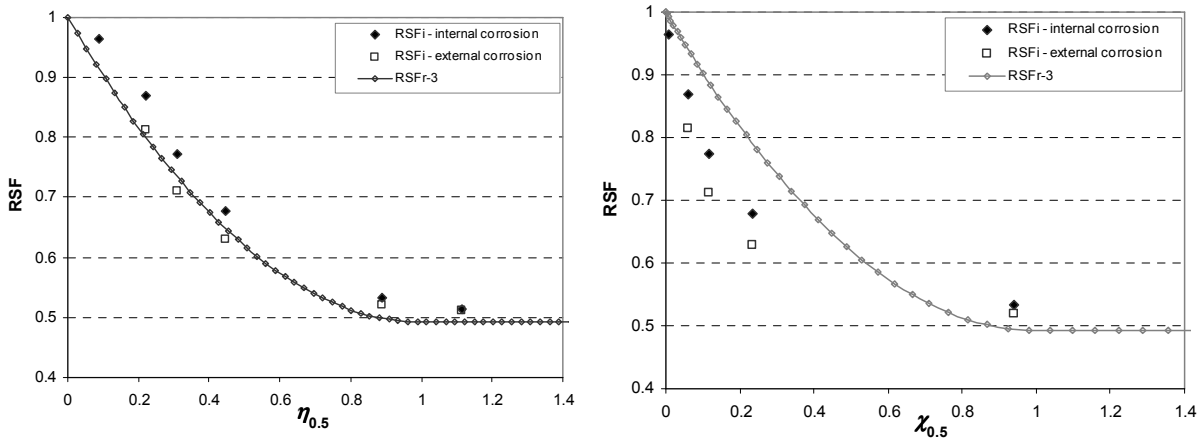

(a) (b)

Figure 8.134 Comparison of RSF_i and RSF_{r-3} for a cylinder (R/h = 32.6) with corrosion damage $h_c = h/2$ using (a) linear interaction curve (b) elliptic interaction curve

Similarly, the normalized variables for elliptic interaction curve is calculated by the left-hand side of Eq. (8.4), viz,

$$\chi_\beta = \beta\left(\frac{b}{x_l}\right)^2 + (1-\beta)\left(\frac{a}{x_c}\right)^2 \tag{8.29}$$

It can be seen that RSF_{r-3} calculated from linear interaction curves provides conservative estimations for almost all cases whereas RSF_{r-3} calculated by using elliptic interaction curves can be unconservative. Thus, linear interaction curves are preferable.

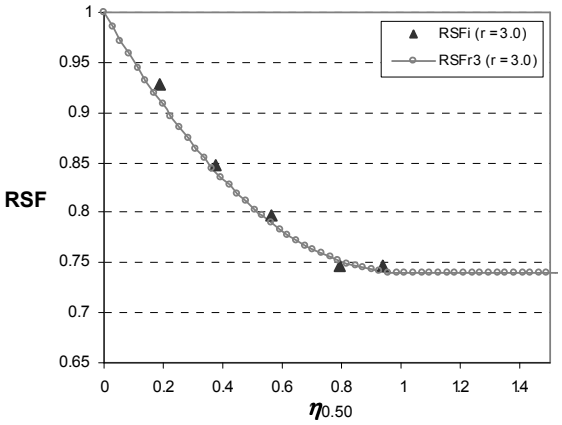

(a)

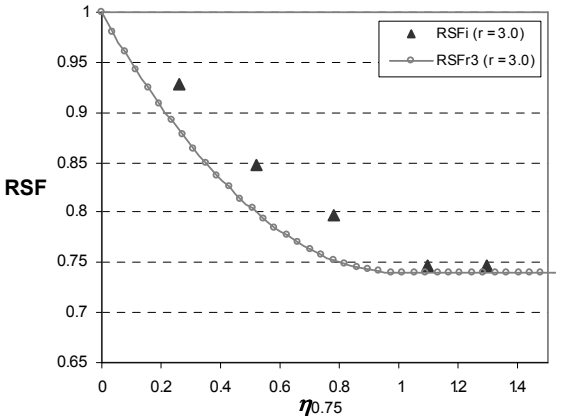

(b)

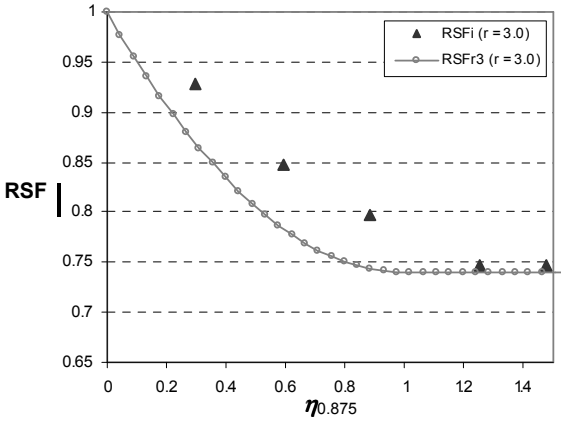

(c)

Figure 8.145 Comparisons of RSF_i and RSF_{r-3} for thermal hot spot with $r = 3.0$

(a) $\alpha = 0.50$ (b) $\alpha = 0.75$ (c) $\alpha = 0.875$

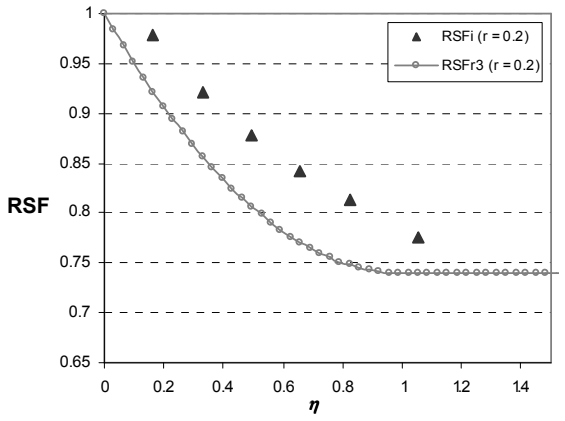

(a)

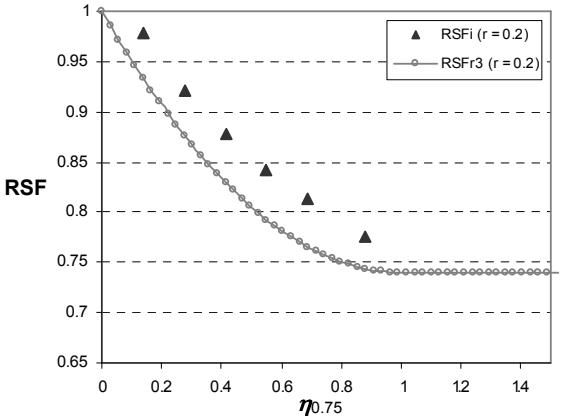

(b)

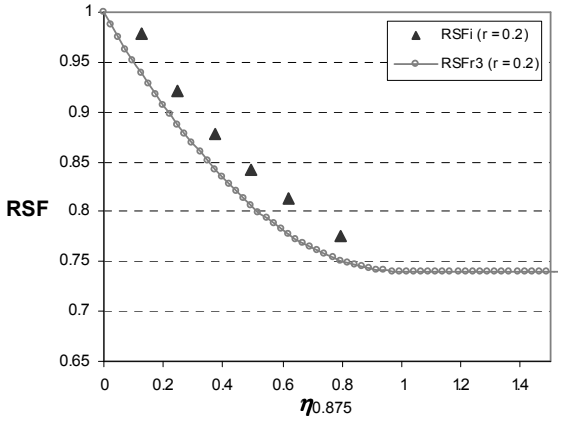

(c)

Figure 8.156 Comparisons of RSF_i and RSF_{r-3} for thermal hot spot with $r = 0.2$

(a) $\alpha = 0.50$ (b) $\alpha = 0.75$ (c) $\alpha = 0.875$

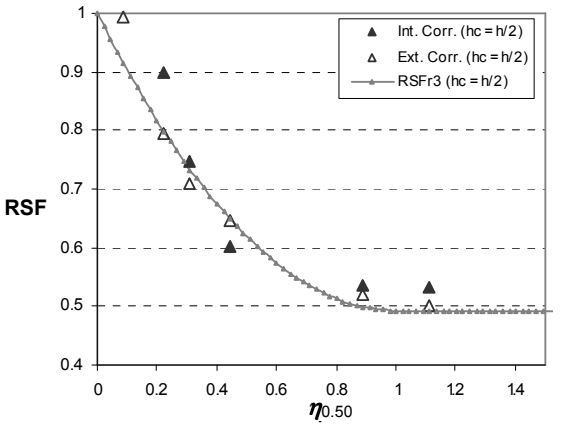

(a)

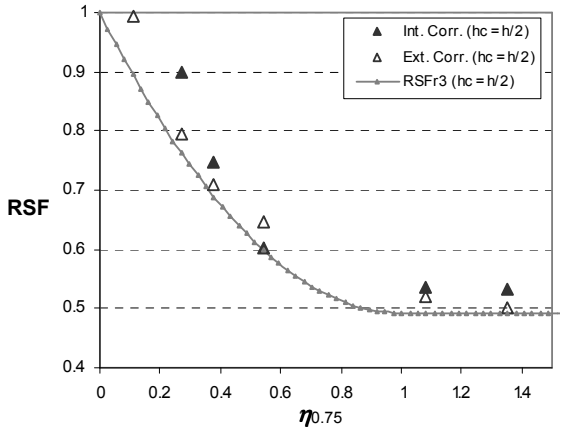

(b)

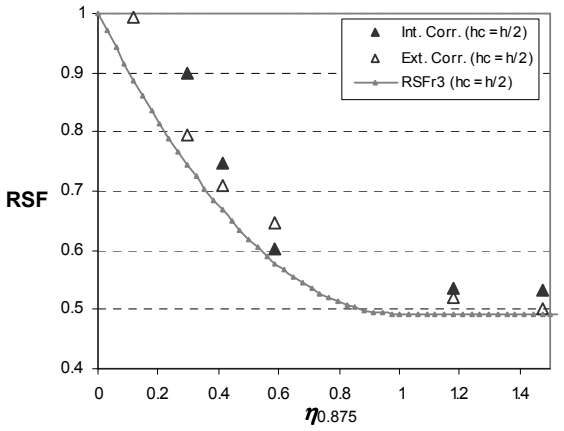

(c)

Figure 8.167 Comparisons of RSF_i and RSF_{r-3} for corrosion damage with $r = 1.0$

(a) $\alpha = 0.50$ (b) $\alpha = 0.75$ (c) $\alpha = 0.875$

It is observed from FEA results that a narrow long damage along the circumferential direction of cylindrical shell (represented by larger r, such as r = 5.0) affects structural capacity of the shell structure less than a narrow damage of the same length in the axial direction (represented by small r). Moreover, it can be also observed that the linear interaction curve with α of 0.5 underestimates the limit for local damage of long damages along the circumferential direction (Figure 8.13c). This results in rather conservative $RSF_{r\text{-}3}$ in such cases.

This can be improved upon by increasing the slope parameter α. As α increases, the linear interaction curve is steeper. Thus, the extent of local damage in the circumferential direction becomes larger and much more than the decay length x_c. The extent of local damage in axial direction is smaller and closer to the decay length in that direction, x_l (Figure 8.2). In addition, it can be seen that as α changes, the change in the extent of local damage in the circumferential direction is more rapid than that in the axial direction.

Recommended RSF_{r-3} using linear interaction curve with α = 0.50, 0.25 and 0.125 for different cases are shown in Figures 8.15 to 8.17. Note that the x-axis for each graph is the normalized variable η_α corresponding to each of the applied α. Hence, the actual dimensions of the damages where the variables are equal are, in fact, not identical.

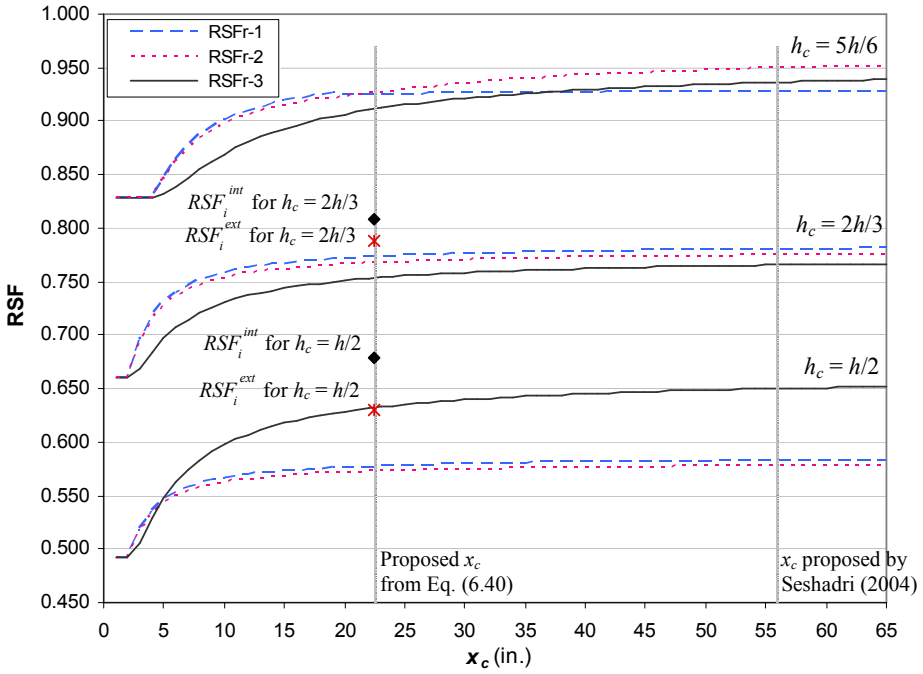

(a) $a = b = 5$ in. ($r = 1$)

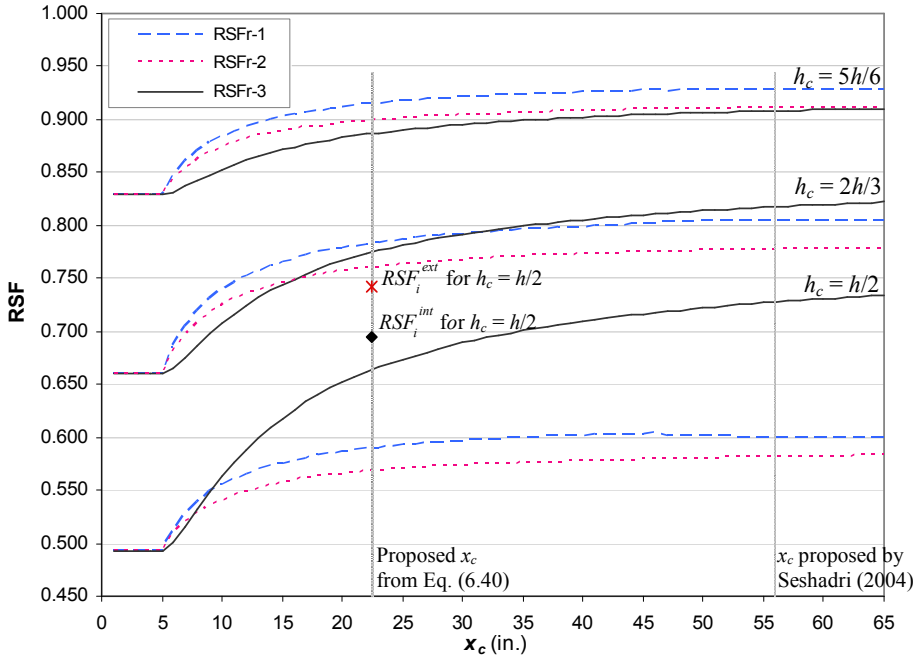

(b) $a = 15$ in. $b = 3$ in. ($r = 0.2$)

Figure 8.17 Recommended RSF_r for corrosion damage calculated by using different x_c

It can be concluded from these comparisons that the linear interaction curve with α = 0.75 offers the best recommended RSF_{r-3} . For this case, almost the same conservatism is present for different profiles of corrosion damage and thermal hot spots, viz., hot spot temperatures, corroded thickness and dimensions of the damaged spot. Therefore, this curve is used as the interaction line for damage in cylindrical shells.

8.7.3. Comparison RSF for Different Circumferential Decay Lengths

In this section, the effect of the circumferential decay length x_c on the recommended RSF is studied. Figure 8.18 shows the three recommended RSF calculated by using different choices for the value of x_c for corrosion damage in cylinder (R_i = 53.3 cm, h = 1.58 cm.). The proposed x_c for this case (from Eq. 8.1) is 22.8 in. (57.8 cm).

It can be seen that RSF increases as the decay length x_c is chosen to be larger. The effects of x_c on RSF are more noticeable in the cases where the damage is more severe (e. g., $h_c \leq h/2$) or the damage aspect ratio r is small (narrow damage lying along the circumferential direction). In addition, recommended RSF can be unconservative if a much larger circumferential decay length is used instead of the proposed one.

Note that the choice of x_c value also affects the limit for local damage. When x_c is chosen to be very small, this limit is small and the damaged area of interest may be considered as global damage. Hence, RSF's for very small choices of x_c values are constant and are equal to RSF_L.

8.8. SUMMARY

This chapter discusses the application of elastic decay lengths to defining the extent of local damage in cylindrical shells. For damaged area with aspect ratio (b/a) other than x_l/x_c, a linear interaction curve is proposed. Three alternative methods are proposed similar to those for spherical shells.

The remaining strength factors are suggested depending on the size and aspect ratio of damaged spot. For damaged spots larger than the extent for local damage, the lower bound remaining strength factor RSF_L is recommended in all three methods.. For very small damaged spots, the recommendations involve using the m_α-multiplier and integral mean of yield criterion or a transition between two limit points. For intermediate size damaged spots, a linear or parabolic transition is shown to work well.

The first recommended method is more conservative than the others for very small damaged spots but is also more theoretically grounded in an overall sense. The second recommendation involves a simplified analysis to identify the threshold between dominance of stretching and bulging effects. It uses the m_α-multiplier for the intermediate limit and linear transitions between this limit and the zero damage point as well as between this limit and the maximum local damage. Third recommended approach involves a simple parabolic transition between the zero damage case and the lower bound RSF limit for large damaged areas.

The “local” damage limits and mutual influence of decay in longitudinal and circumferential directions is studied using an interaction equation.

All the three proposed recommended methods are shown to provide good lower bound estimations compared to inelastic FEA results. Excessive deformation in bulging can be prevented by limiting the out-of-roundness ratio of the shell to 1.01.

CHAPTER 9

CONCLUSIONS AND RECOMMENDATIONS

This chapter summarizes the main work carried out and the key ideas proposed in the present thesis. The main conclusions of the research are presented and recommendations for future work are given.

9.1. SUMMARY

The present thesis proposes Level 2 procedures for evaluating Fitness-for-Service of pressure vessels containing corrosion damage or thermal hot spots. They are based on variational methods, m_α-multipliers, reference volume and the concept of decay lengths in shells.

The principles leading an improved lower bound limit load called the m_α-method (as developed in earlier studies) are discussed in detail in Chapters 2 and 3. These include theorem of nesting surfaces, leap-frogging of iterations to the limit state and Mura's

extended variational formulation. The m_α-method has been shown to provide acceptable approximations to limit load of various mechanical components and thus is employed as the basis of the calculation of the recommended remaining strength factors proposed in the current study.

The effects of local loads on a shell structure are normally restricted to a limited volume in the vicinity of the loads. This kinematically active volume participates in plastic action when local damage occurs in a component and is termed as the reference volume. The use of reference volume instead of the entire volume of the structure gives better approximation of limit load multipliers. In the present research, reference volume is characterized by using decay lengths of shells.

A decay length can be defined as the distance from the applied force (or moment) to the point where the effect of the force is almost completely dissipated or becomes negligible. In the current study, decay lengths for spherical and cylindrical shells are derived based on elastic shell theories. Decay lengths were shown to depend on shell radius and thickness. They were derived as functions of $\sqrt{Rh}$. A decay length for thin shell is smaller than that for thicker shell. It was also concluded that decay lengths in shells with large curvature are likely to be smaller than shells with small curvature. Therefore, thinner and highly curved shells possess smaller reference volume (or influence zones). Small reference volume implies more severe damage.

The derived decay lengths are also used to specify the limit of what can be called “local” damage. The local damage limit is defined by the maximum size of damage for

which the edge effects at the discontinuities have not damped out at the centre of the damage. For this case, the pure membrane stress effect is not expected to occur at any place inside the damaged area. If the damaged spot is larger than this limit, the “failure” will be due to pure membrane action inside the damaged spot as if a “global” damaged spot has occurred. This also implies that interaction between two local damaged areas will not occur if the distance between the outer edges of the damaged areas is at least equal to twice the decay lengths. A linear interaction curve based on decay lengths in the axial and circumferential directions is also proposed for cylindrical shells.

The main factors considered to influence the behaviors of pressurized components containing corrosion damage or thermal hot spots are material characteristics and geometric properties of the damaged spot and the shell. Three alternative methods to calculate remaining strength factors (RSF) for spherical and cylindrical shells with local damage are recommended.

In all the three methods, the lower bound RSF_L is suggested for global damage. The first recommended method uses RSF_α for small damaged spots and a linear transition between RSF_α and RSF_L for intermediate spots. It was shown that for highly localized damage, the first recommended method can offer highly conservative estimation. This is due to dominance of stretching action in the shell with very small damage rather than bulging effect. The threshold to dominance of membrane (as opposed to bulging) is suggested using an approximate method. The second recommended procedure uses linear transitions from the point of no damage to RSF_α at the threshold to dominance of

membrane effect and from that point to RSF_L. The third method recommends a parabolic variation from the point of no damage to the local damage limit.

The usefulness and effectiveness of the three recommended methods are demonstrated through illustrative examples. The recommended approaches are validated by full scale inelastic finite element analysis which is regarded as a Level 3 assessment.

9.2. CONCLUSIONS

Major conclusions of the present research are summarized below.

1. The present research developed recommendations for Level 2 structural integrity assessment procedures to evaluate the remaining strength factors for spherical and cylindrical pressure vessels containing corrosion damages or thermal hot spots. The recommendations use limit load multipliers. Three methods based on the concept of reference volume and the m_α-method are proposed. They are validated using nonlinear FE analysis.

2. Decay lengths for spherical and cylindrical shells based on elastic solutions subject to local actions are proposed. These decay lengths are used to identify the extent of reference volume participating in plastic action. Some observations on decay lengths can be concluded as follows:

- Decay lengths in both spheres and cylinders are functions of $\sqrt{Rh}$, where, R is shell radius and h is shell thickness.

- Thinner shells possess smaller decay lengths than thicker shells (with the same radius). In other words, damage in thin shells is more localized and hence more severe.

- Shells with larger curvature possess smaller decay lengths. Thus, decay length of a spherical shell possessing double curvature (in two directions) is smaller than that of a similar cylindrical shell with single curvature.

3. In the present work, local damage is defined as a damaged area inside which pure membrane action is not present. For damaged areas larger than the local damaged limit, the effects from discontinuities have dissipated and become negligible at the middle of the damaged spot. This limit is estimated by using decay lengths. Pressure vessels with damaged spots larger than the limit will therefore "fail" by pure membrane action inside the damaged area and the remaining strength is calculated by using classical lower bound RSF_L.

4. Interaction of damage in circumferential and axial directions of cylindrical shells can be determined by using a linear interaction curve. The slope of the proposed envelope is calibrated using limit analyses. It was shown that damage in the circumferential direction deteriorates structural integrity of the cylinder less than that in the axial direction. This is because hoop stress is twice of longitudinal stress.

5. It is shown that stretching action dominates the behavior of pressure components with highly localized damage. The damaged spot tends to open up instead of forming a bulge. This gives rise to the second limit which considers the threshold to dominance of stretching action using an approximate equilibrium equation.

6. For intermediate and large damaged spots, bulging occurs. Bulging displacement is proposed to be estimated by using geometries of the damaged spot and the pressure vessel and is used as another limit criterion (for serviceability).

7. The remaining strength factors used in the present study are observed to possess shape independence feature. They are only a function of the geometrical and material property ratios for a given situation and are independent of the actual applied (or operating) load. Hence, the theory for the calculation of RSF is very likely common to all shapes and sizes of pressure vessels. The shape influences the decay lengths and the reference volumes. The same arguments as discussed in the current research should apply to other types of geometries. Therefore, similar simplified level 2 estimations of RSF can be proposed.

8. Some observations have been made based on results from inelastic FEA:

- in most cases, RSF for external corrosion is slightly lower than the RSF for internal corrosion.
- R/h ratio, rather than the individual values of R and h, affects RSF of shells containing local damage.

- Sims (1992) recommended RSF for spherical shell to be independent of the *R*/*h* ratio. It was shown that although the RSF for thinner and thicker shells are not much different for very small or very large damaged areas, the difference can be significant for intermediate size damage.

- The use of an elastic-perfectly plastic model with maximum stress equal to flow stress instead of yield stress to account for material strain hardening is justifiable.

9.3. RECOMMENDATIONS FOR FUTURE RESEARCH

Recommendations for future work are as following.

1. In the present research, an irregular profile of corrosion damage or a thermal hot spot is represented by an equivalent circular area in a sphere or an equivalent rectangular damaged area in a cylindrical pressure vessel. In reality, damaged spots generally have irregular profiles. Although the proposed approach assumes uniform damage and does not account for the irregularity, the method can be extended to determine the remaining strength factors for an irregular profile including irregular damaged area and thickness loss (Figure 9.1). The Level 2 Assessment rules of API 579 (Sec. 5.4.1.2) provide for a better estimate of the structural integrity of a component when significant variations in the thickness profile occur within the region of metal loss. A proper assessment including such variation will be beneficial particularly in the cases where the geometries of

damaged spots considerably change and the assumption of uniform damage is conservative but can greatly overestimate the damage (the shaded zones).

2. Equivalent damaged areas used in the current study are obtained by the outside bound of the irregular damaged areas as well as the minimum corroded thickness. For damage with highly irregular geometries, more suitable equivalent properties must be examined.

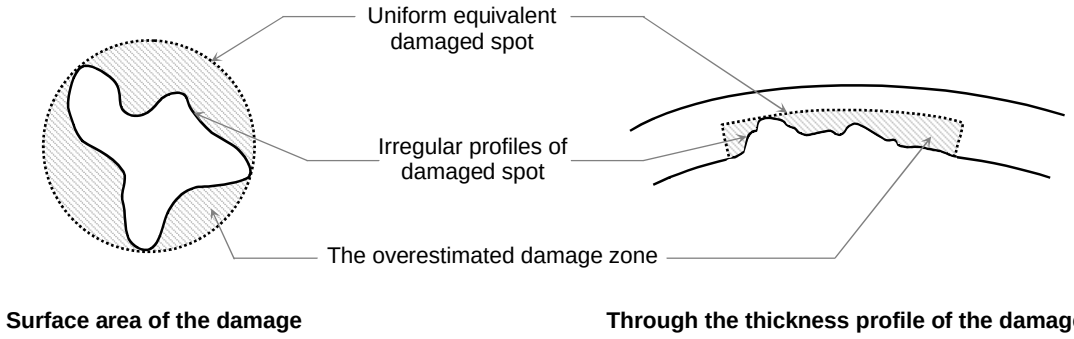

Figure 9.1 An example of a highly irregular damaged spot

3. The present research studied corrosion and hot spot damage which is sufficiently remote from other major structural discontinuities (such as nozzles, elbows, tees, etc.) or geometry changes (i.e., cone-to-cylinder junctions, knuckles in hemispherical heads, etc.). Therefore, they are not affected by them. However, these areas are important since they are common in piping systems that experience Flow Accelerated Corrosion. Two adjacent damage areas are also assumed not to interact. Procedures to calculate the remaining strength factor of pressure vessels with damaged spots near structural discontinuities or multiple interacting damaged spots need to be studied.

4. It is shown that internal and external corrosion damage of the same size have a different effect on the structural integrity of pressure vessels. However, the procedure proposed in the present study does not differentiate between the two types of damage and offers the same remaining strength factor for internal and external corrosion with the same damaged area and thickness loss. Further study on an approach to incorporate this distinction would be useful.

5. The proposed Fitness-for-Service assessments in the current research have been shown to offer lower bound remaining strength factor estimates to pressure vessels of spherical and cylindrical shapes. Since the remaining strength factors used in the present study are expected to be shape-independent, the method can also be employed to evaluate corrosion damage and hot spots in other shapes of pressure vessels. However, decay lengths for each shape of pressure component need to be investigated prior to implementation of the proposed method.

6. The changeover from the dominance of stretching action to bulging action has been estimated using approximate equilibrium equations. A more thorough analysis of small shell geometries (with fixed edges) subject to pressure can be included to improve Method II.

7. Interaction of damage in the axial and circumferential directions of cylindrical shells was investigated in the present study. Similar interaction curves can also be examined for spherical shells with elliptical damaged areas.

8. The current study investigates pressure vessels which operating condition is not in the creep range of material. This can be quite a severe restriction for thermal hot spots. Study of creep effects can be in such cases can be of interest.

9. An experimental study with strain gauges set up can be conducted to obtain the collapse pressure of a corroded component as well as to investigate the behavior of the damaged pressure components at limit state. Results from such experiments can be used to validate the accuracy and effectiveness of the proposed methods.

REFERENCES AND BIBLIOGRAPHY

REFERENCES

American Petroleum Institute (API), 2000. *Fitness-for-Service, API 579*. Washington, D.C.

American Society of Mechanical Engineers (ASME), 2002. *ASME Boiler and Pressure Vessel Code, Section III and VIII*. New York.

ANSYS, 2005. Educational version, Release 10.0, SASIP, Inc.

Arup, H. and Parkins, R. N., 1979. *Stress Corrosion Research*, NATO Science Series E. Springer, New York.

ASME, 1984. *Manual for Determining the Remaining Strength of Corroded Pipelines*, American National Standards Institute (ANSI)/ American Society of Mechanical Engineers (ASME) B31G.

Baumann, R. A. and Weisgerber, F. E., 1985. "Yield-line analysis of slabs-on-grade." *Journal of Structural Engineering*, **109**, pp 1553-1568.

Bednar, H. H., 1985. *Pressure Vessel Design Handbook*. Second Edition, Van Nostrand Reinhold Company, New York.

Beer, F. P., Johnston, E. R., Jr. and DeWolf, J. T., 2002. *Mechanics of Materials*, Third Edition. McGraw-Hill Companies, Inc.

Bolar, A. A. and Adluri, S. M. R., 2005. "Robust Estimation of Limit Loads of Plates." *33rd Annual General Conference of the Canadian Society of Civil Engineering*, Toronto, ON, Canada. June 2-4, 2005.

Bolar, A. A., 2002. *Robust Estimation of Limit Loads of Plates Using Secant Rigidity*, Master's Thesis, Memorial University of Newfoundland, St. John's, Canada.

Boyle, J. T., 1982. "The Theorem of Nesting Surfaces in Steady Creep and Its Application to Generalized Models and Limit Reference Stress." *Res Mechnica*, **4**, pp. 275-294.

Calladine, C. R., 1983. *Theory of Shell Structures*. Cambridge University Press, Cambridge.

Calladine, C. R., 2000. *Plasticity for Engineers: Theory and Application.* Horwood Publishing, Chichester.

Calladine, C. R. and Drucker, D. C., 1962. "Nesting Surfaces of Constant Rate of Energy Dissipation in Creep." *Quarterly of Applied Mathematics*, **20(1)**, pp. 70-84.

Chen, W. F. and Han, D. J., 1988. *Plasticity for Structural Engineers*. Springer-Verlag, New York.

Chouchaoui, B.A., and Pick, R.J., 1994. “A Three Level Assessment of the Residual Strength of Corroded Line Pipe”, *Pipeline Technology*, OMAE – Volume V, pp. 9-18.

Cottis, R. A., 2000. *Stress Corrosion Cracking*. National Corrosion Service (NCS), UK.

Coulson, K. E. W. and Worthingham, R. G., 1990. “Standard Damage-Assessment Approach is Overly Conservative.” *Oil and Gas Journal*. **88(15)**, pp. 56-59.

DePadova, T. A. and Sims, J. R., “Fitness for Continued Service: Local Thin Areas.” *International Conference on Pressure Vessel Technology*, **2**, pp. 175-181.

Donnell, L. H., 1933. **“**Stability of Thin-Walled Tubes Under Torsion.” *Report National Advisory Committee for Aeronautics*, **479**, pp. 95-116.

Du Preez, R. J., 1995. “Assessment of thermal stresses and ratcheting in reactor vessels..” *International Journal of Pressure Vessels and Piping*, **61(2-3)**, pp. 411-425.

Fineberg, 2006. “BP North Slope Spill Reveals A History of Substandard Environmental Performance.” *A Preliminary Report to the Alaska Forum for Environmental Responsibility*, Mar. 15, 2006.

Flugge, 1973. *Stresses in Shells*. Second Edition. Springer-Verlag, New York.

Folias, E. S., December 1969. “On the Effect of Initial Curvature on Cracked Flat Sheets.” *International Journal of Fracture Mechanics*, **5(4)**, pp. 327-346.

Harvey, J. F., 1991. *Theory and Design of Pressure Vessels*, Second Edition. Chapman & Hall, New York.

Hill, R., 1950. *The Mathematical Theory of Plasticity*. Oxford University Press, London.

Hodge, P. G., 1959. *Plastic Analysis of Structures*. McGraw Hill Book Company, New York.

Hoff, N. J., 1954. "Approximate Analysis of Structures in the Presence of Moderately Large Creep Deformations." *Quarterly of Applied Mathematics*, **12(1)**, pp. 49-55.

Hoff, N. J., Kempner, J. and Pohle, F. V., 1954. "Line Load Applied Along Generators of Thin-walled Circular Cylindrical Shells of Finte Length." *Quarterly of Applied Mathematics*, **11(4),** pp. 211-245.

Indermohan, H., and Seshadri, R., 2004. "Fitness-for-service Methodology based on Variational Principles in Plasticity." *ASME Pressure Vessels Piping Div Publ PVP*, **473**, pp. 83-91.

Johansen, K. W., 1972. *Yield-line theory*. Cement and Concrete Association, London.

Kachanov, L.M., 1971. *Foundations of the Theory of Plasticity*. North-Holland Publishing Company, Amsterdam.

Kiefner, J.F., 1990. “The Remaining Strength of Corroded Pipe”, *API Pipeline Conference*, API, April 1990.

Kiefner, J. F. and Vieth, P.H., 1989. *A Modified Criterion for Evaluating the Remaining Strength of Corroded Pipe (with RSTRENG)*. American Gas Association, Catalog No. L51609, PR3-805.

Kraus, H., 1967. *Thin Elastic Shell*. John Wiley & Son, Inc., New York.

Loy, W., 2006. “Workers respond to Prudhoe spill -- North Slope: Leak may be one of the largest in 29 years of production,” *Anchorage Daily News*, Mar. 4, 2006.

Lukasiewicz, S., 1979. *Local Loads in Plates and Shells*. PWN-Polish Scientific Publishers, Warszawa.

Mangalaramanan, S. P., 1997. *Robust Limit Loads Using Elastic Modulus Adjustment Techniques*, Ph.D. Dissertation, Faculty of Engineering and Applied Science, Memorial University of Newfoundland, St. John’s, Canada.

Maxey, W. A., Kiefner, J. F., Eiber, R. J., and Duffy, A. R., 1972. “Ductile Fracture Initiation, Propagation and Arrest in Cyindrical Vessels.” *Fracture Toughness, Proceedings of the 1971 National Symposium on Fracture Mechanics, Part II*, ASTM STP 514, pp. 70-81.

Mendelson, A., 1968. *Plasticity: Theory and Application*. MacMillan Company, New York.

Mura, T., and Koya, T., 1992. *Variational Methods in Mechanics.* Oxford University Press, .New York.

Mura, T., and Lee, S. L., 1963. “Application of Variational Principles to Limit Analysis.” *Quarterly of Applied Mathematics*, **21(3)**, pp. 243-348.

Mura, T., Rimawi, W. H., and Lee, S .L., 1965. “Extended Theorems of Limit Analysis.” *Quarterly of Applied Mathematics*, **23**, pp. 171-179.

Nuclear Electric, 1995. *R6, Assessing the Integrity of Structures Containing Defects*. Berkeley, U.K.

Osage, D. A., 1997. “New Development in API 579.” *International Journal of Pressure Vessels and Piping*, **71**, pp. 93-106.

Osage, D. A., Krishnaswamy, P. , Stephens, D.R., Scott, P., Janelle, J., Mohan, R., Wilkowski, G. M., 2001. “Technologies for the evaluation of non-crack-like flaws in pressurized components-erosion/corrosion, pitting, blisters, shell out-of-roundness, weld misalignment, bulges and dents.” *Welding Research Council Bulletin*, **465**, pp. 1-25.

Pan, L. and Seshadri, R., November 2002. “Limit Load Estimation Using Plastic Flow Parameter in Repeated Elastic Finite Element Analyses.” *Journal of Pressure Vessel Technology*, **124**, pp. 433-439.

Quintas, V., 2003. “Two Main Methods for Yield Line Analysis of Slabs.” *Journal of Engineering Mechanics*, **129(2)**, pp. 223-231.

Radakovic, D. J., Zhao, Y. and Lucas M., 2004. “Investigation of blast furnace bustle pipe failures and repair.” *AISTech 2004 - Iron and Steel Technology Conference Proceedings*, **1**, pp. 111-118.

Ramkumar, B. 2005, *Fitness for Service Assessment of Corroded Pipelines*. M. Eng. Thesis. Faculty of Engineering and Applied Science, Memorial University of Newfoundland, St. John’s.

Ramkumar, B. and Seshadri R., June 2005. “Fitness for Service Assessment of Corroded Pipelines Based on Variational Principles in Plasticity,” *Journal of Pipeline Integrity*, **2**, pp. 99-116.

Reinhardt, W. D. and Seshadri, R., February 2003. “Limit Load Bounds for the m_α Multiplier.” *Journal of Pressure Vessel Technology*, **125**, pp. 11-18.

Seshadri, R., 2004. “Integrity Assessment of Pressure Components with Local Hot Spots.” *ASME Pressure Vessels Piping Div Publ PVP*, **480**, pp. 177-185.

Seshadri, R., and Mangalaramanan, S .P., 1997. “Lower Bound Limit Loads Using Variational Concepts: the mα - method.” *International Journal of Pressure Vessels and Piping*, **71**, pp. 93-106.

Sims, J. R., Hantz, B. F., and Kuehn, K. E., 1992. “A Basis for the Fitness for Service Evaluation of Thin Areas in Pressure Vessels and Storage Tanks.” *Pressure Vessel Fracture, Fatigue and Life Management*, ASME PVP, **233**, pp. 51-58.

Sobotka, Z., 1989. *Theory of plasticity and limit design of plates*. Elsevier, New York.

Szilard, R., 2004. *Theories and Applications of Plate Analysis: Classical, Numerical, and Engineering Methods*. John Wiley, Hoboken, New Jersey.

Tantichattanont, P., Adluri, S. M. R., and Seshadri, R., 2006a (Accepted). “Fitness-for-Service Assessment of Spherical Pressure Vessels with Hot Spots.” *International Journal of Pressure Vessels & Piping*.

Tantichattanont, P., Adluri, S. M. R., and Seshadri, R., 2006b (Accepted). “Structural Integrity Evaluation for Corrosion in Spherical Pressure Vessels.” *International Journal of Pressure Vessels & Piping.*

Tantichattanont, P., Seshadri, R., and Adluri, S. M. R., 2006c. “Integrity Assessment of Spherical Pressure Components with Local Corrosion and Hot Spots.” *Proceedings of PVP2006-ICPVT-11, 2006 ASME Pressure Vessels and Piping Division Conference*, Vancouver, July 23-27, 2006.

Tee. G. J., 2005, “Surface Area and Capacity of Ellipsoids in *n* dimensions.” *New Zealand Journal of Mathematics*, **34**, pp. 165-198

Timoshenko, S., 1970. *Theory of Plates and Shells*. Second Edition. McGraw-Hill, Inc., New York:

Ugural, A. C., 1999. *Stresses in Plates and Shells*, Second Edition. McGraw-Hill, Inc., New York:

Walker, A. C. and Williams, K. A .J , 1995. “Strain Based Design of Pipelines.” *Pipeline Technology*, OMAE, **5**, pp. 345-350.

Westwood, S. and Hopkin, P., 2004. “Smart Pig Defect Tolerances Quantifying the Benefits of Standard and High Resolution Pigs..” *Proceedings of IPC 2004 International Pipeline Conference*, October 4 - 8, 2004. Calgary, Alberta, Canada.

BIBLIOGRAPHY

Anderson, T. L., and Osage, D. A., 2000. “API 579: a Comprehensive Fitness-for-service Guide.” *International Journal of Pressure Vessels and Piping*, **77**, pp. 953-963.

Berak, E. G., and Gerdeen, J.C., 1990. “A Finite Element Technique for Limit Analysis of Structures.” *Transactions of ASME: Journal of Pressure Vessel Technology*, **112**, pp. 138-144.

Carter, P. Marriott, D. L. and Swindeman, M. J., 2004. “Fitness for service assessments of bulging and out-of-round structures.” *ASME Pressure Vessels and Piping Division (Publication) PVP, Fitness for Service, Life Extension, Remediation, Repair, and Erosion/Corrosion Issues for Pressure Vessels and Components - 2004*, **471**, pp. 81-84.

Dym, C. L., 1990. *Introduction to the Theory of Shells*. Hemisphere Publishing Corporation, New York.

Fowler, C. G., 1998. *Robust Estimation of Limit Loads for Cracked Components*. M. Eng. Thesis, Faculty of Engineering and Applied Science, Memorial University of Newfoundland, St. John's.

Hay, M. G., 2001. “Fitness-for-purpose Material Testing for Sour Gas Service- an Overview.” *Corrosion*, **57(3)**, pp. 236-252.

Holand, J., 1961. “Influence Surfaces fro Bending Moments in Circular Cylindrical Shells.” *International Association for Bridge and Structural Engineering Publications*, **21**, pp. 111 - 128.

Hopkins, H. G. and Prager, W., 1953. “The Load Carrying Capacity of Circular Plates.” *Journal of Mechanics and Physics of Solids*, **2**, pp. 1-13.

Hopkins, P. and Jones, D. G., 1992. “A Study of the Behavior of Long and Complex-Shaped Corrosion in Transmission Pipelines.” *British Gas plc*, OMAE-92-1004.

Janosch, J. J., Huther, M., Kocak, M. and Taylor, N., 2005. “European Fitness-for-Service Network (FITNET) – Fatigue Module Development.” *Proceedings of the International Conference on Offshore Mechanics and Arctic Engineering – OMAE*, **3**, pp. 329-338.

Jaske, C. E. and Beavers, J., 2000. “Fitness-for-service Assessment for Pipelines Subject to Stress-Corrosion Cracking.” *Corrosion Prevention and Control*, **47(1)**, pp. 15-24.

Jones, D. G., Turner, T. and Ritchie, D., 1992. “Failure Behavior of Internally Corroded Linepipe.” *British Gas plc*, OMAE-92-1045.

Kocak, M., 2005. “Fitness for Service Analysis of Structures Using the FITNET Procedure: An Overview.” *Proceedings of the International Conference on Offshore Mechanics and Arctic Engineering – OMAE*, **3**, pp. 321-328.

Kuvin, B. F., 1991. “Fitness for Service-Steady Progress.” *Welding Design & Fabrication*. **64**, pp. 32.

McCabe, J. F., 2002. “Fitness for service evaluations and non-linear analysis – 2000.” *ASME Pressure Vessels and Piping Division (Publication) PVP*, **442**, 173p.

Milne, I., Ainsworh, R. A., Dowling, A. R., and Stewart, A. T., 1988. “Assessment of the Integrity of Structures Containing Defects.” *International Journal of Pressure Vessels and Piping*, **32**, pp. 3-104

Mok, D. R. B., Pick, R. J., and Glover, A. G., 1990. “Behavior of Line Pipe with Long External Corrosion.” *Material Performance*, **29(5)**, pp. 75-79.

Mok, D. R. B., Pick, R. J., Glover, A. G. and Hoff, R., 1991. “Bursting of Line Pipe with Long External Corrosion.” *International Journal of Pressure Vessels & Piping.*, **46**, pp. 195-216.

Mollmann, H, 1981. *Introduction to the Theory of Thin Shells*. John Wiley & Sons, Chichester.

Morris, G. A. and Packer, J. A., 1988. “Yield line Analysis of Cropped-web Warren Truss Joints.” *Journal of Structural Engineering*, **114**, pp. 2210-2224.

Newman, R. C. and Marcus, P., 2002. “Stress-Corrosion Cracking Mechanisms”, *Corrosion Mechanisms in Theory and Practice.* Second Edition. Marcel Dekker, New York.

Osage, D. A., Janelle, J., and Henry, P. A., 2000. “Fitness-For-Service Local Metal Loss Assessment Rules in API 579”, *ASME Pressure Vessels Piping Div Publ PVP*, **411**, pp. 143-176.

Pan, L., 2003. *Limit Load Estimation for Structures Under Mechanical Loads*. Ph. D. Dissertation. Faculty of Engineering ad Applied Science, Memorial University of Newfoundland, St. John's.

Ralph F. E., 2000. *Robust Methods of Finite Element Analysis: Evaluation of Non-linear, Lower Bound Limit Loads of Plated Structures and Stiffening Members.* M. Eng. Thesis. Faculty of Engineering ad Applied Science, Memorial University of Newfoundland, St. John's.

Rodery, C. D., 2005. "Determining Effective Thickness of Cylinders in Pressure Equipment with Significant Thickness Variations for Fitness for Service Assessments." *Proceedings of the ASME Pressure Vessels and Piping Conference 2005 - Design and Analysis, PVP2005,* **3**, pp. 181-186.

Rodery, C. D., Takagi, Y., Mura, N. Seipp, T. G., Iyer, S., Cohn, M. .J. and McCabe, J. F., 2004. "Fitness for Service, Life Extension, Remediation, Repair, and Erosion/Corrosion Issues for Pressure Vessels and Components – 2004. *ASME Pressure Vessels and Piping Division PVP*, **471**, 171 p.

Ruggles-Wrenn, M. B., Martin, J., Koves, W. J., Martens, D. H., Becht IV, C., 2003. "Design and Analysis Methods and Fitness for Service Evaluation for Pressure Vessels and Components." *ASME PVP*, *Design and Analysis Methods and Fitness for Service Evaluations for Pressure Vessels and Components*, **459**, 165p.

Sang, Z. F., Wang, H. F., Xue, L. P., and Widera, G. E. O., 2006. " Plastic Limit Loads of Pad Reinforced Cylindrical Vessels Under Out-of-Plane Moment of Nozzle." *Journal of Pressure Vessel Technology*, **128**, pp. 49-56.

Sehgal, R., Tiwari, A. and Sood, V., 2005. “A Study on Fitness-for-service Assessment for Crack-like Defects and Corrosion in Nuclear Reactor Pressure Tubes.” *Reliability Engineering and System Safety*, **89(2)**, pp. 227-235.

Smith, J. H. and Rana M. D., 2002. “The use of "fitness for service" assessment procedures to establish allowable flaw sizes in steel cylinders.” *ASME Pressure Vessels and Piping Division (Publication) PVP*, **442**, pp. 99-109.

Smith, J. H., Rana, M. D. and Hall, C., 2003. “The Use of “Fitness for Service” Assessment Procedures to Establish Critical Flaw Sizes in High-Pressure Gas Cylinders.” *Journal of Pressure Vessel Technology, Transactions of the ASME*, **125(2)**, pp. 177-181.

Thakkar, B. and Pandey, P. C., 2006. “Damage-Coupled Progressive Failure and Yield Line Analyses of Metal Plates.” *Journal of Engineering Mechanics*, **132(5)**, pp. 487-497.

Zhu, X. K. and Leis, B. N., 2005. “Influence of Yield-to-Tensile Strength Ratio on Failure Assessment of Corroded Pipelines.” *Transactions of the ASME*, **127**, pp. 436-441.

APPENDIX A

NUMERICAL RESULTS

This section presents some supplementary results for the inelastic remaining strength factors of damaged spheres and cylinders to those given in Chapter 7 and 8.

Tables A.1 to A.19 and Figure A.1 to A.6 show comparisons of the inelastic RSF obtained from FEA and the recommended RSF's for different cases. It can be seen that the recommended RSF's are comparable and conservative in all the cases.

Table A.1 RSF for spherical shell (R/h =20) with remaining corroded thickness 5h/6

φ_a	RSF_U	RSF_α	RSF_L	$RSF_{r\text{-}1}$	$RSF_{i\text{-}external}$	$RSF_{i\text{-}internal}$
3°	0.997	0.928	0.826	0.927	0.974	0.979
5°	0.994	0.926	0.826	0.926	0.961	0.976
8°	0.987	0.922	0.826	0.920	0.930	0.969
12°	0.976	0.917	0.826	0.894	0.893	0.947
15°	0.969	0.913	0.826	0.875	0.872	0.926
20°	0.957	0.907	0.826	0.842	0.851	0.882
25°	0.957	0.901	0.826	0.826	0.834	0.852
35°	0.946	0.891	0.826	0.826	0.824	0.824

Table A.2 RSF for spherical shell (R/h =20) with remaining corroded thickness $2h/3$

φ_a	RSF_U	RSF_α	RSF_L	$RSF_{r\text{-}1}$	$RSF_{i\text{-}external}$	$RSF_{i\text{-}internal}$
3°	0.993	0.802	0.656	0.801	0.961	0.975
5°	0.984	0.800	0.656	0.800	0.915	0.965
8°	0.968	0.796	0.656	0.789	0.833	0.953
12°	0.944	0.791	0.656	0.749	0.767	0.868
15°	0.927	0.787	0.656	0.720	0.718	0.784
20°	0.901	0.779	0.656	0.670	0.685	0.705
25°	0.878	0.772	0.656	0.656	0.675	0.673
35°	0.841	0.758	0.656	0.656	0.661	0.655

Table A.3 RSF for spherical shell (R/h =20) with remaining corroded thickness $h/2$

φ_a	RSF_U	RSF_α	RSF_L	$RSF_{r\text{-}1}$	$RSF_{i\text{-}external}$	$RSF_{i\text{-}internal}$
3°	0.987	0.590	0.488	0.591	0.942	0.969
5°	0.969	0.594	0.488	0.594	0.861	0.941
8°	0.938	0.600	0.488	0.587	0.725	0.864
12°	0.897	0.603	0.488	0.554	0.590	0.625
15°	0.868	0.605	0.488	0.531	0.544	0.557
20°	0.826	0.605	0.488	0.491	0.514	0.511
25°	0.791	0.603	0.488	0.488	0.503	0.500
35°	0.761	0.600	0.488	0.488	0.497	0.486

Table A.4 Comparison of RSF_r from the three methods and RSF_i for spherical shells (R/h =20, remaining corroded thickness $h_c = 5h/6$)

φ_a	RSF_U	$RSF_{r\text{-}1}$	$RSF_{r\text{-}2}$	$RSF_{r\text{-}3}$	$RSF_{inelastic}^{internal}$	$RSF_{inelastic}^{external}$
3°	0.997	0.928	0.967	0.953	0.993	0.975
5°	0.994	0.926	0.946	0.929	0.983	0.939
8°	0.987	0.920	0.917	0.898	0.949	0.891
12°	0.976	0.894	0.892	0.843	0.896	0.865
15°	0.969	0.875	0.873	0.863	0.866	0.849
20°	0.957	0.842	0.842	0.828	0.842	0.835
25°	0.946	0.826	0.826	0.826	0.834	0.832
35°	0.918	0.826	0.826	0.826	0.824	0.825

Table A.5 Comparison of RSF_r from the three methods and RSF_i for spherical shells (R/h =20, remaining corroded thickness $h_c = 2h/3$)

φ_a	RSF_U	$RSF_{r\text{-}1}$	$RSF_{r\text{-}2}$	$RSF_{r\text{-}3}$	$RSF^{\text{internal}}_{inelastic}$	$RSF^{\text{external}}_{inelastic}$
3°	0.994	0.791	0.887	0.916	0.961	0.975
5°	0.986	0.790	0.812	0.866	0.915	0.965
8°	0.970	0.787	0.770	0.801	0.833	0.953
12°	0.948	0.751	0.739	0.732	0.767	0.868
15°	0.931	0.724	0.715	0.693	0.718	0.784
20°	0.906	0.679	0.675	0.654	0.685	0.705
25°	0.883	0.645	0.645	0.645	0.675	0.673
35°	0.845	0.645	0.645	0.645	0.661	0.655

Table A.6 Comparison of RSF_r from the three methods and RSF_i for spherical shells (R/h =20, remaining corroded thickness $h_c = h/2$)

φ_a	RSF_U	$RSF_{r\text{-}1}$	$RSF_{r\text{-}2}$	$RSF_{r\text{-}3}$	$RSF^{\text{internal}}_{inelastic}$	$RSF^{\text{external}}_{inelastic}$
3°	0.990	0.590	0.709	0.879	0.942	0.968
5°	0.976	0.593	0.587	0.807	0.861	0.941
8°	0.950	0.596	0.571	0.713	0.725	0.864
12°	0.914	0.569	0.550	0.613	0.590	0.625
15°	0.888	0.548	0.534	0.557	0.544	0.557
20°	0.848	0.514	0.508	0.501	0.514	0.511
25°	0.814	0.488	0.488	0.488	0.503	0.500
35°	0.758	0.488	0.488	0.488	0.497	0.486

Table A.7 Comparison of RSF_r from the three methods and RSF_i for spherical shells (R/h =58.9, remaining corroded thickness $h_c = 5h/6$)

φ_a	RSF_U	$RSF_{r\text{-}1}$	$RSF_{r\text{-}2}$	$RSF_{r\text{-}3}$	$RSF_{inelastic}^{internal}$	$RSF_{inelastic}^{external}$
3°	0.994	0.925	0.964	0.952	0.975	0.993
5°	0.986	0.916	0.914	0.895	0.939	0.983
8°	0.973	0.884	0.883	0.854	0.891	0.949
12°	0.958	0.842	0.841	0.825	0.862	0.896
15°	0.947	0.822	0.822	0.822	0.849	0.867
20°	0.932	0.822	0.822	0.822	0835	0.842
25°	0.920	0.822	0.822	0.822	0.832	0.834

Table A.8 Comparison of RSF_r from the three methods and RSF_i for spherical shells (R/h =58.9, remaining corroded thickness $h_c = 2h/3$)

φ_a	RSF_U	$RSF_{r\text{-}1}$	$RSF_{r\text{-}2}$	$RSF_{r\text{-}3}$	$RSF^{\text{internal}}_{inelastic}$	$RSF^{\text{external}}_{inelastic}$
3°	0.986	0.803	0.831	0.869	0.935	0.976
5°	0.970	0.795	0.782	0.799	0.832	0.949
8°	0.944	0.749	0.741	0.721	0.754	0.811
12°	0.912	0.688	0.685	0.665	0.692	0.714
15°	0.890	0.659	0.659	0.659	0.678	0.687
20°	0.861	0.659	0.659	0.659	0.669	0.672
25°	0.837	0.659	0.659	0.659	0.671	0.664

Table A.9 Comparison of RSF_r from the three methods and RSF_i for spherical shells (R/h =58.9, remaining corroded thickness $h_c = h/2$)

φ_a	RSF_U	$RSF_{r\text{-}1}$	$RSF_{r\text{-}2}$	$RSF_{r\text{-}3}$	$RSF^{\text{internal}}_{inelastic}$	$RSF^{\text{external}}_{inelastic}$
3°	0.976	0.605	0.601	0.806	0.868	0.967
5°	0.948	0.604	0.581	0.702	0.715	0.828
8°	0.905	0.568	0.553	0.587	0.598	0.592
12°	0.853	0.519	0.514	0.505	0.518	0.526
15°	0.820	0.496	0.496	0.496	0.507	0.508
20°	0.776	0.496	0.496	0.496	0.501	0.503
25°	0.741	0.496	0.496	0.496	0.499	0.497

Table A.10 Comparison of RSF_r from the three methods and RSF_i for spherical shells (R/h =20) with thermal hot spots T_h = 316 °C

φ_a	RSF_U	$RSF_{r\text{-}1}$	$RSF_{r\text{-}2}$	$RSF_{r\text{-}3}$	$RSF_{inelastic}$
8°	0.985	0.868	0.867	0.854	0.922
12°	0.973	0.836	0.834	0.804	0.865
18°	0.955	0.787	0.786	0.755	0.795
25°	0.936	0.740	0.740	0.740	0.745

Table A.11 Comparison of RSF_r from the three methods and RSF_i for spherical shells (R/h =20) with thermal hot spots T_h = 204 °C

φ_a	RSF_U	$RSF_{r\text{-}1}$	$RSF_{r\text{-}2}$	$RSF_{r\text{-}3}$	$RSF_{inelastic}$
8°	0.991	0.940	0.939	0.920	0.957
12°	0.984	0.919	0.918	0.892	0.932
18°	0.974	0.887	0.887	0.865	0.931
25°	0.963	0.857	0.857	0.857	0.913

Table A.12 Comparison of RSF_r from the three methods and RSF_i for spherical shells (R/h =20) with thermal hot spots T_h = 94.4 °C

φ_a	RSF_U	$RSF_{r\text{-}1}$	$RSF_{r\text{-}2}$	$RSF_{r\text{-}3}$	$RSF_{inelastic}$
8°	0.994	0.965	0.965	0.950	0.967
12°	0.990	0.951	0.951	0.932	0.952
18°	0.983	0.929	0.930	0.915	0.931
25°	0.976	0.910	0.910	0.910	0.913

Table A.13 Comparison of RSF_r from the three methods and RSF_i for spherical shells (R/h =58.9) with thermal hot spots T_h = 316 °C

φ_a	RSF_U	$RSF_{r\text{-}1}$	$RSF_{r\text{-}2}$	$RSF_{r\text{-}3}$	$RSF_{inelastic}$
5°	0.969	0.864	0.875	0.847	0.931
7°	0.974	0.836	0.842	0.804	0.886
10°	0.959	0.794	0.798	0.760	0.828
15°	0.936	0.740	0.740	0.740	0.764
20°	0.916	0.740	0.740	0.740	0.747

Table A.14 Comparison of RSF_r from the three methods and RSF_i for spherical shells (R/h =20) with thermal hot spots T_h = 204 °C

φ_a	RSF_U	$RSF_{r\text{-}1}$	$RSF_{r\text{-}2}$	$RSF_{r\text{-}3}$	$RSF_{inelastic}$
5°	0.991	0.937	0.942	0.915	0.950
7°	0.985	0.919	0.923	0.892	0.947
10°	0.976	0.892	0.894	0.868	0.915
15°	0.963	0.857	0.857	0.857	0.878
20°	0.952	0.857	0.857	0.857	0.863

Table A.15 Comparison of RSF_r from the three methods and RSF_i for spherical shells (R/h =20) with thermal hot spots T_h = 94.4 °C

φ_a	RSF_U	$RSF_{r\text{-}1}$	$RSF_{r\text{-}2}$	$RSF_{r\text{-}3}$	$RSF_{inelastic}$
5°	0.994	0.963	0.967	0.947	0.983
7°	0.990	0.951	0.954	0.932	0.971
10°	0.985	0.933	0.935	0.917	0.951
15°	0.979	0.910	0.910	0.910	0.927
20°	0.969	0.910	0.910	0.910	0.915

Table A.16 Comparison of RSF from the three recommended methods and inelastic analysis for corrosion damage in cylindrical shells (R/h =33.6, $h_c = 2h/3$, r = 1.0)

a (in.)	RSF_u	$RSF_{r\text{-}1}$	$RSF_{r\text{-}2}$	$RSF_{r\text{-}3}$	$RSF_{inelastic}^{internal}$	$RSF_{inelastic}^{external}$
2.5	0.991	0.805	0.794	0.859	0.903	0.948
3.5	0.984	0.798	0.778	0.814	0.846	0.892
5.0	0.972	0.769	0.753	0.756	0.788	0.809
10.0	0.933	0.670	0.671	0.661	0.702	0.694
12.5	0.915	0.660	0.660	0.660	0.692	0.682

Table A.17 Comparison of RSF from the three recommended methods and inelastic analysis for corrosion damage in cylindrical shells (R/h =33.6, $h_c = h/2$, r = 0.2)

a (in.)	RSF_u	$RSF_{r\text{-}1}$	$RSF_{r\text{-}2}$	$RSF_{r\text{-}3}$	$RSF^{\text{internal}}_{inelastic}$	$RSF^{\text{external}}_{inelastic}$
5.0	0.988	0.598	0.674	0.870	0.967	0.957
10.0	0.967	0.601	0.585	0.759	0.828	0.885
15.0	0.945	0.596	0.568	0.668	0.742	0.694
20.0	0.924	0.575	0.550	0.595	0.646	0.617
30.0	0.885	0.533	0.515	0.508	0.550	0.550

Table A.18 Comparison of RSF from the three recommended methods and inelastic analysis for thermal hot spots in cylindrical shells (R/h =33.6, T_h = 316 °C, r =1**)**

a (in.)	b (in.)	RSF_U	RSF_{r-1}	RSF_{r-2}	RSF_{r-3}	$RSF_{inelastic}$
2.0	2.0	0.997	0.873	0.888	0.912	0.957
3.0	3.0	0.993	0.872	0.861	0.875	0.919
5.0	5.0	0.985	0.841	0.830	0.814	0.842
7.0	7.0	0.976	0.806	0.799	0.760	0.799
10.0	10.0	0.963	0.753	0.740	0.740	0.766
15.0	15.0	0.940	0.740	0.740	0.740	0.743
18.0	18.0	0.930	0.740	0.740	0.740	0.739

Table A.19 Comparison of RSF from the three recommended methods and inelastic analysis for thermal hot spot in cylindrical shells (R/h =33.6, T_h = 316 °C, r =0.3)

a (in.)	b (in.)	RSF_U	RSF_{r-1}	RSF_{r-2}	RSF_{r-3}	$RSF_{inelastic}$
5.0	1.5	0.995	0.872	0.877	0.915	0.957
10.0	3.0	0.986	0.867	0.844	0.847	0.880
15.0	4.5	0.976	0.832	0.815	0.796	0.833
20.0	6.0	0.967	0.796	0.786	0.761	0.798
24.0	7.2	0.959	0.768	0.763	0.745	0.777
28.8	8.6	0.951	0.740	0.740	0.740	0.766
32.0	9.6	0.946	0.740	0.740	0.740	0.759

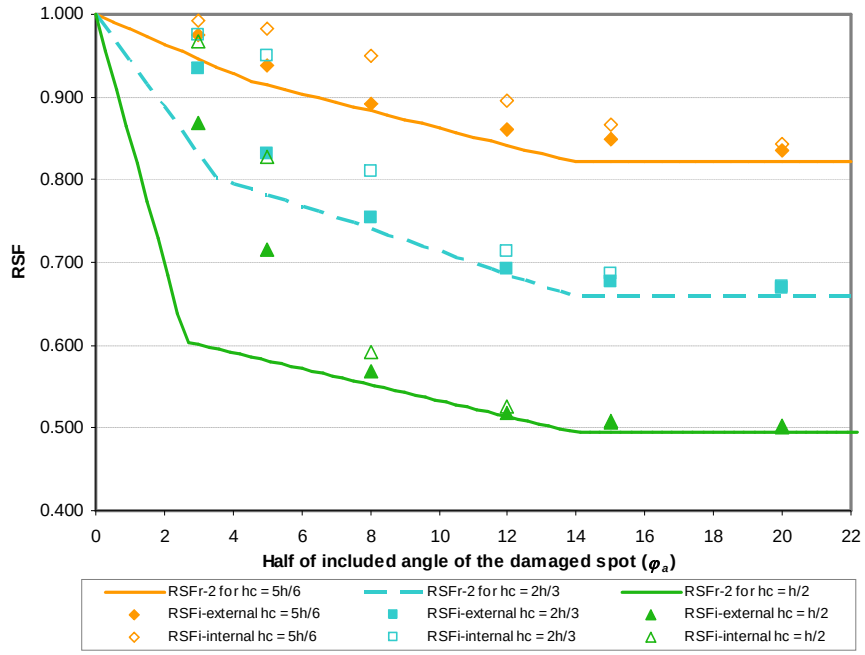

Figure A.1 Method II recommendation: RSF_{r-2} and RSF_i for corrosion damage in spherical shells with R/h ratio = 58.9

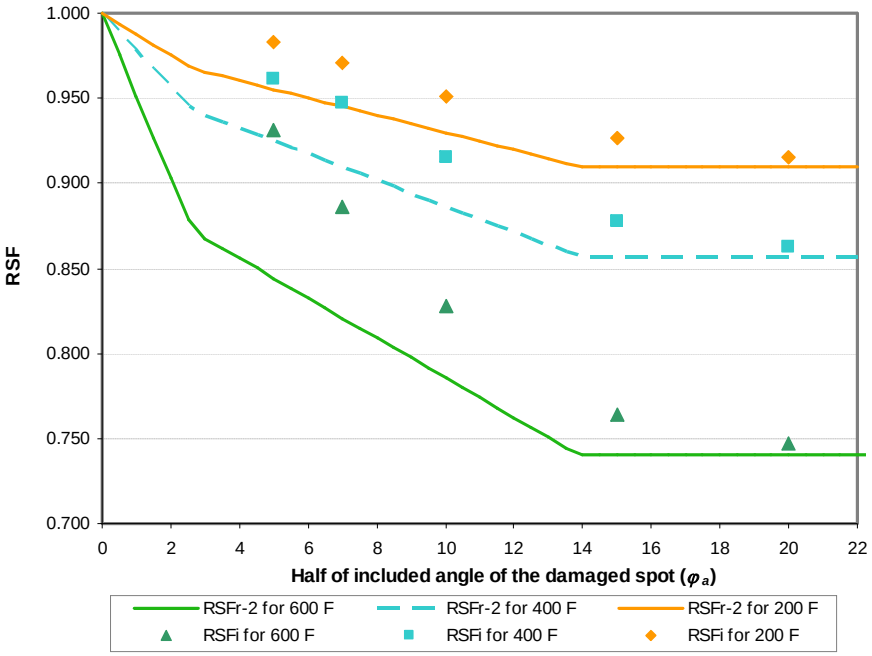

Figure A.2 Method II recommendation: RSF_{r-2} and RSF_i for thermal hot spots in spherical shells with R/h ratio = 58.9

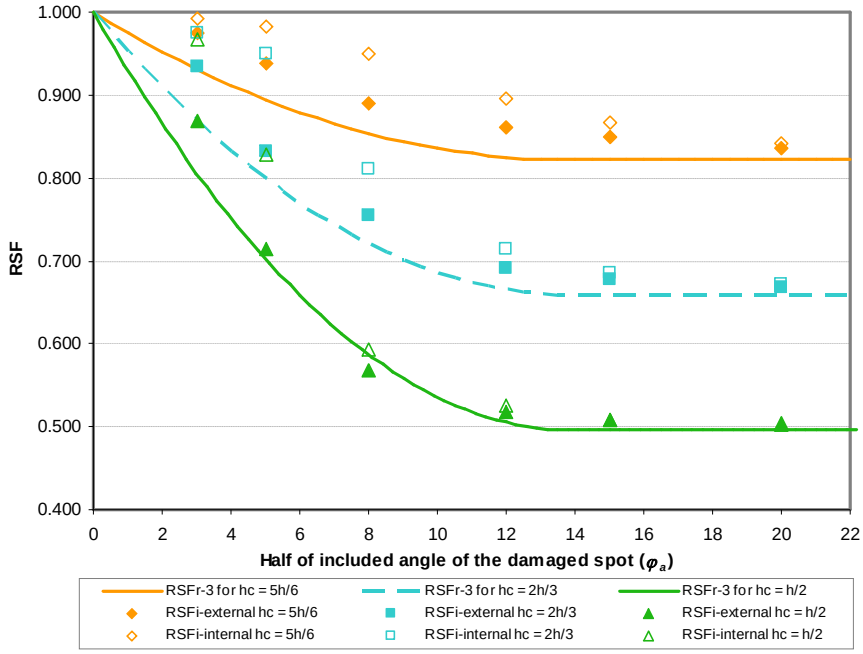

Figure A.3 Method III recommendation: RSF_{r-3} and RSF_i for corrosion damage in spherical shells with R/h ratio = 58.9

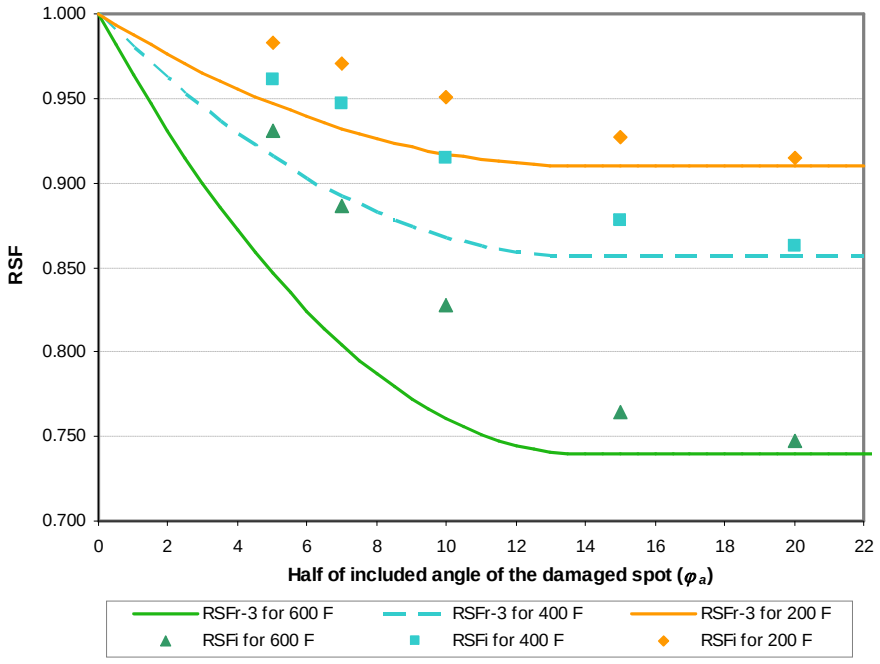

Figure A.4 Method III recommendation: RSF_{r-3} and RSF_i for thermal hot spots in spherical shells with R/h ratio = 58.9

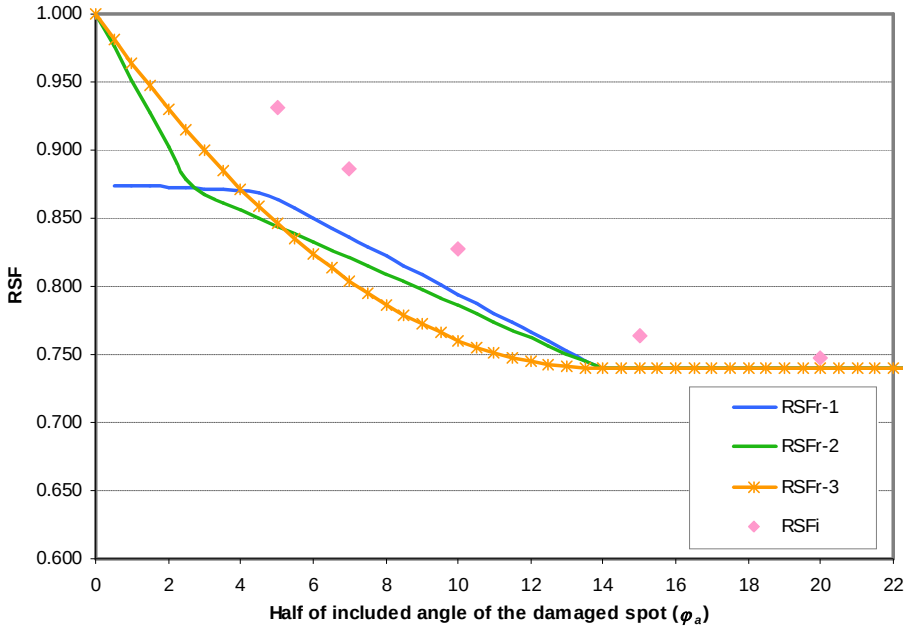

Figure A.5 Comparison of recommended RSF and RSF_i for thermal hot spots in a spherical shell with R/h ratio = 58.9

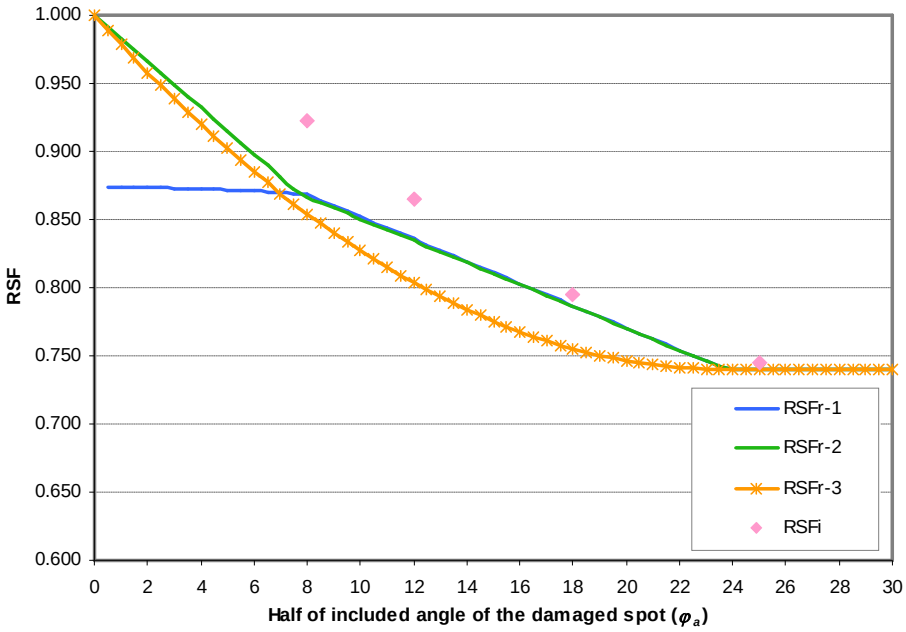

Figure A.6 Comparison of recommended RSF and RSF_i for thermal hot spots in a spherical shell with R/h ratio = 20

APPENDIX B

AIDS FOR RSF ASSESSMENT

The current section provides useful aids for Level 2 RSF evaluation of damaged spheres and cylinders. This includes MATLAB command files and Excel spreadsheet files that can be easily used or customized to obtain the recommended remaining strength factors. They can be adapted by changing the input data to correspond to the case of interest. The MATLAB command files to calculate RSF and estimated bulging displacement are listed along with examples of input data and output arguments. The Excel spreadsheet files are recorded in a compact disc attached with the dissertation. Sample prints of the spreadsheet files are also presented. The spreadsheet files can do all the calculations for RSF and can be used as alternative means for MATLAB functions

B.1. MATLAB SCRIPTS FOR RSF CALCULATION

The MATLAB script and functions (M-files) implemented to determine the recommended remaining strength factors are listed below.

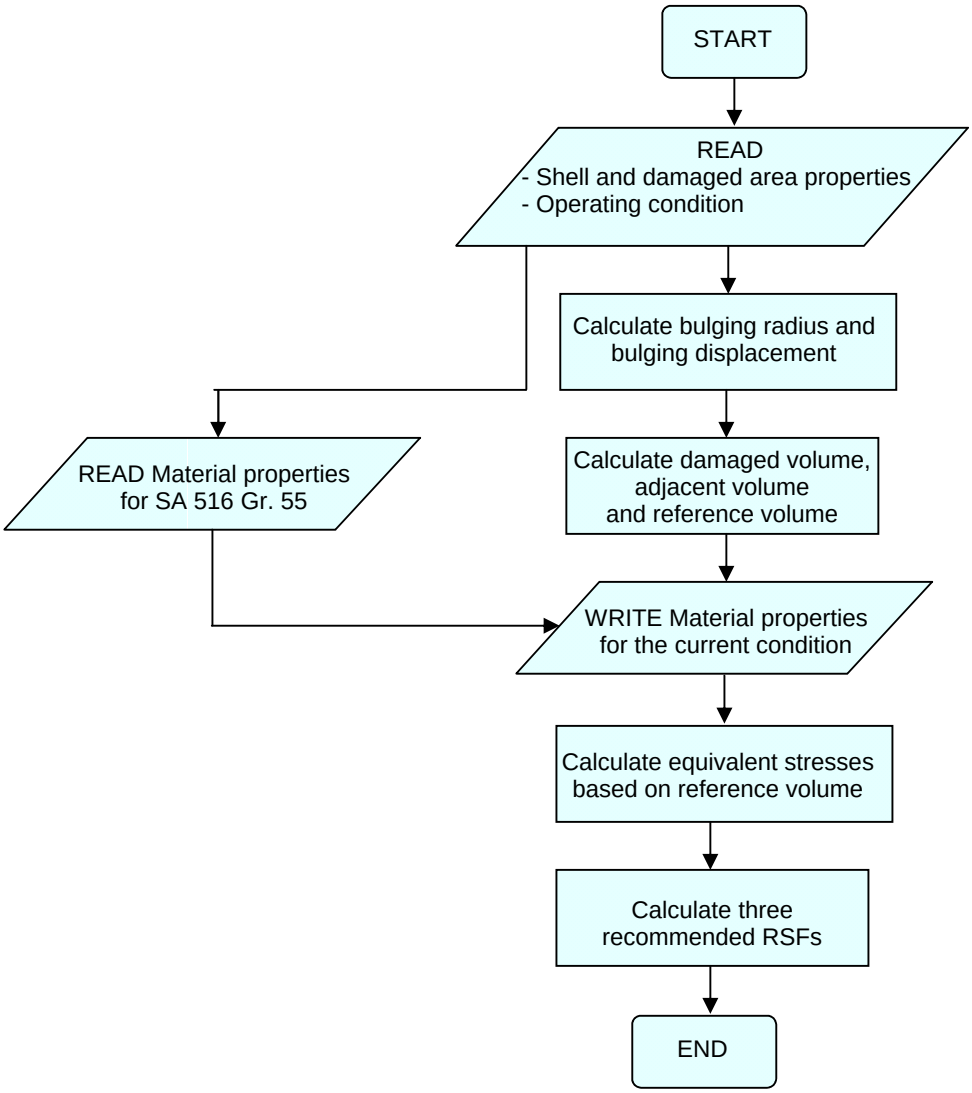

Figure B.1 Flow Chart for the MATLAB script

When the main script is executed, The user is asked to input necessary data such as shell and damaged area properties and operating condition. The *data_input* m-file stores the input properties which will be used through out the program. Function *bulge* determines an approximate bulging radius and displacement. Volume of the damaged spot, adjacent volume and reference volume are obtained by using function *RefVol*. The present program automatically acquires material properties for SA 516 grade 55 based on

operating temperature and stored in parameter *mp_data* (a column array with 4 quantities in the order: Young's modulus, coefficient of thermal expansion, yield stress at temperature of hot spot, yield stress at operating temperature). For other materials with known properties, this array can be input directly to the main program and the execution of function *MP* can be omitted. The RSF from the three recommended methods are then calculated based on Tresca or von-Mises criteria depending upon the user demand. Note that each of the m-files can also be executed on its own if only some particular parameters are of interest (provided that the necessary data are stored at the right places).A simple flow chart of the process described above is provided in Figure B.1.

B.1.1. Main Script

```
% Main Program
% Data input
[ShapeType, Data] = data_input

% Calculate bulging radius and displacement
[delta_b] = bulge(ShapeType, Data);

% Obtain Reference Volume
mp_data = [0 0 0 0];
[V] = RefVol(ShapeType, Data, mp_data);

% Get Material Properties
[mp_data] = MP(ShapeType, Data, V);

% Calculate Equivalent stresses
[se, se_c] = eqvS(ShapeType, Data, mp_data);

% Calculate Three Recommended Remaining Strength Factors
[RSF] = RSFs(ShapeType, Data, mp_data, V, se, se_c)
```

B.1.2. M-File for Data Input

```
% Function for data input

function [ShapeType, Data] = data_input
clc

% input shell and damaged spot geometries
disp('  ')
disp ('                    DATA INPUT ')
check = 'N';

while (check ~= 'Y') && (check ~= 'y')
% continue the loop as long as check is not Y or y
    disp('  ')
    disp('------------------------------------------------------------')
    disp ('   Pressure vessel Geometries')
    disp('------------------------------------------------------------')
    disp('  ')
    shape = input('Pressure vessel shape (C for cylinder, S for sphere): ','s');
    Ri = input('Inner Radius (in.): ');
    h  = input('Shell Thickness (in.): ');
    disp('  ')
    disp('------------------------------------------------------------')
    disp('   Operating conditions.')
    disp('------------------------------------------------------------')
    disp('  ')
    Pd = input('Design Internal Pressure (psi): ');
    Tc = input('Operating Temperature (F): ');
    disp('  ')
    disp('------------------------------------------------------------')
    disp('   Damage conditions and dimensions.')
    disp('------------------------------------------------------------')
    disp('  ')
    type = input('Type of damaged spot (H for hot spot, C for corrosion): ',
     's');
    if (type == 'H') || (type == 'h')
        Th = input('Temperature of the hot spot (F): ');
    elseif (type == 'C') || (type == 'c')
        hc = input('Remaining thickness (in.): ');
```

```
else
    disp('Invalid type of damaged spot.')
    check = 'N';
end
if (shape == 'S') || (shape == 's')
    phi_a_degree = input('Included angle of damaged spot (degree): ');
    % Half of the included angle
    phi_a = phi_a_degree/180*pi/2;
elseif (shape == 'C') || (shape == 'c')
    A = input('Size of damaged spot along the circumferential direction
     (in.): ');
    B = input('Size of damaged spot along the axial direction (in.): ');
    a = A/2; b = B/2;
else
    disp('Invalid pressure vessel shape.')
    check = 'N';
end
disp('  ')
disp('Please check all your input data.')
check = input('Is your input correct? (y,n): ', 's');

% Output data
ShapeType = [shape; type];

if (ShapeType(1,1) == 'C') || (ShapeType(1,1) == 'c')
    if (ShapeType(2,1) == 'C') || (ShapeType(2,1) == 'c')
        Data = [Ri, h, Pd, Tc, hc, a, b];
    elseif (ShapeType(2,1) == 'H') || (ShapeType(2,1) == 'h')
        Data = [Ri, h, Pd, Tc, Th, a, b];
    else
        disp('Some input is invalid. Please enter your data again.')
    end
elseif (ShapeType(1,1) == 'S') || (ShapeType(1,1) == 's')
    if (ShapeType(2,1) == 'C') || (ShapeType(2,1) == 'c')
        Data = [Ri, h, Pd, Tc, hc, phi_a];
    elseif (ShapeType(2,1) == 'H') || (ShapeType(2,1) == 'h')
        Data = [Ri, h, Pd, Tc, Th, phi_a];
    end
else
    check = 'N';
```

```
        disp('Some input is invalid. Please enter your data again.')
    end
end
% Output
```

B.1.3. M-File for Bulging Displacement Calculation

```
% Function used to estimate bulging displacement in spherical or
cylindrical shells

function [delta_b] = bulge(ShapeType, Data);

% For corrosion - ShapeType(2,1) = 'C'
% For hot spot  - ShapeType(2,1) = 'H'
% For cylinder  - ShapeType(1,1) = 'C'; Data = [Ri, h, Pd, Tc, Th, a, b]
% For sphere    - ShapeType(1,1) = 'S'; Data = [Ri, h, Pd, Tc, Th, phi_a]

disp('  ')
disp('------------------------------------------------------------')
disp ('           CALCULATION OF BULGE DISPLACEMENT')
disp('------------------------------------------------------------')
disp('  ')
strain = input('Please enter the limit strain for bulging [default = 0.01]: ');

%If there is no input argument, strain = 0.01 by default
if isempty(strain)
    strain = 0.01;
end

% For cylindrical shells
if (ShapeType(1,1) == 'C') || (ShapeType(1,1) == 'c')
    Ri = Data(1,1);                                          % Inner radius
    h  = Data(1,2); a = Data(1,6); b = Data(1,7);            % Shell thickness
    c  = sqrt(a^2 + b^2);                                    %radius of damaged area
    Ro = Ri + h;                                             Shell outside radius
    theta_o = c/Ro;                                  Included angle of damaged area
% For spherical shells
elseif (ShapeType(1,1) == 'S') || (ShapeType(1,1) == 's')
    Ri = Data(1,1); h  = Data(1,2); theta_o = Data(1,6);     % Inner radius
    Ro = Ri + h;                                             Shell outside radius
```

```
else
    disp('Invalid pressure vessel shape. Please enter your data again.')
end

r_h     = Ro*sin(theta_o);
delta_o = Ro-sqrt(Ro^2-r_h^2);

Rb_thetab = strain*Ro*theta_o + Ro*theta_o;

% Input bound for Rb to calculate Rb and theta b numerically
check1 = 0;
% continue the loop as long as check1 = 0
while check1 == 0
    check2 = 0;
    while check2 == 0
        jRb = input('Please enter your estimate bound for bulging radius (in.)
        :');
        kRb = input('and (in.): ');
        if jRb < kRb
            Rb = jRb:0.0005:kRb;              % variables for bulging radius Rb
            check2 = 1;
        elseif kRb < jRb
            Rb = kRb:0.0005:jRb;
            check2 = 1;
        else
            disp('   The two values are equal. Please re-enter the esimate
            bound.')
        end
    end

    % numbers of Rb
    iRb = size(Rb); nRb = iRb(1,2);

    % Solve for Rb and thetab that give the y equation zero
    for i = 1:nRb
        y(i) = Rb(i)*sin(Rb_thetab/Rb(i)) - r_h;
    end

    done = 0;
    for i = 1:nRb
```

```
        if done == 0
            if y(i)>0
                R_b = Rb(i);
                % bulge included angle (radians)
                theta_b = Rb_thetab/R_b;
                % bulge included angle (degrees)
                theta_b_deg = theta_b/pi*180;
                % bulge displacement
                delta_b = (R_b-delta_o)-(sqrt(R_b^2-r_h^2));
                done = 1;
            end
        end
    end
    disp('  ')
    disp('Estimate bulging Radius (in.): ')
    disp(R_b)

    if (R_b ~= jRb) && (R_b ~= kRb)
        disp('Estimate bulging displacement (in.):')
        disp(delta_b)
        disp('   ')
        check1 = 1;
    else
        disp('If the calculated bulging radius is equal to your either bound,
         please consider changing the bound.')
        % If the bound for bulge radius (Rb) does not give y = 0, the loop will
        restart and the program will ask for new bound for Rb.
    end
end
```

B.1.4. M-File for Calculation of Reference Volume

```
% Reference Volume Calculation

function [V] = RefVol(ShapeType, Data, mp_data)

% For cylinder  - Data = [Ri, h, Pd, Tc, Th (or hc), a, b]
% For sphere    - Data = [Ri, h, Pd, Tc, Th (or hc), phi_a]
```

```
Ri = Data(1,1);      h = Data(1,2);      Pd = Data(1,3);
s_y = mp_data(1,3);                          % stress at operating temperature

% For corrosion damage, obtain corroded thickness (hc) from the Data(1,5)
if (ShapeType(2,1) == 'C') || (ShapeType(2,1) == 'c')
    hc = Data(1,5);
else
    % For hot spot damage, hc = shell thickness (h)
    hc = h;
end

% Calculation
Rm    =  Ri + h/2;                                                  % Mean radius

% For spherical shell
if (ShapeType(1,1) == 'S') || (ShapeType(1,1) == 's')
    phi_a = Data(1,6);                              % Included angle for damaged
spot
    psi_d = 2.14*sqrt(h/Rm);                   % Decay angle for spherical shell

    VD = 2*pi*Rm^2*(1-cos(phi_a))*hc;                   % Volume of damaged spot
    VI = 2*pi*Rm^2*(cos(phi_a)-cos(psi_d))*h;          % Volume of adjacent zone
    VR = VD + VI;                                              % Reference volume
else
    % For cylindrical shell
    a = Data(1,6);              % Half damage size in circumferential direction
    b = Data(1,7);                          % Half damage size in axial direction
    xc = 6.3*sqrt(h*Rm);             % Decay length in circumferential direction
    xl = 2.5*sqrt(h*Rm);                        % Decay length in axial direction

    VD = 4*a*b*hc;                                      % Volume of damaged spot
    VI = 4*h*((a+xc)*(b+xl)-a*b);                      % Volume of adjacent zone
    VR = VD + VI;                                              % Reference volume
end


% Output (Damaged volume, Adjacent volume, Reference volume)

V = [VD VI VR];
```

B.1.5. M-File for Material Properties

```
% Material Properties for SA 516 Grade 55
% Young's modulus, thermal expansion coefficient and yield stress.

function [mp_data] = MP(ShapeType, Data, V)

% For cylinder  - Data = [Ri, h, Pd, Tc, Th (or hc), a, b]
% For sphere    - Data = [Ri, h, Pd, Tc, Th (or hc), phi_a]

checkC = 0;

    % For hot spot damage, operating temperature (Tc) = Data(1,4) and hot spot
    temperature (Th) = Data(1,5).
if (ShapeType(2,1) == 'H') || (ShapeType(2,1) == 'h')
    Tc = Data(1,4); Th = Data(1,5);
    checkH = 0;
% For corrosion damage, operating temperature (Tc) = Data(1,4) and hot spot
    temperature (Th) is set as zero.
elseif (ShapeType(2,1) == 'C') || (ShapeType(2,1) == 'c')
    Tc = Data(1,4); Th = 0;
    checkH = 1;     s_yh = 0;
else
    checkC = 1;     checkH = 1;
end

% Material Properties
Tt   = [    100     200     300     400     500     600];
Et   = [ 2.93e7  2.88e7  2.83e7  2.77e7  2.73e7  2.67e7];
alpt = [5.53e-6 5.89e-6 6.26e-6 6.61e-6 6.91e-6 7.17e-6];
s_yt = [ 3.00e4  2.73e4  2.66e4  2.57e4  2.45e4  2.22e4];

n = 1; iTt = size(Tt); nTt = iTt(1,2);

while checkC == 0
    if n < nTt
        if Tc < Tt(n)
            i = n-1;
            if i == 0
```

```
                disp ('Invalid input for operating temperature. The minimum
                 temperature is (F) :')
                disp(Tt(1))
                Ec = 0; alpc = 0; s_yc = 0;
                checkC = 1;
            else
                deltaT = Tc - Tt(i);
                Ec     = Et(i) + deltaT*(Et(n)-Et(i))/(Tt(n)-Tt(i));
                alpc   = alpt(i) + deltaT*(alpt(n)-alpt(i))/(Tt(n)-Tt(i));
                s_yc   = s_yt(i) + deltaT*(s_yt(n)-s_yt(i))/(Tt(n)-Tt(i));
                checkC = 1;
            end
        elseif Tc == Tt(n)
            Ec = Et(n);
            alpc = alpt(n);
            s_yc = s_yt(n);
            checkC = 1;
        else
            n = n+1;
        end
    else
        disp ('Invalid input for operating temperature. The maximum temperature
         is (F):')
        disp(Tt(nTt))
        Ec = 0; alpc = 0; s_yc = 0;
        checkC = 1;
    end
end

n = 1;
while checkH == 0
    if n < nTt
        if Th < Tt(n)
            i = n-1;
            if i == 0
                disp ('Invalid input for hot spot temperature. The minimum
                 temperature is (F):')
                disp(Tt(1))
                Eh = 0; alph = 0; s_yh = 0;
                checkH = 1;
```

```
            elseif Th == Tt(n)
                Eh = Et(i);
                alph = alpt(i);
                s_yh = s_yt(i);
                checkH = 1;
            else
                deltaT = Th - Tt(n);
                Eh    = Et(i) + deltaT*(Et(n)-Et(i))/(Tt(n)-Tt(i));
                alph  = alpt(i) + deltaT*(alpt(n)-alpt(i))/(Tt(n)-Tt(i));
                s_yh = s_yt(i) + deltaT*(s_yt(n)-s_yt(i))/(Tt(n)-Tt(i));
                checkH = 1;
            end
        else
            n = n+1;
        end
    elseif Th == Tt(n)
        Eh = Et(n);
        alph = alpt(n);
        s_yh = s_yt(n);
        checkH = 1;
    else
        disp ('Invalid input for hot spot temperature. The maximum temperature
         is (F):')
        disp(Tt(nTt))
        Eh = 0; alph = 0; s_yh = 0;
        checkH = 1;
    end
end

VD = V(1,1);                                          % Volume of damaged spot
VI = V(1,2);                                         % Volume of adjacent zone
VR = V(1,3);                                               % Reference volume

% For hot spot problem, calculate effective Young's modulus and thermal
% coefficient by weight average of the volume involved
if (ShapeType(2,1) == 'H') || (ShapeType(2,1) == 'h')
    Ee   = (Eh*VD + Ec*VI)/VR;
    alpe = (alph*VD + alpc*VI)/VR;
elseif (ShapeType(2,1) == 'C') || (ShapeType(2,1) == 'c')
    Ee = Ec;
```

```
    alpe = alpc;
end

% Output
% Ee = Effective Young's modulus; alpe = Effective thermal coefficient
% s_yc = yield stress of the material at operating temperature
% s_yh = yield stress of the material inside the hot spot
mp_data = [Ee alpe s_yc s_yh];
```

B.1.6. M-File for Calculation of Equivalent Stress

```
% Equivalent stresses

function [se, se_c] = eqvS(ShapeType, Data, mp_data)

Ri = Data(1,1);     h   = Data(1,2);       Pd = Data(1,3);
Tc = Data(1,4);     hc  = Data(1,5);
Ee = mp_data(1,1);  alpe = mp_data(1,2);

if (ShapeType(2,1) == 'H') || (ShapeType(2,1) == 'h')
    Th = Data(1,5);
    se  = abs(Pd*Ri/(2*h) - Ee*alpe*(Th-Tc)/2);
    se_c = 0;
elseif (ShapeType(2,1) == 'C') || (ShapeType(2,1) == 'c')
    hc = Data(1,5);
    se  = Pd*Ri/(2*h);
    se_c = Pd*Ri/2/hc;
else
    disp(' Invalid type of damage.')
end
```

B.1.7. M-File for Calculation of Recommended RSFs

```
% RSF Recommendations

function [RSF] = RSFs(ShapeType, Data, mp_data, V, se, se_c)

Ri   = Data(1,1);     h    = Data(1,2);      Pd   = Data(1,3);
```

```
s_yc = mp_data(1,3);

Rm  = Ri + h/2;                                                    % Mean radius

% For corrosion damage, corroded thickness (hc) = Data(1,5)
if (ShapeType(2,1) == 'C') || (ShapeType(2,1) == 'c')
    hc = Data(1,5);
else
% For hot spot damage, corroded thickness (hc) is set to be equal to shell
% thickness
    hc = Data(1,2);
end

% For Spherical Shells
if (ShapeType(1,1) == 'S') || (ShapeType(1,1) == 's')

    phi_a = Data(1,6);

    % Decay angle for sphere
    psi_d = 2.14*sqrt(h/Rm);

    % Transition point (1/3 of the extent for damaged spot)
    Data(1,6) = psi_d/3;

    % Determine Reference volume for the transition point
    [Vt] = RefVol(ShapeType, Data, mp_data);

    % Threshold to dominance of membrane action
    phi_star = 0.5*hc/Rm*sqrt(3*s_yc/2/Pd);

    % Determine Reference volume for the threshold
    Data(1,6) = phi_star;
    [Vc] = RefVol(ShapeType, Data, mp_data);
    Data(1,6) = phi_a;

    % Calculate multipliers
    [All_m] = Multiplier(ShapeType, Data, mp_data, V, Vt, Vc, se, se_c);

    % Calculate RSF for sphere
    [RSF] = RSFsphere(Data, All_m , hc, psi_d, phi_star);
```

```
% For Cylindrical Shells

elseif (ShapeType(1,1) == 'C') || (ShapeType(1,1) == 'c')
    a = Data(1,6);   b = Data(1,7);
    r = b/a;

    % Decay length in the circumferential direction
    xc = 6.3*sqrt(h*Rm);
    % Decay length in the axial direction
    xl = 2.5*sqrt(h*Rm);

    % Normalize variable for dimensions of damaged spot
    xi = a/4/xc + 3*b/4/xl;

    % Transition point (1/3 of the extent for damaged spot)
    at = 4*xc*xl/(r*xc+3*xl)/3;
    Data(1,6) = at;
    % bt
    Data(1,7) = r*at;
    % Determine Reference volume for the transition point
    [Vt] = RefVol(ShapeType, Data, mp_data);

    % Threshold to dominance of membrane action
    star_test = 0;   w1 = 0.01;  w2 = w1*r;
    Plim = s_yc*5/8/Ri/(1+0.6*5/8/Ri);              % Maximum applied pressure
    while star_test == 0
        if r < 1                                                % w1 = shorter size
            x_star = (w2*sqrt(w2^2+3*w1^2)-w2^2)/w1;
            p_star = 3*s_yc*hc^2*(w1*x_star+w2^2)/(w2*x_star*(3*w1*w2
                      - w2*x_star));
        else                                                    % w2 = shorter size
            x_star = (w1*sqrt(w1^2+3*w2^2)-w1^2)/w2;
            p_star = 3*s_yc*hc^2*(w2*x_star+w1^2)/(w1*x_star*(3*w2*w1
                      - w1*x_star));
        End
        % Stretching action dominates when pressure more than p_star
        if Plim > p_star
            star_test = 1;                                      % Terminate loop
            a_star = 0.6*w1;                              % Empirical factor = 0.6
        else
```

```
            w1 = w1 + 0.01;                % Continue the loop by increasing w1
            w2 = w1*r;
        end
    end

    Data(1,6) = a_star;
    % b_star
    Data(1,7) = r*a_star;
    % Determine Reference volume for the threshold
    [Vc] = RefVol(ShapeType, Data, mp_data);

    xi_star   = 0.5*(a_star/4/xc + 3*a_star*r/4/xl);
    Data(1,6) = a;   Data(1, 7) = b;

    % Calculate multipliers
    [All_m] = Multiplier(ShapeType, Data, mp_data, V, Vt, Vc, se, se_c);

    % Calculate RSF for cylinder
    [RSF] = RSFcylinder(Data, All_m, hc, xi, xi_star);
end
```

B.1.8. M-File for RSF in Sphere

```
% Recommended RSF for sphere

function [RSF] = RSFsphere(Data, All_m, hc, psi_d, phi_star)

Ri  = Data(1,1);     h    = Data(1,2);      Pd   = Data(1,3);
phi_a = Data(1,6);
RSF_L = All_m(1,2);  RSF_alp = All_m(1,3);  RSF_alpt = All_m(1,4);
RSF_alpc = All_m(1,5)

Rm = Ri + h/2;

%-------------------------------------------------------------------------
% Calculation of RSF_r1
%-------------------------------------------------------------------------

% Define Poisson's ratio = 0.3
```

```
nu     = 0.3;
% Shell constant
lambda = (3*(1-nu^2)*(Rm/h)^2)^(1/4);

% Transition point at one-third of decay angle
if phi_a < psi_d/3
    % For included angle less than the transition angle
    RSF_r1 = RSF_alp;
elseif phi_a < psi_d
    % For intermediate damage spot (larger than the transition angle, smaller
    % than the decay angle)
    RSF_r1 = (1.5-0.637*lambda*phi_a)*RSF_alpt + (0.637*lambda*phi_a-0.5)*RSF_L;
else
    % For global damage (included angle larger than decay angle)
    RSF_r1 = RSF_L;
End

disp('   ')
disp('------------------------------------------------------------')
disp('   ')
disp('  Recommended RSF from the first method (RSF-r1): ')
disp(RSF_r1)

%-------------------------------------------------------------------------
% Calculation of RSF_r2
%-------------------------------------------------------------------------

% For included angle less than the threshold to dominance of membrane effect
if phi_a < phi_star;
    RSF_r2 = 1 - (1-RSF_alpc)*(phi_a/phi_star);
elseif phi_a < psi_d
    % For intermediate damage spot (larger than the threshold, smaller than the
    %decay angle)
    RSF_r2 = RSF_alpc - (RSF_alpc-RSF_L)/(psi_d-phi_star)*phi_a;
Else
    % For global damage (included angle larger than decay angle)
    RSF_r2 = RSF_L;
end
disp('  Recommended RSF from the second method (RSF-r2): ')
disp(RSF_r2)
```

```
%-------------------------------------------------------------------------
% Calculation of RSF_r3
%-------------------------------------------------------------------------

if phi_a < psi_d
    % For local damage (included angle smaller than decay angle)
    RSF_r3 = (1-RSF_L)/(psi_d^2)*(phi_a^2) - 2*(1-RSF_L)/psi_d*phi_a + 1;
Else
    % For global damage (included angle larger than decay angle)
    RSF_r3 = RSF_L;
end
disp('  Recommended RSF from the third method (RSF-r3): ')
disp(RSF_r3)

% Output
RSF = [RSF_r1 RSF_r2 RSF_r3];
```

B.1.9. M-File for RSF in Cylinder

```
% Recommended RSF for cylinder

function [RSF] = RSFcylinder(Data, All_m, hc, xi, xi_star)

Ri  = Data(1,1);     h    = Data(1,2);      Pd   = Data(1,3);
a   = Data(1,6);     b    = Data(1,7);
RSF_L = All_m(1,2);  RSF_alp = All_m(1,3);  RSF_alpt = All_m(1,4);
RSF_alpc = All_m(1,5)

Rm = Ri + h/2;
%-------------------------------------------------------------------------
% Calculation of RSF_r1
%-------------------------------------------------------------------------
% Transition point at one-third of decay angle
if xi < 1/3
    RSF_r1 = RSF_alp;
elseif xi < 1
    RSF_r1 = RSF_alpt - 1.5*(RSF_alpt - RSF_L)*(xi-1/3);
else
```

```
    RSF_r1 = RSF_L;
End

disp('   ')
disp('-------------------------------------------------------------')
disp('   ')
disp('  Recommended RSF from the first method (RSF-r1): ')
disp(RSF_r1)

%-------------------------------------------------------------------------
% Calculation of RSF_r2
%-------------------------------------------------------------------------
if xi < xi_star;
    RSF_r2 = 1 - (1-RSF_alpc)*(xi/xi_star);
elseif xi < 1
    RSF_r2 = RSF_alpc - (RSF_alpc-RSF_L)*(xi-xi_star)/(1-xi_star);
else
    RSF_r2 = RSF_L;
end
disp('  Recommended RSF from the second method (RSF-r2): ')
disp(RSF_r2)

%-------------------------------------------------------------------------
% Calculation of RSF_r3
%-------------------------------------------------------------------------
if xi < 1
    RSF_r3 = (1-RSF_L)*(xi^2 - 2*xi) + 1;
else
    RSF_r3 = RSF_L;
end
disp('  Recommended RSF from the third method (RSF-r3): ')
disp(RSF_r3)

% Output
RSF = [RSF_r1 RSF_r2 RSF_r3];
```

B.1.10. M-File for Limit Load Multipliers

```
% Calculation of m_u, m_L and m_alpha
```

```
function [All_m] = Multiplier(ShapeType, Data, mp_data, V, Vt, Vc, se, se_c)

Ri  = Data(1,1);     h    = Data(1,2);      Tc = Data(1,4);
phi_a = Data(1,6);
Ee  = mp_data(1,1);  alpe = mp_data(1,2);   s_yc = mp_data(1,3);
s_yh = mp_data(1,4);
VD  = V(1,1);        VI   = V(1,2);         VR   = V(1,3);
VDt = Vt(1,1);       VIt  = Vt(1,2);        VRt  = Vt(1,3);
VDc = Vc(1,1);       VIc  = Vc(1,2);        VRc  = Vc(1,3);

Rm = Ri + h/2;                                                    % Mean radius

% Specify yield criterion
disp('  ')
disp('-------------------------------------------------------')
disp('         CALCULATION OF LIMIT LOAD MULTIPLIERS')
disp('-------------------------------------------------------')
disp('  ')
cr = input('Please specify yield criterion (T for Tresca, V for von Mises) [V]:
', 's');
% set yield criterion to be von Mises by default
if isempty(cr)
    cr = 'V';
end

% Calculation of lowerbound multiplier based on Mura's extended variational
% principle, m_d

check = 0;
while check == 0
    % For von Mises criterion
    if (cr == 'V') || (cr == 'v')
        % For corrosion problem, corroded thickness (hc) = Data (1,5)
        if (ShapeType(2,1) == 'C') || (ShapeType(2,1) == 'c')
            hc = Data(1,5);
            m_d = sqrt((s_yc^2*VI + s_yh^2*VD)/(se^2*VR));
        else
            % For hot spot problem, set corroded thickness to shell thickness
            hc = Data(1,2);
            m_d = sqrt((s_yc^2*VR)/(se^2*VI + se_c^2*VD));
```

```
        end
        check = 1;
    % For Tresca criterion
    elseif (cr == 'T') || (cr == 't')
        % For corrosion problem, corroded thickness = Data (1,5)
        if (ShapeType(2,1) == 'C') || (ShapeType(2,1) == 'c')
            hc = Data(1,5);
            m_d = (s_yc*VI + s_yh*VD)/(se*VR);
        else
            % For hot spot problem, set corroded thickness to shell thickness
            hc = Data(1,2);
            m_d = (s_yc*VR)/(se*VI + se_c*VD);
        end
        check = 1;
    else
        disp('Invalid yield criterion.')
        cr = input ('Please re-enter yield criterion (T for Tresca, V for von
         Mises): ');
        % restart the loop, if the user specifies yield criterion other than T
         or V
    end
end

% Classical upperbound multiplier, m_u
m_u   = s_yc/se;
RSF_U = m_d/m_u;

% Classical lowerbound multiplier, m_L
if (ShapeType(2,1) == 'H') || (ShapeType(2,1) == 'h')
    m_L   = s_yh/se;
else
    m_L   = se_c/se;
end
RSF_L = m_L/m_u;

% Improved lowerbound multiplier, m-alpha
z     = m_d/m_L;
m_alp = 2*m_d*((2*z^2+sqrt(z*(z-1)^2*(1+sqrt(2)-z)*(z-1+sqrt(2))))/...
        ((z^2+2-sqrt(5))*(z^2+2+sqrt(5))));
RSF_alp = m_alp/m_u;
```

```
% Calculate m-alpha at the transition point

check = 0;
while check == 0
    % For von Mises criteria
    if (cr == 'V') || (cr == 'v')
        % calculation of m_d at the transition angle for hot spot problems
        if (ShapeType(2,1) == 'H') || (ShapeType(2,1) == 'h')
            m_dt = sqrt((s_yc^2*VIt + s_yh^2*VDt)/(se^2*VRt));
        else
            % calculation of m_d at the transition angle for corrosion problems
            m_dt = sqrt((s_yc^2*VRt)/(se^2*VIt+se_c^2*VDt));
        end
        check = 1;
    % For Tresca criteria
    elseif (cr == 'T') || (cr == 't')
        if (ShapeType(2,1) == 'H') || (ShapeType(2,1) == 'h')
            m_dt = (s_yc*VIt + s_yh*VDt)/(se*VRt);
        else
            m_dt = (s_yc*VRt)/(se*VIt + se_c*VDt);
        end
        check = 1;
    end
end

zt     = m_dt/m_L;
m_alpt = 2*m_dt*((2*zt^2+sqrt(zt*(zt-1)^2*(1+sqrt(2)-zt)*(zt-1+sqrt(2))))/...
        ((zt^2+2-sqrt(5))*(zt^2+2+sqrt(5))));
RSF_alpt = m_alpt/m_u;


% Calculate m-alpha at the threshold to dominance of membrane effect
% (phi = phi_star)
check = 0;
while check == 0
    % For von Mises criteria
    if (cr == 'V') || (cr == 'v')
        % calculation of m_d at the threshold for hot spot problems
        if (ShapeType(2,1) == 'H') || (ShapeType(2,1) == 'h')
```

```
            m_dc = sqrt((s_yc^2*VIc+s_yh^2*VDc)/(se^2*VRc));
        else
            % calculation of m_d at the threshold for corrosion problems
            m_dc = sqrt((s_yc^2*VRc)/(se^2*VIc+se_c^2*VDc));
        end
        check = 1;
    % For Tresca criteria
    elseif (cr == 'T') || (cr == 't')
        % calculation of m_d for hot spot problems
        if (ShapeType(2,1) == 'H') || (ShapeType(2,1) == 'h')
            m_dc = (s_yc*VIc + s_yh*VDc)/(se*VRc);
        else
           % calculation of m_d for corrosion problems
            m_dc = (s_yc*VRc)/(se*VIc + se_c*VDc);
        end
        check = 1;
    end
end

% Calculation of RSF_alpha at the threshold to dominance of membrane effects
zc     = m_dc/m_L;
m_alpc = 2*m_dc*((2*zc^2+sqrt(zc*(zt-1)^2*(1+sqrt(2)-zc)*(zc-1+sqrt(2))))/...
        ((zc^2+2-sqrt(5))*(zc^2+2+sqrt(5))));
RSF_alpc = m_alpc/m_u;

% Output
% RSF_U = Classical upperbound multiplier
% RSF_L = Classical lowerbound multiplier
% RSF_alp = RSF_alpha for the damaged spot
% RSF_alpt = RSF_alpha at the transition angle (1/3 of the decay angle)
% RSF_alpc = RSF_alpha at the threshold to dominance of membrane effect
All_m = [RSF_U RSF_L RSF_alp RSF_alpt RSF_alpc];
```

B.2. SAMPLES OF OUTPUT AND RESULTS FROM MATLAB FILES

Samples of the return output arguments from the MATLAB functions given in the previous section are given in this section.

B.2.1. Hot Spot in Spherical Shell

```
                    DATA INPUT

-------------------------------------------------------
   Pressure vessel Geometries
-------------------------------------------------------

Pressure vessel shape (C for cylinder, S for sphere): S
Inner Radius (in.): 21.0
Shell Thickness (in.): 0.375

-------------------------------------------------------
   Operating conditions.
-------------------------------------------------------

Design Internal Pressure (psi): 600
Operating Temperature (F): 100

-------------------------------------------------------
   Damage conditions and dimensions.
-------------------------------------------------------

Type of damaged spot (H for hot spot, C for corrosion): H
Temperature of the hot spot (F): 600
Included angle of damaged spot (degree): 10

Please check all your input data.
Is your input correct? (y,n): y
```

```
-----------------------------------------------------
           CALCULATION OF BULGE DISPLACEMENT
-----------------------------------------------------

Please enter the limit strain for bulging [default = 0.01]: 0.01
Please enter your estimate bound for bulging radius (in.) :10
and (in.): 30

Estimate bulging Radius (in.):
    10

If the calculated bulging radius is equal to your either bound, please consider
changing the bound.
Please enter your estimate bound for bulging radius (in.) :5
and (in.): 10

Estimate bulging Radius (in.):
    7.2695

Estimate bulging displacement (in.):
    0.1614

-----------------------------------------------------
         CALCULATION OF LIMIT LOAD MULTIPLIERS
-----------------------------------------------------

Please specify yield criterion (T for Tresca, V for von Mises) [V]: v

All_m =

    0.9784    0.7400    0.8664    0.8650    0.8641

RSF_alpc =

    0.8641
-----------------------------------------------------

  Recommended RSF from the first method (RSF-r1):
    0.8664
```

```
  Recommended RSF from the second method (RSF-r2):
    0.8120

  Recommended RSF from the third method (RSF-r3):
    0.8650
```

B.2.2. Corrosion in Cylindrical Shell

```
                    DATA INPUT

-----------------------------------------------------------
   Pressure vessel Geometries
-----------------------------------------------------------

Pressure vessel shape (C for cylinder, S for sphere): C
Inner Radius (in.): 21
Shell Thickness (in.): 0.625

-----------------------------------------------------------
   Operating conditions.
-----------------------------------------------------------

Design Internal Pressure (psi): 600
Operating Temperature (F): 100

-----------------------------------------------------------
   Damage conditions and dimensions.
-----------------------------------------------------------

Type of damaged spot (H for hot spot, C for corrosion): C
Remaining thickness (in.): 0.4
Size of damaged spot along the circumferential direction (in.): 15
Size of damaged spot along the axial direction (in.): 10

Please check all your input data.
Is your input correct? (y,n): y
```

```
-----------------------------------------------------------
           CALCULATION OF BULGE DISPLACEMENT
-----------------------------------------------------------

Please enter the limit strain for bulging [default = 0.01]: 0.01
Please enter your estimate bound for bulging radius (in.) :10
and (in.): 20

Estimate bulging Radius (in.):
   18.8755

Estimate bulging displacement (in.):
    0.3017

-----------------------------------------------------------
         CALCULATION OF LIMIT LOAD MULTIPLIERS
-----------------------------------------------------------

Please specify yield criterion (T for Tresca, V for von Mises) [V]: T

All_m =

    0.9687    0.5250    0.6491    0.6486    0.6455

RSF_alpc =

    0.6428
-----------------------------------------------------------

  Recommended RSF from the first method (RSF-r1):
    0.6191

  Recommended RSF from the second method (RSF-r2):
    0.6021

  Recommended RSF from the third method (RSF-r3):
    0.6473
```

B.3. EXAMPLES OF SPREADSHEET EXCEL FILES

Excel spreadsheet files for calculation of recommended RSF are provided in the CD attached to the dissertation. Sample outputs of the files are shown in this section.

B.3.1. Corrosion in Spherical Shell

Spherical shell and damaged spot properties

Inner radius (in.) =	**21.9**		Shell thickness (in.) =	**0.375**
Corroded thickness (in.) =	**0.25**			
Included angle of damaged spot (deg.) =	**30**		Operating Temperature (°F) =	**100**

R/h =	58.4				
Design pressure =	392.10	psi			
Outside radius =	22.275	in.			
lambda =	9.8231				
decay angle =	0.2399	rad	**13.74**	**degree**	
Transition angle =	0.0800	rad	4.58	degree	
Threshold to bending =	0.0611	rad	3.50	degree	
E =	29300000	psi			
σ_y =	30000	psi			
α =	5.530E-06				
σ_{ec} =	17272	psi	Classical upperbound, m_u =	2.620	
σ_{ea} =	11449	psi	Classical lowerbound, m_L =	1.737	
Limit pressure =	1100.0	psi	RSF_α at ψ_T =	0.8042	
			RSF_α at ψ_L =	0.8061	

Recommended Remaining Strength Factors

phi_a(deg)	phi_a (rad)	V_D	V_A	V_R	m_d	z	m_a	RSF_U	RSF_α	RSF_L	RSF_{r-1}	RSF_{r-2}	RSF_{r-3}
0	0.000	0.00	33.47	33.47	2.6202	1.5086	2.1210	1.0000	0.8095	0.6629	0.809	1.000	1.000
1	0.017	0.12	38.31	38.43	2.6151	1.5056	2.1201	0.9980	0.8091	0.6629	0.809	0.945	0.953
2	0.035	0.47	43.14	43.62	2.6022	1.4982	2.1176	0.9931	0.8082	0.6629	0.808	0.889	0.909
3	0.052	1.07	47.96	49.03	2.5846	1.4880	2.1141	0.9864	0.8069	0.6629	0.807	0.834	0.869
4	0.070	1.90	52.76	54.66	2.5640	1.4762	2.1099	0.9786	0.8052	0.6629	0.805	0.799	0.832
5	0.087	2.97	57.55	60.52	2.5420	1.4635	2.1051	0.9701	0.8034	0.6629	0.798	0.785	0.799
6	0.105	4.27	62.32	66.59	2.5192	1.4504	2.0998	0.9614	0.8014	0.6629	0.782	0.771	0.770
7	0.122	5.81	67.07	72.88	2.4964	1.4372	2.0943	0.9527	0.7993	0.6629	0.767	0.757	0.744
8	0.140	7.58	71.80	79.38	2.4738	1.4243	2.0885	0.9441	0.7971	0.6629	0.751	0.743	0.722
9	0.157	9.60	76.51	86.10	2.4517	1.4116	2.0827	0.9357	0.7948	0.6629	0.736	0.729	0.703
10	0.175	11.84	81.19	93.03	2.4303	1.3992	2.0767	0.9275	0.7926	0.6629	0.721	0.715	0.688
11	0.192	14.32	85.85	100.17	2.4097	1.3873	2.0707	0.9197	0.7903	0.6629	0.705	0.701	0.676
12	0.209	17.03	90.48	107.52	2.3899	1.3759	2.0647	0.9121	0.7880	0.6629	0.690	0.687	0.668
13	0.227	19.98	95.09	115.07	2.3708	1.3650	2.0588	0.9048	0.7857	0.6629	0.674	0.673	0.664
14	0.244	23.15	99.67	122.82	2.3526	1.3545	2.0529	0.8979	0.7835	0.6629	0.663	0.663	0.663
15	0.262	26.56	104.21	130.77	2.3351	1.3444	2.0471	0.8912	0.7813	0.6629	0.663	0.663	0.663
16	0.279	30.19	108.73	138.92	2.3185	1.3348	2.0414	0.8848	0.7791	0.6629	0.663	0.663	0.663
17	0.297	34.06	113.21	147.27	2.3025	1.3256	2.0358	0.8787	0.7769	0.6629	0.663	0.663	0.663
18	0.314	38.15	117.66	155.80	2.2873	1.3169	2.0303	0.8729	0.7748	0.6629	0.663	0.663	0.663
19	0.332	42.46	122.07	164.53	2.2727	1.3085	2.0249	0.8674	0.7728	0.6629	0.663	0.663	0.663
20	0.349	47.00	126.44	173.45	2.2587	1.3004	2.0196	0.8620	0.7708	0.6629	0.663	0.663	0.663
21	0.367	51.77	130.78	182.55	2.2454	1.2927	2.0145	0.8569	0.7688	0.6629	0.663	0.663	0.663
22	0.384	56.75	135.08	191.83	2.2326	1.2854	2.0094	0.8520	0.7669	0.6629	0.663	0.663	0.663
Transition angle =	**4.58**	**0.080**	**2.49**	**55.55**	**58.04**	**2.5513**	**1.4689**	**2.1072**	**0.9737**	**0.8042**	**0.6629**			
Threshold to stretching =	**3.50**	**0.061**	**1.46**	**50.38**	**51.84**	**2.5745**	**1.4822**	**2.1121**	**0.9825**	**0.8061**	**0.6629**			
15.00	**0.262**	**26.56**	**104.21**	**130.77**	**2.3351**	**1.3444**	**2.0471**	**0.8912**	**0.7813**	**0.6629**	**0.663**	**0.663**	**0.663**

Bulging calculations for spherical vessels

Assume that the bulge has a spherical shape and extends over all the damaged area

maximum permissible strain at the crown of the bulge, ε_b = 0.01

φ_a =	0.5236	radians	
δ_0 =	0.746	in.	
$r = R_o/R_b$ =	1.35221	(Choose to be greater than 1)	

Use the solver option of the spreadsheet to set the target cell identified as "equation LHS" to zero by changing the value of the cell identified with $r = R_o/R_b$

Each time the input data is changed, go to Tools >Solver and select "solve"
In the next pop-up window, select "keep solver solution" option if the result is acceptable.

equation LHS **4.86E-07** (Should be zero)

Bulge radius, R_b =	16.20	in.
Bulge included angle, φ_b =	0.3575	radians
=	20.49	degrees

Bulging displacement, δ_b = 0.2780 in.

B.3.2. Hot Spot in Cylindrical Shell

Cylindrical shell and damaged spot properties

Outer radius (in.) =	**21.0**	Shell thickness (in.) =	**0.625**
Size of damaged spot along the circumferential direction (in.) =	**15**	Aspect ratio of damaged spot (b/a) =	**1.0**
Operating Temperature (°F) =	**100**	Hot spot Temperature (°F) =	**600**

R/h =	33.1	
Design pressure =	600.00	psi
Inner radius =	20.4	in.

decay length in circumferential direction (x_c) = 22.48 in.

decay length in axial direction (x_l) = 8.92 in.

*Use the solver option of the spreadsheet to set the target cell identified as "LHS" to zero by changing the value of the cell identified with a**

Each time the input data is changed, go to Tools >Solver and select "solve"
In the next pop-up window, select "keep solver solution" option if the result is acceptable.

Threshold to bending:	LHS =	2.20E-07	x =	3.79
	a^* =	3.79	b^* =	3.79
	ξ^* =	0.2167		

Material Properties at operating temperature

E =	2.930E+07	psi
σ_y =	30000	psi
α =	5.530E-06	
σ_{el} =	25511	psi
Limit pressure =	1807.2	psi

Material Properties at hot spot temperature

E =	2.670E+07	psi
σ_y =	22200	psi
α =	7.170E-06	
Classical upperbound, m_u =	1.176	
Classical lowerbound, m_L =	0.870	
RSF_α at ψ_T =	0.8713	
RSF_α at ψ_L =	0.8725	

Recommended Remaining Strength Factors $\alpha =$ 0.75

	a (in.)	b (in.)	ξ	V_D	V_A	V_R	E_a	σ_{ya}	α_a	σ_e
	0.00	0.00	0.000	0.00	501.42	501.42	2.930E+07	30000	5.530E-06	9569
	0.50	0.50	0.048	0.63	540.67	541.29	2.930E+07	29991	5.532E-06	9577
	1.00	1.00	0.095	2.50	579.92	582.42	2.929E+07	29967	5.537E-06	9600
	1.50	1.50	0.143	5.63	619.18	624.80	2.928E+07	29930	5.545E-06	9635
	2.00	2.00	0.190	10.00	658.43	668.43	2.926E+07	29883	5.555E-06	9678
	2.50	2.50	0.238	15.63	697.68	713.31	2.924E+07	29829	5.566E-06	9728
	3.00	3.00	0.286	22.50	736.94	759.44	2.922E+07	29769	5.579E-06	9784
	3.50	3.50	0.333	30.63	776.19	806.82	2.920E+07	29704	5.592E-06	9844
	4.00	4.00	0.381	40.00	815.45	855.45	2.918E+07	29635	5.607E-06	9908
	4.50	4.50	0.428	50.63	854.70	905.33	2.915E+07	29564	5.622E-06	9974
	5.00	5.00	0.476	62.50	893.95	956.45	2.913E+07	29490	5.637E-06	10042
	5.50	5.50	0.524	75.63	933.21	1008.83	2.911E+07	29415	5.653E-06	10110
	6.00	6.00	0.571	90.00	972.46	1062.46	2.908E+07	29339	5.669E-06	10180
	6.50	6.50	0.619	105.63	1011.72	1117.34	2.905E+07	29263	5.685E-06	10250
	7.00	7.00	0.666	122.50	1050.97	1173.47	2.903E+07	29186	5.701E-06	10320
	7.50	7.50	0.714	140.63	1090.22	1230.85	2.900E+07	29109	5.717E-06	10390
	8.00	8.00	0.762	160.00	1129.48	1289.477	2.898E+07	29032	5.733E-06	10459
	8.50	8.50	0.809	180.63	1168.73	1349.36	2.895E+07	28956	5.750E-06	10528
	9.00	9.00	0.857	202.50	1207.98	1410.48	2.893E+07	28880	5.765E-06	10597
	9.50	9.50	0.904	225.63	1247.24	1472.86	2.890E+07	28805	5.781E-06	10664
	10.00	10.00	0.952	250.00	1286.49	1536.49	2.888E+07	28731	5.797E-06	10731
	10.50	10.50	0.999	275.63	1325.75	1601.37	2.885E+07	28657	5.812E-06	10797
	11.00	11.00	1.047	302.50	1365.00	1667.50	2.883E+07	28585	5.828E-06	10861
	11.50	11.50	1.095	330.63	1404.25	1734.88	2.880E+07	28514	5.843E-06	10925
	12.00	12.00	1.142	360.00	1443.51	1803.51	2.878E+07	28443	5.857E-06	10988
	12.50	12.50	1.190	390.63	1482.76	1873.39	2.876E+07	28374	5.872E-06	11049
Transition angle =	**3.22**	**3.22**	**0.306**	**25.86**	**753.92**	**779.78**	**2.921E+07**	**29741**	**5.584E-06**	**9810**
Threshold to bending =	**2.28**	**2.28**	**0.217**	**12.96**	**680.14**	**693.09**	**2.925E+07**	**29854**	**5.561E-06**	**9705**
	7.50	**7.50**	**0.71**	**140.63**	**1090.22**	**1230.85**	**2.900E+07**	**29109**	**5.717E-06**	**10390**

a (in.)	b (in.)	ξ	m_u	m_L	m_d	z	m_α	RSF_U	RSF_α	RSF_L	RSF_{r-1}	RSF_{r-2}	RSF_{r-3}
0.00	0.00	0.000	3.135	2.3200	3.1351	1.3514	2.7397	1.0000	0.8739	0.7400	0.874	1.000	1.000
0.50	0.50	0.048	3.132	2.3179	3.1315	1.3510	2.7370	0.9997	0.8738	0.7400	0.874	0.972	0.976
1.00	1.00	0.095	3.125	2.3124	3.1218	1.3500	2.7297	0.9990	0.8735	0.7400	0.874	0.944	0.953
1.50	1.50	0.143	3.114	2.3042	3.1074	1.3486	2.7189	0.9980	0.8732	0.7400	0.873	0.916	0.931
2.00	2.00	0.190	3.100	2.2939	3.0893	1.3468	2.7054	0.9966	0.8727	0.7400	0.873	0.888	0.910
2.50	2.50	0.238	3.084	2.2820	3.0685	1.3446	2.6897	0.9950	0.8722	0.7400	0.872	0.869	0.891
3.00	3.00	0.286	3.066	2.2689	3.0455	1.3423	2.6725	0.9933	0.8716	0.7400	0.872	0.861	0.873
3.50	3.50	0.333	3.047	2.2551	3.0211	1.3397	2.6542	0.9914	0.8710	0.7400	0.866	0.853	0.856
4.00	4.00	0.381	3.028	2.2406	2.9957	1.3370	2.6351	0.9894	0.8703	0.7400	0.857	0.845	0.840
4.50	4.50	0.428	3.008	2.2258	2.9696	1.3341	2.6155	0.9873	0.8696	0.7400	0.848	0.837	0.825
5.00	5.00	0.476	2.988	2.2108	2.9431	1.3312	2.5956	0.9851	0.8688	0.7400	0.839	0.829	0.811
5.50	5.50	0.524	2.967	2.1958	2.9165	1.3282	2.5756	0.9829	0.8680	0.7400	0.830	0.821	0.799
6.00	6.00	0.571	2.947	2.1807	2.8899	1.3252	2.5556	0.9807	0.8672	0.7400	0.821	0.813	0.788
6.50	6.50	0.619	2.927	2.1658	2.8636	1.3221	2.5358	0.9784	0.8664	0.7400	0.812	0.804	0.778
7.00	7.00	0.666	2.907	2.1511	2.8375	1.3191	2.5162	0.9761	0.8656	0.7400	0.803	0.796	0.769
7.50	7.50	0.714	2.887	2.1367	2.8118	1.3160	2.4969	0.9738	0.8647	0.7400	0.794	0.788	0.761
8.00	8.00	0.762	2.868	2.1225	2.7865	1.3129	2.4779	0.9715	0.8639	0.7400	0.785	0.780	0.755
8.50	8.50	0.809	2.849	2.1086	2.7618	1.3098	2.4592	0.9692	0.8631	0.7400	0.776	0.772	0.749
9.00	9.00	0.857	2.831	2.0950	2.7376	1.3067	2.4410	0.9670	0.8622	0.7400	0.767	0.764	0.745
9.50	9.50	0.904	2.813	2.0817	2.7139	1.3037	2.4231	0.9647	0.8614	0.7400	0.758	0.756	0.742
10.00	10.00	0.952	2.796	2.0688	2.6908	1.3007	2.4057	0.9625	0.8605	0.7400	0.749	0.748	0.741
10.50	10.50	0.999	2.779	2.0562	2.6683	1.2977	2.3887	0.9603	0.8597	0.7400	0.740	0.740	0.740
11.00	11.00	1.047	2.762	2.0440	2.6463	1.2947	2.3721	0.9581	0.8588	0.7400	0.740	0.740	0.740
11.50	11.50	1.095	2.746	2.0320	2.6250	1.2918	2.3560	0.9559	0.8580	0.7400	0.740	0.740	0.740
12.00	12.00	1.142	2.730	2.0205	2.6042	1.2889	2.3403	0.9538	0.8571	0.7400	0.740	0.740	0.740
12.50	12.50	1.190	2.715	2.0092	2.5839	1.2860	2.3250	0.9517	0.8563	0.7400	0.740	0.740	0.740
3.22	**3.22**	**0.306**	**3.058**	**2.2630**	**3.0351**	**1.3412**	**2.6647**	**0.9925**	**0.8713**	**0.7400**	**0.871**	**0.857**	**0.865**
2.28	**2.28**	**0.217**	**3.091**	**2.2875**	**3.0781**	**1.3456**	**2.6969**	**0.9958**	**0.8725**	**0.7400**	**0.872**	**0.872**	**0.900**

Transition angle =
Threshold to bending =

7.50	**7.50**	**0.71**	**2.887**	**2.1367**	**2.8118**	**1.3160**	**2.4969**	**0.9738**	**0.8647**	**0.7400**	**0.794**	**0.788**	**0.761**

Bulging calculations for cylindrical vessels

Assume that the bulge has a spherical shape and extends over all the damaged area

maximum permissible strain at the crown of the bulge, ε_b = 0.01

φ_a =	1.9619	radians	
δ_0 =	9.597	in.	
$r = R_o/R_b$ =	1.01832	(Choose to be greater than 1)	

Use the solver option of the spreadsheet to set the target cell identified as "equation LHS" to zero by changing the value of the cell identified with $r = R_o/R_b$

Each time the input data is changed, go to Tools >Solver and select "solve"
In the next pop-up window, select "keep solver solution" option if the result is acceptable.

equation LHS **4.95E-07** (Should be zero)

Bulge radius, R_b =	21.24	in.
Bulge included angle, φ_b =	1.0089	radians
=	57.81	degrees

Bulging displacement, δ_b = 0.3253 in.

APPENDIX C

ANSYS INPUT FILES AND COMMAND LISTING

Typical ANSYS batch files for different models used in determination of inelastic remaining strength factors of spherical and cylindrical shells containing hot spots and corrosion damages as discussed in Chapter 5 are provided in this section. ANSYS 9.0 is the version used for the analysis. The electronic versions of the files are included in the CD attached with the dissertation.

C.1. INPUT AND MACROS FOR SPHERICAL SHELLS

Two models are used in nonlinear finite element analysis for spherical shells with damages. The first model uses an 8-node plane element (PLANE82) for an axisymmetric problem. The other model is for a quarter of a complete sphere by using an 8-node shell element (SHELL91 for hot spot problems and SHELL93 for corrosion). The results from the axisymmetric and shell models are shown to be comparable. The PLANE82 model requires less computational time and hence is favorable when appropriate. Typical ANSYS batch files for the two models are listed below. As mentioned in the main thesis,

no thermal analysis is included in the hot spot problem. The temperature of the damaged and undamaged zones is assumed and the appropriate material properties are input in the present analysis.

C.1.1. Axisymmetric Model for Hot Spot Damage in Spherical Shells

```
/COM, HOT SPOT IN SPHERICAL SHELL

! Sphere dimensions (in.)

*SET, Ri, 21.9                          ! Inner radius
*SET, R_h, 58.9                         ! R/h ratio
*SET, h, Ri/R_h                         ! Shell thickness
*SET, Ro, Ri+h                          ! Outer radius

! Damaged spot dimensions

*SET, PI, 3.14159265359

*SET, phia, 7/180*pi                    ! Half of included angle (measure from y axis) (rad)
*SET, a, phia*Ro                        ! Half arc length at the outside surface

*SET, rai, Ro*sin(phia)
*SET, s, Ri*cos(phia)

! Applied internal pressure (psi)

*SET, P, 1000

! Number of element divisions

*SET, hsp_div, 150                      ! Inside the hot spot
*SET, top_div, 400                      ! The rest of the top part of the sphere
*SET, bot_div , 150                     ! The bottom part of the sphere


! --- P R E P R O C E S S O R ---
/PREP7                                  ! Enter Preprocessor
/TITLE, Spherical shell, hot spot, axisymmetric
/UNITS, BIN

! NOTE: For each analysis change : phia and choose the proper MP

! --M O D E L I N G--

CSYS,2                                  ! Spherical coordinate system

! Create keypoints
```

```
K, 1, 0, 0, 0
K, 2, Ri, 0, 0
K, 3, Ri+h, 0, 0

K,12, Ri,  -90, 0
K,13, Ri+h, -90, 0

K,22, Ri, 90-phia*180/PI, 0

K,23, Ri+h, 90-phia*180/PI,0

K,32, Ri, 90, 0
K,33, Ri+h, 90, 0

! Create lines
LARC,12, 2, 1, Ri                    ! Arc line 1 to 6
LARC,13, 3, 1, Ri+h
LARC, 2,22, 1, Ri
LARC, 3,23, 1, Ri+h
LARC,22,32, 1, Ri
LARC,23,33, 1, Ri+h

L,2,3                                ! Line 7 to 10
L,12,13
L,22,23
L,32,33

! Create areas from lines
AL,10,5,9,6                          ! Area 1 to 3
AL, 9,3,4,7
AL, 7,1,8,2

! --E L E M E N T   D I V I S I O N --

LSEL,S,line,,1,2
LESIZE,ALL,,,bot_div

LSEL,S,line,,3,4
LESIZE,ALL,,,top_div,0.35

LSEL,S,line,,5,6
LESIZE,ALL,,,hsp_div

LSEL,S,line,,7,8
LESIZE,ALL,,,4

LSEL,S,line,,9,10
LESIZE,ALL,,,10

! -- E L E M E N T   A N D   M A T E R I A L   P R O P E R T I E S--

ET,1,PLANE82,,,1                     ! Use PLANE82 element for axisymmetric model

! Properties for hot region
```

```
! Material type 1

! Properties at temperature 600 deg.F
!MP,EX,1,26.7E6                  ! Young's modulus
!MP,PRXY,1,0.3                   ! Poisson's ratio
!TB,BKIN,1,,,1                   ! Bilinear kinematic strain hardening

!TBDATA,,22182,2E3               ! Table data: Yield point and plastic modulus

! Properties at temperature 400 deg.F
!MP,EX,1,27.7E6
!MP,PRXY,1,0.3
!TB,BKIN,1,,,1
!TBDATA,,25682,2E3


! Properties at temperature 200 deg.F
MP,EX,1,28.8E6
MP,PRXY,1,0.3
TB,BKIN,1,,,1
TBDATA,,27282,2E3

! Meshing the hot spot
TYPE,1
MAT,1
ASEL,S,AREA,,1
AMESH,ALL

! Properties at temperature 100 deg F (cold region)
! Material type 2

MP,EX,2,29.3E6
MP,PRXY,2,0.3
TB,BKIN,2,,,1
TBDATA,,29982,2E3

! Meshing the rest of the sphere
TYPE,1
MAT,2
ASEL,S,AREA,,2,3
AMESH,ALL

ASEL,ALL

CSYS,0

! Boundary Conditions

NSEL,S,LOC,X,Ri
NSEL,R,LOC,Y,0
D,ALL,UY,0
NSEL,ALL

CHECK
```

```
FINISH                                  ! Exit Preprocessor

! -- S O L  U T I  O N  M O D U L E--

/SOLU                                   ! Enter Solution module

LSEL,S,line,,1,5,2                      ! Apply uniform internal pressure
SFL,ALL,PRES,P
LSEL,ALL
SFTRAN                                  ! Transfer surface load to the FE model

ANTYPE,STATIC                           ! Static Analysis
SOLCONTROL,ON                           ! Nonlinear analysis
AUTOT,ON                                ! Automatic time stepping
NSUBST,200                              !Initial number of substeps
OUTRES,ALL,ALL

SOLVE
SAVE                                    ! Save Database
FINISH                                  ! Exit Solution Routine

! -- P O S T  P R O C E S S O R  M O D U L E --

/POST1                                  ! Enter post processor
RSYS,2                                  ! Spherical coordinate
PLESOL,EPTO,EQV                         ! Plot element solution, von Mises strain
*GET,bulge_strain,node,2,epto,eqv       ! Obtain bulging strain at the crown of the sphere

EXIT
```

C.1.2. Axisymmetric Model for Internal Corrosion in Spherical Shells

```
/COM, INTERNAL CORROSION IN SPHERICAL SHELL

! Sphere dimensions (in.)

*SET, Ri, 21.9                          ! Inner radius
*SET, h, 3/8                            ! Original shell thickness
*SET, Ro, Ri+h                          ! Outer radius

! Damaged spot dimensions

*SET, c , h/2                           ! Corrosion depth
*SET, hc, h-c                           ! Corroded thickness

*SET, phia, 10/180*pi                   ! Half of included angle (measure from y axis) (rad)
*SET, a, phia*Ro                        ! Half arc length at the outside surface

*SET, rai, Ro*sin(phia)
```

```
*SET, s, Ri*cos(phia)

! Applied internal pressure (psi)

*SET, P, 1000

! Number of element divisions

*SET, hsp_div, 100                    ! Inside the damaged spot
*SET, top_div, 400                    ! The rest of the upper part of the sphere
*SET, bot_div , 150                   ! The bottom part of the sphere

*SET, PI, 3.14159265359


! -- P R E P R O C E S S O R   M O D U L E -

/PREP7                                ! Enter Preprocessor
/TITLE, Spherical shell, internal corrosion, axisymmetric
/UNITS, BINS

! NOTE:for each case, change : corrosion depth (c) and included angle of damaged spot (phia)

! -- M O D E L I N G --

CSYS,2                                ! Spherical coordinate system

! Create keypoints

K, 1,  0, 0, 0
K, 2, Ri, 0, 0
K, 3, Ri+c,  0, 0
K, 4, Ri+h, 0, 0

K,12, Ri,  -90, 0
K,13, Ri+c, -90, 0
K,14, Ri+h, -90, 0

K,22, Ri, 90-phia*180/PI, 0
K,23, Ri+c, 90-phia*180/PI, 0
K,24, Ri+h, 90-phia*180/PI,  0

K,33, Ri+c, 90, 0
K,34, Ri+h, 90, 0

! Create lines by keypoints

LARC,12, 2, 1, Ri                     ! Arc line 1 to 3
LARC,13, 3, 1, Ri+c
LARC,14, 4, 1, Ri+h

LARC, 2,22, 1, Ri                     ! Arc line 4 to 6
LARC, 3,23, 1, Ri+c
LARC, 4,24, 1, Ri+h
```

```
LARC,23,33, 1, Ri+c                    ! Arc line 7 to 8
LARC,24,34, 1, Ri+h

L,2,3                                  ! Line 9 to 15
L,3,4
L,12,13
L,13,14
L,22,23
L,23,24
L,33,34

! Create fillet inside the corroded spot
LFILLT,7,13,0.1.0
LDIV,16,0.5
L,23,7

! Create areas by lines
AL,1,11,2,9                            ! Area 1

AL,2,12,3,10                           ! Area 2 to 5
AL,4,9,5,18,17,13
AL,5,10,6,14
AL,7,16,18,14,8,15

! --E L E M E N T   D I V I S I O N S --

LSEL,ALL

LSEL,S,line,,1,3
LESIZE,ALL,,,bot_div

LSEL,S,line,,4,6
LESIZE,ALL,,,top_div,0.35

LSEL,S,line,,7,8
LESIZE,ALL,,,hsp_div

LSEL,S,line,,10
LSEL,A,line,,12,13
LESIZE,ALL,,,4

LSEL,S,line,,16,18
LESIZE,ALL,,,2

LSEL,S,line,,9
LSEL,A,line,,11
LESIZE,ALL,,,4

LSEL,S,line,,14
LESIZE,ALL,,,8

LSEL,S,line,,15
LESIZE,ALL,,,8
```

```
LSEL,ALL

! --E L E M E N T  A N D  M A T E R I A L  P R O P E R T I E S --

! Element type 1
ET,1,PLANE82,,,1                    ! Plane 82

! Material type 1, Properties at temperature 100 F
MP,EX,1,29.3E6                      ! Young's modulus
MP,PRXY,1,0.3                       ! Poisson's ratio
TB,BKIN,1,,,1                       ! Bilinear kinematic hardening
TBDATA,,30E3,2E4                    ! Yield point = 30E3, Platic modulus = 50E4

! Meshing
ASEL,ALL
AMESH,ALL

CSYS,0                              ! Cartesian coordinate system

! Boundary Conditions

NSEL,S,LOC,X,Ri
NSEL,R,LOC,Y,0
D,ALL,UY,0
NSEL,ALL

CHECK
FINISH                              ! Exit Preprocessor!


! --S O L U T I O N  M O D U L E --

/SOLU                               ! Enter solution routine

LSEL,S,line,,1,7,3
SFL,ALL,PRES,P                      ! Apply internal pressure
LSEL,ALL
SFTRAN

ANTYPE,STATIC                       ! Static analysis
SOLCONTROL,ON                       ! Nonlinear analysis
AUTOT,ON                            ! Automatic time stepping
NSUBST,200                          ! Initial number of substep
OUTRES,ALL,ALL                      ! Basic output

SOLVE
SAVE                                ! Save Database
FINISH                              ! Exit Solution Routine


! --P O S T  P R O C E S S O R --

/POST1                              ! Enter postprocessor
RSYS,2                              ! Spherical coordinate system
```

```
PLESOL,EPTO,EQV                 ! Plot element solution, equivalent strain
*GET,bulge_strain,node,2,epto,eqv   ! Obtain bulging strain at the crown

EXIT
```

C.1.3. Axisymmetric Model for External Corrosion in Spherical Shells

```
/COM, EXTERNAL CORROSION IN SPHERICAL SHELL

! Sphere dimensions (in.)

*SET, Ri, 21.9                  ! Inner radius
*SET, h, 3/8                    ! Original shell thickness
*SET, Ro, Ri+h                  ! Outer radius

! Damaged spot dimensions

*SET, c , h/2                   ! Corrosion depth
*SET, hc, h-c                   ! Corroded thickness

*SET, phia, 10/180*pi           ! Half of included angle (measure from y axis) (rad)
*SET, a, phia*Ro                ! Half arc length at the outside surface

*SET, rai, Ro*sin(phia)
*SET, s, Ri*cos(phia)

! Applied internal pressure (psi)

*SET, P, 1000

! Number of element divisions

*SET, hsp_div, 100              ! Inside the damaged spot
*SET, top_div, 400              ! The rest of the upper part of the sphere
*SET, bot_div , 150             ! The bottom part of the sphere

*SET, PI, 3.14159265359


! --- P R E P R O C E S S O R   M O D U L E ---
/PREP7                          ! Enter preprocessor
/TITLE, Spherical shell, external corrosion, axisymmetric
/UNITS, BINS

! NOTE:for each case, change : corrosion depth (c) and included angle of damaged spot (phia)

! ---M O D E L L I N G ---

CSYS,2                          ! Spherical coordinate system

! Create keypoints
```

```
K, 1,  0, 0, 0
K, 2, Ri, 0, 0
K, 3, Ri+hc, 0, 0
K, 4, Ri+h, 0, 0

K,12, Ri, -90, 0
K,13, Ri+hc, -90, 0
K,14, Ri+h, -90, 0

K,22, Ri, 90-phia*180/PI, 0
K,23, Ri+hc, 90-phia*180/PI, 0
K,24, Ri+h,  90-phia*180/PI,       0

K,32, Ri,  90, 0
K,33, Ri+hc, 90, 0

! Create lines by keypoints

LARC,12, 2, 1, Ri                       ! Arc line 1 to 3
LARC,13, 3, 1, Ri+hc
LARC,14, 4, 1, Ri+h

LARC, 2,22, 1, Ri                       ! Arc line 4 to 6
LARC, 3,23, 1, Ri+hc
LARC, 4,24, 1, Ri+h

LARC,23,33, 1, Ri+hc                    ! Arc line 7 to 8
LARC,24,34, 1, Ri+h

L,2,3                                   ! Line 9 to 15
L,3,4
L,12,13
L,13,14
L,22,23
L,23,24
L,32,33

! Create fillet inside the corroded spot
LFILLT,8,14,0.1.0
LDIV,16,0.5
L,23,7

! Create areas by lines
AL,1,11,2,9                             ! Area 1 to 5
AL,2,12,3,10                            !
AL,5,10,6,14,17,18
AL,13,4,9,5
AL,7,13,18,16,8,15

! ---E L E M E N T   D I V I S I O N S ---

LSEL,ALL

LSEL,S,line,,1,3
```

```
LESIZE,ALL,,,bot_div

LSEL,S,line,,4,6
LESIZE,ALL,,,top_div,0.3

LSEL,S,line,,7,8
LESIZE,ALL,,,hsp_div

LSEL,S,line,,10
LSEL,A,line,,12,14,2
LESIZE,ALL,,,4

LSEL,S,line,,16,18
LESIZE,ALL,,,2

LSEL,S,line,,9
LSEL,A,line,,11
LESIZE,ALL,,,4

LSEL,S,line,,12,15,2
LESIZE,ALL,,,12
LSEL,ALL

!--- E L E M E N T  A N D  M A T E R I A L  P R O P E R T I E S ---

! Element type 1
ET,1,PLANE82,,,1                    ! Plane 82

! Material type 1, Properties at temperature 100 F
MP,EX,1,29.3E6                      ! Young's modulus
MP,PRXY,1,0.3                       ! Poisson's ratio
TB,BKIN,1,,,1                       ! Bilinear kinematic hardening
TBDATA,,30E3,2E4                    ! Yield point = 30E3, Platic modulus = 50E4

! Meshing
ASEL,ALL
AMESH,ALL

CSYS,0                              ! Cartesian coordinate system

! Boundary Conditions

NSEL,S,LOC,X,Ri
NSEL,R,LOC,Y,0
D,ALL,UY,0
NSEL,ALL

CHECK
FINISH                              ! Exit preprocessor


!--- S O L U T I O N  M O D U L E ---

/SOLU                               ! Enter solution routine
```

```
LSEL,S,line,,1,7,3
SFL,ALL,PRES,P                  ! Apply internal pressure
LSEL,ALL
SFTRAN                          ! Transfer surface load to FE model

ANTYPE,STATIC
SOLCONTROL,ON                   ! Nonlinear analysis
AUTOT,ON                        ! Automatic time stepping
NSUBST,200
OUTRES,ALL,ALL                  ! Obtain all output results

SOLVE
SAVE                            ! Save database
FINISH                          ! Exit solution routine


!--- P O S T P R O C E S S O R   M O D U L E ---

/POST1                          ! Enter postprocessor
RSYS,2                          ! Spherical coordinate system
PLESOL,EPTO,EQV                 ! Plot element solution, equivalent strain
*GET,bulge_strain,node,2,epto,eqv   ! Obtain bulging strain at the crown

EXIT
```

C.1.4. Shell Element Model for Hot Spot Damage in Spherical Shells

```
/COM, HOT SPOT IN SPHERICAL SHELL

! Sphere dimensions (in.)

*SET, Ri, 21.9                  ! Inner radius
*SET, Ro, 22.275                ! Outside radius (case 1 R/h = 58.4)
!*SET, Ro, 22.995               ! Outside radiuis (case 2 R/h = 20)
*SET,  h, Ro - Ri               ! Shell thickness
*SET, Rm, (Ri+Ro)/2             ! Mean radius

! Damaged spot dimensions

*SET, phia, 10/180*pi           ! Half of included angle (measure from y axis) (rad)
*SET, a, phia*Ro                ! Half arc length at the outside surface

*SET, rai, Ro*sin(phia)
*SET, s, Ri*cos(phia)

! Applied internal pressure (psi)

*SET, P, 1000

! Number of element divisions
```

```
*SET, hsp_div, 14                    ! Inside the hot spot along y axis
*SET, hspa_div, 14                   ! Inside the hot spot along the arclength
*SET, hor_div, 40                    ! Along the equator of the sphere
*SET, ver_div , 150                  ! Along the rest of the upper part of the sphere

*SET, PI, 3.14159265359


! --- P R E P R O C E S S O R ---
/PREP7
/TITLE, Spherical shell, hot spot , Shell model
/UNITS, BIN

! NOTE: Change: hot spot size (phia) and choose the proper material properties (MP)

! ---M O D E L I N G ---

CSYS,2                               ! Spherical coordinate system

! Create keypoints

K, 1,  0, 0, 0
K, 2, Rm, 0, 90
K, 3, Rm, 0, 0
K, 4, Rm, 90, 0
K, 5, Rm, -90, 0

K, 6, Rm, 90, phia*180/PI
K, 7, Rm, 90-phia*180/PI, 0

K, 8, Rm*cos(phia),   90, 0

! Create lines by keypoints

LARC, 2, 3, 1, Rm                    ! Arc lines 1 to 8
LARC, 3, 7, 1, Rm
LARC, 7, 4, 1, Rm
LARC, 4, 6, 1, Rm
LARC, 6, 2, 1, Rm
LARC, 2, 5, 1, Rm
LARC, 5, 3, 1, Rm
LARC, 6, 7, 8, Rm*sin(phia)

! Create areas by lines
AL, 3, 4, 8                          ! Area 1 (hot spot area)
AL, 1, 2, 8,5                        ! Area 2 and 3 (cold region)
AL, 7, 1, 6


! ---- E L E M E N T   D I V I S I O N ---

LSEL,S,LINE,, 1                      ! Select lines by line number,, vmin,vmax,vinc
LSEL,A,LINE,, 6, 7
```

```
LESIZE,ALL,,,hor_div                ! Number of element divisions

LSEL,S,LINE,,2
LSEL,A,LINE,,5
LESIZE,ALL,,,ver_div

LSEL,S,LINE,, 3, 4
LESIZE,ALL,,,hspv_div

LSEL,S,LINE,, 8
LESIZE,ALL,,,hspa_div

LSEL,ALL

! ----E L E M E N T   A N D   M A T E R I A L   T Y P E S ---

! Element type 1
ET,1,SHELL93                        ! Shell93
R,1,h                               ! Real constant set no. 1, thickness
KEYOPT,1,8,2

! Material properties for hot region
! At temperature 600 deg.F
!MP,EX,1,26.7E6                     ! Young's modulus
!MP,PRXY,1,0.3                      ! Poisson ratio
!TB,BKIN,1,,,1                      ! Bilinear kinematic strain hardening
!TBDATA,,22182,2E3                  ! Data table, Yield point, Plastic modulus

! At temperature 400 deg.F
MP,EX,1,27.7E6
MP,PRXY,1,0.3
TB,BKIN,1,,,1
TBDATA,,25682,2E3

! At temperature 200 deg.F
!MP,EX,1,28.8E6
!MP,PRXY,1,0.3
!TB,BKIN,1,,,1
!TBDATA,,27282,2E3

! Mesh the hot spot  area
TYPE,1
MAT,1
ASEL,S,AREA,,1
AMESH,ALL

! Material properties for cold region
! At design temperature 100 deg.F, Material type 2
MP,EX,2,29.3E6                      ! Young's modulus
MP,PRXY,2,0.3                       ! Poisson ratio
TB,BKIN,2,,,1                       ! Bilinear kinematic strain hardening
TBDATA,,29982,2E3                   ! Data table, Yield point, Plastic modulus

! Mesh the rest of the sphere
```

```
TYPE,1                          ! Element type
MAT,2                           ! Material type
ASEL,S,AREA,,2,3                ! Select cold region
AMESH,ALL

ASEL,ALL

CSYS,0                          ! Cartesian coordinate system

! Boundary Conditions

NSEL,S,LOC,Z,0
DSYM,SYMM,Z,0                   ! Symmetry along Z = 0 (create a quarter of the model)

NSEL,S,LOC,X,0
DSYM,SYMM,X,0                   ! Symmetry along X = 0

NSEL,S,LOC,X,0                  ! Constrain the bottom node
NSEL,R,LOC,Z,0
NSEL,R,LOC,Y,-Rm
D,ALL,UY,0

NSEL,ALL

CHECK
FINISH                          ! Exit preprocessor


!--- S O L U T I O N   M O D U L E ---

/SOLU                           ! Enter solution module

ASEL,S,AREA,,1,3
SFA,ALL,,PRES,1000              ! Apply internal pressure
SFTRAN                          ! Transfer surface load to the FE model

ANTYPE,STATIC
SOLCONTROL,ON                   ! Nonlinear analysis
AUTOTS,ON                       ! Automatic time stepping
NSUBST,100                      ! Initial number of substep
OUTRES,ALL,ALL                  ! Obtain all output results

SOLVE
SAVE                            ! Save database
FINISH                          ! Exit solution routine


! ---- P O S T P R O C E S S O R   M O D U L E ---

/POST1                          ! Enter postprocessor
RSYS,2                          ! Obtain results using global spherical coordinate system

SHELL,TOP                       ! Read results at the top of the shell
*GET,bulge_strain,node,2,epto,eqv  ! Get strain at the crown (node 2)
```

```
SHELL,MID                          ! Read results at the middle of the shell
*GET,bulge_strain,node,2,epto,eqv  ! Get strain at the crown
SHELL,BOT                          ! Read results at the bottom of the shell
*GET,bulge_strain,node,2,epto,eqv  ! Get strain at the crown

SHELL,MID
*GET,disp,node,2,U,X               ! Get displacement at node 2

!Read results along a defined path
!PATH,P1,59
!PPATH,P

!PDEF,UX,U,X
!PDEF,EPTOEQV,EPTO,EQV
!PLPATH,UX
!PLPATH,EPTOEQV

!PSEL,S,P1                         ! Select path
!PASAVE,ALL,patha                  ! Store path in a file name 'patha'
!PARESU,ALL,patha                  ! Retrieve path

EXIT
```

C.1.5. Shell Element Model for Internal Corrosion in Spherical Shelsl

```
/COM, INTERNAL CORROSION IN SPHERICAL SHELL

! Sphere dimensions (in.)

*SET, Ri, 21.9                    ! Inner radius
*SET, Ro, 22.275                  ! Outer radius for R/h = 58.4
!*SET, Ro, 22.995                 ! Outer radius for R/h = 20

*SET, h,Ro-Ri                     ! Original shell thickness
*SET, Ro, Ri+h                    ! Outer radius

! Damaged spot dimensions

*SET, c , h/3                     ! Corrosion depth
*SET, hc, h-c                     ! Corroded thickness

*SET, phia, 8/180*pi              ! Half of included angle (measure from y axis) (rad)
*SET, a, phia*Ro                  ! Half arc length at the outside surface

*SET, rai, Ro*sin(phia)
*SET, s, Ri*cos(phia)

! Applied internal pressure (psi)

*SET, P, 1000
```

```
! Number of element divisions

*SET, hsp_div, 50                    ! Inside the corrodedt spot along y axis
*SET, hspa_div, 50                   ! Inside the corroded spot along the arclength
*SET, hor_div, 50                    ! Along the equator of the sphere
*SET, ver_div , 120                  ! Along the rest of the upper part of the sphere


*SET, PI, 3.14159265359


! --- P R E P R O C E S S O R  M O D U L E ---

/PREP7                               ! Enter preprocessor
/TITLE, Spherical shell, internal corrosion, Shell model
/UNITS, BIN

! ---M O D E L L I N G  A  Q U A R T E R  O F  T H E  S P H E R E ---

CSYS,2                               ! Spherical coordinate system

! Create keypoint in the current CS
K, 1,  0, 0, 0
K, 2, Ro, 0, 90
K, 3, Ro, 0, 0
K, 4, Ro, 90, 0
K, 5, Ro, -90, 0
K, 6, Ro, 90, phia*180/PI

K, 7, Ro, 90-phia*180/PI, 0

K, 8, Ro*cos(phia),   90, 0

! Create lines by keypoints

LARC, 2, 3, 1, Ro                    ! Arc lines 1 to 8
LARC, 7, 3, 1, Ro
LARC, 7, 4, 1, Ro
LARC, 4, 6, 1, Ro
LARC, 6, 2, 1, Ro
LARC, 2, 5, 1, Ro
LARC, 5, 3, 1, Ro
LARC, 6, 7, 8, Ro*sin(phia)

! Create areas by lines
AL, 3, 4, 8                          ! Areas 1 to 3
AL, 1, 2, 8,5
AL, 7, 1, 6

! --- E L E M E N T  D I V I S I O N S ---

LSEL,S,LINE,, 1                      !Select line, line number,,,vmin,vmax,vinc
LSEL,A,LINE,, 6, 7                   ! Select additional lines
```

```
LESIZE,ALL,,,hor_div                ! Element size control, by line

LSEL,S,LINE,,2
LSEL,A,LINE,,5
LESIZE,ALL,,,ver_div,5

LSEL,S,LINE,, 3, 4
LESIZE,ALL,,,hspv_div

LSEL,S,LINE,, 8
LESIZE,ALL,,,hspa_div

LSEL,ALL

!--E L E M E N T  A N D  M A T E R I A L  T Y P E S  ( A T  T E M P E R A T U R E  1 0 0  F )--

! Inside the corroded spot
MP,EX,1,29.3E6                      ! Young's modulus
MP,PRXY,1,0.3                       ! Poisson ratio
TB,BKIN,1,,,1                       ! Bilinear kinematic Hardening
TBDATA,,30E3,2 E4                   ! Yield point = 30E3, Platic modulus = 2E4


ET,1,SHELL91,10,1,,,1               ! SHELL91, Maximum no. of layers = 3
KEYOPT,1,11,2                       ! Nodes located at top surface

R,1,10                              ! Real constant, number of layers
RMORE
RMORE,1,,hc/3                       ! Material number and thickness for layer 1 (bottom)
RMORE,1,,hc/3                       ! Material number and thickness for layer 2 (middle)
RMORE,1,,hc/3                       ! Material number and thickness for layer 3 (top)

! Mesh the corroded spot
TYPE,1                              ! Element type 1
REAL,1                              ! Real constant set no. 1
ASEL,S,AREA,,1                      ! Mesh area 1
AMESH,ALL

! Element type 2
ET,2,SHELL91,16,1,,,1               ! Maximum =  6 layers
KEYOPT,2,11,2                       ! Nodes located at top surface

R,2,6                               ! Number of layers, 6
RMORE
RMORE,1,,c/3                        ! material number and thickness for layer 1 (bottom)
RMORE,1,,c/3                        ! material number and thickness for layer 2
RMORE,1,,c/3
RMORE,1,,hc/3
RMORE,1,,hc/3
RMORE,1,,hc/3                       ! Material number and thickness for layer 6 (top)

! Mesh the rest of the sphere
```

```
TYPE,2                          ! Element type 2
REAL,2                          ! Real constant set no. 2
ASEL,S,AREA,,2,3                ! Mesh area 2 and 3
AMESH,ALL

CSYS,0

! Boundary Conditions

NSEL,S,LOC,Z,0                  ! Symmetry along Z = 0
DSYM,SYMM,Z,0

NSEL,S,LOC,X,0                  ! Symmetry along X = 0
DSYM,SYMM,X,0

NSEL,S,LOC,X,0                  ! Constrain the bottom node
NSEL,R,LOC,Z,0
NSEL,R,LOC,Y,-Ro
D,ALL,UY,0

NSEL,ALL

CHECK
FINISH                          !Exit preprocessor


! ---S O L U T I O N   M O D U L E ---

/SOLU                           ! Enter solution module

ASEL,S,AREA,,1,3                ! Apply internal pressure to areas 1 to 3
SFA,ALL,,PRES,P                 ! Internal pressure = P
SFTRAN                          ! Transfer surface loading to FE models

ANTYPE,STATIC                   ! Static analysis
SOLCONTROL,ON                   ! Nonlinear analysis
AUTOT,ON                        ! Automatic time stepping
NSUBST,300                      ! Initial number of substep

OUTRES,ALL,ALL                  ! Obtain all output results
SOLVE
SAVE                            ! Save database
FINISH                          ! Exit solution routine

EXIT
```

C.2. INPUT AND MACROS FOR CYLINDRICAL SHELLS

Nonlinear finite element analysis for cylindrical shells with damages is executed by using shell element (SHELL91 for hot spot and SHELL93 for corrosion) and solid element (SOLID185) modeling as explained in Chapter 5. Examples of typical macro for such models are listed below.

C.2.1. Shell Element Model for Hot Spot Damage in Cylindrical Shells

```
/COM, HOT SPOT IN CYLINDRICAL SHELL

! Cylinder dimensions
*SET, Ro, 21                          ! Outer radius
*SET, Ri, 20.375                      ! Inner radius
*SET, len,200                         ! Length of the cylinder

*SET, h, Ro-Ri                        ! Shell thickness
*SET, Rm, (Ro+Ri)/2                   ! Mean radius

*SET, pi, 3.141592654

! Applied internal pressure
*SET, P,  900

! Number of element divisions

*SET, bhsp_div, 20                    ! Along axial direction of the hot spot
*SET, ahsp_div , 20                   ! Along circumferential direction of the hot spot
*SET, r1_div, 25                      ! For the rest of the upper part of the cylinder
*SET, r2_div, 20                      ! For the bottom part of the cylinder
*SET, r3_div, 30                      ! For lines along circumference (half of the cylinder)
*SET, lon_div, 30                     ! Along half the total length of the cylinder
*SET, lon_div2, 25                    ! Along the rest of the Z axis exclude the hot spot

! Damaged spot dimension
*SET, a_hsp,15                        ! Half the width of the hot spot along the circumference
*SET, b_hsp, 15                       ! Half the width of the hot spot along the axial direction
*SET, theta_hsp , (a_hsp/Ro)*(180/pi)


! --- P R E P R O C E S S O R ---

/PREP7                                ! Enter preprocessor
!/TITLE, Cylindrical shell, Shell 93, hot spot
```

```
/UNITS,BIN

! --- M O D E L I N G ---

CSYS,0                                  ! Cartesian coordinate system

! Create keypoints

K,  1,  0,  0, 0                        ! Keypoints on Z=0 plane (inner radius)
K,  2, Rm,  0, 0
K,  3,  0, Rm, 0
K,  4,-Rm,  0, 0

K,  6,  0,  0,b_hsp                     ! Keypoint  6 at the center at Z = b_hsp
K,  7, Rm,  0,b_hsp
K,  8,  0, Rm,b_hsp
K,  9,-Rm,  0,b_hsp

K, 11,  0,  0,len                       ! Keypoint 11 at the center at z = len
K, 12, Rm,  0,len
K, 13,  0, Rm,len
K, 14,-Rm,  0,len

K, 16,  0,  0,len+Rm

CSYS,1                                  ! Cylindrical CS with Z as the axis of rotation
K,  5, Rm,theta_hsp,0
K, 10, Rm,theta_hsp,b_hsp
K, 15, Rm,theta_hsp,len
K,18,Rm*cos(theta_hsp/180*pi),0,len

CSYS,0                                  ! Cartesian coordinate system

! Creates lines by keypoints
LARC,2,5,1,Rm                           ! Arcline 1 to 3 at Z = 0
LARC,5,3,1,Rm
LARC,3,4,1,Rm

LARC, 7,10,6,Rm                         ! Arcline 4 to 6 at Z = b_hsp
LARC,10, 8,6,Rm
LARC, 8, 9,6,Rm

LARC,12,15,11,Rm                         ! Arcline 7 to 9 at Z = len
LARC,15,13,11,Rm
LARC,13,14,11,Rm

L, 2, 7                                 ! Line 10 to 13 from Z = 0 to b_hsp
L, 5,10
L, 3, 8
L, 4, 9

L, 7,12                                 ! Line 14 to 17 from Z = b_hsp to len
L,10,15
L, 8,13
```

```
L, 9,14

! Create areas by lines
CSYS,1                                  ! Cylindrical coordinate system
AL, 1,11, 4,10                          ! Area 1 to 6
AL, 2,12, 5,11
AL, 3,13, 6,12
AL, 4,15, 7,14
AL, 5,16, 8,15
AL, 6,17, 9,16

CSKP,11,2,11,12,13                      !Local CS - spherical CS - origin at KP 11
K,17,Rm,0,theta_hsp

LARC,14,16,11,Rm                        ! Lines for spherical head (line 18 to 22)
LARC,16,17,11,Rm
LARC,17,12,11,Rm
LARC,13,16,11,Rm
LARC,15,17,18,Rm*sin(theta_hsp/180*pi)

AL,20, 7,22                             ! Areas for spherical head (area 7 to 9)
AL,19,22, 8,21
AL,18,21, 9

CSYS,0

!--- E L E M E N T   D I V I S I O N ---

LSEL,S,LINE,, 1, 7,3                    !Select line by line no - vmin,vmax,vinc
LESIZE,ALL,,,ahsp_div

LSEL,S,LINE,,10,11,1
LESIZE,ALL,,,bhsp_div

LSEL,S,LINE,, 2, 8,3
LESIZE,ALL,,,r1_div,3

LSEL,S,LINE,,14,17,1
LESIZE,ALL,,,lon_div,4

LSEL,ALL

! --- E L E M E N T   A N D   M A T E R I A L   T Y P E S---

! Element type 1
ET,1,SHELL93                            ! SHELL93
R,1,h                                   ! Real constant, shell thickness
KEYOPT,1,8,2

! Material properties at temperature  600 deg.F
MP,EX,1,26.7E6                          ! Young's modulus
MP,PRXY,1,0.3                           ! Poisson's ratio
TB,BKIN,1,,,1                           ! Rice's Hardening
TBDATA,,22182,2E3                       ! Yield point and plastic modulus
```

```
! Material properties at temperature  400 deg.F
!MP,EX,1,27.7E6
!MP,PRXY,1,0.3
!TB,BKIN,1,,,1
!TBDATA,,25682,2E3

! Material properties at temperature  200 deg.F
!MP,EX,1,28.8E6
!MP,PRXY,1,0.3
!TB,BKIN,1,,,1
!TBDATA,,27282,2E3

! Meshing the hot region
TYPE,1                          ! Select element type
MAT,1                           ! Select material type
ASEL,S,AREA,,1                  ! Mesh area 1
AMESH,ALL

! Material properties at temperature  100 deg.F
MP,EX,2,29.3E6
MP,PRXY,2,0.3
TB,BKIN,2,,,1
TBDATA,,29982,2E3

MAT,2                           ! Select material type 2
ASEL,S,AREA,,7,9                ! Mesh area 7 to 9
DESIZE,,,,,,,0.5                ! Define element size
AMESH,ALL

ASEL,ALL                        ! Select all areas
ASEL,U,AREA,,1                  ! Deselect area 1, 7, 9
ASEL,U,AREA,,7,9
AMESH,ALL                       ! Mesh

ASEL,ALL
FINISH                          ! Exit preprocessor

!--- S O L U T I O N   M O D U L E ---

/SOLU                           ! Enter solution routine

ANTYPE,STATIC                   ! Static analysis
CSYS,0                          ! Global Cartesian corrodiante

! --- B O U N D A R Y   C O N D I T I O N S ---

NSEL,S,LOC,Z,0                  ! Symmetry along Z = 0
DSYM,SYMM,Z,0

NSEL,S,LOC,Y,0                  ! Symmetry along Y = 0
DSYM,SYMM,Y,0

!simply support at the end of the cap
```

```
NSEL,S,LOC,Z,len+Rm
NSEL,R,LOC,Y,0
NSEL,R,LOC,X,0
D,ALL,UX,0

NSEL,ALL
DTRAN                          ! Transfer constraints to the FE model

ASEL,ALL
SFA,ALL,,PRES,P                ! Apply internal pressure
SFTRAN                         ! Transfer surface loading to the FE modle

SOLCONTROL,ON                  ! Nonlinear analysis
AUTOTS,ON                      ! Automatic time stepping
NSUBST, 100                    ! Initial number of substep
OUTRES,ALL,ALL
SOLVE
SAVE                           ! Save database
FINISH                         ! Exit solution routine

EXIT
```

C.2.2. Shell Element Model for Internal Corrosion in Cylindrical Shells

```
/COM, INTERNAL CORROSION IN CYLINDRICAL SHELL

! Cylinder dimensions
*SET, Ro, 21                   ! Outer radius
*SET, Ri, 20.375               ! Inner radius
*SET, len,80                   ! Length of the cylinder

*SET, h, Ro-Ri                 ! Shell thickness
*SET, Rm, (Ro+Ri)/2            ! Mean radius

*SET, pi, 3.141592654

! Damaged spot dimensions
*SET, aspect_ratio, 3          ! Aspect ratio of the damaged spot
*SET, a_hsp, 3                 ! Length of the damaged spot in circumferential direction
*SET, b_hsp,  aspect_ratio*a_hsp   ! Length of the damaged spot in axial direction
*SET, theta_hsp, (a_hsp/Ro)*(180/pi)   ! Angle of the damaged spot in circumferential direction


*SET, c, h/2                   ! Corrosion depth
*SET, hc, h-c                  ! Corroded thickness

! Applied internal pressure
*SET, P,  900
! Number of element divisions

*SET, bhsp_div, 20             ! Along axial direction of the corroded spot
```

```
*SET, ahsp_div , 10                    ! Along circumferential direction of thecorroded spot
*SET, r1_div,40                        ! For the rest of the upper part of the cylinder
*SET, lon_div, 50                      ! Along half the total length of the cylinder

! Damaged spot dimension
*SET, a_hsp,15                         ! Half the width of the corrosion along the circumference
*SET, b_hsp, 15                        ! Half the width of the corrosion along the axial direction
*SET, theta_hsp , (a_hsp/Ro)*(180/pi)


! --- P R E P R O C E S S O R ---

/PREP7                                 ! Enter preprocessor
/TITLE, Cylinder, Shell 91, Internal corrosion
/UNITS,BIN

! ---M O D E L I N G ---

! Create keypoints

CSYS,0                                 ! Cartesian coordinate system
K,  1,  0,  0,0                        ! keypoints 1 to 4 on Z=0 plane (inner radius)
K,  2, Ro,  0,0
K,  3,  0, Ro,0
K,  4,-Ro,  0,0

K,  6,  0,  0,b_hsp                    ! keypoint  6 to 9 at the center at Z = b_hsp
K,  7, Ro,  0,b_hsp
K,  8,  0, Ro,b_hsp
K,  9,-Ro,  0,b_hsp

K, 11,  0,  0,len                      ! keypoint 11 to 14 at the center at Z= len
K, 12, Ro,  0,len
K, 13,  0, Ro,len
K, 14,-Ro,  0,len

K, 16,  0,  0,len+Ro                   ! keypoint 16 at the center at Z = len+Ro

CSYS,1                                 ! Cylindrical axis with Z as the axis of rotation
K,  5, Ro,theta_hsp,0
K, 10, Ro,theta_hsp,b_hsp
K, 15, Ro,theta_hsp,len
K,18,Ro*cos(theta_hsp/180*pi),0,len

! Create lines by keypoints

CSYS,0                                 ! Cartesian coordinate system

LARC,2,5,1,Ro                          ! Arcline 1 to 3 at Z = 0
LARC,5,3,1,Ro
LARC,3,4,1,Ro

LARC, 7,10,6,Ro                        ! Arcline 4 to 6 at Z = b_hsp
LARC,10, 8,6,Ro
```

```
LARC, 8, 9,6,Ro

LARC,12,15,11,Ro                    ! Arcline 7 to 9 at Z = len
LARC,15,13,11,Ro
LARC,13,14,11,Ro

L, 2, 7                             ! line 10 to 13 from 0 to b_hsp
L, 5,10
L, 3, 8
L, 4, 9
L, 7,12                             ! line 14 to 17 from b_hsp to len
L,10,15
L, 8,13
L, 9,14

! Create areas from lines

CSYS,1                              ! Cylindrical coordinate system
AL, 1,11, 4,10                      ! Area 1 to 6
AL, 2,12, 5,11
AL, 3,13, 6,12
AL, 4,15, 7,14
AL, 5,16, 8,15
AL, 6,17, 9,16

CSKP,11,2,11,12,13                  !Local CS - spherical CS - origin at KP 11
K,17,Ro,0,theta_hsp

LARC,14,16,11,Ro                    !Spherical head - arc line 18 to 22
LARC,16,17,11,Ro
LARC,17,12,11,Ro
LARC,13,16,11,Ro
LARC,15,17,18,Ro*sin(theta_hsp/180*pi)

AL,20, 7,22                         ! Create areas (area 7 to 9) by lines
AL,19,22, 8,21
AL,18,21, 9

CSYS,0

! --- E L E M E N T   D I V I S I O N S ---

LSEL,S,LINE,, 1, 7,3                ! Defined by line number,,,Vmin,Vmax,Vinc
LESIZE,ALL,,,ahsp_div

LSEL,S,LINE,,10,13,1
LESIZE,ALL,,,bhsp_div

LSEL,S,LINE,, 2, 8,3
LESIZE,ALL,,,r1_div,4

LSEL,S,LINE,,14,17,1
LESIZE,ALL,,,lon_div,8
```

```
LSEL,ALL

! ---- E L E M E N T  A N D  M A T E R I A L  T Y P E S ---

! Material type 1
MP,EX,1,29.3E6                  ! Temperature = 100 F
MP,PRXY,1,0.3
TB,BKIN,1,,,1                   ! Rice's Hardening
TBDATA,,30000,2E4               ! yield point = 30000, Platic modulus = 2E4

! Element type 1
ET,1,SHELL91,3,1,,,1            ! Shell91, Maximum no. of layers = 3
KEYOPT,1,11,2                   ! Nodes located at 1. bottom 2. top surface
KEYOPT,1,5,1                    ! Print average results at layer middle

! Real constant set no. 1
R,1,3                           ! number of layers
RMORE
RMORE,1,,hc/3                   ! material number and thickness for layer 1 (bottom)
RMORE,1,,hc/3                   ! material number and thickness for layer 2 (middle)
RMORE,1,,hc/3                   ! material number and thickness for layer 3 (top)

! Mesh the damaged spot
TYPE,1                          ! Element type 1
REAL,1                          ! Real constant set 1
ASEL,S,AREA,,1                  ! Select area 1
AMESH,ALL

! Element type 2
ET,2,SHELL91,6,1,,,1             ! Shell91, Maximum no. of layers =  6 layers
KEYOPT,2,5,1                    ! Print average results at layer middle
KEYOPT,2,11,2                   ! Nodes located at 1. bottom 2. top surface

! Real constant set no. 2
R,2,6                           ! number of layers
RMORE
RMORE,1,,c/3                    ! material number and thickness for layer 1
RMORE,1,,c/3                    ! material number and thickness for layer 2
RMORE,1,,c/3                    ! material number and thickness for layer 3
RMORE,1,,hc/3                   ! material number and thickness for layer 4
RMORE,1,,hc/3                   ! material number and thickness for layer 5
RMORE,1,,hc/3                   ! material number and thickness for layer 6

! Mesh the remaining of the cylinder
TYPE,2                          ! Element type 2
REAL,2                          ! Real constant set 2
ASEL,ALL                        ! Select all areas
ASEL,U,AREA,,1                  ! Deselect area 1
DESIZE,,,,,,,0.5                ! Assign element edge size
AMESH,ALL

ASEL,ALL
CSYS,0
```

```
! ---B O U N D A R Y   C O N D I T I O N S ---

NSEL,S,LOC,Z,0                  ! Symmetry along Z = 0
DSYM,SYMM,Z,0

NSEL,S,LOC,Y,0
DSYM,SYMM,Y,0                   ! Symmetry along Y = 0

! Simply support at the end of the cap
NSEL,S,LOC,Z,len+Ro
NSEL,R,LOC,Y,0
NSEL,R,LOC,X,0
D,ALL,UX,0

NSEL,ALL
DTRAN                           ! Transfer constraints to FE model

! Apply internal pressure
ASEL, ALL
SFA,ALL,,PRES,P
SFTRAN                          ! Transfer loads to FE model

CHECK
FINISH                          ! Exit preprocessor


! ---- S O L U T I O N   M O D U L E ---

/SOLU                           ! Enter solution routine

ANTYPE,STATIC                   ! Static analysis
SOLCONTROL,ON                   ! Nonlinear analysis
AUTOTS,ON                       ! Automatic time stepping
NSUBST,200                      ! Initial number for substep

SOLVE
SAVE                            ! Save database
FINISH                          ! Exit solution routine


! ----P O S T P R O C E S S O R   M O D U L E ---
/POST1                          ! Enter postprocessor

RSYS,1                          ! Obtain results in cylindrical coordinate system
*get,strain_0,node,1,epto,eqv   ! Obtain strain at the crown of bulging
*get,stress_0,node,1,s,eqv      ! Obtain stress at the crown of bulging
PLESOL,EPTO,EQV                 ! Contour plot for von Mises strain

EXIT
```

C.2.3. Solid Element Model for Internal Corrosion in Cylindrical Shells

```
/COM, INTERNAL CORROSION IN CYLINDRICAL SHELL

! Cylinder dimensions (inch)
*SET, Ro, 21                          ! Outer radius
*SET, Ri, 20.375                      ! Inner radius
*SET, len, 80                         ! Length of the cylinder

*SET, h, Ro-Ri                        ! Shell thickness
*SET, Rm, (Ro+Ri)/2                   ! Mean radius

*SET, pi, 3.141592654

! Applied internal pressure
*SET, P, 1050

! Corrosion dimenstion

*SET, aspect_ratio, 3                 ! Aspect ratio of the damaged spot
*SET, a_hsp, 3                        ! Half the width of the damaged spot along circumference
*SET, b_hsp, aspect_ratio*a_hsp       ! Half the width of the damaged spot along axial direction
*SET, theta_hsp, (a_hsp/Ro)*(180/pi)

*SET, c,  h/2                         ! Corrosion depth
*SET, hc, h-c                         ! Corroded thickness
*SET, Rc, Ri+c                        ! Inner radius inside the corroded spot

! Number of element divisions

*SET, bhsp_div, 12                    ! Inside the corroded area - axial direction
*SET, ahsp_div, 6                     ! Inside the corroded area - circumferential direction
*SET, r1_div, 10                      ! For the rest of the upper part of the cylinder
*SET, lon_div, 40                     ! Along the length of the cylinder
*SET, hc_div, 10                      ! Through thickness inside the corrosion
*SET, h_div,  5                       ! Through thickness outside the corrosion

*SET, SL, -(P*Ri*Ri)/(2*Rm*h)
*SET, arc1, pi/2*Rc
*SET, arc4, pi/2*Ri
*SET, arc5, pi/2*Ro
*SET, arc2, (pi*theta_hsp*Rc)/180
*SET, arc3, (pi*theta_hsp*Ri)/180
*SET, arc6, (pi*theta_hsp*Ro)/180
*SET, a, arc2/arc1
*SET, a1, arc3/arc4
*SET, a2, arc6/arc5


! ---- P R E P R O C E S S O R ----

/PREP7                                ! Enter the preprocessor
/TITLE, Cylindrical shell, Solid 185, Internal corrosion
```

```
/UNITS,BIN

! ---M A T E R I A L  P R O P E R T I E S  A N D  E L E M E N T  T Y P E S---

! Element type 1
ET,1,SOLID185                    ! SOLID185

! Material properties for temperature 100 deg. F
MP,EX,1,29.3E6                   !  Young's modulus
MP,PRXY,1,0.3                    ! Poisson's ratio
TB,BKIN,1,1,2,1                  ! Bilinear kinematic strain hardening
TBDATA,,29982,2E4                ! Data table, yield stress, plastic modulus

! ---- M O D E L I N G  ---

! Create keypoints on the current CS
K,1,0,0,0
K,2,Ri,0,0
K,3,0,Ri,0
K,4,0,-Ri,0
K,5,Ro,0,0
K,6,0,Ro,0
K,7,0,-Ro,0
K,8,0,0,len

! Create lines from keypoints
LARC,2,3,1,Ri                    ! Arc line 1 to 4
LARC ,5,6,1,Ro
LARC ,2,4,1,Ri
LARC ,5,7,1,Ro

L,2,5                            ! Line 5 to 8
L,3,6
L,4,7
L,1,8

! Create areas by lines
AL,5,1,6,2                       ! Area 1 and 2
AL,5,3,7,4
ASEL, ALL
VDRAG,1,2,,,,,8                  ! Create volume by dragging areas along line 8

! Create internal corroded spot
K,15,0,Rc,0
K,16,Rc,0,0
LARC,15,16,1,Rc
LDIV,22,a,17
LDIV,1,1-a,18
L,17,18
LCSL,6,22                        ! Divide intersecting lines at points of intersection
AL,26,22,25,24                   ! Create areas by lines
VEXT,12,,,,,b_hsp                ! Generates additional volumes by extruding areas
VSBV,1,3                         ! Subtract volume 3 from volume 1
```

```
! Create different portions for meshing
LDIV,2,1-A2,51                  ! Line along longitudinal direction at a_hsp
L,18,51
LDIV,12,1-A2,52
LDIV,16,A1,53
L,52,53
A,52,53,18,51
VSBA,4,1                        ! Subtract area 1 from volume 4

K,54,Ro+10,Ro+10,b_hsp          !Line along circumferential direction at a_hsp
K,55,-(Ro+10),Ro+10,b_hsp
K,56,-(Ro+10),-(Ro+10),b_hsp
K,57,(Ro+10),-(Ro+10),b_hsp
A,54,55,56,57
VSBA,3,1                        ! Subtract area 1 from vol 3 (inside the corroded area)

K,54,Ro+10,Ro+10,b_hsp
K,55,-(Ro+10),Ro+10,b_hsp
K,56,-(Ro+10),-(Ro+10),b_hsp
K,57,(Ro+10),-(Ro+10),b_hsp
A,54,55,56,57
VSBA,1,1                        ! Subtract area 1 from vol 1 (upper part of the cylinder)

K,54,Ro+10,Ro+10,b_hsp
K,55,-(Ro+10),Ro+10,b_hsp
K,56,-(Ro+10),-(Ro+10),b_hsp
K,57,(Ro+10),-(Ro+10),b_hsp
A,54,55,56,57
VSBA,2,1                        ! Subtract area 1 from volume 2 (lower part)

! ---- E L E M E N T   D I V I S I O N S ----

lesize,35,,,lon_div,6           ! Along longitudinal direction
lesize,40,42,,lon_div,6
lesize,48,49,,lon_div,6
lesize,58,59,,lon_div,6

lesize,1 ,2,,r1_div,4           ! Along circumferential direction (upper part)
lesize,12,,,r1_div,4
lesize,23,,,r1_div,4
lesize,31,,,r1_div,4
lesize,51,52,,r1_div,4

lesize,3 ,4,,12                 ! Along circumferential direction (lower part)
lesize,17,,,12
lesize,21,,,12
lesize,38,,,12
lesize,56,,,12

lesize,15,16,,ahsp_div          ! Inside the corroded spot (along circumference)
lesize,22,,,ahsp_div
lesize,26,30,2,ahsp_div
lesize,45,,,ahsp_div
```

```
lesize,6 ,,,hc_div                    ! Through corroded thickness
lesize,25,29,2,hc_div
lesize,39,,,hc_div
lesize,46,47,,hc_div

lesize,32,34,,bhsp_div                ! Inside the corroded spot (along axial direction)
lesize,37,,,bhsp_div
lesize,43,44,,bhsp_div
lesize,53,55,,bhsp_div

! ---- M E S H I N G ----

! Preparation for mapped meshing
LREVERSE,1                            ! Reverse the normal of selected lines
LREVERSE,2
LREVERSE,12
LREVERSE,35
LREVERSE,41
LREVERSE,42
LREVERSE,58
LREVERSE,59

LCCAT,25,39                           ! Concatenates lines into one line for mapped meshing
LCCAT,47,29
LCCAT,46,6
LCCAT,15,2
LCCAT,43,48
LCCAT,44,49
LCCAT,40,34
LCCAT,37,59
LCCAT,54,42
LCCAT,53,41

ACCAT,12,2                            ! Concatenates areas into one area for mapped meshing
ACCAT,16,19
ACCAT,18,13

! Mesh volume
VMESH,ALL                             ! Mesh volume

! ---- B O U N D A R Y   C O N D I T I O N S ---
DA,2 ,symm                            ! Apply symmetric boundary conditions
DA,7 ,symm
DA,12,symm
DA,14,symm
DA,23,symm
DA,26,symm
DA,34,symm

DK,5,UY,0                             ! Constrain disp along axial direction at keypoint 5

SFA,15,1,PRES,P                       ! Apply internal pressure to inside surface areas
SFA,24,1,PRES,P
SFA,29,1,PRES,P
```

```
SFA,21,1,PRES,P
SFA,3 ,1,PRES,P
SFA,35,1,PRES,P

SFA,22,1,pres,SL                ! Apply pressure to the end of the cylinder
SFA,6,1,pres,SL
SFA,11,1,pres,SL

DTRAN                           ! Transfer constraints to FE model
SFTRAN                          ! Transfer surface load to FE model
FINISH                          ! Exit preprocessor


! ---- S O L U T I O N   M O D U L E ---

/SOLU                           ! Enter solution routine
NSUBST,500                      ! Initial number of substep
OUTRESS,ALL,ALL
SOLVE
SAVE                            ! Save database
FINISH                          ! Exit solution routine

EXIT
```

C.2.4. Solid Element Model for External Corrosion in Cylindrical Shells

```
/COM, EXTERNAL CORROSION IN CYLINDRICAL SHELL

! Cylinder dimensions (inch)
*SET, Ro, 21                    ! Outer radius
*SET, Ri, 20.375                ! Inner radius
*SET, len, 100                  ! Length of the cylinder

*SET, h, Ro-Ri                  ! Shell thickness
*SET, Rm, (Ro+Ri)/2             ! Mean radius

*SET, pi, 3.141592654

! Applied internal pressure
*SET, P, 1050

! Corrosion dimenstion

*SET, aspect_ratio, 3           ! Aspect ratio of the damaged spot
*SET, a_hsp, 3                  ! Half the width of the damaged spot along circumference
*SET, b_hsp, aspect_ratio*a_hsp ! Half the width of the damaged spot along axial direction
*SET, theta_hsp, (a_hsp/Ro)*(180/pi)

*SET, c,  h/2                   ! Corrosion depth
*SET, hc, h-c                   ! Corroded thickness
*SET, Rc, Ri+c                  ! Inner radius inside the corroded spot
```

```
! Number of element divisions

*SET, bhsp_div, 12                  ! Inside the corroded area - axial direction
*SET, ahsp_div, 6                   ! Inside the corroded area - circumferential direction
*SET, r1_div, 10                    ! For the rest of the upper part of the cylinder
*SET, lon_div, 40                   ! Along the length of the cylinder
*SET, hc_div, 10                    ! Through thickness inside the corrosion
*SET, h_div,  5                     ! Through thickness outside the corrosion

*SET, SL, -(P*Ri*Ri)/(2*Rm*h)
*SET, arc1, pi/2*Rc
*SET, arc4, pi/2*Ri
*SET, arc5, pi/2*Ro
*SET, arc2, (pi*theta_hsp*Rc)/180
*SET, arc3, (pi*theta_hsp*Ri)/180
*SET, arc6, (pi*theta_hsp*Ro)/180
*SET, a, arc2/arc1
*SET, a1, arc3/arc4
*SET, a2, arc6/arc5


! ---- P R E P R O C E S S O R ----

/PREP7                              ! Enter preprocessor
/TITLE, Cylindrical shell, Solid 185, External corrosion
/UNITS,BIN

! M A T E R I A L   P R O P E R T I E S

ET,1,solid185                       ! SOLID185 element

MP,EX,1,29.3e6                      ! Young's modulus
MP,PRXY,1,0.3                       ! Poisson's ratio
TB,BKIN,1,1,2,1                     ! Bilinear kinematic strain hardenting
TBDATA,,29982,2e4                   ! Yield point, plastic modulus

! ---M O D E L I N G ---

! Create keypoints on the current CS
K,1,0,0,0                           ! At the center of the cylinder
K,2,Ri,0,0                          ! Along the circumference of the inner radius
K,3,0,Ri,0
K,4,0,-Ri,0
K,5,Ro,0,0                          ! Along the circumference of the outter radius
K,6,0,Ro,0
K,7,0,-Ro,0
K,8,0,0,len

! Create lines from keypoints
LARC,2,3,1,Ri                       ! Arc line 1 to 4
LARC ,5,6,1,Ro
LARC ,2,4,1,Ri
LARC ,5,7,1,Ro
```

```
L,2,5                                   ! Line 5 to 8
L,3,6
L,4,7
L,1,8

! Create areas by lines
AL,5,1,6,2                              ! Area 1 and 2
AL,5,3,7,4
ASEL, ALL
VDRAG,1,2,,,,,8                         ! Create volume by dragging areas along line 8

! Create external corroded spot
K,15,0,Rc,0
K,16,Rc,0,0
LARC,15,16,1,Rc
LDIV,22,a,17
LDIV,2,1-a2,18
L,17,18
LCSL,6,22                               ! Divide intersecting lines at points of intersection
AL, 22,27,24,25                         ! Create areas by lines
VEXT,12,,,,,b_hsp                       ! Generates additional volumes by extruding areas
VSBV,1,3                                ! Subtract volume 3 from volume 1

! Create different portions for meshing
LDIV, 1,1-a1,51                         ! Line along longitudinal direction at a_hsp
L,18,51
LDIV, 12,1-a2,52
LDIV,16,a1,53
L,52,53
A,52,53,51, 18
VSBA,4,1                                ! Subtract area 1 from volume 4

K,54,Ro+10,Ro+10,b_hsp                  !Line along circumferential direction at a_hsp
K,55,-(Ro+10),Ro+10,b_hsp
K,56,-(Ro+10),-(Ro+10),b_hsp
K,57,(Ro+10),-(Ro+10),b_hsp
A,54,55,56,57
VSBA,3,1                                ! Subtract area 1 from vol 3 (inside the corroded area)

K,54,Ro+10,Ro+10,b_hsp
K,55,-(Ro+10),Ro+10,b_hsp
K,56,-(Ro+10),-(Ro+10),b_hsp
K,57,(Ro+10),-(Ro+10),b_hsp
A,54,55,56,57
VSBA,1,1                                ! Subtract area 1 from vol 1 (upper part of the cylinder)

K,54,Ro+10,Ro+10,b_hsp
K,55,-(Ro+10),Ro+10,b_hsp
K,56,-(Ro+10),-(Ro+10),b_hsp
K,57,(Ro+10),-(Ro+10),b_hsp
A,54,55,56,57
VSBA,2,1                                ! Subtract area 1 from volume 2 (lower part)
```

```
! ---- E L E M E N T   D I V I S I O N S ----

lesize,35,,,lon_div,6                  ! Along longitudinal direction
lesize,40,42,,lon_div,6
lesize,48,49,,lon_div,6
lesize,58,59,,lon_div,6

lesize,1 ,2,,r1_div,4                  ! Along circumferential direction (upper part)
lesize,12,,,r1_div,4
lesize,23,,,r1_div,4
lesize,34,,,r1_div,4
lesize,51,52,,r1_div,4

lesize,3 ,4,,12                        ! Along circumferential direction (lower part)
lesize,17,,,12
lesize,21,,,12
lesize,38,,,12
lesize,56,,,12

lesize,6,,,ahsp_div                    ! Inside the corroded spot (along circumference)
lesize,13,16,3,ahsp_div
lesize,22,,,ahsp_div
lesize,27,29,2,ahsp_div
lesize,45,,,ahsp_div

lesize,26 ,,,hc_div                    ! Through corroded thickness
lesize,39,,,hc_div
lesize,43,44,,hc_div

lesize,25,,,h_div                      ! Through the shell thickness
lesize,28,,,h_div
lesize,30,,,h_div

lesize,31,33,,bhsp_div                 ! Inside the corroded spot (along axial direction)
lesize,37,,,bhsp_div
lesize,46,47,,bhsp_div
lesize,53,55,,bhsp_div

! ---- M E S H I N G ----

! Preparation for mapped meshing
LREVERSE,1                             ! Reverse the normal of selected lines
LREVERSE,2
LREVERSE,12
LREVERSE,35
LREVERSE,41
LREVERSE,42
LREVERSE,58
LREVERSE,59

LCCAT,25,39                            ! Concatenates lines into one line for mapped meshing
LCCAT,47,29
LCCAT, 3, 1
LCCAT, 4, 2
```

```
LCCAT, 1,13
LCCAT,12,17
LCCAT,16,34
LCCAT,27,12
LCCAT,28,44
LCCAT,33,40
LCCAT,34,21
LCCAT,41,53
LCCAT,42,54
LCCAT,43,30
LCCAT,46,48
LCCAT,58,55
LCCAT,59,37

ACCAT,6,13                    ! Concatenates areas into one area for mapped meshing
ACCAT,15,19

! Mesh volume
VMESH,ALL                     ! Mesh volume

! ---- B O U N D A R Y   C O N D I T I O N S ---

DA,2 ,symm                    ! Apply symmetric boundary conditions
DA,12 ,symm
DA,16,symm
DA,18,symm
DA,22,symm
DA,26,symm
DA,34,symm

DK,5,UY,0                     ! Constrain disp along axial direction at keypoint 5

SFA,3 ,1,PRES,P               ! Apply internal pressure to inside surface areas
SFA, 7,1,PRES,P
SFA,21,1,PRES,P
SFA,25,1,PRES,P
SFA,29,1,PRES,P
SFA,35,1,PRES,P

SFA,5,1,pres,SL               ! Apply pressure to the end of the cylinder
SFA,11,1,pres,SL
SFA,23,1,pres,SL

DTRAN                         ! Transfer constraints to FE model
SFTRAN                        ! Transfer surface load to FE model
FINISH                        ! Exit preprocessor


! ---- S O L U T I O N   M O D U L E ---

/SOLU                         ! Enter solution routine
NSUBST,500                    ! Initial number of substep
OUTRESS,ALL,ALL
SOLVE
```

```
SAVE                                    ! Save database
FINISH                                  ! Exit solution routine

EXIT
```